PROCEEDINGS

of the

Fifth International Conference on the Ultrasonic Measurement and Imaging of Tissue Elasticity©

Snowbird, Utah, USA
October 8 – 11, 2006

PROCEEDINGS

of the
Fifth International Conference
on the Ultrasonic Measurement and Imaging
of Tissue Elasticity©

Snowbird, Utah, USA
October 8–11, 2006

Table of Contents

QUESTIONS OR COMMENTS ARE WELCOME AT ANY TIME AT <elasticity.conference@uth.tmc.edu>

Some abstracts may have been edited by the reviewers for clarity of presentation.

FOREWORD

Dear Conference Delegate:

Welcome to the 5th Anniversary year of the International Conference on the Ultrasonic Measurement and Imaging of Tissue Elasticity©.

This year we are continuing to experience a phenomenal year–over–year growth in the number of abstracts submitted to the Conference; over the last four years since the first Conference, the number of accepted abstracts has increased by nearly 70%, bringing the total number of abstracts this year to 121. We are also seeing a steady increase in the number of clinical papers presented at the Conference, as well as the participation of more research groups from related disciplines and from Industry and students. The international participation in this Conference is reflected by delegates from some 20 countries, including virtually all global entities engaged in research, development and practice in the field. We believe that this continually increasing level of participation bodes well for the future of the field.

Last year's Conference feedback was unanimous in the desire for continuation of the Sunday tutorial series. We are pleased that Drs. Armen Sarvazyan (USA) and Brian Garra (USA) have agreed to present this year's exciting tutorials on the basic science and clinical progress and prospects of imaging the elastic properties of tissue. We are also continuing last year's popular format of the formal Poster Session, where each presenter has the opportunity to give a brief oral summary of his/her poster, and we thank Dr. Jeff Bamber (UK) for his continuing enthusiastic organization of this event.

The Monday evening Conference Dinner will conclude with a 5th Anniversary special classical guitar concert performed by Mr. Michael Lucarelli, an accomplished concert soloist. Mr. Lucarelli will play a variety of classical and Latin works as well as some of his own compositions.

We would like to thank all the delegates, the reviewers and the session chairs for their continuing support of the Conference. Special thanks are in order to our enthusiastic support staff that has worked above and beyond. Ms Manette Price (USA) of the Conference Secretariat's office has spent much time and effort handling most of the Conference organizational duties, hotel negotiations, correspondence and budgets; Ms Karen Ophir (USA) volunteered to design the conference's artwork, scientific program and publications, and to edit all abstracts in the Conference Proceedings; Ms Betsy Christiansen (USA) has updated and greatly improved the Conference website.

The Conference is conducted under the joint auspices of the University of Rochester Center for Biomedical Ultrasound and the Ultrasonics Laboratory in the Department of Diagnostic and Interventional Imaging at the University of Texas Medical School at Houston. These organizations have contributed in personnel, equipment and financial support. Most funding for the Conference is derived from registration fees, and with your continued support in abstract submissions and attendance, we are committed to improve and expand the Conference in the years to come. We appreciate your written and oral feedback that always helps us in planning for future Conferences.

We hope that you will enjoy this year's scientific and social programs as well as the Snowbird Ski and Summer Resort location and amenities. We plan to hold next year's Conference in the USA again, and in 2008 it will be hosted by Dr. Yongping Zheng (HK) of the Hong Kong Polytechnic University.

J. Ophir and K.J. Parker
Conference Organizers
Snowbird, Utah, October 8, 2006

CONFERENCE–AT–A–GLANCE

Fifth International Conference on the Ultrasonic Measurement and Imaging of Tissue Elasticity©
Snowbird Ski and Summer Resort – Snowbird, Utah, USA October 8–11, 2006

Sunday, October 8		**9:00A – 7:30P**	
9:00A – 12:00P		**Presentation & Exhibit Set Up**	Ballroom I, II, III
9:00A – 7:30P		Registration Desk & Conference Office Open	Ballroom Lobby
12:00P – 7:30P	**Session EEX:**	Equipment Exhibit *(during breaks)*	Ballroom III
1:00P – 3:00P	**Session TUT:**	**Tutorials: Imaging of Tissue Elasticity – Progress & Prospects of Basic & Clinical Science**	Ballroom I
3:00P – 3:30P		*Coffee Break*	Ballroom II
3:30P – 5:30P	**Session POS:**	**Poster Session – Live Oral Summaries**	Ballroom II
5:30P – 7:30P		*Opening Oktoberfest Dinner Reception*	Ballrooms II & III
Monday, October 9		**7:00A – 10:30P**	
7:00A – 8:00A		*Group Continental Breakfast*	Golden Cliff Room
7:00A – 5:30P		Registration Desk & Conference Office Open	Ballroom Lobby
8:00A – 5:30P	**Session POS:**	Posters	Ballrooms II & III
8:00A – 5:30P	**Session EEX:**	Equipment Exhibit	Ballrooms II & III
9:00A – 9:30A		*Tourist Information*	Golden Cliff Room
7:45A – 8:00A		Opening Remarks	Ballroom I
8:00A – 10:00A	**Session CAA-1:**	**Clinical and Animal Applications – I**	Ballroom I
10:00A – 10:30A		*Coffee Break*	Ballroom III
10:30A – 12:00P	**Session SIP–1:**	**Signal and Image Processing – I**	Ballroom I
12:00P – 1:30P		*Group Lunch*	Golden Cliff Room
1:30P – 2:30P	**Session CVE–1:**	**Cardiovascular Elasticity – I**	Ballroom I
2:30P – 3:30P	**Session CMM:**	**Complementary and Multi–Modality Techniques**	Ballroom I
3:30P – 4:00P		*Coffee Break*	Ballroom III
4:00P – 5:30P	**Session MIP–1:**	**Methods for Imaging Elastic Tissue Properties – I**	Ballroom I
7:30P – 10:30P		*Conference Dinner & 5th Anniversary Concert featuring Classical Guitar Soloist Michael Lucarelli*	Ballroom I
Tuesday, October 10		**7:00A – 6:45P**	
7:00A – 8:00A		*Group Continental Breakfast*	Golden Cliff Room
7:00A – 5:45P		Registration Desk & Conference Office Open	Ballroom Lobby
8:00A – 5:45P	**Session POS:**	Posters	Ballrooms II & III
8:00A – 5:45P	**Session EEX:**	Equipment Exhibit	Ballrooms II & III
8:00A – 9:45A	**Session MIP–2:**	**Methods for Imaging Elastic Tissue Properties – II**	Ballroom I
9:45A – 10:15A		*Coffee Break*	Ballroom III
10:15A – 11:30A	**Session FIP–1:**	**Forward and Inverse Problems – I**	Ballroom I
11:30A – 12:30P	**Session MMT–1:**	**Mechanical Measurement Techniques for Tissues – I**	Ballroom I
12:30P – 2:00P		*Group Lunch*	Golden Cliff Room
2:00P – 3:30P	**Session SIP–2:**	**Signal and Image Processing – II**	Ballroom I
3:30P – 4:00P		*Coffee Break*	Ballroom III
4:00P – 5:45P	**Session CAA–2:**	**Clinical and Animal Applications – II**	Ballroom I
5:45P – 6:45P		*Group Photo*	Chickadee Hill
Wednesday, October 11		**7:00A – 10:00P**	
7:00A – 8:00A		*Group Continental Breakfast*	Golden Cliff Room
7:00A – 4:30P		Registration Desk & Conference Office Open	Ballroom Lobby
8:00A – 4:30P	**Session POS:**	Posters	Atrium Overlook & Mezzanine Lobby
8:00A – 4:30P	**Session EEX:**	Equipment Exhibit	Atrium Overlook & Mezzanine Lobby
8:00A – 10:15A	**Session INS:**	**Instrumentation**	Ballroom I
10:15A – 10:45A		*Coffee Break*	Atrium Overlook & Mezzanine Lobby
10:45A – 12:15P	**Session MIP–3:**	**Methods for Imaging Elastic Tissue Properties – III**	Ballroom I
12:15P – 1:45P		*Group Lunch*	Aerie Dining Room Level 10
1:45P – 3:00P	**Session CVE–2:**	**Cardiovascular Elasticity – II**	Ballroom I
3:00P – 4:00P	**Session FIP–2:**	**Forward and Inverse Problems – II**	Ballroom I
4:00P – 4:30P		*Coffee Break*	Atrium Overlook & Mezzanine Lobby
4:30P – 5:45P	**Session MMT–2:**	**Mechanical Measurement Techniques for Tissues – II**	Ballroom I
7:00P – 10:00P		*Closing Pizza Party (Proceedings Book Signing)*	Atrium Lounge & Patio

PROGRAM

Fifth International Conference
on the Ultrasonic Measurement and Imaging
of Tissue Elasticity©
Snowbird, Utah, USA
October 8–11, 2006

Sunday, October 8 9:00A – 7:30P

9:00A – 12:00P Presentation & Exhibit Set Up
All Oral Presenters load presentations onto Conference computers (via CD or jump drive) Ballroom I
Poster Presenters set up presentations Ballroom II
Exhibitors set up exhibits Ballroom III

9:00A – 7:30P
Registration Desk & Conference Office Open Ballroom Lobby

12:00P – 1:00P 3:00P – 3:30P 5:30P – 7:30P
Session EEX: Equipment Exhibit Ballroom III

Sunday 1:00P – 3:00P
Session TUT: Tutorial: Imaging of Tissue Elasticity – Progress & Prospects of Basic & Clinical Science

Chair: JM Rubin, USA *Co-Chair: SF Levinson, USA* Ballroom I

Page No.

1:00P – 1:45P
122 TISSUE VISCOELASTICITY: PAST AND FUTURE, UNEXPLORED AREAS AND BRAVE PROJECTIONS. **25**
A Sarvazyan[1].*
[1]Artann Laboratories, Trenton, NJ, USA.

1:45P – 2:00P Discussion

2:00P – 2:45P
124 IMAGING OF TISSUE ELASTICITY: WILL IT BECOME AN IMPORTANT CLINICAL TOOL? **26**
BS Garra[1].*
[1]The University of Vermont, Burlington, VT, USA.

2:45P – 3:00P Discussion

3:00P – 3:30P
COFFEE BREAK Ballroom III

Sunday 3:30P – 5:30P
(Posters will be open for viewing and Coffee Break Discussion through Wednesday, October 11, 4:30P)
Session POS: Poster Session – Live Oral Presentations

Chair: JC Bamber, UK *Co-Chair: JL Gennisson, France* Ballroom I

Page No.

Oral summary times are approximate and subject to change.

3:30P – 3:32P
002 A NOVEL STRAIN FORMATION ALGORITHM FOR ULTRASONIC STRAIN IMAGING. **27**
J Jiang[1], TJ Hall[1], AM Sommer[1].*
[1]University of Wisconsin–Madison, Madison, WI, USA.

(Session POS continues on next page)

(Session POS continued from previous page) **Page No.**

3:32P – 3:34P

007 TOWARDS NON INVASIVE VISCO–ELASTIC VESSEL WALL MECHANICAL CHARACTERIZATION USING ULTRASOUND MEASUREMENTS. **28**

S Balocco[1,3], C Cachard[1], G Courbebaisse[2], E Boni[3], E Brusseau[2], P Tortoli[3], O Basset[2].*

[1]CREATIS, Université Claude Bernard Lyon 1, Lyon, FRANCE; [2]CREATIS, INSA Lyon, Lyon, FRANCE; [3]Università di Firenze, Firenze, ITALY.

3:34P – 3:36P

008 ROTATIONAL TISSUE MOTION QUANTIFICATION IN IVUS WITH OPTICAL FLOW. **29**

MG Danilouchkine[1], F Mastik[1], AFW van der Steen[1,2].*

[1]Erasmus Medical Center, Rotterdam, The NETHERLANDS; [2]Interuniversity Cardiology Institute of the Netherlands, Utrecht, The NETHERLANDS.

3:36P – 3:38P

010 INCREASE OF ACCURACIES OF MCSPGM, MAM and MDM. **30**

C Sumi[1], T Noro[1], T Ebisawa[1], T Tooyama[1].*

[1]Sophia University, Tokyo, JAPAN.

3:38P – 3:40P

014 A MULTISCALE VARIATIONAL OPTICAL FLOW METHOD TO ESTIMATE DISCONTINUOUS MOTION FIELDS FOR ULTRASOUND ELASTOGRAPHY. **31**

D Sosa–Cabrera[1], J González–Fernández[1], CA Castaño–Moraga[2], L Gómez–Déniz[1], L Alvarez–Leon[2], J Ruiz–Alzola[1,3].*

[1,2]University of Las Palmas de Gran Canaria, Las Palmas de Gran Canaria, Canary Islands, SPAIN; [3]Canary Islands Institute of Technology, Santa Lucía, Canary Islands, SPAIN.

3:40P – 3:42P

016 DEVELOPMENT OF A ROBUST ALGORITHM FOR IMAGING COMPLEX TISSUE ELASTICITY. **32**

Y Zhang[1], RW Kramer[1], DB Goldgof[2], V Manohar[2].*

[1]Youngstown State University, Youngstown, OH, USA; [2]University of South Florida, Tampa, FL, USA.

3:42P – 3:44P

019 BENCHMARKING OF THE MECHANICAL PROPERTIES OF ENGINEERED TISSUE. **33**

J Helfenstein[1], E Mazza[1].*

[1]Swiss Federal Institute of Technology, Zürich, SWITZERLAND.

3:44P – 3:46P

020 PHANTOM EXPERIMENTS AND COMPUTER SIMULATIONS OF ELASTOGRAPHY FOR BREAST CANCER USING WATER BAG PRESSURE. **34**

Y Hayakawa[1], K Ishida[1], K Tsuji[1], H Doi[1], Y Amano[1], M Nakamura[2].*

[1]Toin University of Yokohama, Yokohama, Kanagawa-ken, JAPAN; [2]Yokohama General Hospital, Yokohama, Kanagawa–ken, JAPAN.

3:46P – 3:48P

023 LOW–COST OPEN–SOURCE ELECTROCARDIOGRAPH FRONT–END FOR *IN–VIVO* TISSUE MOTION SYNCHRONIZATION. **35**

J González–Fernández[1], L Gómez–Déniz[1], J Ruiz–Alzola[1,2].*

[1]University of Las Palmas de Gran Canaria, Las Palmas de Gran Canaria, Canary Islands, SPAIN; [2]Canary Islands Institute of Technology, Canary Islands, SPAIN.

3:48P – 3:50P

024 RHEOLOGICAL MODELING OF THE TIME–DEPENDANT BEHAVIOR OF POROELASTIC MATERIALS UNDER CREEP TEST EXPERIMENTS. **36**

JJ Ammann[1], R Rivera[1], J. Ophir[2].*

[1]Universidad de Santiago de Chile, Santiago, CHILE; [2]The University of Texas Health Science Center Houston Medical School, Houston, TX, USA.

3:50P – 3:52P

039 REFERENCE POSITION VS. CONTRAST–TO–NOISE RATIO (CNR) ON 1D SHEAR MODULUS RECONSTRUCTION OBTAINED BY STRAIN RATIO. **37**

C Sumi[1].*
[1]Sophia University, Tokyo, JAPAN.

3:52P – 3:54P

043 ASSESSMENT OF LIVER FIBROSIS AND PORTAL HYPERTENSION BY TRANSIENT ELASTOGRAPHY IN PATIENTS WITH CHRONIC LIVER DISEASE. **38**

C Fournier[1], V Miette[1], C Corpechot[2], R Poupon[2], JA Carrion[3], X Forns[3], L Sandrin[1].*
[1]Echosens, Paris, FRANCE; [2]Hôpital Saint Antoine, Paris, FRANCE; [3]Institut d'Investigacions Biomediques August Pi i Sunyer (IDIBAPS), Barcelona, SPAIN.

3:54P – 3:56P

044 NEW COPOLYMER–IN–OIL PHANTOM MATERIALS FOR ELASTOGRAPHY. **39**

J Oudry[1], V Miette[1], L Sandrin[1].*
[1]Echosens, Paris, FRANCE.

3:56P – 3:58P

055 1D AND 2D STRAIN IMAGING WITH INTRAVASCULAR ULTRASOUND: AN *IN VIVO* STUDY. **40**

W Khaled[1], W Bojara[2], M Lindstaedt[2], A Pesavento[3], A Lorenz[3], H Ermert[1].*
[1,2]Ruhr-University Bochum, Bochum, GERMANY; [3]LP–IT Innovative Technologies GmbH, Bochum, GERMANY.

3:58P – 4:00P

062 COMPUTING STRAIN ELASTOGRAMS OF SKIN USING AN OPTICAL FLOW BASED METHOD. **41**

*Y Zhang[1], JR Sullins[1], DB Goldgof[2], V Manohar[2]. represented by RW Kramer[1]**
[1]Youngstown State University, Youngstown, OH, USA; [2]University of South Florida, Tampa, FL, USA.

4:00P – 4:02P

063 MECHANICAL PROPERTIES OF HELA CELLS BY HIGH-FREQUENCY TIME–RESOLVED ACOUSTIC MICROSCOPE. **42**

PV Zinin[1], EC Weiss[2], P Anastasiadis[2], RM Lemor[2].*
[1]University of Hawaii, Honolulu, HI, USA; [2]Fraunhofer–Institute for Biomedical Technology, St. Ingbert, GERMANY.

4:02P – 4:04P

072 STUDY OF MR-ELASTOGRAPHY RECONSTRUCTION METHODS USING AN ANTHROPOMORPHIC BREAST PHANTOM. **43**

B Robert[1], R Sinkus[1], EL Madsen[2], M Fink[1].*
[1]Laboratoire Ondes et Acoustique, ESPCI, Paris, FRANCE; [2]University of Wisconsin–Madison, Madison, WI, USA.

4:04P – 4:06P

074 SOFT TISSUE ELASTOMETER. **44**

S Tsyuryupa[1], S Kanilo[1], V Egorov[1], A Sarvazyan[1].*
[1]Artann Laboratories, Trenton, NJ, USA.

4:06P – 4:08P

075 TISSUE MIMICKING MATERIALS AND PHANTOMS. **45**

V Egorov[1], S Airapetian[1], A Sarvazyan[1].*
[1]Artann Laboratories, Trenton, NJ, USA.

(Session POS continues on next page)

(Session POS continued from previous page) **Page No.**

4:08P – 4:10P

078 IMAGE QUALITY ISSUES IN POROELASTOGRAPHY. **46**
R Righetti[1], S Srinivasan[2], A Thitai Kumar[1,3], J Ophir[1,3], TA Krouskop[4].*
[1]The University of Texas Health Science Center Houston Medical School, Houston, TX, USA; [2]Siemens Acuson Ultrasound, Mountain View, CA, USA; [3]University of Houston, Houston, TX, USA; [4]Baylor College of Medicine, Houston, TX, USA.

4:10P – 4:12P

081 A NEW SYSTEM TO EVALUATE VISCOELASTIC PROPERTIES OF SMALL SAMPLES. **47**
DPF Padula[1], O Baffa[1], AAO Carneiro[1].*
[1]Universidade de São Paulo, Ribeirão Preto–SP, BRAZIL.

4:12P – 4:14P

083 MAGNETIC RESONANCE ELASTOGRAPHY (MRE) OF AN ANTHROPOMORPHIC BREAST PHANTOM. **48**
MA Hobson[1], SA Kruse[2], JL Kugel[2], RL Ehman[2], EL Madsen[1].*
[1]University of Wisconsin–Madison, Madison, WI, USA; [2]Mayo Clinic College of Medicine, Rochester, MN, USA.

4:14P – 4:16P

084 GRADING OF THYROID NODULE STIFFNESS USING THE FINE NEEDLE AS PROXY FOR CLINICAL PALPATION: A PROSPECTIVE *IN VIVO* STUDY. **49**
N Ragavendra[1], J Sayre[2], S Hirschowitz[3].*
[1,2,3]University of California at Los Angeles, Los Angeles, CA, USA.

4:16P – 4:18P

091 NONLINEARITY OF CORNEAL BIOMECHANICAL PROPERTIES MEASURED BY AN ULTRASONIC SYSTEM. **50**
X He[1], J Liu[1].*
[1]The Ohio State University, Columbus, OH, USA.

4:18P – 4:20P

092 CLINICAL APPLICATIONS OF A REAL–TIME ELASTOGRAPHY TECHNIQUE IN BREAST IMAGING. **51**
RG Barr[1,2].*
[1]Radiology Consultants, Youngstown, OH, USA; [2]Northeastern Ohio University College of Medicine, Rootstown, OH, USA.

4:20P – 4:22P

096 MECHANICAL MEASUREMENT OF VISCOELASTIC PROPERTIES OF HUMAN PROSTATE INCLUDING CORRELATION WITH PATHOLOGY. **52**
*M Zhang[1], P Nigwekar[1], PA di Sant'Agnese[1], J Joseph[1], E Messing[1], DJ Rubens[1], KJ Parker[1]. presented by B Castañeda**
[1]University of Rochester, Rochester, NY, USA.

4:22P – 4:24P

101 ANALYSES OF BLOCK MATCHING ON ELASTOGRAPHIC IMAGES. **53**
LP Neves[1], J Jiang[2], TJ Hall[2], T Varghese[2], E Madsen[2], JA Zagzebski[2], AAO Carneiro[1].*
[1]Universidade de São Paulo, Ribeirão Preto, São Paulo, BRAZIL; [2]University of Wisconsin–Madison, Madison, WI, USA.

4:24P – 4:26P

103 INTERFACE BONDING STRENGTH IN AXIAL–SHEAR STRAIN ELASTOGRAPHY. **54**
A Thitai Kumar[1,2], J Ophir[1,2], TA Krouskop[1,3], BS Garra[4].*
[1]The University of Texas Health Science Center Houston Medical School, Houston, TX, USA; [2]University of Houston, Houston, TX, USA; [3]Baylor College of Medicine, Houston, TX, USA; [4]The University of Vermont, Burlington, VT, USA.

* *indicates Presenter*

4:26P – 4:28P

107 DEVELOPMENT OF 1–D SONOMYOGRAPHY SYSTEM TO DYNAMICALLY MONITOR DIMESIONAL CHANGE OF FOREARM MUSCLES DURING WIRST EXTENSION AND FLEXION. **55**
JY Guo[1], YP Zheng[1], QH Huang[1], X Chen[1].*
[1]The Hong Kong Polytechnic University, Hong Kong, CHINA.

4:28P – 4:30P

112 STRESS AND STRAIN RELAXATION MECHANISMS IN SOFT TISSUES. **56**
R Leiderman[1], G Berry[2], NH Gokhale[1], MS Richards[1], CE Rivas[1], JC Bamber[2], AA Oberai[3], PE Barbone[1].*
[1]Boston University, Boston, MA, USA; [2]Institute of Cancer Research, Royal Marsden Hospital, Sutton, Surrey, England, UK; [3]Rensselaer Polytechnic Institute, Troy, NY, USA.

4:30P – 4:32P

120 TRANSIENT RADIATION FORCE ELASTOGRAPHY: A PRELIMINARY COMPARISON WITH SURFACE PALPATION ELASTOGRAPHY. **57**
D MelodeLima[1], JC Bamber[1], GP Berry[1], NL Bush[1], FA Duck[2], JA Shipley[2], L Xu[1].*
[1]Institute of Cancer Research and Royal Marsden NHS Trust, Sutton, Surrey, England, UK; [2]Royal United Hospital, Bath, England, UK.

4:32P – 4:34P

123 ANALYSIS OF ULTRASOUND FRAME RATE REQUIREMENTS FOR CARDIAC ELASTOGRAPHY. **58**
H Chen[1,3], T Varghese[1], PS Rahko[2], JA Zagzebski[1].*
[1,2,3]University of Wisconsin–Madison, Madison, WI, USA.

4:34P – 4:36P

125 TRACKING OF APONEUROSIS MOTION DURING VOLUNTARY CONTRACTIONS OF THE TIBIALIS ANTERIOR MUSCLE. **59**
JW Farron[1], T Varghese[2,3], BC Heiderscheit[4], DG Thelen[1,3,4].*
[1,2,3,4]University of Wisconsin–Madison, Madison, WI, USA.

4:36P – 5:30P **Discussion**

Sunday 5:30P – 7:30P

Opening Oktoberfest Dinner Reception *Proceedings Book Signing* Ballrooms II & III

Monday, October 9 7:00A – 10:30P

7:00A – 8:00A
GROUP CONTINENTAL BREAKFAST — Golden Cliff Room

7:00A – 5:30P
Registration Desk & Conference Office Open — Ballroom Lobby

8:00A – 5:30P **Session POS: Posters** — Ballrooms II & III
Session EEX: Equipment Exhibit — Ballrooms II & III

9:00A – 9:30A *Tourist Information* — Golden Cliff Room

Monday 7:45A – 8:00A

OPENING REMARKS
KJ Parker, J Ophir — Ballroom I

Monday 8:00A – 10:00A

Session CAA–1: Clinical and Animal Applications – I

Chair: WF Weitzel, USA *Co-Chair: R Souchon, France* Ballroom I

Page No.

8:00A – 8:15A

098 CLINICAL BREAST ELASTOGRAPHY: BLINDED READER PERFORMANCE AND STRATEGIES FOR IMPROVING READER PERFORMANCE. **60**

BS Garra[1], LM Mobbs[1], CM Chant[1], J Ophir[2].*

[1]University of Vermont College of Medicine & Fletcher Allen Health Care, Burlington, VT, USA; [2]The University of Texas Health Science Center at Houston, Houston, TX, USA.

8:15A – 8:30A

033 ROC ANALYSIS OF BREAST ULTRASOUND ELASTICITY IMAGING. **61**

ES Burnside[1], TJ Hall[1] AM Sommer[1], GA Sisney[1], GK Hesley[2], NJ Hangiandreou[2], WE Svensson[3].*

[1]University of Wisconsin–Madison, Madison, WI, USA; [2]Mayo Clinic, Rochester, MN, USA; [3]Charing Cross Hospital, London, England, UK.

8:30A – 8:45A

041 CYST CHARACTERIZATION VIA DIFFERENTIAL CORRELATION COEFFICIENT VALUES FROM 2D AND 3D BREAST ELASTOGRAPHY. **62**

RC Booi[1], PL Carson[1], M O'Donnell[1], MA Roubidoux[1], AL Hall[2], JM Rubin[1].*

[1]University of Michigan, Ann Arbor, MI, USA; [2]General Electric Healthcare, Milwaukee, WI, USA.

8:45A – 9:00A

042 LIVER STIFFNESS MEASUREMENT IN MORBID AND MALIGNANT OBESITY BY TRANSIENT ELASTOGRAPHY. **63**

V Miette[1], C Fournier[1], L Sandrin[1].*

[1]Echosens, Paris, FRANCE.

9:00A – 9:15A

100 STRAIN CONTRAST FOR *IN VIVO* BREAST TISSUE. **64**

AM Sommer[1], TJ Hall[1], ES Burnside[1], J Jiang[1].*

[1]University of Wisconsin–Madison, Madison, WI, USA.

9:15A – 9:30A

065 HIGH RESOLUTION MAGNETIC RESONANCE ELASTOGRAPHY AT 7T: APPLICATION TO RHEOLOGY. **65**

B Larrat[1], R Sinkus[1], M Tanter[1], M Fink[1].*

[1]Laboratoire Ondes et Acoustique, ESPCI, Paris, FRANCE.

9:30A – 9:45A

068 *IN VIVO* 3D ELASTOGRAPHY OF INDUCED SKELETAL MUSCLE CONTRACTION. **66**

RGP Lopata[1], MM Nillesen[1], H van Dijk[2], IH Gerrits[1], JM Thijssen[1], CL de Korte[1].*

[1,2]Radboud University Nijmegen Medical Centre, Nijmegen, The NETHERLANDS.

9:45A – 10:00A

071 THREE–DIMENSIONAL SONOELASTOGRAPHY FOR THERMAL LESION DETECTION IN AN *IN VIVO* SWINE MODEL. **67**

M Zhang[1], B Castañeda[1], J Christensen[1], W Saad[1], DJ Rubens[2], KJ Parker[1].*

[1,2]University of Rochester, Rochester, NY, USA.

10:00A – 10:30A

COFFEE BREAK Ballroom III

Monday 10:30A – 12:00P

Session SIP–1: Signal and Image Processing – I

Chair: TJ Hall, USA *Co-Chair: K Hoyt, USA* Ballroom I

Page No.

10:30A – 10:45A

004 EFFICIENT ELIMINATION OF DROPOUTS IN DISPLACEMENT TRACKING. **68**
GM Treece[1], JE Lindop[1], AH Gee[1], RW Prager[1].*
[1]University of Cambridge, Cambridge, England, UK.

10:45A – 11:00A

088 RESOLUTION OF AXIAL-SHEAR STRAIN ELASTOGRAPHY. **69**
A Thitai Kumar[1,2], R Righetti[1], J Ophir[1,2], TA Krouskop[1,3].*
[1]The University of Texas Health Science Center Houston Medical School, Houston, TX, USA; [2]University of Houston, Houston, TX, USA; [3]Baylor College of Medicine, Houston, TX, USA.

11:00A – 11:15A

001 A NOVEL REAL–TIME SPECKLE TRACKING ALGORITHM USING DYNAMIC PROGRAMMING. **70**
J Jiang[1], TJ Hall[1].*
[1]University of Wisconsin–Madison, Madison, WI, USA.

11:15A – 11:30A

006 RF SIGNAL PROCESSING USING FAST GAUSS–NEWTON OPTIMIZATION. **71**
J Fehrenbach[1], R Souchon[2].*
[1]Laboratoire MIP, Toulouse, FRANCE; [2]INSERM U556, Lyon, FRANCE.

11:30A – 11:45A

054 DISPLACEMENT ESTIMATORS IN ULTRASONIC ELASTOGRAPHY FOR FINITE DEFORMATIONS. **72**
W Khaled[1], S Reichling[2], OT Bruhns[2], H Ermert[1].*
[1,2]Ruhr–University Bochum, Bochum, GERMANY.

11:45A – 12:00P

057 APPLICATION OF 2–D OPTIMIZED STRAIN ESTIMATION ALGORITHM TO DEFORMATION IMAGING OF BOVINE LIVERS *IN VITRO*. **73**
E Brusseau[1], JF Déprez[1], O Basset[1].*
[1]CREATIS UMR CNRS 5515 INSERM U630, Lyon, FRANCE.

12:00P – 1:30P

GROUP LUNCH Golden Cliff Room

Monday 1:30P – 2:30P

Session CVE–1: Cardiovascular Elasticity – I

Chair: G Cloutier, Canada *Co-Chair: M Bilgen, USA* Ballroom I

Page No.

1:30P – 1:45P

034 IMAGING MYOCARDIAL HETEROGENEITY USING PROPAGATION OF PULSED VIBRATION FOR HEALTHY SUBJECTS AND PATIENTS WITH OLD MYOCARDIAL INFARCTION. **74**
H Kanai[1], S Watanabe[2], Y Saijo[1], M Tanaka[1].*
[1]Tohoku University, Sendai, Miyagi, JAPAN; [2]Miyagi Shakaihoken Hospital, Sendai, Miyagi, JAPAN.

1:45P – 2:00P

067 *IN VIVO* 3D CARDIAC ELASTOGRAPHY IN AN ANIMAL MODEL AND HUMAN HEART. **75**
RGP Lopata[1], MM Nillesen[1], FN van de Vosse[3], IH Gerrits[1], JM Thijssen[1], L Kapusta[2], CL de Korte[1].*
[1,2]Radboud University Nijmegen Medical Centre, Nijmegen, The NETHERLANDS; [3]Eindhoven University of Technology, Eindhoven, The NETHERLANDS.

(Session CVE–1 continues on next page)

(Session CVE-1 continued from previous page) **Page No.**

2:00P – 2:15P

047 TRANSIENT MR–ELASTOGRAPHY OF THE HEART. **76**
B Robert[1], R Sinkus[1], JL Gennisson[1], M Tanter[1], M Fink[1].*
[1]Laboratoire Ondes et Acoustique, ESPCI, Paris, FRANCE.

2:15P – 2:30P

048 NON–INVASIVE ELASTOGRAPHY OF CAROTID ARTERIES. **77**
H Ribbers[1], RGP Lopata[1], S Holewijn[2], G Pasterkamp[3], JD Blankensteijn[2], CL de Korte[1].*
[1,2]Radboud University Nijmegen Medical Center, Nijmegen, The NETHERLANDS; [3]University Medical Center Utrecht, Utrecht, The NETHERLANDS.

Monday 2:30P – 3:30P
Session CMM: Complementary & Multi–Modality Elasticity Imaging Techniques

Chair: R Sinkus, France *Co-Chair: JR Resnick, USA* Ballroom I

Page No.

2:30P – 2:45P

090 MULTIMODALTY IMAGING WITH ELASTICITY ASSESSMENT. **78**
A Sarvazyan[1].*
[1]Artann Laboratories, Trenton, NJ, USA.

2:45P – 3:00P

013 INHOMOGENEITY OF THE TISSUE THERMAL PARAMETER OF EBBINI'S MODEL AND ITS DEPENDENCY ON TEMPERATURE. **79**
C Sumi[1], H Yanagimura[1], T Ooba[1], K Inoue[1].*
[1]Sophia University, Tokyo, JAPAN.

3:00P – 3:15P

036 ULTRASOUND INDUCED THERMAL STRAIN IMAGING (TSI). **80**
K Kim[1], SW Huang[1], R Witte[1], TL Hall[1], M O'Donnell[1].*
[1]University of Michigan, Ann Arbor, MI, USA.

3:15P – 3:30P

029 ULTRASOUND BASED TEMPERATURE IMAGING FOR MONITORING RADIOFREQUENCY ABLATION. **81**
M Daniels[1], J Jiang[1], T Varghese[1], EL Madsen[1], JA Zagzebski[1].*
[1]University of Wisconsin–Madison, Madison, WI, USA.

3:30P – 4:00P

COFFEE BREAK Ballroom III

Monday 4:00P – 5:30P
Session MIP–1: Methods for Imaging Elastic Tissue Properties – I

Chair: JC Bamber, UK *Co-Chair: JR Yoon, USA* Ballroom I

Page No.

4:00P – 4:15P

061 TOWARD LIVER FIBROSIS STAGING WITH IMPULSIVE ACOUSTIC RADIATION FORCE. **82**
KR Nightingale[1], KD Frinkley[1], L Zhai[1], GE Trahey, ML Palmeri[1].*
[1]Duke University, Durham, NC, USA.

4:15P – 4:30P

030 REAL–TIME TISSUE COMPRESSION QUALITY FEEDBACK FOR OPTIMIZED FREEHAND ELASTICITY IMAGING. **83**
EG Radulescu[1], R Alexandru[1], R Hooley[2], LE Philpotts[2], H Frimmer[2].*
[1]Aloka, US R&D, Wallingford, CT, USA; [2]Yale University School of Medicine, New Haven, CT, USA.

* *indicates Presenter*

Page No.

4:30P – 4:45P

031 SONOELASTOGRAPHIC SHEAR VELOCITY IMAGING: AN APPLICATION OF CRAWLING WAVES. **84**
K Hoyt[1], KJ Parker[1], DJ Rubens[2].*
[1,2]University of Rochester, Rochester, NY, USA.

4:45P – 5:00P

040 FEASIBILITY OF MUSCLE STRAIN IMAGING USING ULTRASOUND ELASTOGRAPHY DURING THERAPEUTIC BODY MOVEMENTS. **85**
JJ Triano[1], HM Langevin[2], JR Fox[3], EE Konofagou[4].*
[1]Canadian Memorial Chiropractic College, Toronto, ON, CANADA; [2,3]University of Vermont, Burlington, VT, USA; [4]Columbia University, New York, NY, USA.

5:00P – 5:15P

022 DYNAMIC MECHANICAL RESPONSE OF ELASTIC SPHERICAL INCLUSIONS TO ACOUSIC RADIATION FORCE EXCITATION. **86**
ML Palmeri[1], SA McAleavey[2], KL Fong[1], GE Trahey[1], KR Nightingale[1].*
[1]Duke University, Durham, NC, USA; [2]University of Rochester, Rochester, NY, USA.

5:15P – 5:30P

077 CONGRUENCE OF SONOELASTOGRAPHY CRAWLING WAVES AND MECHANICAL MEASUREMENTS FOR ESTIMATION OF VISCOELASTIC PROPERTIES OF SOFT TISSUES. **87**
B Castañeda[1], M Zhang[1], ZC Wu[1], DJ Rubens[2], KJ Parker[1].*
[1,2]University of Rochester, Rochester, NY, USA.

Monday 7:30P – 10:30P

7:30P – 10:30P

Conference Dinner & 5th Anniversary Concert *Proceedings Book Signing*
Concert: *Classical Guitar selections performed by soloist Michael Lucarelli*
Ballroom I **24**

Tuesday, October 10 7:00A – 6:45P

7:00A – 8:00A
GROUP CONTINENTAL BREAKFAST — Golden Cliff Room

7:00A – 5:45P
Registration Desk & Conference Office Open — Ballroom Lobby

8:00A – 5:45P **Session POS: Posters** — Ballrooms II & III
Session EEX: Equipment Exhibit — Ballrooms II & III

Tuesday 8:00A – 9:45A

Session MIP-2: Methods for Imaging Elastic Tissue Properties – II

Chair: KR Nightingale, USA *Co-Chair: Y Zheng, China* Ballroom I

Page No.

8:00A – 8:15A

115 STIFFNESS RECONSTRUCTION OF HUMAN MUSCLE TISSUE. **88**
JR Yoon[1], JR McLaughlin[2], SF Levinson[3].*
[1]Clemson University, Clemson, SC, USA; [2]Rensselaer Polytechnic Institute, Troy, NY, USA; [3]Wayne State University, Detroit, MI, USA.

8:15A – 8:30A

117 BIOLOGICAL IMPLICATIONS OF MUSCLE ELASTICITY AND VISCOSITY. **89**
SF Levinson[1], A Sarvazyan[2], JR Yoon[3], JR McLaughlin[4], OV Rudenko[5].*
[1]Wayne State University, Detroit, MI, USA; [2]Artann Laboratories, Inc., Trenton, NJ, USA; [3]Clemson University, Clemson, SC, USA; [4]Rensselaer Polytechnic Institute, Troy, NY, USA; [5]M.V. Lomonosov Moscow State University, Moscow, RUSSIA.

(Session MIP-2 continues on next page)

(Session MIP-2 continued from previous page) **Page No.**

8:30A – 8:45A

025 TWO–DIMENSIONAL MULTI–LEVEL STRAIN ESTIMATION FOR DISCONTINUOUS TISSUE. **90**
H Shi[1], T Varghese[1].*
[1]University of Wisconsin–Madison, Madison, WI, USA.

8:45A – 9:00A

079 THE FEASIBILITY OF IMAGING THE TIME-DEPENDENT MECHANICAL BEHAVIOR OF POROELASTIC MATERIALS USING AXIAL STRAIN ELASTOGRAPHY. **91**
R Righetti[1], M Righetti[2], J Ophir[1], TA Krouskop[3].*
[1]The University of Texas Health Science Center Houston Medical School, Houston, TX, USA; [2]University of Florence, Florence, ITALY; [3]Baylor College of Medicine, Houston, TX, USA.

9:00A – 9:15A

064 THE SPATIO–TEMPORAL BEHAVIOUR OF THE STRAIN FIELD IN LAYERED POROELASTIC MEDIA. **92**
GP Berry[1], NL Bush[1], JC Bamber[1].*
[1]Institute of Cancer Research, Sutton, Surrey, England, UK.

9:15A – 9:30A

104 CALIBRATION CURVES FOR NONLINEAR QUANTIFICATION OF TISSUE ELASTICITY WITH SCANNING ACOUSTIC MICROSCOPY. **93**
JL Katz[1,2], O Marangos[1], Y Wang[2], P Spencer[2], A Misra[1].*
[1,2]University of Missouri–Kansas City, Kansas City, MO, USA.

9:30A – 9:45A

021 CONTRAST–TRANSFER EFFICIENCY FOR ELECTRODE DISPLACEMENT ELASTOGRAPHY. **94**
S Bharat[1], T Varghese[1].*
[1]University of Wisconsin–Madison, Madison, WI, USA.

9:45A – 10:15A

COFFEE BREAK Ballroom III

Tuesday 10:15A – 11:30A

Session FIP–1: Forward and Inverse Problems – I

Chair: PE Barbone, USA *Co-Chair: EEW Van Houten, New Zealand* Ballroom I

Page No.

10:15A – 10:30A

087 FORWARD SIMULATIONS FOR DETERMINING THE DETECTABILITY OF SMALL INCLUSIONS WITH DYNAMIC ELASTOGRAPHY. **95**
J McNamara[1], L Goldmints[1], AM Maniatty[1].*
[1]Rensselaer Polytechnic Institute, Troy, NY, USA.

10:30A – 10:45A

038 SOME RESULTS ON THE CONDITIONING OF THE INVERSE PROBLEM OF IMAGING IN MAGNETIC RESONANCE ELASTOGRAPHY. **96**
DJN Wall[1], P Olsson[2], EEW Van Houten[3].*
[1,3]University of Canterbury, Christchurch, NEW ZEALAND; [2]Chalmers University of Technology, Gothenburg, SWEDEN.

10:45A – 11:00A

116 VARIANCE CONTROLLED SHEAR STIFFNESS IMAGING IN MAGNETIC RESONANCE ELASTOGRAPHY. **97**
JR McLaughlin[1], D Renzi[1], JR Yoon[2].*
[1]Rensselaer Polytechnic Institute, Troy, NY, USA; [2]Clemson University, Clemson, SC, USA.

** indicates Presenter*

Page No.

11:00A – 11:15A

113 NONLINEAR ELASTICITY IMAGING: RECOVERING NONLINEAR ELASTIC PARAMETERS USING HIGHER ORDER FINITE ELEMENTS. **98**
NH Gokhale[1], MS Richards[1], CE Rivas[1], R Leiderman[1], PE Barbone[1], AA Oberai[1,2].*
[1]Boston University, Boston, MA, USA; [2]Rensselaer Polytechnics Institute, Troy, NY, USA.

11:15A – 11:30A

111 ESTIMATION OF TISSUE ELASTICITY PARAMETERS USING A SIMILARITY BASED APPROACH. **99**
J Li[1], Y Chi[1], M Kalisch[1], A Noble[1].*
[1]University of Oxford, Oxford, England, UK.

CANCELLED

Tuesday 11:30A – 12:30P

Session MMT–1: Mechanical Measurement Techniques for Tissues – I

Chair: JL Katz, USA *Co-Chair: BB Guzina, USA* Ballroom I

Page No.

11:30A – 11:45A

082 VISCOELASTIC TISSUE PROPERTY MEASUREMENT USING HIGH FREQUENCY ULTRASOUND. **100**
D Liu[1], ES Ebbini[2].*
[1,2]University of Minnesota, Minneapolis, MN, USA.

11:45A – 12:00P

108 ESTIMATION OF POISSON'S RATIO BY USING FORCE AND DEFORMATION INFORMATION FROM SIGNLE INDENTATION. **101**
YP Zheng[1], APC Choi[1], CHY Ling[1].*
[1]The Hong Kong Polytechnic University, Hong Kong, CHINA.

12:00P – 12:15P

070 APPLICATION OF A 2D ELASTOGRAPHIC TECHNIQUE FOR EARLY DETECTION OF PRESSURE ULCERS: PRELIMINARY RESULTS. **102**
JF Déprez[1], E Brusseau[1], O Basset[1].*
[1]CREATIS, Lyon, FRANCE.

12:15P – 12:30P

052 ULTRAFAST ULTRASONIC DEVICE APPLIED TO MEASUREMENTS OF *IN VIVO* MUSCLE CONTRACTION FEATURES. **103**
T Deffieux[1], JL Gennisson[1], M Tanter[1], M Fink[1].*
[1]Laboratoire Ondes et Acoustique, ESPCI, Paris, FRANCE.

12:30P – 2:00P

GROUP LUNCH Golden Cliff Room

Tuesday 2:00P – 3:30P

Session SIP–2: Signal and Image Processing – II

Chair: T Varghese, USA *Co-Chair: E Brusseau, France* Ballroom I

Page No.

2:00P – 2:15P

005 LOCATION ESTIMATION INCREASES THE ACCURACY OF ULTRASONIC STRAIN ESTIMATES. **104**
JE Lindop[1], GM Treece[1], AH Gee[1], RW Prager[1].*
[1]University of Cambridge, Cambridge, England, UK.

2:15P – 2:30P

060 THE K-SIGMA FILTER: A NEW CORRELATION–BASED FILTER FOR STRAIN IMAGING. **105**
R Souchon[1], JY Chapelon[1].*
INSERM UMR 556, Lyon, FRANCE.

(Session SIP-2 continues on next page)

(Session SIP-2 continued from previous page) **Page No.**

2:30P – 2:45P

009 COMPARISON OF MULTIDIMENSIONAL DISPLACEMENT VECTOR AND STRAIN TENSOR MEASUREMENT METHODS THROUGH SIMULATIONS AND PHANTOM EXPERIMENTS. **106**
C Sumi[1], T Ebisawa[1].*
[1]Sophia University, Tokyo, JAPAN.

2:45P – 3:00P

003 A NOVEL LATERAL MOTION TRACKING ALGORITHM AND ITS APPLICATIONS IN SHEAR STRAIN IMAGING: A FEASBILITY STUDY. **107**
J Jiang[1], TJ Hall[1].*
[1]University of Wisconsin–Madison, Madison, WI, USA.

3:00P – 3:15P

089 SNR, CNR AND THEIR TRADE–OFF WITH RESOLUTION IN AXIAL–SHEAR STRAIN ELASTOGRAPHY. **108**
A Thitai Kumar[1,2], J Ophir[1,2], TA Krouskop[1,3].*
[1]The University of Texas Health Science Center Houston Medical School, Houston, TX, USA; [2]University of Houston, Houston, TX, USA; [3]Baylor College of Medicine, Houston, TX, USA.

3:15P – 3:30P

105 REAL–TIME LEAST–SQUARES STRAIN ESTIMATOR FOR ELASTOGRAPHY. **109**
R Zahiri–Azar[1], SE Salcudean[1].*
[1]University of British Columbia, Vancouver, BC, CANADA.

3:30P – 4:00P

COFFEE BREAK — Ballroom III

Tuesday 4:00P – 5:45P

Session CAA–2: Clinical and Animal Applications – II

Chair: BS Garra, USA *Co-Chair: CL de Korte, The Netherlands* Ballroom I

Page No.

4:00P – 4:15P

085 ELASTICITY IMAGING IN THE TREATMENT OF LOBULAR BREAST CARCINOMA: A CASE STUDY. **110**
JR Resnick[1], S Good[1], D Paul[1], L Fan[1], S Barnes[1], J Hanson[2].*
[1]Siemens Medical Solutions USA, Inc., Mountain View, CA, USA; [2]Swedish Medical Center, Seattle, WA, USA.

4:15P – 4:30P

050 MR–ELASTOGRAPHY IS CAPABLE OF INCREASING THE SPECIFICITY OF MR-MAMMOGRAPHY – INFLUENCE OF RHEOLOGY ON THE DIAGNOSTIC GAIN. **111**
R Sinkus[1], K Siegmann[2], M Tanter[1], T Xydeas[2], M Fink[1].*
[1]Laboratoire Ondes et Acoustique, ESPCI, Paris, FRANCE; [2]University Tübingen, Tübingen, GERMANY.

4:30P – 4:45P

093 CLINICAL APPLICATIONS OF A REAL TIME ELASTOGRAPHY TECHNIQUE IN BREAST IMAGING. **112**
RG Barr[1,2].*
[1]Radiology Consultants, Youngstown, OH, USA; [2]Northeastern Ohio University College of Medicine, Rootstown, OH, USA.

4:45P – 5:00P

099 BREAST LESION SIZE IN ELASTICITY IMAGING. **113**
AM Sommer[1], ES Burnside[1], GA Sisney[1], GK Hesley[2], TJ Hall[1].*
[1]University of Wisconsin, Madison, WI, USA; [2]Mayo Clinic, Rochester, MN, USA.

5:00P – 5:15P

049 VASCULAR ACOUSTIC RADIATION FORCE IMPULSE IMAGING (ARFI) IMAGING OF POPLITEAL AND CAROTID ARTERIES: *IN VIVO* RESULTS. **114**
D Dumont[1], J Dahl[1], E Miller[1], J Allen[1], G Trahey[1].*
[1]Duke University, Durham, NC, USA.

** indicates Presenter*

Page No.

5:15P – 5:30P

094 PRELIMINARY POROELASTOGRAPHY RESULTS ON LYMPHEDEMATOUS TISSUES *IN VIVO*. **115**
R Righetti[1], BS Garra[2], LM Mobbs[2], CM Chant[2], J Ophir[1].*
[1]The University of Texas Health Science Center Houston Medical School, Houston, TX, USA; [2]The University of Vermont, Burlington, VT, USA.

5:30P – 5:45P

086 THYROID STIFFNESS INDEX FROM THYROID ELASTOGRAPHY USING CAROTID ARTERY PULSATION: CORRELATION WITH FINE NEEDLE ASPIRATION BIOPSY. **116**
U Bae[1], M Dighe[1], V Shamdasani[1], Y Kim[1].*
[1]University of Washington, Seattle, WA, USA.

Tuesday 5:45P – 6:45P
Group Photo

Chickadee Hill

Wednesday, October 11 7:00A – 10:00P

7:00A – 8:00A
GROUP CONTINENTAL BREAKFAST — Golden Cliff Room

7:00A – 4:30P
Registration Desk & Conference Office Open — Ballroom Lobby

8:00A – 4:30P **Session POS: Posters** — Atrium Overlook & Mezzanine Lobby Level C
Session EEX: Equipment Exhibit — Atrium Overlook & Mezzanine Lobby Level C

Wednesday 8:00A – 10:15A
Session INS: Instrumentation

Chair: A Sarvazyan, USA *Co-Chair: L Sandrin, France* — Ballroom I

Page No.

8:00A – 8:15A

102 EXPERIMENTAL VALIDATION OF TISSUE MOTION TRACKING RESOLUTION LIMITS FOR THE DIGITAL PULSED PHASE LOCKED LOOP. **117**
T Lynch[1], S Guy[1], R Saunders[1].*
[1]Luna Innovations Incorporated, Hampton, VA, USA.

8:15A – 8:30A

032 ANTHROPOMORPHIC UTERINE PHANTOMS FOR TESTING ELASTOGRAPHY SYSTEMS. **118**
MA Hobson[1], GR Frank[1], T Varghese[1], EL Madsen[1].*
[1]University of Wisconsin–Madison, Madison, WI, USA.

8:30A – 8:45A

059 ULTRASOUND ELASTOGRAPHY AND BACKSCATTER ATTENUATION TOMOGRAPHY AS METHODS FOR IONIZING RADIATION DOSIMETRY: A FEASIBILITY STUDY. **119**
JC Bamber[1], NL Bush[1], J Trap[1], M Partridge[1].*
[1]Institute of Cancer Research and Royal Marsden NHS Trust, Sutton, Surrey, England, UK.

8:45A – 9:00A

026 NON–CONTACT FOCUSED ACOUSTIC RADIATION FORCE TECHNIQUE FOR THE BIOMECHANICAL CHARACTERISATION OF AN AMPUTEE'S RESIDUAL LIMB. **120**
H Mulvana[1], S Cochran[2], B Spence[1], S Solomonidis[1].*
[1]University of Strathclyde, Glasgow, UK; [2]University of Paisley, Paisley, UK.

(Session INS continues on next page)

(Session INS continued from previous page) **Page No.**

9:00A – 9:15A

069 QUANTIZATION OF TISSUE VISCO–ELASTICITY FROM MEASURED DISPERSION OF SHEAR WAVE SPEED: A PRACTICAL STUDY. **121**
S Chen[1], R Kinnick[1], JF Greenleaf[1].*
[1]Mayo Clinic College of Medicine, Rochester, MN, USA.

9:15A – 9:30A

076 BREAST MECHANICAL IMAGER – AN ELASTICITY IMAGING DEVICE BASED ON DYNAMIC MEASUREMENT OF SURFACE STRESS PATTERNS. **122**
V Egorov[1], J Son[2], S Airapetian[1], A Sarvazyan[1].*
[1]Artann Laboratories, Trenton, NJ, USA; [2]Medical Tactile, Inc., Los Angeles, CA, USA.

9:30A – 9:45A

028 MULTI-LAYERED PLAQUE VASCULAR PHANTOMS FOR ACOUSTIC RADIATION FORCE IMPULSE IMAGING. **123**
D Dumont[1], M Mathis[1], L Zhai[1], B Fahey[1], G Trahey[1].*
[1]Duke University, Durham, NC, USA.

9:45A – 10:00A

106 DEVELOPMENT OF A THREE–DIMENSIONAL TISSUE ELASTICITY MICROSCOPE. **124**
T Shiina[1], M Yoshida[1], M Yamakawa[1], N Nitta[2], T Mitake[3].*
[1]University of Tsukuba, Tsukuba, JAPAN; [2]National Institute of Advanced Industrial Science and Technology, Tsukuba, JAPAN; [3]Hitachi Medical Corporation, Kashiwa, JAPAN.

10:00A – 10:15A

121 VOLUME ELASTICITY IMAGING WITH A 2–D CAPACITIVE MICRO–MACHINED ULTRASOUND TRANSDUCER (CMUT) ARRAY. **125**
TG Fisher[1], TJ Hall[1], S Panda[2], J Jiang[1], J Resnick[2], S Barnes[2], EL Madsen[1].*
[1]University of Wisconsin–Madison, Madison, WI, USA; [2]Siemens Medical Solutions USA, Inc., Mountain View, CA, USA.

10:15A – 10:45A

COFFEE BREAK — Atrium Overlook & Mezzanine Lobby Level C

Wednesday 10:45A – 12:15P

Session MIP–3: Methods for Imaging Elastic Tissue Properties – III

Chair: KJ Parker, USA *Co-Chair: C Sumi, Japan* Ballroom I

Page No.

10:45A – 11:00A

118 ANALYZING THE EFFECT OF VISCOELASTICITY IN SHEAR WAVE SPEED IMAGES WITH SUPERSONIC IMAGING DATA. **126**
JR McLaughlin[1], D Renzi[1], J Klein[1], JR Yoon[2].*
[1]Rensselaer Polytechnic Institute, Troy, NY, USA; [2]Clemson University, Clemson, SC, USA.

11:00A – 11:15A

015 SHEAR STRAIN ELASTOGRAMS INDUCED BY SHEAR DEFORMATION. **127**
M Rao[1], EL Madsen[1], T Varghese[1].*
[1]University of Wisconsin–Madison, Madison, WI, USA.

11:15A – 11:30A

053 ELASTIC IMAGING AT FINITE DEFORMATIONS. **128**
S Reichling[1], W Khaled[2], OT Bruhns[1], H Ermert[2].*
[1,2]Ruhr–University Bochum, Bochum, GERMANY.

* *indicates Presenter*

Page No.

11:30A – 11:45A

058 SIMULATIONS OF MOTION DETECTION USING A COMBINED ARRAY FOR LOCALIZED HARMONIC MOTION IMAGING. **129**
J Heikkilä[1], K Hynynen[2].*
[1]University of Kuopio, Kuopio, FINLAND; [2]Sunnybrook Health Sciences Centre, Toronto, ON, CANADA.

11:45A – 12:00P

027 PRINCIPAL COMPONENT ANALYSIS: SHEAR STRAIN EFFECTS. **130**
H Chen[1], T Varghese[1].*
[1]University of Wisconsin–Madison, Madison, WI, USA.

12:00P – 12:15P

051 A 3D TRANSIENT ELASTOGRAPHY SYSTEM DESIGNED FOR *IN VIVO* BREAST EXAMINATION. **131**
JL Gennisson[1], T Deffieux[1], R Sinkus[1], M Pernot[1], M Tanter[1], M Fink[1].*
[1]Laboratoire Ondes et Acoustique, ESPCI, Paris, FRANCE.

12:15P – 1:45P

GROUP LUNCH — Aerie Dining Room Level 10

Wednesday 1:45P – 3:00P

Session CVE–2: Cardiovascular Elasticity – II

Chair: H Kanai, Japan *Co-Chair: EG Radulescu, USA* Ballroom I

Page No.

1:45P – 2:00P

066 NON–INVASIVE VASCULAR ULTRASOUND ELASTOGRAPHY OF CAROTID ARTERIES: AN UPDATE ON A PHASE 1 CLINICAL STUDY. **132**
G Cloutier[1], RL Maurice[1], C Schmitt[1], MF Giroux[2], G Soulez[2].*
[1]University of Montréal Hospital Research Center, Montréal, Quebec, CANADA; [2]University of Montréal Hospital, Montréal, Quebec, CANADA.

2:00P – 2:15P

037 STRAIN ESTIMATION OF ARTERIAL WALL WITH GLOBAL MOTION TRACKING: A PHANTOM STUDY. **133**
H Hasegawa[1], H Kanai[1].*
[1]Tohoku University, Sendai, Miyagi, JAPAN.

2:15P – 2:30P

110 GAINING NEW INSIGHTS ON THE RELATIONSHIP BETWEEN STRUCTURE, PROPERTY AND FUNCTION IN THE DIABETIC HEART USING ELASTOGRAPHY IMAGING. **134**
M Bilgen[1,2], J Gauch[3], R Loganathan[4], MD Alenezy[5], E Popel[3], T Alrefae[5], IV Smirnova[4].*
[1,2,4]University of Kansas Medical Center, Kansas City, KS, USA; [3,5]Kansas University, Lawrence, KS, USA.

2:30P – 2:45P

046 MECHANICAL VISCOELASTIC VARIATIONS OF *IN VIVO* CAROTID ATHEROMAS USING EXTERNAL ULTRASOUND. **135**
M McCormick[1], H Shi[1], C Mitchell[1], MA Kliewer[1], R Dempsey[1], T Varghese[1].*
[1]University of Wisconsin–Madison, Madison, WI, USA.

2:45P – 3:00P

035 LOCAL UNDISTENDED ARTERIAL ELASTIC MODULUS RECONSTRUCTION USING *IN VIVO* STRAIN IMAGING AND PULSE WAVE VELOCITY. **136**
K Kim[1], WF Weitzel[2], C Jia[1], JM Rubin[3], TJ Kolias[2], M O'Donnell[1].*
[1,2,3]University of Michigan, Ann Arbor, MI, USA.

Wednesday 3:00P – 4:00P
Session FIP–2: Forward and Inverse Problems – II

Chair: D Renzi, USA *Co-Chair: GM Treece, UK* Ballroom I

Page No.

3:00P – 3:15P

114 INVESTIGATION OF LOCALLY CONSTANT ASSUMPTION FOR INVERSE PROBLEM IN ELASTOGRAPHY. **137**
K Lin[1], JR McLaughlin[1].*
[1]Rensselaer Polytechnic Institute, Troy, NY, USA.

3:15P – 3:30P

119 MODEL–BASED VISCOELASTIC TISSUE CHARACTERIZATION FROM HIGH FREQUENCY ULTRASOUND MEASUREMENTS. **138**
BB Guzina[1], ES Ebbini[2], K Tuleubekov[1], D Liu[2].*
[1,2]University of Minnesota, Minneapolis, MN, USA.

3:30P – 3:45P

012 COMPARISON OF MULTIDIMENSIONAL SHEAR MODULUS RECONSTRUCTION METHODS THROUGH SIMULATIONS AND PHANTOM EXPERIMENTS. **139**
C Sumi[1], D Kikuchi[1], Y Shimada[1], S Nojiri[1].*
[1]Sophia University, Tokyo, JAPAN.

3:45P – 4:00P

097 DOMAIN DECOMPOSITION OF THE ELASTICITY IMAGING PROBLEM: EXPERIENCE WITH A SUBZONE BASED MAGNETIC RESONANCE ELASTOGRAPHY APPROACH. **140**
EEW Van Houten[1], HU Berger[1], MD McGarry[1], MM Doyley[2], JB Weaver[3], KD Paulsen[2].*
[1]University of Canterbury, Christchurch, NEW ZEALAND; [2]Dartmouth College, Hanover, NH, USA; [3]Dartmouth–Hitchcock Medical Center, Lebanon, NH, USA.

4:00P – 4:30P

COFFEE BREAK Atrium Overlook & Mezzanine Lobby Level C

Wednesday 4:30P – 5:45P
Session MMT–2: Mechanical Measurement Techniques for Tissues – II

Chair: SF Levinson *Co-Chair: R Righetti, USA* Ballroom I

Page No.

4:30P – 4:45P

045 MEASUREMENTS OF ATTENUATION IN COPOLYMERS–IN–OIL PHANTOMS USING TRANSIENT ELASTOGRAPHY. **141**
C Bastard[1], V Miette[1], L Sandrin[1].*
[1]Echosens, Paris, FRANCE.

4:45P – 5:00P

056 SKIN ELASTOGRAPHY IN BREAST CANCER RELATED LYMPHOEDEMA PATIENTS UNDER SURFACE TENSILE LOADING. **142**
LV Coutts[1], JC Bamber[1], NR Miller[1], P Mortimer[1].*
[1]Institute of Cancer Research and Royal Marsden NHS Trust, Sutton, Surrey, England, UK.

5:00P – 5:15P

073 ASSESSMENT OF MECHANICAL PROPERTIES AND GEOMETRICAL FEATURES OF THE PROSTATE BY A MECHANICAL IMAGING DEVICE. **143**
V Egorov[1], S Airapetian[1], A Sarvazyan[1].*
[1]Artann Laboratories, Trenton, NJ, USA.

5:15P – 5:30P

080 WAVE ATTENUATION AND POISSON'S RATIO IN DEFORMED MOUSE MAMMARY TUMOR. **144**
H Kobayashi[1], R Vanderby[1].*
[1]University of Wisconsin–Madison, Madison, WI, USA.

** indicates Presenter*

5:30P – 5:45P

5:45P – 7:00P *No Conference Activities*

Wednesday 7:00P – 10:00P

Closing Pizza Party *Proceedings Book Signing* Atrium Lounge & Patio

Session EEX: Equipment Exhibit

See Sunday – Tuesday: Ballroom III; Wednesday: Atrium Overlook & Mezzanine Lobby Level C

Luna Innovations Incorporated.
Blacksburg, VA, USA.

Siemens Medical Solutions Ultrasound Group.
Issaquah, WA, USA.

Ultrasonix Medical Corporation
Burnaby, BC, CANADA.

AUTHOR INDEX

AUTHOR INDEX

Fifth Anniversary Concert

Michael Lucarelli

Classical Guitar

Michael Lucarelli was born on August 18, 1959 in Cincinnati, Ohio. He began his music education in 1973 on the electric guitar after hearing the group Led Zepplin. Later, Michael discovered the classical guitar and began his studies with Peruvian Guitarist Ricardo Linares. Michael went on to receive his Bachelor of Music degree in 1989 from the University of Utah and his Master of Music in 1992 from the University of Arizona in Guitar performance.

Currently Michael lives in Salt Lake City with his wife Shahla, where he has an active schedule performing, recording, teaching, and composing for the classical guitar. Michael teaches Guitar and Yoga through the University of Utah "LifeLong Learning" as well as private guitar instruction at his home studio. Michael performs extensively for weddings, receptions, concerts, festivals, and private events throughout the U.S.A.

Some of his Utah performances have included appearances at Capitol Theatre, Gardner Hall, Peery's Egyptian Theatre, Temple Square Concert Series, Utah State University, BYU, Dixie College, Snow College, and Westminster College. He has performed regularly at the Utah Arts Festival, Helper Arts festival, Brown Bag Concert series, and First Night. During the 2002 Winter Olympics, Michael had the honor of performing for the Athletes at the Olympic Village. He has appeared on several radio and television programs including the TV series "Touched by an Angel". Michael has been on the Utah Performing Arts Tour roster for several seasons, and in 1995 he was the recipient of an Individual Artist Grant from the Utah Arts Council and the National Endowment of the Arts. Michael's six CDs have received enthusiastic reviews worldwide.

Tonight's concert spans three centuries of music that includes many styles and sounds, which demonstrate the wide range of the classical guitar. From the Baroque music of Bach to the Classical music of the "Beethoven of the Guitar", Fernando Sor – from the Spanish styles of Albéniz to the Latin composers such as Piazzolla and Barrios – to the unique traditional "ultra" sonority of the 13–string Japanese Koto of Yocoh's Variations on Sakura, and Michael's own composition, Untitled Dream.

A detailed program will be available at the Conference Dinner.
Monday, October 9, 2006
Performance will start at 9 pm

ABSTRACTS

Fifth International Conference
on the Ultrasonic Measurement and Imaging
of Tissue Elasticity©
Snowbird, Utah, USA
October 8–11, 2006

Session TUT: Tutorial: Imaging of Tissue Elasticity – Progress & Prospects of Basic & Clinical Science

Sunday, October 8 1:00P – 3:00P

122 **TISSUE VISCOELASTICITY: PAST AND FUTURE, UNEXPLORED AREAS AND BRAVE PROJECTIONS.**

Armen Sarvazyan[1]*.
[1]Artann Laboratories, 1459 Lower Ferry Rd., Trenton, NJ 08618, USA.

Since most of the participants of this Conference are active researchers in the tissue elasticity field and are closely familiar with the main concepts and applications of viscoelasticity, this tutorial will provide just a brief overview of the subject and will focus mainly on the least–known aspects of the problem. Whenever possible, preference will be given to posing questions rather than to discussing well established facts.

Starting with a brief historical introduction to tissue viscoelasticity assessment, the relationships of the main mechanical parameters of tissue, such as shear elasticity, dynamic viscosity, creep and anisotropy, to tissue structural characteristics on the molecular, cellular and supracellular levels will be discussed.

Until recently, biomechanical assessment of tissue conditions was largely based only on the evaluation of relative changes in the modulus of elasticity. The main target of ultrasound and MRI elasticity imaging techniques has been to visualize variations in tissue hardness using different means of inducing tissue strain, such as by remote loading with transient acoustic radiation force or by various types of surface loading. Another technique for elasticity visualization is stress imaging which mimics manual palpation and utilizes measurement of the stress pattern on the surface of the compressed tissue. Temporal and spatial changes in the stress pattern while moving the pressure sensor array over the examined tissue provide information on the mechanical properties and the structure of the examined tissue.

Viscosity of tissues became the subject of active interest of researchers only in last few years. Now it is known that the range of variation of tissue viscosity can be comparable to or even greater than that of elasticity and that quantitative assessment of viscosity may serve as a means for differentiating tissue conditions. The literature data on tissue viscosity are very scarce despite great diagnostic information value of this parameter. Real–time assessment of viscosity of skeletal muscle and cardiac tissue may dramatically improve diagnostics and monitoring of great number of diseases. Viscosity of skeletal muscle, which is the largest amount of tissue in the human body (about 40% of the body mass), is closely related to a fundamental physiological function of muscle: dissipation of mechanical energy of external impacts to absorb mechanical shock. This fundamental function of skeletal muscle, to the best of our knowledge, was overlooked by physiologists and biomechanics researchers. The ability of muscle to redistribute the energy of impact in time and space and unload skeletal joints is of key importance in physical activities, such as running, playing basketball and soccer, jumping and wrestling. It appeared that the viscosity of the skeletal muscle is a variable parameter which can be voluntarily controlled by changing the tension of the isometrically contracted muscle. We will present a hypothesis on a highly efficient molecular mechanism of muscle–controlled viscosity created by biological evolution for absorbing and dissipating mechanical impacts.

The presentation will conclude with an overview of several novel areas of application of tissue viscoelasticity assessment in biomedical and clinical fields.

124 **IMAGING OF TISSUE ELASTICITY: WILL IT BECOME AN IMPORTANT CLINICAL TOOL?**

Brian S. Garra[1].*
[1]University of Vermont College of Medicine & Fletcher Allen Health Care, Burlington, VT, USA.

The estimation of tissue stiffness by palpation is one of the key methods traditionally used by physicians to diagnose disease. A mass or nodule only becomes palpable if its hardness is greater or lesser than the surrounding tissue. In addition, the subjective estimation of organ firmness is a critical part of the physical diagnosis of many organs including the liver, spleen, thyroid gland and even the eye. Given the importance of tissue elasticity estimation in physical diagnosis, it is almost surprising that imaging of this important parameter is just emerging as a usable clinical tool. Beginning with the description of ultrasound elasticity imaging (elastography) in the early 1990's, research has resulted in improved image quality, real time imaging and novel methods of performing elasticity imaging on organs and structures not readily accessible to direct mechanical manipulation.

Recently, other mechanical parameters such as stiffness nonlinearity, viscosity, Poisson's ratio and its time course have been imaged or estimated. These parameters may contain additional diagnostically useful information.

Currently, the major modalities used for elasticity imaging are ultrasound and magnetic resonance imaging. Each has advantages and disadvantages and, though ultrasound elasticity imaging emerged first and is the most common method, MRI techniques are improving rapidly and could surpass ultrasound methods in several areas of the body.

The potential applications for elasticity imaging that have shown promise so far are:

1 Detection and characterization of superficial and deep soft tissue masses including breast cancer, thyroid nodules, lymph nodes, prostate cancer and other masses.
2 Quantitative and semi–quantitative estimation of changes in organ stiffness due to disease such as hepatic cirrhosis, uterine softening during pregnancy, renal disease and thyroiditis.
3 Vascular studies: Evaluation of atheromatous plaque and wall stiffness in arteries and evaluation of thrombosis in veins.
4 Estimation of effective treatment volume during ablation therapy including RF ablation, ethanol ablation and cryoablation.
5 Monitoring tissue fluid translocation in disease processes such as lymphedema.

With several manufacturers already producing or ready to produce working clinical elasticity imaging instruments, we should be seeing a surge in clinical trials further testing some of the potential applications above. Clinical applications from among those above should soon follow. Some of the reasons for delays in implementing clinical applications and new clinical trials will be discussed.

MRI and US elasticity imaging will likely become important diagnostic tools, not replacing other methods that look at other features of disease, but complimenting them. This will improve both diagnostic accuracy and our ability to effectively monitor new ablative therapies.

002 **A NOVEL STRAIN FORMATION ALGORITHM FOR ULTRASONIC STRAIN IMAGING.**

J Jiang[1], TJ Hall[1] and AM Sommer[1].*
[1]Medical Physics Department, University of Wisconsin–Madison, Madison, WI, USA.

Background and Aims: Ultrasonic strain imaging systems are gaining rapid attention for breast tumor differentiation [1,2], despite the fact that consistently obtaining long sequences of high quality *in vivo* strain images is still a persistent challenge. Freehand scanning often induces non–uniform deformation and variations in strain image quality. To improve image quality of such systems, much effort has been devoted to developing more sophisticated motion tracking algorithms. This study takes an alternate route and investigates a new strain formation scheme for improving *in vivo* strain image quality by utilizing a displacement quality metric (DQM) method [3] in pairing frames of echo data for strain image formation. This new strain image formation method is a retrospective processing technique and is not restricted to a particular motion tracking algorithm. A block–matching algorithm [4] was used for our convenience.

Methods: To obtain a strain image using this method, three radio–frequency (RF) echo frames are automatically selected from RF data captured online and stored in memory as a sequence. Those data are used to generate two parent strain images located in the same physical grid from which a high quality composite strain image may be calculated by averaging. This approach allows averaging the two parent strain images (that reside in the same physical grid) to obtain higher quality strain images without the penalty of reduction in spatial resolution. This image formation strategy was tested with three approaches to pairing RF echo frames for displacement estimation (pairing consecutive RF frames, pairing to achieve a specified frame–average strain [2,5] and pairing to achieve the best possible DQM values [3]). The DQM is the product of the cross correlations among the two pairs of motion–compensated RF echo fields (a measure of motion tracking accuracy) and the cross correlation among the parent strain images (a measure of strain image consistency) [3]. RF echo data acquired from a Siemens Elegra with freehand scanning of *in vivo* breast tissue [2] were used to validate this method.

Results: Through processing of *in vivo* breast tissue data (>10 data sets with different types of lesions and roughly 1000 RF echo frames in total), our findings demonstrated that higher quality strain images can be obtained through pairing to achieve the maximum DQM. For instance, in one fibroadenoma data, the average DQM using this method (0.57 ± 0.15) was significantly improved, compared to pairing bases on a targeted frame–average strain (0.33 ± 0.25) and pairing adjacent frames [0.43 ± 0.19], while reducing the quality fluctuation (lower standard deviation) in a sequence of estimated strain images. Among all data investigated, the proposed three–frame strain formation method outperformed the two–frame method typically used, and pairing to achieve the maximum DQM provides the highest quality strain images with both techniques.

Conclusions: A new offline strain formation algorithm is presented here, and our results show that this method can obtain high quality strain images more consistently, thereby enhancing diagnostic confidence using ultrasonic strain imaging.

Acknowledgements: This work is supported in part by grants from NIH–R01CA100373 and the University of Wisconsin–Madison.

References:

[1] B. S. Garra, E. I. Céspedes, J. Ophir, S. R. Spratt, R. A. Zuurbier, C. M. Magnant, and M. F. Pennanen, "Elastography of breast lesions: initial clinical results," *Radiology*, vol. 202, pp. 79–86, 1997.
[2] T. J. Hall, Y. Zhu, and C. S. Spalding, "*In vivo* realtime freehand palpation imaging," *Ultrasound in Medicine & Biology*, vol. 29, pp. 427–35, 2003.
[3] J. Jiang, T. J. Hall, and A. M. Sommer, "A novel performance descriptor for ultrasonic strain imaging: A preliminary study," *IEEE Trans. on UFFC*, vol. 53, pp. 1088–1102, 2006.
[4] Y. Zhu and T. J. Hall, "A modified block matching method for real-time freehand strain imaging," *Ultrasonic Imaging*, vol. 24, pp. 161–76, 2002.
[5] M. A. Lubinski, S. Y. Emelianov, and M. O'Donnell, "Adaptive strain estimation using retrospective processing," *IEEE Trans. on UFFC*, vol. 46, pp. 97–107, 1999.

007 **TOWARDS NON INVASIVE VISCO–ELASTIC VESSEL WALL MECHANICAL CHARACTERIZATION USING ULTRASOUND MEASUREMENTS.**

S. Balocco[1,3], C. Cachard[1], G. Courbebaisse[2], E. Boni[3], E. Brusseau[2], P. Tortoli[3], O. Basset[2].*
[1]CREATIS, Université Claude Bernard Lyon 1, CNRS UMR 5515, INSERM U630, Lyon, FRANCE; [2]CREATIS, INSA Lyon, CNRS UMR 5515 INSERM U630, Lyon, FRANCE; [3]Microelectronic Systems Design Laboratory, Università di Firenze, Firenze, ITALY.

Background: The inflammation of the arterial wall is characterized by changes in its elasticity. This phenomenon often leads to the development of atherosclerotic plaques in vessels. The constant monitoring of mechanical vessel properties could help physicians to classify patient illness, but reaching this goal non–invasively is difficult.

Aims: This work presents an approach which allows quantifying the mechanical properties of vessel wall tissues using ultrasound Doppler measurements.

Methods: Blood flow induces hydrostatic radial pressure on the inner surface of the vessels. Experimental tests on human arteries have shown that applied radial pressure and wall displacements are out of phase. The simple Hooke law is not suited to describe the wall kinematics. Biological tissues must be considered as a viscoelastic medium because of the time–dependent response. The "Zener" mechanical model of a membrane (thin viscoelastic plate) has thus been considered. It is composed of two parallel branches, one with a single spring and the other with a spring and a damper. The model is characterized by three parameters: the Young modulus, E, representing the elasticity of the system, the μ coefficient, that can be interpreted as the relative stiffness (viscosity) of the damper, and the τ constant, corresponding to the relaxation time. For a given structural geometry, the finite element simulator based on these three parameters can describe the dynamic behavior of the wall and blood in a vessel.

This approach can be exploited to solve the inverse problem, i.e. to show that it is possible to estimate the tissue viscoelastic properties from the simultaneous measurement (based on, e.g., ultrasound dual–beam Doppler methods) of vessel hydrostatic pressure and wall displacements. The stress waveform is considered as the input of our model and the time varying wall displacement represents the output. The transfer function of the system depends on the three aforementioned mechanical parameters. An identification technique based on an autoregressive moving average (ARMA) curve fitting approach is used to estimate the optimal set for such parameters.

Results: The feasibility of this approach has been validated from simulated reference data: the input pressure and the system, defined by a set of parameters, are established and the resulting output is provided by the finite element tool. From the simulated stress and strain (input and output), the parameters of the system transfer function are deduced and compared to the reference set of parameters. This current test has shown that the parameters of the model (E, μ, τ) can be estimated with a relative error of about 4%.

Conclusions: In this work, a promising non invasive approach for the evaluation of vessel wall properties is presented. However, the feasibility has been shown on simulated data corresponding to a simple single layer cylindrical phantom. Future work will be oriented to a multi–layer structure, involving fluid-structure interaction.

** indicates Presenter*

008 **ROTATIONAL TISSUE MOTION QUANTIFICATION IN IVUS WITH OPTICAL FLOW.**

Mikhail G. Danilouchkine[1], Frits Mastik[1], Anton F.W. van der Steen[1,2].*
[1]Erasmus Medical Center, Rotterdam, The NETHERLANDS; [2]Interuniversity Cardiology Institute of the Netherlands, Utrecht, The NETHERLANDS.

Background: Semi–invasive characterization of atherosclerotic plaque vulnerability in coronary arteries plays an important role in preventing cardiac events. High strain regions along the vessel wall give a clear indication of the rupture–prone locations and can be identified by means of Intravascular (IVUS) palpography. The latter quantifies the strain profile by cross–correlating the radio–frequency signals at different systemic pressures. However, inter–frame misalignment due to IVUS catheter rotation gives rise to strain errors.

Aims: This study reports a novel algorithm for the quantitative assessment of apparent tissue motion in two consecutive frames due to the rotation of the catheter in IVUS images.

Methods: The optical flow (OF) algorithm computes a vector field that characterizes inter–frame tissue displacement. It was specifically adapted for ultrasonic speckle with rich edge– and corner–like image features. A novel weighting scheme assigns heavier weights to the reliably traceable edges and corners, while the regions with the homogeneous intensity level are assumed to have lesser contributions to the OF solution. Additionally, the scale–space representation of the OF equations was derived for the affine model of tissue. It allows noise suppression and more robust responses of the employed differential operators. The abovementioned modifications gave rise to enhanced performance of the algorithm.

The algorithm's accuracy and robustness were demonstrated on a tissue–mimicking phantom, subjected to a controlled amount of simulated rotation. Knowing the catheter's rotation angle, the true motion vectors were computed. The relative magnitude error has been employed. It was equal to the absolute magnitude difference between the true and OF displacement vectors divided over the magnitude of the true displacement expressed as a percentage. The relative magnitude error was computed for each point and subsequently averaged over the outlined vessel wall.

Results: Figure 1A shows the computed OF field, overlaid on the IVUS image. The non-uniformity of the vector field orientation and magnitude correctly suggests the counterclockwise rotation of the phantom around the center of the catheter. Figure 2 summarizes the dependency between the average relative magnitude error and the catheter's rotation.

Conclusions: The results of the validation on the tissue–mimicking phantom demonstrated robust, encouraging performance for the catheter rotation up to 3.5°. The relative magnitude error remains stable at the level of 1.9%. The accuracy of the predicted tissue displacements with OF quickly deteriorates for the higher degrees of catheter rotation.

Acknowledgements: This research was funded by Dutch Foundation for Technical Sciences (STW) and Volcano Therapeutics Inc. (Rancho Cordova, CA, USA).

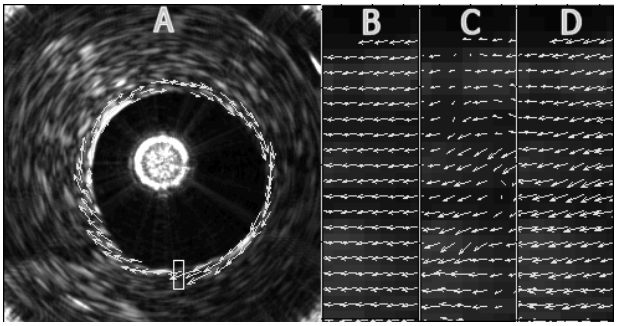

Figure 1: (A) The optical flow field describing the counterclockwise rotational displacement of the catheter in the tissue–mimicking phantom (the enlarged sparse vector field is displayed for the clarity of presentation). The white rectangle indicates the region of magnification. (B) The true rotational displacement of the tissue; (C) the optical flow field computed with the uniform and (D) feature–based weighting schemes.

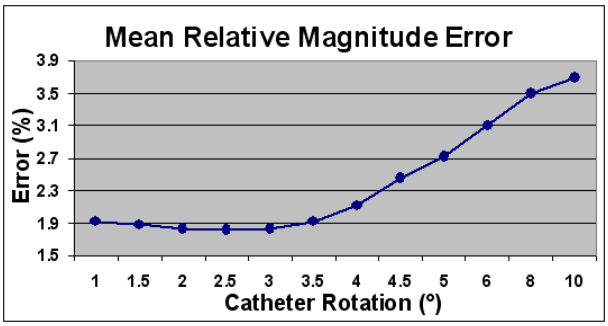

Figure 2: The results of the quantitative assessment of tissue motion tracking with the optical flow algorithm depending on amount of catheter rotation (horizontal axis) in terms of the mean relative magnitude errors (vertical axis).

010 **INCREASING THE ACCURACY OF MCSPGM, MAM and MDM DISPLACEMENT VECTOR ESTIMATION METHODS.**

Chikayoshi Sumi[1], Toshitaka Noro[1], Tomonori Ebisawa[1] and Takashi Tooyama[1].*
[1]Sophia University, 7-1, Kioicho, Chiyodaku, Tokyo, JAPAN.

Background: We have reported three methods of measuring a multidimensional displacement vector, i.e., the multidimensional autocorrelation method (MAM); multidimensional Doppler method (MDM) [1]; multidimensional cross–spectrum phase gradient method (MCSPGM) [2]. All the multidimensional methods realize more accurate measurements of tissue axial displacement/axial strain as well as tissue vector motion/strain tensor than their corresponding 1D methods. This indicates that the use of these multidimensional methods together with our previously proposed lateral Gaussian envelope cosine modulation method (LGECMM) [1] or multidimensional synthetic aperture method (MDSAM) [3] realizes accurate vector measurement. Last year, by using actual data, we also reported the effectiveness of regularization on stabilizing the MCSPGM together with a shear modulus reconstruction method [4]. The regularization parameters were set at each position using the local correlation value, echo SNR, or variances of displacements or strains obtained by the estimation [4] or measurement [5].

Aims: For the displacement vector measurement, we report the following: (1) *MDSAM:* The suitable directions of synthesizing the beams for obtaining an accurate displacement vector. (2) *LGECMM:* For our tissue shear modulus reconstruction, the modulation frequency is significantly increased compared with that observed in the reported application of the lateral modulation to blood flow measurement. Thus, a conventional spherical focusing is introduced instead of axicon focusing. Moreover, because the designed lateral modulation frequency and lateral bandwidth cannot be realized due to the inappropriateness of the Fraunhofer's approximation, we introduce the compensation parameters [1]. We also try to use the Hanning functions instead of Gaussian functions in the apodization function. (3) *Regularization:* We investigate the effectiveness of the regularization on the convergence speed of the iterative phase matching. The regularization is properly performed at each position for the respective displacement components. The measurement results are also shown for MAM and MDM (phantom experiments).

Methods and Results: (1) *MDSAM:* The measurement accuracies of the displacement components are evaluated in a geometrical sense. For instance, in 2D measurement, the region of measurement error of the displacement vector has a diamond shape. When the angle between the synthesized two beams is θ and the measurement error of the displacements is $\pm a/2$, the area is $a2/\sin\theta$ regardless the directions of the two beams. The error region rotates by the simultaneous rotation of the two beams without changing the area. When $\theta = \pi/2$ [rad], the area becomes the smallest, i.e., a2 (the error region: a square). The directional error of the beamforming can also be evaluated. (2) *LGECMM:* We calculate the point spread function (PSF) and spectra using Field II. For both spherical and axicon focusing, the bandwidths for all the depths become narrower than the designed ones, particularly by axicon focusing. The position of the center of PSF also differs from the designed focus depth, particularly for a large focus depth, although, for spherical focusing, the position slightly differs from the designed depth. Moreover, for all the depths, the bandwidth compensation was effective only for spherical focusing. Furthermore, the modulation frequencies for all the depths became lower than the designed ones. The compensation of the lateral modulation frequency was also effective, although this compensation made the bandwidth narrower. Use of the Hanning functions enabled the decrease of the effective aperture size without resulting in ringing. (3) The regularization was effective for stably measuring a displacement vector distribution, particularly, a lateral displacement distribution. The regularization enabled the decrease of the required number of phase matchings. The measured lateral strains using MAM were shown in Figure 1a-1c (agar phantom including a stiff cylindrical inclusion; results of MDM omitted). Only the lateral displacement was regularized (Figure 1b). Compared with the result obtained using the low pass filtering (Figure 1c), the result was effectively stabilized.

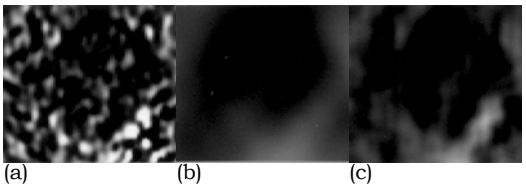

(a) (b) (c)

Figure 1: Lateral strains.
(a) MAM. (b) Regularized MAM.
(c) Low-pass filtered.

Conclusions: The MDSAM, LGECMM and regularization were effective for MCSPGM, MAM and MDM.

References:

[1] C. Sumi, Proc. of IEEE International Ultrasonics Symposium (CD-ROM), pp. 1771-1776, 2005.
[2] C. Sumi, IEEE Trans. on UFFC, vol. 46, pp. 158-166, 1999.
[3] C. Sumi, IEEE Trans. on UFFC, vol. 52, pp. 1670-1689, 2005.
[4] C. Sumi, Proc. of The 4th Intl. Conf. on the Ultrason. Meas. and Imag. of Tissue Elasticity, p. 114, 2005.
[5] C. Sumi et al., Proc. of the 2000 Spring Meeting of the Acoustical Society of Japan, pp. 1085-1086, March 2000.

* *indicates Presenter*

014 **A MULTISCALE VARIATIONAL OPTICAL FLOW METHOD TO ESTIMATE DISCONTINUOUS MOTION FIELDS FOR ULTRASOUND ELASTOGRAPHY.**

D Sosa–Cabrera[1], J González–Fernández[1], CA Castaño–Moraga[2], L Gómez–Déniz[1], L Alvarez-Leon[2], J Ruiz–Alzola[1,3].*

[1]CTM Center for Technology in Medicine, Signals and Communications Dept.; [2]AMI Análisis Matemático de Imágenes Research Group, Computer Science Dept., University of Las Palmas de Gran Canaria, Canary Islands, SPAIN; [3]Canary Islands Institute of Technology, Canary Islands, SPAIN.

Introduction: Different approaches have been developed to estimate and image the elastic properties of tissue. In ultrasound elastography, the estimation of the displacement and strain fields is mostly based on measurements performed on the RF signals (time–domain cross–correlation, among others). Pellot-Barakat et al. [1] have proposed a multi–scale optical flow method where the estimation of regularized displacement fields is obtained from two consecutive B–mode images. Following this idea, we propose a multi–scale variational method to estimate the displacement field, but our method uses a regularization term that allows preservation of discontinuities in the flow. We are able to obtain a better estimation on the boundaries of the inclusions in the tissue with our method.

Methods: A tissue–mimicking phantom was modeled as a 10x10x5 cm region containing a centered 10mm cylindrical inclusion three times stiffer than the surrounding material, and its elastic behavior was simulated using COMSOL Multiphysics 3.2 software. Synthetic pre– and post–compression (1%) B-mode images were computer generated using FIELD II [3] ultrasound simulator. Afterward, the algorithm was tested with a commercial CIRS breast elastography phantom, applying a 2% freehand compression. To estimate the flow, we used a variational method which consists of the minimization of an energy function that is constrained by echo amplitude conservation and neighborhood smoothness of the displacement vector field, but allowed discontinuities in such flow. To speed up the algorithm and to avoid spurious local minima, we used a pyramidal approach from coarse to fine scale. Concerning the implementation, we used a robust and efficient semi–implicit numerical scheme to solve the equation.

Results and Discussion: Results are presented in Figure 1. As it can be seen, we obtained the expected displacement fields. In the synthetic experiment (shown on the left), the elastogram reveals the modeled inclusion and the high strain areas around it. In the elastogram of the commercial phantom (shown on the right), we appreciate two isoechoic inclusions, a bigger one visible in the B–mode, and a smaller one that can hardly be seen without the elastogram. Although other researchers have used optical flow methods for elastography, as far as we know, isoechoic inclusions had not been detected using this method. Ongoing research includes clinical validation and comparison with other displacement estimation methods in elastography.

Acknowledgement: Supported by: USIMAG grant (TEC2004–06647–C03–02) from the Spanish Government, SIMILAR Network of Excellence (FP6–507609) from the CEE and the FLUID Specific Targeted Research project (No 513633) from the CEE.

References:

[1] C. Pellot–Barakat, F. Frouin, M. F. Insana, A. Helrment: Ultrasound elastography based on multiscale estimations of regularized displacement fields, IEEE Trans. Med. Imag. 23(2), pp 153–163, 2004.

[2] L. Alvarez J. Weickert and J. Sánchez "Reliable Estimation of Dense Optical Flow Fields with Large Displacements", International Journal of Computer Vision, 39(1), pp. 41–56, 2000.

[3] J. A. Jensen. Field: A program for simulating ultrasound systems. Med. Biol. Eng. Comp., 10th Nordic-Baltic Conference on Biomedical Imaging, Vol. 4, Supplement 1, Part 1:351–353, 1996b. http://www.es.oersted.dtu.dk/staff/jaj/field/.

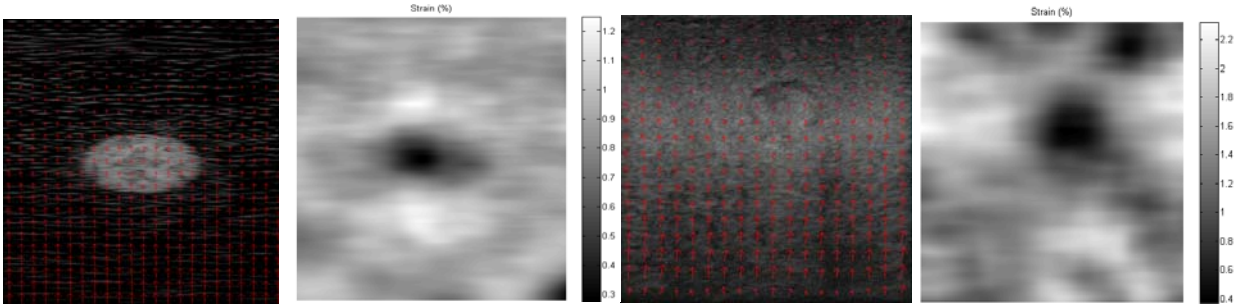

Figure 1: Displacement Field superposed to the sonogram and the corresponding axial strain elastogram for the synthetic experiment (left) and the commercial phantom experiment (right).

016 **DEVELOPMENT OF A ROBUST ALGORITHM FOR IMAGING COMPLEX TISSUE ELASTICITY.**

Yong Zhang[1], Robert W. Kramer[1], Dmitry B. Goldgof[2], Vasant Manohar[2].*
[1]Youngstown State University, Meshell Hall, One University Plaza, Youngstown, OH, 44555, USA;
[2]University of South Florida, ENB 118, 4202 East Fowler Avenue, Tampa, FL, 33620, USA.

Background: Imaging elastic properties of soft tissue is an emerging technology that holds great promise in medical diagnosis [1]. Two steps are usually involved: (1) A dynamic or static displacement field is obtained from any one of various imaging modalities; (2) Desired parameters such as Young's modulus or Poisson's ratio are then estimated by minimizing the discrepancy between the measured data and the outputs of a forward model. This type of inverse problem is likely nonlinear and ill–posed. Iterative gradient descent methods with regularization are often employed to obtain a stable solution [2,3,4].

Aims: Gradient–based methods are sensitive to initial conditions and local minima. We present a generic algorithm that is constrained by prior knowledge to ensure a good solution from noisy data. The aim is to develop a robust recovery algorithm that can handle more complex elasticity distributions.

Methods: To link a 2D–3D finite element model to a 1D chromosome in a genetic pool, a one–to–one mapping scheme is devised to encode elasticity. In this way, a direct correspondence is established between finite elements and genes. Rank tables are used to implement a penalty term that represents prior knowledge (equivalent to the smoothness constraint in a Tikhonov functional). The rank–based approach allows less quantitative information to be incorporated into the regularization process. A Gaussian mutation operator with a relatively high mutation rate helps maintain solution diversity. A one-point crossover operator is used to generate children from parents that are selected randomly by a K-2 tournament procedure. Best solutions are kept through generations by the elitism mechanism.

Results: A finite element model is used to simulate deformation of a square–shaped soft tissue model (Figure 1). The model has a dimension of 6 by 6 cm^2 that is discretized to a 300 by 300 quadrilateral mesh. Two hard inclusions are embedded in the model with Young's modulus values that are five and ten times higher than that of background tissues, respectively. The model has a Dirichlet boundary condition at the bottom and is compressed from the top by a specified Neumann condition. Displacement data were generated by running a forward model and then was altered by 1% additive white noise. In experiments with various initial conditions, both inclusions were successfully recovered with good resolutions, indicating the high potential of the proposed algorithm (Figure 2).

Conclusions: Results suggest that, given noisy data, a constrained generic algorithm is a robust solution strategy for ill–posed elasticity imaging problems. The stochastic nature allows the algorithm to avoid local solutions and hence be more effective in dealing with complex elasticity distributions.

Acknowledgements: This work is supported in part by URC Grant 2006–2007 #16–07, Youngstown State University, OH, USA.

References:

[1] J. Ophir, E. I. Cespedes, H. Ponnekanti, Y. Yazdi, and X. Li, "Elastography: a quantitative method for imaging the elasticity of biological tissues", Ultrasonic Imaging, vol. 13, pp. 111–134, 1991.
[2] F. Kallel and M. Bertrand "Tissue elasticity reconstruction using linear perturbation method", IEEE Trans. Medical Imaging, vol. 15, pp. 299–313, 1996.
[3] M. Doyley, P. Meaney, and J. Bamber, "Evaluation of an iterative reconstruction method for quantitative elastography", Phys. Med. Biol. vol. 45, pp. 1521–1540, 2000.
[4] Y. Zhu, T. J. Hall, and J. Jiang, "A finite–element approach for Young's modulus reconstruction", IEEE Trans. Medical Imaging, vol. 22, pp. 890–901, 2003.

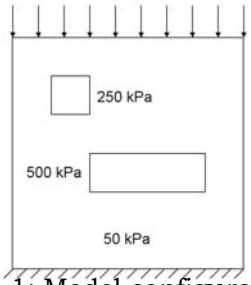

Figure 1: Model configuration with two hard inclusions.

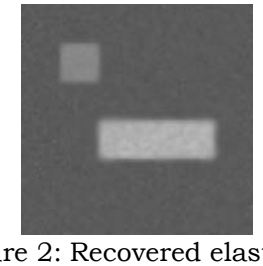
Figure 2: Recovered elasticity in grayscale image.

* *indicates Presenter*

019 **BENCHMARKING OF THE MECHANICAL PROPERTIES OF ENGINEERED TISSUE.**

Jörg Helfenstein[1], Edoardo Mazza[1].*
[1]ETH Zurich, Swiss Federal Institute of Technology, 8092 Zurich, SWITZERLAND.

Background: Intervertebral discs allow relative movement between adjacent vertebral bodies. The disc must withstand the forces and moments acting on it without being excessively squeezed nor damaged. The disc itself consists of an outer ring of collagen fiber reinforced material called the annulus fibrous and a soft central region called the nucleus pulposus. Collageneous plates build up the inferior and superior ends. Intervertebral disc damage (for example herniated discs), causes low–back pain. Mechanical characterization of intervertebral discs is useful for (1) understanding the reasons for disc failure (prevention), and (2) development of tissue replacements from *in vitro* cultured tissue samples. Of particular interest to persons in tissue engineering is how the application of mechanical loads during the culturing process influences the characteristics of the resulting tissue.

Aims: This presentation illustrates a research project on the mechanical behavior of intervertebral discs and corresponding tissue–engineered replacements. Whilst a great deal of attention has been placed on characterizing the biochemistry and composition of tissue–engineered constructs to reach target levels, the relationship of the composition to the macro–mechanical behavior is often not quantified. Recent experiments on articular cartilage showed their mechanical behavior to be nonlinear, time–dependent and charge–dependent. In this project novel structure–composition–function constitutive models will be developed and validated. Tissue–engineered constructs will be tested and evaluated with the model. In this manner the main contributors to the mechanical behavior can be identified and targeted during soft-tissue culturing.

Methods: Several experimental techniques for testing tissue engineered constructs are carried out and procedures for mechanical response characterization are validated. Standard measures as uniaxial compression is performed to obtain reference data for the global mechanical behavior of uncultured agar samples. Other techniques such as magnetic resonance elastography (MRE) for the determination of volumetric data will be applied. The macro–mechanical behavior of intervertebral discs is studied on an entire human lumbar spine. CT–scans are used to obtain original geometry data. Different constitutive models will be evaluated with comparison of experimental data and finite element (FE) simulations of the spine.

The intervertebral disc classification is performed in terms of structure (histology), composition (high-performance spectrophotometry), and mechanical behavior of the whole organ (macro) and individual components (micro). Using these data, novel constitutive models (based upon the composition of the intervertebral disc) will be developed and validated with respect to experimental data.

Results: Experimental results of mechanical tests on agar probes that are used in tissue culturing are presented. Experiments are performed using an aspiration experiment [1] and a torsional resonator device [2] in order to get reference data on the mechanical properties of the agar gel over a wide frequency range. Critical aspects for correct mechanical characterization are discussed.

References:

[1] Nava A., Mazza E., Kleinermann F., Avis N.J., McClure J., Bajka M., Technology and Health Care 12 (2004), 269-280.
[2] Valtorta, D., Mazza E., Medical Image Analysis 9 (2005), 481-490.

Figure 1: Agar probe under the torsional resonator device

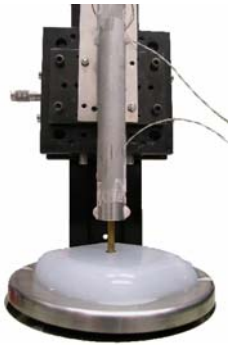

020 **PHANTOM EXPERIMENTS AND COMPUTER SIMULATIONS OF ELASTOGRAPHY FOR BREAST CANCER USING WATER BAG PRESSURE.**

Y Hayakawa[1], K Ishida[1], K Tsuji[1], H Doi[1], Y Amano[1], M Nakamura[2].*
[1]Toin University of Yokohama, 1614 Kuroganecho, Aoba–ku, Yokohama, Kanagawa–ken, JAPAN;
[2]Yokohama General Hospital, 2201 Kuroganecho, Aoba–ku, Yokohama, Kanagawa–ken, JAPAN.

Background: Breast cancer has a larger elastic modulus as compared to mammary gland tissue and benign lesions [1]. Thus, the measurement of the elastic modulus *in vivo* seems to enable differentiation of cancer and benign tissue. By compressing the breast with an ultrasound transducer, strains in lesions can be measured [2,3]. The information obtained, however, is not the elastic modulus as the stress is not known. In this study, a phantom was made of 10 weight percent gelatin with a thickness of 40mm, in which a Plexiglas cylinder with a diameter of 10 mm, mimicking a cancer, was placed at a depth of 10mm or 20mm from each surface. Phantoms were then placed on the desk and pressed by a balloon filled with water. The height of the vessel of water connected to the balloon was adjusted to change the pressure in the balloon. Deformation in the phantom was detected by the ultrasound echo technique, using an ultrasound frequency of 11MHz. The gelatin phantom (density of 1.03) was deformed around the Plexiglas cylinder by water pressure of 1.1 to 2.4 kPa. The experiment was simulated by computer using a Finite Element Method (ANSYS 9.0) to confirm the experimental findings. The elastic modulus of the gelatin phantom was compared to computer simulation assuming the Poisson's ratio of gelatin of 0.49 and/or 0.45 to give the elastic modulus of gelatin to be 6 kPa to 9 kPa The dispersion of elastic modulus seems to be due to the stretching force in the rubber material of the water filled balloon.

Aims: Compression by static water pressure gives a simpler stress distribution compared to compression with a planar transducer. Measurement of the elastic modulus by this method is under development in our laboratories. Basic experiments were performed by compressing breast cancer phantoms with a water bag and computer simulation by Finite Element Method is under development for future experiments.

Methods: The numerical phantom is 80 mm in width and 40 mm in height. The main structure of the phantom is fat in which a circular mammary gland (10 mm diameter) and cancer (10mm diameter) are situated. In one phantom, the center of the circular mammary gland tissues is 15 mm (Figure 1a) from the upper surface, and in another 25 mm (Figure 1b).

Results: The results are shown in Figure 1a & b, where the elliptical deformation of the mammary gland is evident. The height–to–width ratio of the mammary gland and cancer was nearly independent of tissue depth.

Conclusions: Present results show the feasibility of using a water bag to compress the sample. The effect of the balloon rubber tension should be avoided by employing softer materials. The height–to–width ratio of the mammary gland and cancer was nearly independent of tissue depth in the computer simulation also.

References:

[1] Krouskop TA, Wheeler TM, Kallel K, et al., (1998) Ultrasonic Imaging 26, 260-274.
[2] Ophir J, Cespedes I, Ponnekanti H, et al., (1991) Ultrasonic Imaging 13:111-13.
[3] Yamakawa M, Shiina T, et al., (2001) Jpn. J. Appl. Phys. 40:3872-3876.

(a) 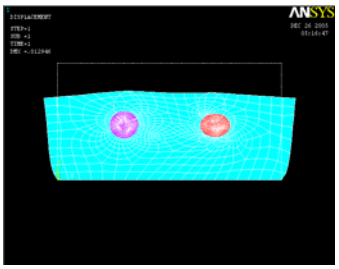

(b) 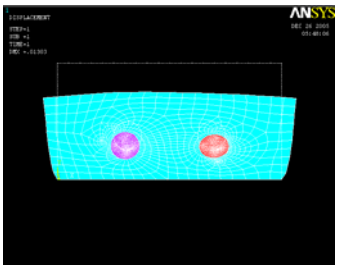

Figure 1: Results of computer simulation experiment. The size of numerical phantom (80 mm W x 40 mm H) of fat with elastic modulus of 18kPa was assumed [1]. Also assumed are circular mammary gland of the diameter of 10 mm (on the left side of the figures) with elastic modulus of 28 kPa and cancer of the diameter of 10mm (in the right) with elastic modulus of 106 kPa inside the fat. The assumed water pressure is 5 kPa. Poisson's ratio was assumed to be between 0.49 and 0.35 (in the above image it is 0.40). Elliptic deformation of mammary gland is evident, while that of cancer is not. In Figure 1(a), the depth of the centers of the circular lesions is 15 mm from the surface and in Figure 1(b), it is 25 mm. The height-to-width ratio of tissues was nearly independent of depth.

* *indicates Presenter*

023 **LOW–COST OPEN–SOURCE ELECTROCARDIOGRAPH FRONT–END FOR *IN–VIVO* TISSUE MOTION SYNCHRONIZATION.**

Javier González–Fernández[1], Luís Gómez–Déniz[1], Juan Ruiz–Alzola[2].*
[1]University of Las Palmas de Gran Canaria, CTM–Center for Technology in Medicine, Las Palmas de Gran Canaria, Canary Islands, SPAIN; [2]Canary Islands Institute of Technology, Canary Islands, SPAIN.

Background: Pulsation–induced tissue motion may be used as a convenient way of obtaining compressions in elastography [1]. Traditionally, such motion has been detected making use of Doppler related information from circulating blood in close proximity. However, at present real–time elastography makes use of computationally intensive algorithms and, hence, the accrual of supplementary calculations might become totally unviable.

Aims: This motion can be frozen at particular frames of interest (at predefined pre– and post-compression states) with the addition of a simple electronic device, that monitors the heartbeat, connected to an ultrasound scanner, allowing user control of the acquisition process via an interruption–driven routine. In this manner, synchronization with tissue motion can be performed in hardware by an embedded DSP-enabled microcontroller, so as to lessen main CPU–cost and consequently not affecting other major real–time computations.

Methods: The complete system consists of a battery operated microcontroller–based heartbeat detector, which can be connected to a PC–based ultrasound scanner via a wireless, thus electrically isolated, link to provide communications for setup and results retrieval. Heartbeats are monitored across the chest using three simple electrodes. The electronic equipment is comprised of a commercially available instrumentation amplifier and associated analog circuitry. The band–limited and amplified signal is then fed to a 10–bit A/D converter which samples the signal at 500 Hz. Additional digital band–pass filtering is used to attenuate noise outside the ECG spectrum and remove DC voltage. Analog filtering is also critical in removing interference from other physiological processes and 50–60 Hz mains noise. The block diagram for the signal processing path is shown in Figure 1. The system can operate whether outputting the entire waveform to the main computer for display or examination, or signaling a precise pre-configurable instant of cardiac cycle, characteristically the QRS complexes. The latter is achieved by careful analysis of the ECG waveform with the aid of real–time detection methods described in [2,3]. Communication latency can be taken into account and corrected in advance.

Results and Conclusions: Timing accuracy and detection reliability of the system was initially tested with synthetically generated ECG signals corrupted with random noise (Figure 2). Afterwards, real physiologic test signals [4] were input, in accordance with ANSI standards. In both cases, successful and accurate results were obtained. Embedded firmware is open–source C–language and consists of easily modifiable operating algorithms. Interrupt–driven acquisition has been preliminarily tested on an Ultrasonix RP500 ultrasound scanner. Ongoing research will involve clinical validation for *in–vivo* abdominal and vascular elastography, and comparison with other tissue–motion detection methods.

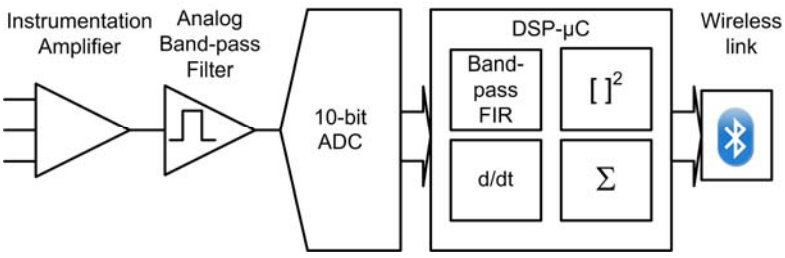

Figure 1: Functional block diagram

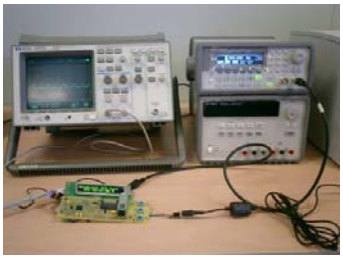

Figure 2: Prototype testing

Acknowledgements: This work has been supported by USIMAG grant (TEC2004-06647-C03-02/TCM) from the Spanish Government and SIMILAR Project FP6-507609.

References:

[1] Wilson, Robinson, Dadd: Elastography – The movement begins. Phys. Med. Biol. 45 (2000) 1409–1421.
[2] Pan J, Tompkins W: A Real-Time QRS Detection Algorithm. IEEE Transactions on Biomedical Engineering, Vol. BME–32, No.3, March 1985: 230–236.
[3] Köhler, Hennig, Orglmeister: The Principles of Software QRS Detection. IEEE Engineering In Medicine and Biology, Jan–Feb 2002: 42–57.
[4] PhysioBank Archive Index: Physiologic signal archives for biomedical research ECG Database. http://www.physionet.org/physiobank/database/#ecg

024 **RHEOLOGICAL MODELING OF THE TIME-DEPENDANT BEHAVIOR OF POROELASTIC MATERIALS UNDER CREEP TEST EXPERIMENTS.**

Jean Jacques Ammann[1], Ricardo Rivera[1], Jonathan Ophir[2].*
[1]Universidad de Santiago de Chile, Physics Department, Santiago, CHILE; [2]The University of Texas Health Science Center Houston Medical School, Houston, TX, USA.

Background: In addition to giving access to local elastic coefficients, elastography can be applied to evaluate the mechanical behavior of the specimen as a function of time, offering an additional characteristic set of viscoelastic parameters to locally determine the anelastic nature of the tissue. Creep test experiments have proved to be valuable for accessing the anelastic (or viscoelastic) behavior of poroelastic materials [1,2].

Aims: We present an experimental method for extracting local sets of elastic and viscous parameters by applying a continuous bimodal rheological model to the strain vs. time curves obtained from a series of time–dependent 1D elastograms.

Methods: The behavior of measured time–strain curves at constant depth, acquired during the application of a constant axial load at the specimen surface, is shown here to follow a continuous rheological model formed by an elastic element (E_{elast}) in series with a continuous Kelvin–Voigt element holding bimodal Gaussian distributions of the viscosity coefficient:

$$\varepsilon(t) = \frac{\sigma_0}{E_{Elast}} + \frac{\sigma_0}{E_{Anel}} \frac{1}{\eta_{máx} - \eta_{mín}} \int_{\eta_{mín}}^{\eta_{máx}} \left\{ G_{01}\, e^{-\frac{(\eta-\eta_{01})^2}{2\sigma_{01}^2}t} + G_{02}\, e^{-\frac{(\eta-\eta_{02})^2}{2\sigma_{02}^2}t} \right\} * \left(1 - e^{-tE_{Anel}/\eta}\right) d\eta \qquad \text{Equation 1}$$

The experiment consists in placing the specimen in a water immersion chamber above a 5.0 MHz broadband transducer mounted on the bottom wall with its acoustical axis oriented vertically. The load is applied on top of the specimen through a loading device composed of an acrylic disk larger than the specimen with mobility in the vertical direction only. The loading device is loaded with the corresponding weight and successive RF traces are acquired. The local displacement is extracted from the RF data through a running cross–correlation between each pair of the successive traces and the strain determined by applying the gradient operator to the integrated displacement (Figure 1). After processing, the viscoelastic parameters {E_{anel}, G_i, η_i and σ_i (i = 1,2)} are obtained through the fit of the strain vs. time curves, extracted at any specific location along the depth axis (Figure 2), according to Equation 1, by trial and error.

Results: As an illustration, the method is applied to a sample of soft white cheese of 50 mm diameter and 45 mm height with a weight of 200 g (σ_0= 100 Pa). RF traces (34) are acquired during approximately 30 minutes. Fits have been performed at three different depths yielding the values shown in the table. It is noticeable that, though required, the second Gaussian distribution (for long relaxation times) does not vary significantly through the set of real time/strain curves. However, the elastic modulus E_{anel} common to the Kelvin–Voigt cell distributions and the first Gaussian distribution parameters, corresponding to short relaxation times ($\tau = \eta/E$), are critical in characterizing the white cheese local anelastic behavior.

Depth [m]	E_{anel} [kPa]	G_1	η_1 [MPa s]	τ_1 [s]	σ_1 [MPa s]
0.020	20.0	48.2	-2.2	110	4.0
0.030	13.2	48.2	-2.4	181	4.0
0.035	8.5	15.7	-2.4	282	3.0
G_2=50, η_2=40MPa s, τ2=2000s, σ_2=15MPa s Uncertainty on all parameters: 5%.					

Conclusions: The method we propose here is able to yield a set of various parameter maps of the specimen including elastic and viscous coefficients for diagnostic/characterization purpose. It requires considerable signal processing and an acquisition time of several minutes to yield reliable values. It can be easily generalized to 2D or 3D images allowing for motion compensation.

Acknowledgements: This work is supported by Fondecyt project No. 1040206, Chile and Fondap project No. 11980002, Chile.

References:

[1] R. Righetti, J. Ophir, and T. A. Krouskop, Ultrasound in Med. & Biol., Vol. 31, No. 6, pp. 803–816, 2005.
[2] J.J. Ammann, R. Rivera1, J. Ophir, Proc. of The Fourth International Conference on the Ultrasonic Measurement and Imaging of Tissue Elasticity, Lake Travis, Texas, USA, October 16–19, 2005, p. 54.

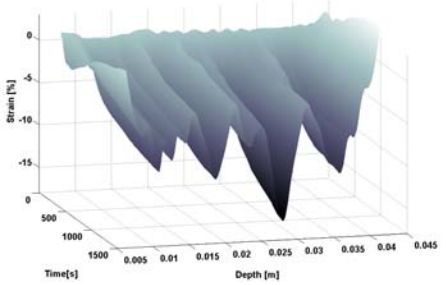

Figure 1: Strain Surface vs. Depth and Time.

Figure 2: Experimental strain vs. time curves (symbols) at three specific depths with corresponding simulation (continuous lines) through the Bimodal Rheological Model.

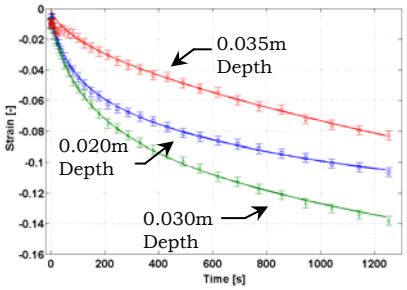

* *indicates Presenter*

039 **REFERENCE POSITION VS. CONTRAST–TO–NOISE RATIO (CNR) ON 1D SHEAR MODULUS RECONSTRUCTION OBTAINED BY STRAIN RATIO.**

Chikayoshi Sumi[1].*
[1]Sophia University, Tokyo, JAPAN.

Background: Last year, our previously developed three methods of 1D shear modulus reconstruction using strain (elongation or compression) ratio were reviewed [1], and the usefulness of the methods was summarized. The reconstructed shear modulus values of the stiff and soft inclusion are respectively improved by setting the references in the stress–concentrated regions or stress weak regions in front of and behind the inclusions. The effectiveness was confirmed in simulations [1] and phantom experiments [2] etc. Calculation of strain ratio provides a relative or absolute elastic modulus image that is more similar to the original elastic modulus image than the measured strain itself [2]. However, when evaluating strains at reference regions with a high spatial resolution, reconstruction often becomes laterally unstable [1]. To cope with this instability, reconstruction of the inverse of the shear modulus obtained by strain ratio is efficiently low–pass filtered rather than reconstruction of the shear modulus [1]. Otherwise, when using homogeneous region as reference such as block of reference material, fatty tissue, parenchyma, muscle, or skin etc., evaluation of strain at reference regions with a low spatial resolution is also effective (this yields a high spatial resolution reconstruction) [1].

Aims: In this study, we evaluate the position of the reference line in the stress–concentrated region vs. the detectability of the inclusion when using raw strain ratio, the 2D moving averaging of the reference strain and the 2D low-pass filtering of raw strain ratio.

Methods: For the noise–filled case (white noise was added to the displacement data) together with the no-noise-filled case, we evaluate the position of the reference line vs. our newly defined contrast-to-noise ratio (CNR) using the respective original shear moduli G_I and G_S (2.0 vs. 1.0 x 10^5 N/m^2) in a spherical inclusion (dia. = 10 mm at depth 25 mm) and surrounding region and the respectively calculated squared means of the reconstruction errors N_I^2 and N_S^2 with respect to G_I and G_S in the inclusion and surrounding region.

Results: The results are shown in Figures 1a and 1b for the two cases in which low and high cutoff frequencies of differential filter are respectively used, i.e., 0.33 and 0.54 mm^{-1}. As a result, the SNRs of the strains are respectively 63.9 and 39.9 dB. For all the reconstructions including the no–noise filled case, by setting the reference points in the stress–concentrated region, CNR is significantly improved.

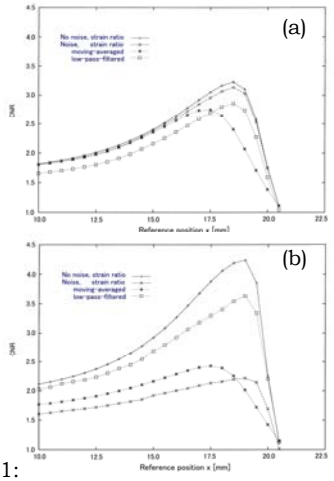

Figure 1:

This means that, the accuracy of the shear modulus reconstruction value of the inclusion is improved. However, as the reference line approaches the inclusion (the edge, x = 20 mm), all CNRs begin to decrease. In particular, the moving averages of the reference strain begin to decrease fast (from x = 17.5 mm) and for the high-SNR case, its CNR is lower than that of the raw strain ratio. That is, the accuracy of 1D reconstruction value des not become high because the strain that significantly varies at the stress-concentrated region is moving–averaged. Thus, the spatial resolution of the strains in the reference region cannot always be reduced. This also explains the superiority of the low–pass filtering of strain ratio in such a case in that a highly accurate reconstruction value of inhomogeneity can be obtained.

For the low–pass filtering of raw strain ratio (cutoff frequency, 0.25 mm^{-1}), for the low–SNR case, CNR is the highest, whereas for the high–SNR case, CNR is the lowest. However, although required practical plural low–pass filtering significantly decreases spatial resolution, the obtained accuracy of the reconstruction value of the inclusion is higher than that of the moving averaging of the reference strain when the reference strain significantly varies as described above (if not smoothed too much).

Conclusions: We confirmed that, when reducing artifacts of 1D shear modulus reconstruction, the utilization of low spatial resolution reference strain yields a low–accuracy reconstruction value of inhomogeneity. In contrast, in such a case the low–pass filtering of strain ratio yields a more accurate reconstruction value if not smoothed too much. Both the above mentioned stabilization methods should be properly used (i.e., switched on) in conventional ultrasonic equipment when considering the application of the reconstruction (i.e., in accordance with the measurement accuracy of strains and the occurrence of artifacts).

References:

[1] C. Sumi, "Real-time Reconstruction of Shear Modulus Distribution by Calculating Strain Ratio," *Proc. of 27th Ann. Int. Conf. of IEEE Eng. in Med. and Biol. Soc.* (CD-ROM), September 2005.
[2] Sumi, IEICE Trans. Fundamentals, E78-A, pp. 1655-1664, 1995.

043 **ASSESSMENT OF LIVER FIBROSIS AND PORTAL HYPERTENSION BY TRANSIENT ELASTOGRAPHY IN PATIENTS WITH CHRONIC LIVER DISEASE.**

Céline Fournier[1], Véronique Miette[1], Christophe Corpechot[2], Raoul Poupon[2], Jose A Carrion[3], Xavier Forns[3], Laurent Sandrin[1].*

[1]Echosens, Research and Development Department, 153 avenue d'Italie, 75013 Paris, FRANCE; [2]Service d'Hépatologie, Centre National de Référence des Maladies Inflammatoires du Foie et des Voies Biliaires, Hôpital Saint Antoine, Paris, FRANCE; [3]Liver Unit, Institut de Malalties Digestives, Hospital Clinic, Institut d'Investigacions Biomediques August Pi i Sunyer (IDIBAPS), Barcelona, SPAIN.

Background: The use of invasive procedures such as liver biopsy or hepatic vein pressure gradient (HVPG) measurement is required in the follow–up of patients suffering from liver disorders or biliary diseases. Those diseases usually result in the development of liver fibrosis which leads to an increase of liver stiffness. Fibroscan (Echosens, Paris, France) is an ultrasound–based transient elastography device [1] that quantifies liver stiffness in a noninvasive and rapid way by measuring the velocity of a low-frequency elastic shear wave which is induced by a vibrator. More than 100 devices are now routinely used and tested worldwide with numerous clinical indications.

Aims: We aim to evaluate liver stiffness measurement (LSM) carried out by transient elastography for the assessment of liver fibrosis [2] and portal hypertension [3] in patients with chronic liver disease.

Methods: LSMs were carried out with Fibroscan using a standard 3.5 MHz transducer. LSMs were compared to HVPG for the diagnosis of portal hypertension in chronic hepatitis C (HCV) transplanted patients and to histological results obtained from liver biopsy for the assessment of liver fibrosis in patients with biliary diseases. Statistical analysis was performed using the Receiver Operator Characteristics (ROC) curves. Performances were assessed using area under ROC (AUROC) curves.

124 liver–transplant patients with HCV were included in a comparison study between HVPG and LSM for the diagnosis of portal hypertension (HVPG > 6 mmHg) and the diagnosis of significant portal hypertension (HVPG > 10 mmHg). 129 paired HVPG and LSM were performed.

The comparison to liver biopsy in patients with biliary diseases was performed on 101 patients using the histological METAVIR scoring system: F0 no fibrosis, F1 fibrosis without septa, F2 few septa, F3 significant fibrosis, F4 cirrhosis.

Results: LSM and HVPG are strongly correlated (Pearson's coefficient = 0.84, $p < 0.001$). AUROC are respectively 0.93 for the diagnosis of portal hypertension and 0.94 for the diagnosis of significant portal hypertension. The optimal cutoff is 8.74 kPa for the diagnosis of portal hypertension.

Stiffness values ranged from 2.8 to 69.1 kPa in patients with biliary disease. LSMs were strongly correlated to histological stages (Spearman's coefficient = 0.84, $p < 0.0001$). AUROC are respectively 0.92, 0.94 and 0.97 for the diagnosis of patients with F2, F3 and F4 histological stages. Cutoffs are respectively 7.3 kPa, 9.8 kPa and 18.5 kPa.

Conclusions: Results with AUROC superior to 0.92 support that LSM with Fibroscan is a simple, accurate and reliable noninvasive means for the assessment of biliary fibrosis and for the diagnosis portal hypertension. This promising tool is an alternative to liver biopsy and HVPG measurements, especially in patients with bleeding tendency.

References:

[1] Sandrin L et al, Transient elastography: a new noninvasive method for assessment of hepatic fibrosis, Ultrasound in Medicine and Biology 2003;29(12):1705–1713.

[2] Corpechot C et al, Assessment of biliary fibrosis by transient elastography in patients with PBC and PSC, Hepatology 2006;43:1118–1124.

[3] Carrion JA et al, Transient elastography for diagnosis of advanced fibrosis and portal hypertension in patients with hepatitis C recurrence after liver transplantation, Liver Transplantation 2006, in press.

* *indicates Presenter*

044 **NEW COPOLYMER–IN–OIL PHANTOM MATERIALS FOR ELASTOGRAPHY.**

Jennifer Oudry[1], Véronique Miette[1], Laurent Sandrin[1].*
[1]Echosens, Research and Development Department, 153 avenue d'Italie, 75013 Paris, FRANCE.

Background: Phantoms that mimic properties of soft biological tissues are essential to elastic imaging investigation and to elastography device characterization. Several materials including agar/gelatin, PVA (polyvinyl alcohol) and polyacrylamide gel have been successfully used in the past to produce tissue phantoms as reported in the literature. However, it appears to be difficult to find a phantom material with a wide range of stiffness, good stability over time and high resistance to rupture.

Aims: We aim to develop and test new SEBS copolymer (Styrene–Ethylene/Butylene–Styrene) in oil phantom material for elastography.

Methods: Phantoms are made from a mixture of SEBS copolymer and oil plus additives for acoustical scattering (graphite or silica powder). The polymer and additives are dissolved stepwise in low–viscous oil at a temperature of 130–160°C. Once the polymer is totally dissolved and the blend is homogeneous, the resulting solution is cast in a container of desired shape and size and cooled at room temperature to gel formation. Stiffness measurements are performed using a Fibroscan (Echosens, Paris, France) with ultrasound–based transient elastography technique [1].

Results: Six homogeneous phantoms were produced with SEBS concentration ranging from 2.5 to 5.5% and 0.2% graphite for acoustical scattering. Stiffness ranges from 2.2 to 13kPa. As shown in Figure 1, increased concentration of SEBS copolymer produces greater stiffness. The stiffness of phantoms (Young's modulus E) is shown to be linearly proportional to the SEBS concentration. In addition, we observed that phantoms maintain their properties (shape, size, stiffness) over time when stored at room temperature. Stiffness measurements performed during a four–month period confirmed the stability of their acoustic and mechanical properties.

Conclusions: The results suggest that SEBS copolymer–in–oil is an attractive material for ultrasound-based elastography phantoms. Advantageous properties of this material are: ease of production, stability over time, non–toxicity, high resistance to rupture and large range of stiffness (Young's modulus). It is anticipated that SEBS copolymer–in–oil phantoms could be adapted to MR elastography.

References:

[1] Sandrin L, Tanter M, Gennisson JL, Catheline S, Fink M. Shear elasticity probe for soft tissues with 1–D transient elastography. IEEE UFFC 2002; 29 (4): 436–46.

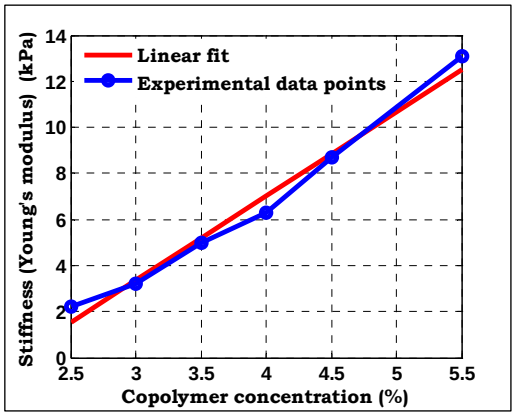

Figure 1: Copolymer–in–oil phantom stiffness as a function of the copolymer concentration.

055 **1D AND 2D STRAIN IMAGING WITH INTRAVASCULAR ULTRASOUND: AN *IN VIVO* STUDY.**

W Khaled[1], W. Bojara[2], M. Lindstaedt[2], A. Pesavento[3], A. Lorenz[3], H Ermert[1].*
[1]Institute of High Frequency Engineering, [2]Institute of Mechanics, Ruhr–University Bochum, Bochum, GERMANY; [3]LP–IT Innovative Technologies GmbH, Bochum, GERMANY.

Background: Coronary atherosclerosis is a common disease in industrialized countries. Acute coronary syndromes are associated with a high mortality rate. They are usually caused by a sudden occlusion of the coronary lumen due to rupture of unstable plaques in the vessel wall, often with less than 50% stenosis. Thus, plaque morphology does not give sufficient information for determining the risk of an acute syndrome. However, the mechanical properties of vulnerable coronary plaques were shown to be different from other plaque types. Therefore, intravascular ultrasound (IVUS) strain imaging can be an important imaging tool for risk assessment. The strain is measured by cross–correlating RF signals acquired at different systemic pressures [1]. However, catheter motion due to cardiac activity causes misalignment of these signals so that strain estimates can be obtained [2].

Aims: The aim of this work is to present a single non–rotating element to calculate 1D strain imaging with a very high frame rate and a rotating 2D strain imaging based on motion compensation using local block matching [3] with contour mapping and to compare both methods.

Methods: A Galaxy IVUS scanner (Boston Scientific, CA, USA) was used for *in vivo* experiments in the catheter lab. Single element rotating transducers (which can be stopped at different positions) with a center frequency of 40 MHz were used for the acquisitions. Analog RF data were sampled at 400 MHz with a 12 Bit A/D converter (DP310 Digitizer, Acqiris, Switzerland). Custom made hardware was used for triggering and signal amplification. The IVUS system has a built-in shielded RF output, which is a prerequisite for clinical use. *In vivo* imaging was performed and full frame RF data was recorded during IVUS examinations in the catheter lab. Simultaneously, the intracoronary pressure signal was recorded along with an electrocardiogram, digitized at 200 Hz and stored on a hard disk. Pressure guide wires were used for pressure measurements and evaluated with the Radi analyzer (Radi, Sweden). Pressure measurements were used to align the RF data of consecutive diastolic frames. For strain calculations only, frames in late diastole were considered, since in this part of the heart cycle, vessel motion and, thus, decorrelation effects are supposed to be minimal. When using the rotating catheter for 2D images, motion compensation methods based on block matching, mainly global rotation block matching and contour mapping, were used to estimate displacements of local tissue regions.

Figure 1:

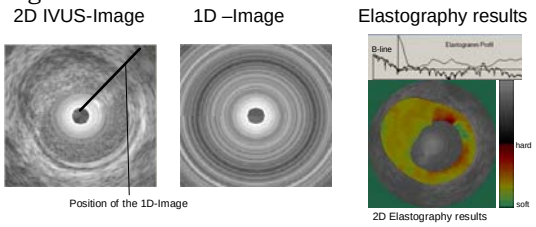

Results: The 1D strain imaging method was calculated and verified with the data calculated from the rotating transducer. The compensation methods were validated on 5 *in vitro* acquisitions and 10 *in vivo* pullback acquisitions. The proposed methods were compared with respect to the stability of the algorithms using phantom and ultrasound measurements.

Conclusions: Based on this comparison, an approach is introduced, which significantly increases the number of valid strain estimates in intravascular elastograms allowing the detection of vulnerable coronary plaques.

Acknowledgements: This work is a project of the Ruhr Center of Excellence for Medical Engineering (Kompetenzzentrum Medizintechnik Ruhr (KMR), Bochum, Germany). Supported by the Federal Ministry of Education and Research, No. 01 IR A 14 B and the Boston Scientific Corp. (Fremont, CA, USA).

References:

[1] Pesavento, A.; Perrey, C.; Kruger, M.; Ermert, H.: A time–efficient and accurate strain estimation concept for ultrasonic elastography using iterative phase zero estimation. IEEE Trans. UFFC. Vol. 46 (1999), pp. 1057–1067.
[2] Perrey, C., Ermert, H.: Correction of non–uniform rotational artefacts in intravascular ultrasound elastography. Biomedizinische Technik, Vol. 49 (2004, Suppl. 2, Pt. 2), pp. 870–871.
[3] D. Boukerroui, J. A. Noble, et al., Velocity Estimation in Ultrasound Images: A Block Matching Approach, Lecture Notes in Computer Science, 2003, pp. 586–598.

* *indicates Presenter*

062 **COMPUTING STRAIN ELASTOGRAMS OF SKIN USING AN OPTICAL FLOW BASED METHOD.**

Yong Zhang[1], John R. Sullins[1], Dmitry B. Goldgof[2], Vasant Manohar[2].*
[1]Youngstown State University, Meshell Hall, One University Plaza, Youngstown, OH, 44555, USA;
[2]University of South Florida, ENB 118, 4202 East Fowler Avenue, Tampa, FL, 33620, USA.

Background: Most elastography studies focus on detecting property anomalies of internal organs such as heart and kidney [1]. We report a preliminary work on computing strain elastograms of human skin. A camcorder was used to capture the deformation of skin surface in a video sequence, upon which tracking was performed with an optical flow method to generate a dense motion field [2]. A strain elastogram is then obtained by convolving the motion field with a gradient filter. Potential applications of the proposed method include skin cancer detection, burn scar assessment and facial surgery simulation [3].

Aims: There are situations where direct contact of imaging devices with patients is not a viable option. For example, skin evaluation of burn patients during the early healing stage. Our primary objective is to develop a practical method for computing skin elastograms with optical images acquired at a distance.

Methods: Using a Sony DCR-TRV camcorder, videos of deformed skin were acquired with a speed of 30 frames per second under normal lighting condition. Skin deformation was caused by manual stretching. The image resolution is 720 by 528 pixels. Displacements between two adjacent frames are in the range of 1-9 pixels. Each frame pair was pre-smoothed by a Laplacian operator with a window size of 3. To improve motion quality, a multi-resolution approach was used to solve the optical flow equation. Experiments indicate that four resolution levels are adequate to obtain an accurate and continuous motion field. Given the vertical and horizontal motions, strain elastograms (normal strain: $(\partial u/\partial x, \partial v/\partial y)$, shear strain: $0.5(\partial u/\partial x + \partial v/\partial y)$, and strain magnitude) were computed by applying a gradient filter.

Results: Two types of skins were used in the experiments: normal skins and skins with scars or moles. Two cases for each type were studied. The skin was gradually stretched during video acquisition. Figure 1 shows a mole with a radius of 2.3 mm. Two components of computed motion field are shown in Figure 2. There exist smooth motion transitions inside deformed skin while discontinuities are observed along the physical boundary of moving objects. Based on our experiments, moderate lighting variation does not cause significant performance degradation of the optical flow algorithm. In strain elastograms (Figure 3), abnormal tissues such as moles are clearly distinguishable from its surrounding skins due to their relatively low strain values. In addition, we found high consistency among strain elastograms obtained using different frame pairs, suggesting the stability of the proposed method.

Conclusions: Experiments show that an optical flow based method is suitable for studying skin elastograms. Its application in skin related diagnosis and modeling will be investigated in future work.

Acknowledgements: This work is supported in part by URC Grant 2006–2007 #16–07, Youngstown State University.

References:

[1] E.E. Konofagou, J. D'hooge, and J. Ophir, "Myocardial Elastography – A feasibility study", Ultrasound in Medicine and Biology, vol. 28, pp. 475–482, 2002.
[2] B.K.P. Horn and B.G. Schunck, "Determining optical flow," AI Memo 572. Massachusetts Institute of Tech., 1980.
[3] Y. Zhang, D. B. Goldgof, S. Sarkar, and L. V. Tsap, "A modeling approach for burn scar assessment using natural features and elastic property", IEEE Transactions on Medical Imaging, vol. 23, pp. 1325–1329, 2004.

Figure 1: Deformed skin with mole.

(a) Frame 1

(b) Frame 2

Figure 1: Deformed skin (mole radius=2.3 mm)

Figure 2: Computed motion field.

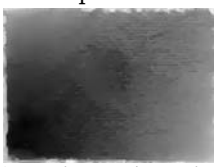

(a) Horizontal motion

(b) vertical motion

Figure 2: Motion fields.

Figure 3: Strain elastograms.

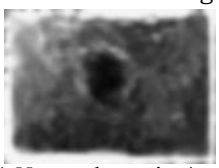

(a) Normal strain (εxx)

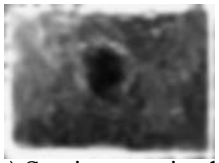

(b) Strain magnitude

Figure 3: Strain elastograms.

* *indicates Presenter*

063 **MECHANICAL PROPERTIES OF HELA CELLS BY HIGH–FREQUENCY TIME–RESOLVED ACOUSTIC MICROSCOPE.**

Pavel V. Zinin[1], Eike C. Weiss[2], Pavlos Anastasiadis[2], Robert M. Lemor[2].*
[1]School of Ocean and Earth Science and Technology, University of Hawaii, Honolulu, USA; [2]Biomedical Ultrasound Research, Fraunhofer Institute for Biomedical Technology, St. Ingbert, GERMANY.

Background: Mechanical factors play an important role in the regulation of cell physiology including cell division, cell motility, etc. Recently, the effects of the cell pathophysiology, in particular the effect of cancer on cell viscoelasticity, have attracted the attention of biomedical researchers since connections between single–cell biomechanics and human cancer have been established. Despite the fact that numerous techniques are available for studying mechanical properties of biological cells such as the micropipette technique, the magnetic twisting cytometry, numerous laser techniques and atomic force microscopy (AFM), most of the techniques allow studying either mechanical properties of only the cell membrane or a combination of the mechanical properties of the cell membrane and the cytoskeleton. Scanning acoustic microscopy (SAM), particularly time–resolved acoustic microscopy, is one of the few techniques that allow studying the mechanical properties of only the cell's interior, the cytosol and nucleus. Unfortunately, time-resolved acoustic microscopes that have been used so far in biology did not provide sufficient resolution to study the elasticity of a single cell.

Aims: In this report, we demonstrated that the high–frequency time–resolved acoustic microscope developed at the Fraunhofer Institute for Biomedical Technology (IBMT), Germany [1], is capable of imaging and characterizing the elastic properties of micron size structures in the cell's cytoskeleton and has a theoretical resolution limit of 10 m/s when measuring sound speed in a single cell.

Results: Measurements were performed on cells of the HeLa cell line derived from human cervices with carcinoma or human cervix carcinoma. SAM measurements of sound speed of adherent HeLa cells at different states of the cell cycle have been conducted. They yielded an average value of 1540 m/s. B–Scan images of HeLa cells at different states of the cell cycle show distinct patterns inside the cell (Figure 1). A method for estimating sound attenuation inside HeLa cells has been presented. Such a method is critical for the determination of cell viscoelasticity.

Conclusions: Despite the well accepted opinion that cells have no internal reflections and can be assumed to be homogeneous, this has been found not to be true for HeLa cells.

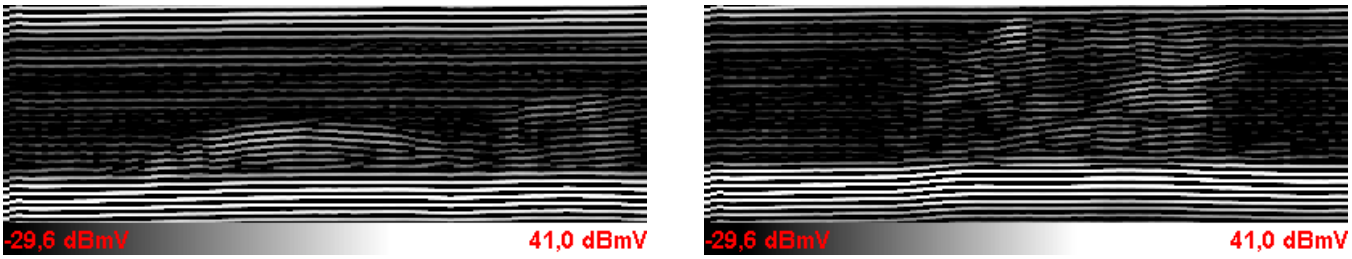

(a) (b)

Figure 1: B–Scan images from an adherent flat HeLa cell (a) and from a round dividing HeLa cell (b) recorded at 1 GHz.

Acknowledgements: The financial support provided by "Alexander von Humboldt Foundation" of Germany is gratefully acknowledged. This work was supported partially by the European Framework Program 6, Project "CellProm".

Reference:

[1] R. Lemor, E. C. Weiss, G. Pilarczyk, and P. V. Zinin, "Measurements of the elastic properties of the cell using high frequency time–resolved acoustic microscope," in *2003 IEEE Ultrasonic Symposium*, D. E. Yuhas, Ed. New York: IEEE, 2004, pp. 881–884.

* *indicates Presenter*

072 **STUDY OF MR–ELASTOGRAPHY RECONSTRUCTION METHODS USING AN ANTHROPOMORPHIC BREAST PHANTOM.**

B. Robert[1], R. Sinkus[1], E.L. Madsen[2], M. Fink[1].*

[1]Laboratoire Ondes et Acoustique, ESPCI, Paris, FRANCE; [2]Medical Physics Department, University of Wisconsin–Madison, Madison, WI, USA.

Background: The potential diagnostic gain of viscoelastic parameters measured by MR–Elastography depends strongly on the correctness of the applied algorithm for reconstruction of the complex shear modulus. Therefore, tests on phantoms serving as benchmarks are essential.

Aims: Assessment of applicability of a reconstruction technique utilizing the curl–operator for removal of the compressional wave using an anthropomorphic breast phantom (Figure 1a). The phantom consisted of a homogenous medium containing inclusions with different viscoelastic properties [1]. It was geometrically calibrated before synthesis (Gd~10 kPa and Gl~1 kPa).

Methods: We used a full 3D based reconstruction algorithm [2] to assess the dynamic modulus (Gd) and the loss modulus (Gl) of the phantom for several frequencies (100–300 Hz). The phantom was excited by a mechanical transducer with longitudinal waves. Due to mode conversion, shear waves were generated within the medium. To build shear properties maps, the longitudinal wave component was deleted via the curl operator application, i.e. the curl of the longitudinal waves was null. Thus, by calculating the curl of the displacement, we were able to invert a medium adapted shear wave equation.

Results: The experimentally-obtained values for Gd and Gl agreed with the expected values within the standard errors, while not using the curl operator led to wrong estimations of the viscoelastic properties. Moreover, it appeared that the viscoelastic parameter estimation was model dependant, i.e. using different rheological models, we obtained different elastic and viscous moduli. The relative low viscosity of the material leads in the steady state to interference patterns causing locally constructive and destructive interferences. Thus, the total amplitude of the displacement was almost zero within certain distinct regions (depending on the boundary conditions), which led to significant problems for the inversion algorithm. This kind of interference patterns was not observed *in–vivo*. The viscoelastic maps were in good agreement with the manufacturer viscoelastic maps of the phantom (Figure 1). Moreover, the inclusions were well localized and characterized on the Gd and Gl maps.

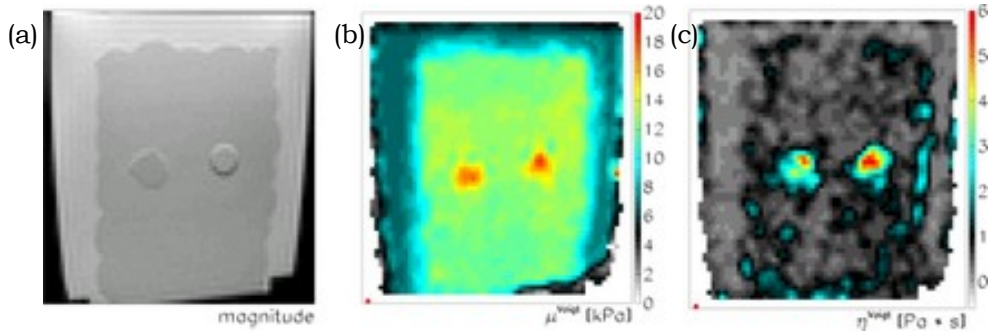

Figure 1: (a) magnitude image of the phantom, (b) Gd map of the phantom, (c) Gl map of the phantom.

Conclusions: The 3D reconstruction algorithm provided correct values for Gd and Gl when benchmarked against the anthropomorphic breast phantom. Future phantom developments might target enhanced viscous properties. Moreover, tissue which is normally considered as "homogeneous" (for instance fatty breast tissue) exhibits micro–heterogeneous properties leading to mode–conversion not only at interfaces but everywhere in the medium. These effects might also be incorporated into the phantom material.

References:

[1] Madsen, E.L. Anthropomorphic breast phantoms for testing elastography systems, PMB, in press.
[2] Sinkus, R. Magn Reson Imaging 23(2), 159–165 (2005).

074 **SOFT TISSUE ELASTOMETER.**

Sergey Tsyuryupa[1], Sergiy Kanilo[1], Vladimir Egorov[1] and Armen Sarvazyan[1].*
[1]Artann Laboratories, 1459 Lower Ferry Rd., Trenton, NJ 08618, USA.

Background: Soft Tissue Elastometer (STE) is based on the design of a similar device named Microelastometer developed at Artann Laboratories for use on core biopsy samples obtained for regular diagnostic purposes. Microelastometer provided measurements of the Young's modulus of biopsy samples ranging from 1 to 1000 kPa with an accuracy of 20% on a small segment of the core. Attempts to use the Microelastometer on tissue samples other than core biopsy specimens were unsuccessful because the stress vs. strain curve is greatly dependant on the shape and dimensions of the specimen.

Aims: The objective of this study is the development and validation of STE, a device for tissue Young's modulus measurement, which can be used in the clinical environment on freshly excised surgical specimens.

Methods: The hardware of STE is comprised of a vertically moving indenter with 3 mm diameter, a force measuring table and a laptop computer. The device provides measurements of the stress–strain curve on specimens of an arbitrary shape with characteristic dimensions from 5 to 50 mm. Indenter displacement is measured with the accuracy of 0.005 mm, and the accuracy of force measurement is 0.1 mN. Each measurement takes 30–60 seconds and collected data are saved in digital format. A mathematical model [1] describing the strain–stress dependence for the indenter being inserted into the sample is used as a base for Young's modulus calculations. Maximum sample deformation is 15%. The measurement procedure is fully automated. The device has been tested on tissue phantoms fabricated from two-component silicon elastomers SEMICOSIL 921 and SEMICOSIL 934 (Wacker Chemical Corporation, USA) and on excised animal tissues.

Results: Experimental results of Young's modulus (E) measurements of tissue phantoms with known mechanical properties and of different geometry are shown in the table below. Limits of ratio of specimen characteristic dimensions to indenter size for the stated measurement errors are 2.5–11. Each sample was measured five (5) times. As seen from the data in Table 1, the elasticity measurement error is less than 5% for the phantoms with E<100 kPa and less than 15% for the samples with E=500 kPa and below. Testing on the excised animal tissue samples (freshly purchased beef, pork, chicken) of arbitrary geometry and Young's modulus in the range of 4–100 kPa yielded reproducibility of elasticity measurements in the range of 5-25%. The tissue samples were shifted and rotated after each measurement.

Conclusions: The results obtained on phantom and soft tissue samples indicate that STE can be successfully used in laboratory and clinical environments for the evaluation of tissue elasticity modulus.

Acknowledgements: This work is partly supported by NIH grant 5 R44 CA091392.

Reference:

[1] S. Timoshenko, J.N. Goodier, "Theory of Elasticity", 2nd Edition, New York, McGraw–Hill Book Company, 1951, pp. 1–506.

Sample form	Young's modulus (E) of tissue phantoms, kPa					
	14.0	**22.0**	**40.0**	**73.0**	**195**	**350**
	Measured Young's modulus of tissue phantoms, kPa					
Rectangular samples	14.4±0.3	23.7±1.1	40.0±0.7	73.7±1.0	186±18	338±37
Pyramidal samples	13.9±0.1	21.3±0.5	43.2±0.6	73.9±1.2	180±11	383±19

Table 1: Experimental results of Young's modulus measurements of tissue phantoms.

* *indicates Presenter*

075 **TISSUE MIMICKING MATERIALS AND PHANTOMS.**

Vladimir Egorov[1], Suren Airapetian[1] and Armen Sarvazyan[1].*
[1]Artann Laboratories, 1459 Lower Ferry Rd., Trenton, NJ 08618, USA.

Background: Several materials including gelatin and polyacrylamide gels, plastisol, PVA hydrogels, silicones and rubbers, etc. have been successfully used in the fabrication of tissue phantoms for elasticity imaging and for training practitioners. In this study, we focus on development of composite breast phantoms based on SEMICOSIL® silicon gels (Wacker Silicon, Corp., MI, USA). As it was shown in our previous studies, these gels meet all the basic requirements of materials for tissue mimicking phantoms, i.e. they provide an adequate range of Young's modulus (E), a reasonable shelf–life and are nontoxic and stable [1].

Aim: The objective of this study is to identify materials and to develop the procedures for fabrication of composite, durable and time–stable tissue–mimicking phantoms of predetermined mechanical properties for training practitioners in conducting palpation examinations and, specifically, for testing and calibrating devices for Mechanical Imaging (MI).

Methods and Results: Numerous breast phantoms varying in dimensions, shapes, elasticity moduli of bulk tissue and containing various inclusions were manufactured. The bulk breast tissue has been mimicked by two–component silicon SEMICOSIL 921 with component ratio (B/A) in the range 0.7 to 1.0 and corresponding range of the Young's modulus E = 4–7 kPa. To produce composite breast phantoms, a variety of structural inclusions mimicking breast lesions were fabricated in separate molds. Inclusions of various shapes, round, oval, lobular, irregular, were fabricated from the SEMICOSIL 745 and SEMICOSIL 934 silicones. Changing the component ratio (B/A) of SEMICOSIL 745 from 3.5 to 1.0, the range of Young's modulus variation of 35–100 kPa has been provided. Reproducibility of elastic property values are within 1–5%, which is influenced by mixing quality of two components, accuracy of component ratio preparation and curing temperature. The component ratio (B/A) of SEMICOSIL 934 from 0.8 to 4.0 corresponded to a Young's modulus variation of 80–600 kPa. Each breast phantom included up to 10 specifically or randomly placed lesions with size range of 4–40 mm. Nontransparent silicone Color Masterbatch CM 166 (tan inorganic pigment) was mixed with SEMICOSIL 921 to add natural visual color to the fabricated phantoms. The three–dimensional design in SolidWork® of the breast molding forms and following rapid prototyping by selective laser sintering technique provided flexibility in building breast phantoms of different shape and size. Typically SEMICOSIL cures fully in 24 hours at room temperature (25ºC) and in 1 hour at 100ºC. The cured breast phantom is easily extracted from the mold if the mold surface is covered by a thin (0.1 mm) wax coat. After the phantom has cured, it is placed on a flat rectangular support plate as shown in Figure 1. Then, the phantom is covered by several sub–millimeter layers of elastic material which mimics the skin and provides mechanical protection.

Conclusions: The results of this study clearly demonstrated that SEMICOSIL silicone gels can be used to produce complex tissue mimicking phantoms with the desired mechanical properties. The phantom basic tissue and enclosed substructure elasticity properties can be manipulated in a wide range close to that of soft tissue [2].

Acknowledgements: This work is partly supported by NIH grant 5 R44 CA091392.

References:

[1] T. Sarvazyan, V. Stolarsky, V. Fishman, A. Sarvazyan, "Development of mechanical models of breast and prostate with palpable nodules", Proceedings of the 20th Annual International Conference IEEE, 1998, vol. 2, pp. 736-739.
[2] A. Sarvazyan, Elastic properties of soft tissues. – In: Handbook of Elastic Properties of Solids, Liquids and Gases, Vol. III, Chap. 5, eds. Levy, Bass and Stern, Acad. Press, 2001, pp. 107–127.

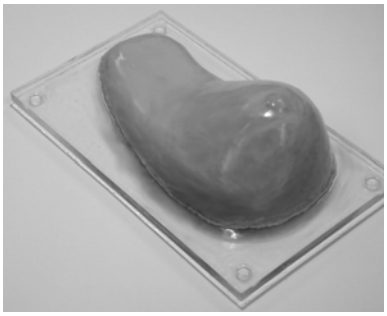

Figure 1: General view of the composite breast phantom

078 **IMAGE QUALITY ISSUES IN POROELASTOGRAPHY.**

Raffaella Righetti[1], Seshadri Srinivasan[2], Arun Thitai Kumar[1,3], Jonathan Ophir[1,3], Thomas A. Krouskop[3].*

[1]University of Texas Health Science Center Houston Medical School, 6431 Fannin St., Houston, TX, 77030, USA; [2]Siemens Acuson Ultrasound, 1230 Shorebird W., Mountain View, CA, 94043, USA; [3]University of Houston Cullen College of Engineering, 4800 Calhoun Rd., Houston, TX, 77204, USA; [4]Baylor College of Medicine, One Baylor Plaza, Houston, TX, 77030, USA.

Background: The quality of strain estimates in traditional elastography may be quantified by several quality factors such as the elastographic signal–to–noise ratio, the elastographic contrast–to–noise ratio, the spatial axial and lateral resolution and the dynamic range. Previous theoretical and simulation work has lead to established upper bounds of these image quality factors in axial strain elastography; however the limits on quality of lateral strain elastography, effective Poisson's ratio elastography and poroelastography are still not well understood.

Aims: In this presentation, we investigate the upper bounds of image quality in lateral strain elastograms, effective Poisson's ratio elastograms and poroelastograms. The term "effective Poisson's ratio elastogram" is used in this context to indicate an image obtained by dividing pixels in the lateral–strain elastogram by the matching pixels in the axial strain elastogram. In the field of porous materials, the effective Poisson's ratio is the Poisson's ratio of the composite material and is related to the experimental conditions under which the material is tested [1]. Since the performance of these elastographic techniques is expected to be significantly inferior to the performance of axial strain elastography, we also focus on the analysis and application of techniques that can be used to improve the performance of these imaging techniques under various experimental conditions.

Methods: Theoretical expressions of the upper bounds of image quality parameters in poroelastographic techniques and their trade–offs are derived using the Strain Filter formalism [2]. Simulations are performed to corroborate these theoretical findings. An analysis of the possible use of some elastographic techniques to increase the predicted performance of effective Poisson's ratio elastography and poroelastography in experimental situations of clinical interest is reported. These techniques include spatial and temporal averaging as well as the use of novel strain estimation algorithms.

Results: The results of the image quality analysis show that the upper bound of the performance of poroelastographic techniques is determined by the performance limitations of lateral strain elastography. Therefore, as in lateral strain elastography, signal–to–noise ratio and contrast–to–noise ratio of effective Poisson's ratio elastography and poroelastography are significantly lower than those predicted for axial strain elastography, under the same system and processing–parameter conditions. The spatial resolution (axial and lateral) of effective Poisson's ratio elastography and poroelastography, instead, is found to be the same as the spatial resolution of axial and lateral strain elastography. A nonlinear trade–off between the signal–to–noise (and contrast–to–noise) ratio and axial and lateral resolution exists for effective Poisson's ratio (and lateral) strain elastography and poroelastography, as it does for axial strain elastography [3].

Conclusions: Effective Poisson's ratio elastograms and poroelastograms of reasonable image quality can be generated in practical applications by using advanced elastographic acquisition and signal processing techniques in combination with methods commonly employed in other imaging modalities to increase signal–to–noise and contrast–to–noise ratio such as spatial and temporal averaging.

Acknowledgements: This work was supported by NCI Program Project PO1–CA64597–12 and by funding from John S. Dunn foundation to The University of Texas Health Science at Houston.

References:

[1] Christensen RM. Effective properties of composite materials containing voids. Proceedings: Mathematical and Physical Sciences, vol. 440(1909): 461–473, 1993.

[2] Varghese T, Ophir J. A theoretical framework for performance characterization of elastography: The strain filter. IEEE Trans. Ultrason. Ferroelec. Freq. Control. 1997. 44: 164–172.

[3] Srinivasan S, Righetti R, Ophir J. Tradeoffs between the axial resolution and the signal–to–noise ratio in elastography. Ultrasound Med. Biol. 2003. 29:847–866.

* *indicates Presenter*

081 **A NEW SYSTEM TO EVALUATE VISCOELASTIC PROPERTIES OF SMALL SAMPLES.**

DPF Padula[1], O Baffa[1], AAO Carneiro[1].*
[1]Departamento de Física e Matemática, FFCLRP, Universidade de São Paulo, Av. Bandeirantes 3900, 1404901, Ribeirão Preto–SP, BRAZIL.

Background: It is well known that changes in tissue mechanical properties such as the elastic modulus can be sensitive indicators of pathology. Changes in mechanical properties may also indicate the physiologic state of the tissue. Strain–stress curves are common in tissue characterization. In a conventional system, the deformation amplitude is fixed by its previous configuration.

Many studies in biological tissues have proposed techniques based on elastic contrast to examine abnormal breast tissues. The elastic stiffness comparison between normal and abnormal breast tissues has long been recognized [1]. Other research has proposed pressure distribution techniques in the tissue surface when it is forced [2].

Aims: In this work, we present a new excitation system with mechanical properties equivalent to the tissue. This system is composed of a modified loudspeaker and a displacement transducer based on magnetic sensors with sensitivity to 10 nm. This is a low cost and highly sensible system to evaluate the mechanical properties of small samples of soft biologic tissues.

Methods: This study applied a dynamic strain to small samples. The axial displacement of a piston and stress on the sample are registered using a magnetic sensor and load cell. The output voltages from the load and displacement transducer were registered using lock–in amplifiers. Test samples with mechanical properties equivalent to biological tissues were used in system characterization. Small changes on the mechanical properties of the samples would also imply variations on amplitude of oscillation of the piston. Both stress and displacement measurements were used for sample characterization.

Results: A periodic load was applied in the frequency range between 20Hz and 250Hz. The tests were made on four samples with different mechanical properties, silicon rubber, bovine liver, crystal paraffin and gel paraffin. Figure 1 shows the response of the axial displacement transducer corresponding to the variation of the oscillation amplitude of the piston. A behavior with two resonant peaks was observed. Figure 2 shows the load cell response to the same measurement conditions. The higher the elasticity of the sample, the smaller the area of this peak. Regarding the paraffin samples, the displacement signal presented the same characteristics, with small changes in the amplitude and frequency of the first resonance peak. In the liver sample, there was a considerable reduction in the amplitude and little change in the frequency of the resonance peak.

Conclusions: These previous studies have shown that with a simplified and low cost system, it is possible to evaluate small changes in the mechanical properties of small samples of soft biological tissue. From Figure 1 and 2 variances are visually notable in the load and displacement curves providing from sample with small differences of elasticity and viscosity. Repeated measurements in the same sample and same procedure of acquisition showed that the system presents a good reproducibility. A mathematical formalism to fit these experimental results is being developed to obtain a quantitative evaluation of the mechanical parameters of samples.

Acknowledgements: To CAPES, FAPESP and CNPq for financial support and to the technicians Lourenço Rocha, José Luiz Aziani and Sérgio Bueno for technical support.

References:

[1] Harris, J. R.; Lippman, M.E.; Morrow, M. and Hellman, S. Diseases of the Breast. Lippincott–Raven. 1996.
[2] Gentle, C. R. Mammobarography: a possible method of mass breast screening. Journal of Biomedical. Engineering 10 (2): 124-0126, 1998.

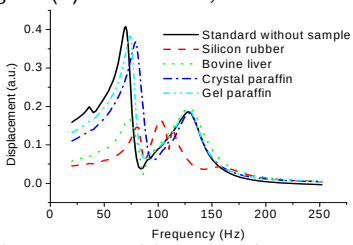

Figure 1: Position transducer response versus frequency.

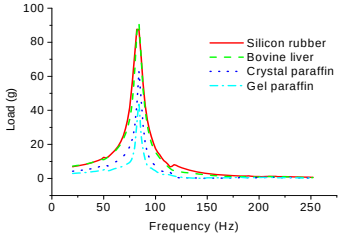

Figure 2: Load transducer response versus frequency.

083 **MAGNETIC RESONANCE ELASTOGRAPHY (MRE) OF AN ANTHROPOMORPHIC BREAST PHANTOM.**

Maritza A. Hobson[1], Scott A. Kruse [2], Jennifer L.Kugel[2], Richard L. Ehman[2], Ernest L. Madsen[1].*
[1]Medical Physics Department, University of Wisconsin–Madison, 1300 University Ave., 1530 MSC, Madison, WI 53706, USA; [2]Radiology Department, Mayo Clinic College of Medicine, 200 First St. SW, Rochester, MN 55905, USA.

Aims: To assess the feasibility of using a well–characterized anthropomorphic breast phantom to develop a technique to characterize MR elastography (MRE).

Background: Currently there are no comparison standards between groups working with MRE. A standard phantom capable of being used at multiple sites could be useful for evaluating different MRE systems.

Methods: An anthropomorphic breast phantom for testing MRE and US elastography (USE) systems was developed by Madsen et al [1] and was used in this study. Phantom production methods, component properties, and designs are given in [1]. MRE was performed on the breast phantom at Mayo Clinic using 200 Hz shear waves. A 2–D multiple slice spin–echo based echo–planar–imaging (SE–EPI) sequence was used with 24 4–mm thick adjacent slices perpendicular to the phantom axis. A SE–EPI magnitude image of the 10th slice is shown in Figure 1a, where BF is a 14–mm (bound) fibroadenoma; IRC is an irregularly shaped cancer and C is a 5 mm diameter cancer. Two different inversion methods were used to obtain the shear modulus distributions for MRE: the local frequency estimator (LFE) method [2], shown in Figure 1b, and the direct inversion (DI) method [3], shown in Figure 1c.

Results: The breast phantom was scanned with no modifications to the current MRE procedure. In addition, the phantom was fully illuminated with shear waves. This resulted in preliminary data detecting both the 14-mm and 10–mm diameter bound fibroadenomas and the irregularly shaped cancer. The tissue–mimicking subcutaneous fat and glandular regions were well differentiated in the MR elastograms. A comparison of the elastic contrasts (ratio of inclusion to the glandular background) is given in Table 1.

Conclusions: The elastic contrasts determined by the MRE system agreed well with the elastic contrast determined from dynamic testing of phantom components. To fully characterize the phantom, multiple scans at various frequencies and resolutions must be preformed.

References:

[1] Madsen, E.L. et al. Anthropomorphic Breast Phantoms for Testing Elastography Systems. Ultrasound in Med. & Biol., 2006, In press.
[2] Manduca, A. et al. SPIE Med Img 2710: 616–623, 1996.
[3] Oliphant, T.E. et al. Complex Valued Stiffness Recon. For MRE by Algebraic Inversion of the Differential Equation. Magnetic Resonance in Medicine 45: 299–301, 2001.

Table 1: Elastic Contrast Comparisons

	MRE at 200 Hz	Dynamic Testing at 50 Hz
Fibroadenoma	2.1	2.8 ± 0.2
Cancer	1.3	1.8 ± 0.2
Fat Sphere	0.76	0.50 ± 0.04
Subcutaneous Fat	0.54	0.47 ± 0.03

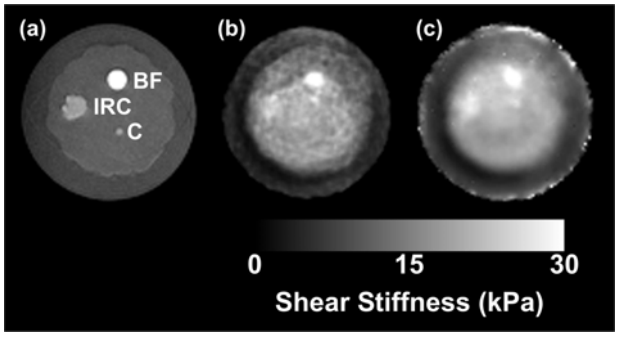

Figure 1: Slice 10
(a) SE–EPI magnitude image indicating inclusion locations,
(b) LFE elastogram,
(c) DI elastogram.

* *indicates Presenter*

084 **GRADING OF THYROID NODULE STIFFNESS USING THE FINE NEEDLE AS PROXY FOR CLINICAL PALPATION: A PROSPECTIVE *IN VIVO* STUDY.**

Nagesh Ragavendra[1], James Sayre[2], Sharon Hirschowitz[3].*
Radiology[1], Biostatistics[2] & Pathology[3] Departments, David Geffen School of Medicine at UCLA, Center for Health Sciences, 10833 LeConte Avenue, Box 951721, Los Angeles, CA 90095, USA.

Background: Sonoelastography is a novel imaging technique that detects differences in tissue stiffness during compression maneuvers. Its validation, however, requires *in vivo* measurement of elastic properties of living tissues. It was observed during thyroid biopsy procedures that variable stiffness of the nodule was readily perceptible by hand via the fine needle used in this case as a substitute for clinical palpation. Thus, a tissue stiffness grading system derived and/or modified from this or other techniques might be useful to validate clinical sonoelastographic images.

Aims: The principal aim of this prospective study is to test the null hypothesis that tissue differences between benign and malignant thyroid nodules are not *perceptible* using the fine needle as a substitute for clinical palpation during biopsy procedures.

Methods: Between May, 2005, and April, 2006, 334 focal solid and complex thyroid nodules were subjected to ultrasound guided non–aspiration fine needle biopsy. Ultrasound guidance for needle placement and tissue sampling were performed by the same radiologist (N Ragavendra). After placing the needle tip on the surface of the nodule, the needle was repeatedly advanced into and withdrawn from the nodule in rapid succession. The needle was not connected to any external suction apparatus or syringe. On the basis of the degree of stiffness encountered by the advancing needle, the nodules were categorized into two groups, "Gritty" and "Spongy". Gritty nodules displayed a crunchy feel while Spongy nodules showed no resistance to the advancing needle. The nodule size was also recorded. The aspirate was sent to the cytologist (S Hirschowitz) for review. The cytologist had no prior knowledge of the tissue stiffness grade. Tissue grade was correlated with final cytological/pathological diagnosis. Stepwise logistic regression was utilized. Size and tissue stiffness grade were predictor variables; presence or absence of malignancy as outcome variables.

Results: Total number of nodules in the study: 334.
Gritty Group: 53 nodules; 26 cytology positive, 27 cytology negative.
Spongy Group: 281 nodules; 9 cytology positive, 272 cytology negative.
Sensitivity 74.29%, Specificity 90.97%, PPV 49.06%, NPV 96.80%, Accuracy 89.22%. $P < 0.001$.

Conclusions: Tissue stiffness differences between malignant and nonmalignant thyroid nodules are sufficiently large for detection by the method described. However, the subjective nature of this technique limits its clinical applicability. Methods to quantify these differences by attaching pressure sensors to the needle tip are under consideration. The results of this study lend support for the potential use of sonoelastography as a method to select patients for fine needle biopsy.

091 **NONLINEARITY OF CORNEAL BIOMECHANICAL PROPERTIES MEASURED BY AN ULTRASONIC SYSTEM.**

Xiaoyin He[1], Jun Liu[1].*
[1]The Ohio State University, 270 Bevis Hall, Columbus, OH, USA.

Background: Glaucoma is one of the leading causes of irreversible blindness [1]. It is characterized by optic nerve head damage associated with high intraocular pressure (IOP). Accurate measurement of IOP is essential for diagnosis and monitoring of glaucoma. Inter–subject variations of corneal biomechanical properties may have introduced significant errors to IOP measurements using the current gold standard - Goldmann Applanation Tonometry [2]. Methods for *in vivo* measurement of corneal biomechanical properties have not been established.

Aims: The aim of this study is to develop an ultrasonic system for non–invasive measurements of corneal biomechanical properties in intact eyes, and to use this method to differentiate corneal biomechanical properties in response to elevated IOPs.

Methods: An ultrasonic measurement technique in combination with a mathematical model for wave propagation in thin layers was developed to estimate corneal biomechanical properties. The measurements were performed on 10 enucleated fresh porcine eyes with the IOPs adjusted at four different levels. An inverse algorithm was used to reconstruct the biomechanical properties of the corneas.

Results: It was observed that corneal thickness and stiffness were decreased with abnormally high IOPs. The results showed that corneas exhibit non–linear stress–strain relationship when IOP exceeds the normal range. It was also demonstrated that the ultrasonic method was sensitive to detecting changes of corneal biomechanical properties associated with changes in IOP.

Conclusions: The ultrasonic method used in the current study has the potential to implement *in vivo* measurements of corneal properties. The phenomenon of corneal "softening" at abnormally high IOPs was not reported in literature. The constitutive relationships of corneas in intact eyes need to be further studied.

Acknowledgements: Funding from Columbus Foundation is gratefully acknowledged. We thank Xueliang Pan for his assistance in statistical analysis of data.

References:

[1] Quigley HA. Number of people with glaucoma worldwide. Br. J. Ophthalmol., 1996; 80(5):389–93.
[2] Liu, J, and CJ Roberts. Influence of corneal biomechanical properties on intraocular pressure measurement. J. Cataract. Refract. Surg., 2005; 31:146–55.

** indicates Presenter*

092 **CLINICAL APPLICATIONS OF A REAL–TIME ELASTOGRAPHY TECHNIQUE IN BREAST IMAGING.**

RG Barr[1,2].*

[1]Radiology Consultants, Youngstown, OH, USA; [2]Northeastern Ohio University College of Medicine, Rootstown, OH, USA.

Background: Elastography can provide diagnostic information of breast masses which is otherwise not available in routine clinical practice. This information can improve both the sensitivity and specificity in ultrasound breast cancer detection.

Aims: This poster reviews the clinical utility of a real–time elastography technique in detection and characterization of breast masses.

Methods: 125 biopsy proven benign and malignant lesions, in which real–time elastography was used to characterize lesions obtained during routine clinical cases were reviewed, and examples where elastography was helpful in clinical diagnosis are presented. Elastograms were obtained on a Siemens Elegra or Antares Ultrasound system utilizing a 13 MHz probe. The additional information obtained from the elastogram is presented and how that information was utilized in the clinical setting is discussed. The characteristic elastographic patterns observed in various benign and malignant breast lesions is presented in pictorial form.

Results: Initial results of adding a real–time breast elastography technique to the characterization of breast lesions in the clinical setting aid in the determination if the lesion is benign or malignant (based on change in lesion size); characterize lesions as cysts (bull's eye pattern) or fat lobules in dense breast tissue (based on relative elasticity). Preliminary results in the clinical setting suggest that this technique has the potential to improve the detection and characterization of breast lesions.

Conclusions: In our initial evaluation of adding real–time elastography to the clinical evaluation of breast abnormalities, the elastogram added additional diagnostic information in a large portion of cases. Preliminary results are encouraging and suggest that this technique will improve characterization of breast lesions and may significantly decrease the number of biopsies or aspirations performed. Larger multi–center trials are needed to confirm our initial findings and determine the sensitivity and specificity of this technique.

Acknowledgements: This work was supported in part by a grant from Siemens Ultrasound.

References:

[1] Ophir, J., Céspedes, I., Maklad, N. F., and Ponnekanti, H.: "Elastography: A Method for Imaging the Elastic Properties of Tissue *In–Vivo*". Chapter 7 In Ultrasonic Tissue Characterization, M. Tanaka et al., eds., Springer Verlag, Publ., Tokyo, pp 95–123, 1996.

[2] Garra, B.S., Céspedes, I., Ophir, J., Spratt, S., Zuurbier, R. A., Magnant, C. M. and Pennanen, M. F.: Elastography of Breast lesions: initial clinical results. Radiology, Vol. 202, pp. 79–86, 1997.

[3] Svensson WE et al. Elasticity Imaging of 67 Cancers and 167 Benign Breast Lesions Shows That It Could Halve Biopsy Rates of Benign Lesions. Proceedings of the 4th Int'l Conference on the Measurement and Imaging of Tissue Elasticity, Lake Travis, Texas, October 2005, p. 87.

096 **MECHANICAL MEASUREMENT OF VISCOELASTIC PROPERTIES OF HUMAN PROSTATE INCLUDING CORRELATION WITH PATHOLOGY.**

Man Zhang[1], Priya Nigwekar[1], P. Anthony di Sant'Agnese[1], Jean Joseph[1], Edward M. Messing[1], Deborah J. Rubens[1], Kevin J. Parker[1].*
[1]University of Rochester, Rochester, NY, 14620, USA.

Background: Prostate cancer is one of the most common cancers among American men, frequently diagnosed by palpation of a firm nodule on digital rectal examination. Viscoelastic characterization of normal and cancerous prostate tissues is, therefore, of great importance for medical applications, such as elasticity imaging and surgical simulation and planning. In this study, we proposed a tissue stress-relaxation experiment to clarify the viscoelastic properties of human prostate tissue.

Aims: To characterize viscoelastic properties of normal and cancerous human prostate tissue *in vitro*, that is essential for assessing the performance of elasticity imaging on prostate cancer detection.

Methods: The human prostate samples were collected immediately following radical prostatectomy at the Pathology Department at the University of Rochester Medical Center. Cylindrical tissue samples (~8 mm diameter, 5–9 mm thickness) were acquired at different locations of each prostate. A 5% compressional strain was applied on each sample for 700 seconds. Three repeated measurements were performed on each sample. The averaged stress–relaxation curve of each sample was fitted to the three–parameter (E_0, η and α) viscoelastic Kelvin–Voigt fractional derivative (KVFD) model. The complex Young's modulus at any frequency was then obtained by Fourier transform of time domain response. After mechanical testing, prostate specimens were sent to pathology for the investigation of correlation between mechanical and pathological findings. Prostate specimens containing more than 50% of cancer were included in the cancerous tissue category.

Results: The mechanical properties of a cancerous specimen and a normal specimen obtained from the same prostate are demonstrated in Figure 1, showing the correlation between the mechanical testing and the pathological inspection. In this case, the magnitudes of the complex Young's moduli at 100 Hz are 57.8 kPa and 17.8 kPa, respectively. The elastic contrast is about 3.3:1 (cancer:non–cancer). The complex Young's modulus of prostate tissue slightly increases with frequency. A total of 15 samples from 7 human prostates were under investigation. The viscoelastic behavior of prostate tissue is well characterized by KVFD model. For both normal (n = 7) and cancerous (n = 8) prostate specimens, there is noticeable inter–patient variability on the mechanical properties. The average magnitudes of the complex Young's moduli are 15.5±4.81 kPa and 37.9±14.9 kPa at 100 Hz, respectively, giving an elastic contrast of 2.5:1. Eight paired t–tests (One normal/cancer pair per prostate except one prostate that has two paired samples) indicate there are significant differences between mechanical properties of normal and cancerous prostate tissues: η ($p << 0.01$) and |E*| ($p=0.002$).

Conclusions: The stress–relaxation tests on prostate specimens produced repeatable results that fit the KVFD model very well. Viscoelastic properties of normal and cancerous human prostates were systematically investigated. The elastic contrast between non–cancerous prostate tissue and other regions with over 50% cancer appears to be 2.5:1 (STD = 0.87) at 100 Hz. This study contributes to current limited knowledge on the elasticity of human prostate, and the inherent contrast produced by cancer.

Acknowledgements: This study was partly supported by NIH grant 5 RO1 AG016317–05.

Reference:

[1] Taylor LS et al., "A Kelvin–Voigt fractional derivative model for viscoelastic characterization of liver tissue", ASME Int. Mechanical Engineering Congress and Exposition, 2002.

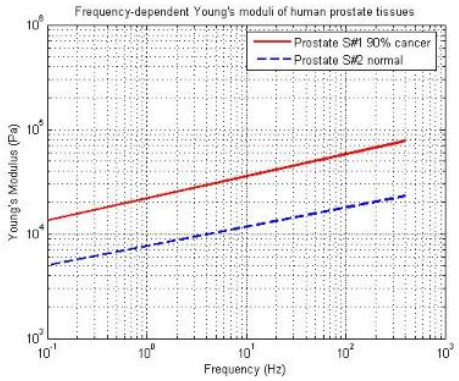

Figure 1: Frequency–dependent Young's moduli of prostate tissue.

* *indicates Presenter*

101 **ANALYSES OF BLOCK MATCHING ON DYNAMIC ELASTOGRAPHIC IMAGES.**

LP Neves[1], J Jiang[2], TJ Hall[2], T Varghese[2], E Madsen[2], JA Zagzebski[2], AAO Carneiro[1].*
[1]Departamento de Física e Matemática, FFCLRP, Universidade de São Paulo, Ribeirão Preto, São Paulo–1404901, BRAZIL. [2]Medical Physics Department, University of Wisconsin–Madison, 1300 University Avenue, 1530 MSC, Madison, WI 53706, USA.

Aims: This work provides a comparison between elasticity imaging obtained using Block Matching (BM), for two different methods of compression: static and dynamic.

Background: Elastography or elasticity imaging is a new imaging modality where elastic tissue parameters related to the structural organization of normal and pathological tissues are imaged [1]. Both static and dynamic techniques have been utilized for inducing tissue deformations that are subsequently used to delineate tissues having different elastic properties. In quasi–static elastography, radiofrequency (RF) signals acquired before and after a small amount of compression are compared. Dynamic methods, on the other hand, may image local deformations within tissues or structures induced by externally applied oscillations using transducers at low frequencies [2].

Methods: In this work, we applied a quasi–static compression to tissue–mimicking phantoms [3], in two different ways, i.e. a dynamic and a static compression. A 9 cm cubic phantom was positioned between two aluminum plates. For compression, the top plate was fixed and contained a rectangular slot to hold the transducer, while the bottom plate was moved up and down in a sinusoidal fashion by a dc motor. RF echo signals were acquired during the motion. The compression frequency and maximum deformation were 56.4 bpm and 1% axial strain. In static compression, a stepper–motor was connected to the same transducer that was used before, but for this method, the bottom plate was fixed, while the top plate was moved down with the transducer. The compression was applied in steps of 0.2%, with a maximum compression of 1%. Displacement maps were obtained using the BM technique, comparing the pre– and post–compressed RF echo data. Strain images were then obtained from the axial gradient of the 2–D displacement data. RF data were acquired using an ultrasound machine with a research interface, the Ultrasonix 500RP, using a linear array transducer. The mean and variance were also compared between both BM and CC for strain maps.

Results: The mean values of strain under those two loading conditions were estimated, as well as their error variances. The estimated mean strain from a cycle of load reversals is plotted out in Figures 1(a) and (b).

Figure 1a: Mean Strain in Dynamic Loading

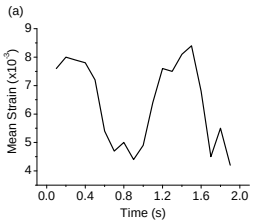

Figure 1b: Mean Strain in Static Loading

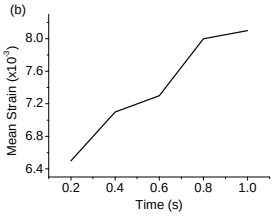

It is easy to see, from Figures 1(a) and (b) that strain profiles match well with the prescribed sinusoidal and static loading pattern. The underestimation among the estimated strains (see Figure 1(a)) may be attributed by mechanical "damping" effect, as observed during experimentation. The frequency of the evaluated mean strain rate was also close to the frequency of applied deformation (i.e. 56 bpm). However, the error variance in the estimated local strains was four times greater under the sinusoidal compression than that obtained under the static compression. This is partially due to the fact that homogenous strain profile is somehow violated in the presence of local mechanical vibration. Therefore, how to quantify the estimated strain error in dynamic loading deserves further attention.

Conclusions: Strain images obtained using two different forms of compression and analyses were compared. In both cases, the BMA [2] can accurately estimate strain.

Acknowledgements: This work was financially supported by CAPES, FAPESP, University of Wisconsin–Madison and the University of São Paulo.

References:

[1] Ophir J et al. 1991. Ultrason. Imaging 13: 111–34.
[2] Zhu Y and Hall TJ 2002. Ultrason. Imaging 24,100–108.
[3] Ernest L Madsen et al 2005 Phys. Med. Biol. 50 5597–5618.

103 **INTERFACE BONDING STRENGTH IN AXIAL–SHEAR STRAIN ELASTOGRAPHY.**

A Thitai Kumar[1,2], J Ophir[1,2], TA Krouskop[1,3] and BS Garra[4].*
[1]The University of Texas Health Science Center Houston Medical School, Houston, TX, USA; [2]University of Houston, Houston, TX, USA; [3]Baylor College of Medicine, Houston, TX, USA; [4]University of Vermont, Burlington, VT, USA.

Background: It is known that among breast lesions, malignant tumors are generally more firmly bonded to their surroundings than are benign tumors [1]. When an inhomogeneous tissue is subjected to an axial compression, it experiences not only normal strains (axial/lateral), but also shear strains. We hypothesize that imaging the shear strain may provide information about the bonding strength at the interface. In this simulation study, we analyze the axial component of the shear strain elastograms to determine a metric that may be indicative of the bonding strength at the interface.

Methods: A 2D model with a circular–inclusion either firmly–bonded or weakly–bonded to the background was used. The weakly–bonded inclusion was modeled assigning a coefficient of friction to the contact elements in FEA software ANSYS®. The inclusion was three times stiffer than the background and an axial compression of 2% was applied. RF–data were obtained by simulating a linear ultrasound transducer with a 5MHz center frequency, 50% fractional bandwidth and a constant -6 dB beamwidth of 1mm. The axial–shear strain was estimated as the gradient of the axial displacements in the lateral direction. The axial–shear strain profile taken perpendicularly across the inclusion/background interface was analyzed. Strain profiles taken at different locations along the interface will be specified by their orientation with the lateral direction. One such example is illustrated in Figure 1. The width at -3dB from the peak value of the strain profile and the average axial–shear strain within the width were investigated as a possible metric to study the bonding strength at the interface. For example, *in–vivo* axial–shear strain elastograms superimposed on corresponding sonograms for the two types are shown in Figure 3.

Results: Results indicate that the width of the strain profile is larger, while the mean strain value within the width is smaller, when the inclusion is firmly–bonded compared to when it is weakly–bonded. In addition, both these measures are orientation dependent (Figure 2).

Conclusions: In summary, we have shown using simulations that a metric that describes some features of the pattern (e.g. width at different orientation) and magnitude of the axial–shear strain near the interface may be exploited to quantify the bonding strength at the interface.

Acknowledgements: This work was supported in part by NIH program project grant P01–EB02105–12 awarded to the University of Texas Health Science Center Houston Medical School.

Reference:

[1] Chen EJ, Adler RS, Carson PL, et al. Ultrasound tissue displacement imaging with application to breast cancer, *Ultrasound in Medicine and Biology* 21(9), 1153–1162 (1995).

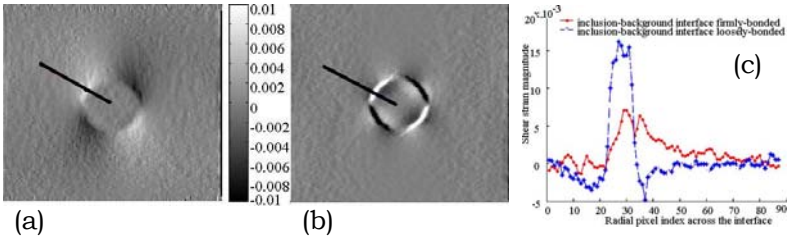

Figure 1: (a) Axial–shear strain elastogram of a firmly–bonded inclusion, (b) weakly-bonded inclusion, and (c) graph of the axial–shear strain profile across the interface along the line indicated in the elastograms.

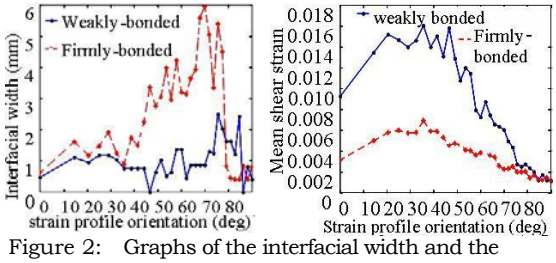

Figure 2: Graphs of the interfacial width and the mean axial–shear strain within the width of the axial–shear strain profiles at different orientation from shear strain elastogram.

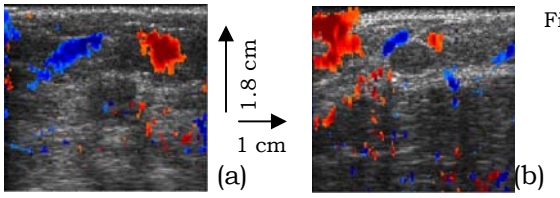

Figure 3: Examples showing the axial–shear strain elastogram (color patches, see CD version) superimposed on the corresponding sonogram of a cancer (a) and a benign lesion (b). Observe that the proximity of the axial-shear strain region to the sonographically visible lesion is different for both the cases.

* *indicates Presenter*

107 **DEVELOPMENT OF 1–D SONOMYOGRAPHY SYSTEM TO DYNAMICALLY MONITOR DIMESIONAL CHANGES OF FOREARM MUSCLES DURING WIRST FLEXSION AND EXTENSION.**

J.Y. Guo[1], Y.P. Zheng[1], Q.H. Huang[1], X. Chen[1].*
[1]The Hong Kong Polytechnic University, Hong Kong, CHINA.

Background: Skeletal muscles play an important role in human movement. The mechanical and bioelectrical properties of muscles are closely related to the structure, such as fascicle length, pennation angle and cross–sectional area. Surface electromyography (SEMG) is one of the most frequently used methods in studying the biological and bioelectrical characteristics of muscles. However, it is difficult to provide the information of the architectural changes of muscles during contraction. Ultrasonography has been recently used for the quantitative measurement of the architectural changes of muscles, fascicles and tendons [1,2]. We used the term sonomyography (SMG) to describe signals representing these changes in muscles [2]. A system was successfully developed to continuously record synchronized ultrasound images, SEMG, torque and joint angle and to analyze them simultaneously. Although the SMG signals obtained using B–mode images are able to offer accurate information of muscle deformation in experiments, A–mode ultrasound may provide a more portable solution to detect SMG for various applications.

Aims: The aim of this study is to develop an A–mode ultrasound system to measure the SMG signals of extensor carpi radialis muscle of nine healthy young adults during the wrist flexion and extension.

Methods: A 10MHz focused ultrasound transducer was placed on the belly of the extensor carpi radialis of the forearm using double–sided adhesive tape to measure the dimensional change of muscle. A custom–developed EMG amplifier was used to amplify the SEMG signals captured from the EMG bipolar Ag–Agcl electrodes, which was attached to the skin surface near the ultrasound transducer. An additional electrode for providing the reference electrical signal was attached to a site near the pisiform bone. The angle of the wrist during the movement of extension and flexion was measured by an electronic goniometer. The A–mode ultrasound signals were digitized by a high speed A/D converter with a sampling rate of 100 MHz. The SEMG and wrist angle signals were continuously collected by a data acquisition card. A multi–threaded program for ultrasound measurement of motion and elasticity (UMME, http://www.tups.org/) was developed using Visual C++ to acquire and analyze the A–mode ultrasound, SEMG and joint angle signals simultaneously. Nine healthy subjects (2 females, 7 males) participated in the experiments. During the experiments, subjects were seated in a comfortable chair and requested to perform the wrist flexion and extension three times at the velocity of 30 beats/minute, 45 beats/minute, 60 beats/minute guided by a metronome. The relationships among the SMG signals, root–mean–square (RMS) amplitudes of SEMG and wrist angle signals were quantitatively studied.

Results: Three parameters were derived from each data set, including the range of wrist angle, the muscle deformation and the root–mean–square (RMS) of SEMG. It was demonstrated that the thickness changes of the extensor carpi radialis muscle during the wrist extension and flexion of the subjects were highly correlated with the wrist angles and SEMG RMS. Quadratic functions could well represent the their relationships. The results of all the subjects showed similar trends and the overall mean R^2 value for the correlation between the wrist angle and muscle deformation was 0.886±0.097 (mean ±S.D.); the overall mean R^2 value between wrist angle and RMS was 0.903±0.083.

Conclusions: We developed an A–mode ultrasound system to record the thickness change of muscles in real–time during their contraction. The present study demonstrated that the quadratic regression could be used to describe the relationships among the wrist angle, muscle deformation and the SEMG RMS signals in the nine healthy subjects. Further studies of SMG signals using this system will be conducted.

Acknowledgements: This project was supported by the The Hong Kong Polytechnic University (G-YE22).

References:

[1] Loram ID, Maganaris CN, Lakie M. Use of ultrasound to make noninvasive *in vivo* measurement of continuous changes in human muscle contractile length. J Appl Physiol 100: 1311–1323, 2006.
[2] Zheng YP, Chan MM, Shi J, Chen X, Huang QH. Sonomyography: Monitoring morphological changes of forearm muscles in actions with the feasibility for the control of powered prosthesis. Med Eng Phys 28: 405–15, 2006.

112 **STRESS AND STRAIN RELAXATION MECHANISMS IN SOFT TISSUES.**

R Leiderman[1], G Berry[2], NH Gokhale[1], MS. Richards[1], CE Rivas[1], JC Bamber[2], AA Oberai[3] and PE Barbone[1].*

[1]Boston University, Boston, MA, USA; [2]Joint Department of Physics, Institute of Cancer Research and Royal Marsden NHS Trust, Downs Road, Sutton, Surrey, SM2 5PT, England, UK; [3]Rensselaer Polytechnics Institute, Troy, NY, USA.

Background: Soft tissue is widely recognized as having both fluid and solid phases which can move independently of each other. Furthermore, the fluid exists within several "compartments" of the soft tissue, notably, the vasculature (including both the hemal and lymphatic vessels) and the extravascular space [1]. Of course, due to permeability of the microvessels in both vascular networks, fluid is often exchanged between these compartments. It is recognized that fluid flow leads to a stress relaxation at fixed strain (or conversely, a strain relaxation at fixed stress) [2,3]. On the other hand, the solid phase of soft tissue is a gel–like polymer network comprised primarily of crosslinked collagen and proteoglycans [4]. When subjected to stress, these molecules can undergo molecular rearrangement, which itself gives rise to macroscopic relaxation phenomena. These distinct microscopic relaxation mechanisms can be captured in mathematical models describing the macroscopic stress strain response of the tissue.

Aims: The aim of this work is to explore the macroscopic effects of different microscopic relaxation mechanisms. In particular, we aim to elucidate the roles of the different mechanisms on the spatio-temporal pattern of strain relaxation.

Methods: We worked with a mathematical model of tissue deformation which was a generalization of [3] to accommodate the viscous relaxation of the solid frame. We used a finite element method to solve the mathematical equations and thus conduct computational experiments. Via these experiments, we explored the parameter space of possibilities. We also extracted from the literature parameter values representative of breast tissue and predicted the magnitudes and time scales of various effects.

Results: We found that, all else being equal, each different microscopic relaxation mechanism resulted in a different spatio–temporal pattern of strain relaxation. The strain relaxation patterns themselves, however, depended strongly on a host of confounding variables such as the stiffness distribution, boundary conditions and the particular relaxation mechanism under consideration.

Conclusions: Different microscopic mechanisms of stress/strain relaxation in soft tissues manifest themselves in different macroscopic behaviors. Mathematical models describing the macroscopic behavior can be derived and solved. These elucidate the macroscopic effects of the microscopic mechanisms. The results point to the potential of indirectly quantifying these mechanisms via macroscopic observation.

Acknowledgements: This work was supported by the DOD Breast Cancer Research Program (Award No W81XWh-04–1–0763) and NSF.

References:

[1] Levick JR. An introduction to cardiovascular physiology, 4th ed. London: Arnold Publishers, 2003.
[2] Mow VC, Kuei SC, Lai WM, Armstrong CG. Biphasic creep and stress relaxation of articular cartilage in compression: theory and experiments. J Biomech Eng 1980;102:73–84.
[3] Netti PA, Baxter LT, Boucher Y, Salak R and Jain RK 1997 Macro– and microscopic fluid transport in living tissues: Application to solid tumors AIChE Journal 43(3) 818–834.
[4] Sridhar M, Liu J, Insana MF: Elasticity imaging of polymeric media, unpublished manuscript, June 2006.

** indicates Presenter*

120 **TRANSIENT RADIATION FORCE ELASTOGRAPHY: A PRELIMINARY COMPARISON WITH SURFACE PALPATION ELASTOGRAPHY.**

David MelodeLima[1], Jeffrey C. Bamber[1], Gearóid P. Berry[1], Nigel L. Bush[1], Francis A. Duck[2], Jacqueline A. Shipley[2], Lijun Xu[1].*

[1]Joint Department of Physics, Institute of Cancer Research and Royal Marsden NHS Trust, Downs Road, Sutton, Surrey, SM2 5PT, England, UK; [2] Royal United Hospital, Bath, England, UK.

Background: The use of ultrasound elastographic methods has generated considerable interest as a means of remotely evaluating with good resolution a range of mechanical properties of tissues *in vivo*. Of the various methods that are under investigation, most apply a nearly static or a slowly varying dynamic load to the tissue surface and use ultrasound to image the resulting tissue strain. Several groups have, however, studied transient acoustic radiation force as a means of applying the load at depth in the tissue. Since we have developed variants of both approaches, we have a good opportunity to make an assessment of their relative advantages and disadvantages. This presentation describes early work toward such an objective.

Aims: To assess some of the advantages and disadvantages of generating tissue strain by deep loading with transient acoustic radiation force versus the use of nearly static surface loading.

Methods: Experiments with gelatin phantoms and finite element models containing cylindrical stiff inclusions in homogeneous backgrounds were employed to measure the relative performance of previously reported methods of pseudo-static freehand elastography [1] and transient radiation force elastography [2]. Images using deep transient loading with radiation force were created using a "pushing" burst of sound at each location of strain estimation; an *F*1.3 focused ultrasound transducer was driven at 1.7 MHz, generating a highly localized force in space (the push area was about 1.5 mm wide by 1 cm deep, centered at a depth of about 22 mm from the acoustic source) and time (the push lasted 8 ms and the measured strain decayed in about 2 ms). Experimentally, a linear array with a centre frequency of 7.5 MHz was used to obtain radio frequency (RF) echo signals. The focused transducer and the linear array were aligned such that the focus of the pushing beam was in the imaging plane. For pseudo–static strain imaging, RF echo data were acquired at full frame rate during freehand palpation using the same linear array. Images of pseudo–static or transient strain, as appropriate, were produced using well–known methods of ultrasound RF correlation–based displacement tracking and least squares strain estimation.

Results: Relative to images obtained with surface loading, radiation force images were found to be less susceptible to artefacts associated with boundary conditions and elastic modulus inhomogeneities, providing strain images that were more closely related to the elastic modulus distributions. In particular, radiation force elastograms were more homogeneous in the background and within the inclusions, and displayed a superior contrast–transfer–efficiency, particularly for regions that had negative modulus contrast or that were disconnected from the background or the anterior medium by a low friction boundary. They also possessed a reduced rate of decay of strain signal–to–noise ratio with depth, when compared with pseudo–static images generated using surface loading.

Conclusions: Elastograms created using the transient strain that arises from a highly localized and impulsive radiation force appear to be of superior quality in many respects, when compared to those generated using pseudo–static surface loading. Currently, however, it takes much longer to scan using radiation force loading. Radiation force elastograms may also, under circumstances not yet studied, show contrast for ultrasonic attenuation and absorption, as well as for tissue stiffness; this needs further investigation, preferably *in vivo*.

Acknowledgements: This work was supported by funding from DoH NEAT project D008, and the EPSRC.

References:

[1] Bamber JC, Barbone PE, Bush NL, Cosgrove DO, Doyley MM, Fuechsel FG, Meaney PM, Miller NR, Shiina T, Tranquart F (2002) Progress in freehand elastography of the breast. IEICE Trans on Information and Systems; 85-D(1):5–14.

[2] Melodelima D, Bamber JC, Duck F, Shipley J, Xu L (2006) Elastography for breast cancer diagnosis using radiation force: system development and performance evaluation. Ultrasound Med Biol; 32(3):387–96.

123 **ANALYSIS OF ULTRASOUND FRAME RATE REQUIREMENTS FOR CARDIAC ELASTOGRAPHY.**

Hao Chen[1,3], Tomy Varghese[1], Peter S. Rahko[2], James A. Zagzebski[1].*
[1]Medical Physics Department, [2]Cardiovascular Medicine, [3]Electrical and Computer Engineering Department, University of Wisconsin–Madison, Madison, WI, USA.

Background: Strain and strain rate imaging, as adjuncts to traditional echocardiography, are developing into techniques that provide new information for evaluation of regional myocardial function [1, 2]. Clinical diagnosis using echocardiography is based on visually–assessed wall motion scoring, which is semi-quantitative and heavily weighted on operator experience and expertise. Cardiac motion estimation methods such as tissue Doppler and elastography can be used to assess myocardial muscle displacements, providing quantitative parameters such as the strain–rate and strain. However, tissue Doppler imaging does not differentiate between active contraction and simple rotation or translation of the heart wall, nor does it differentiate passively following tissue from active contraction. Cardiac elastography can provide two–dimensional strain information, provided radiofrequency (RF) data frames at a sufficient frame rate are acquired.

Aims: The purpose of this study was to evaluate the ultrasound frame rate requirements for accurate estimation of tissue displacements and strain in cardiac elastography. We used a uniformly elastic tissue-mimicking phantom that underwent cyclic compressions at variable compression frequencies and measured tissue displacements and strains estimated using both 1D and a newly developed two–step 2D cross–correlation method [3].

Methods: A cubic TM phantom with 10 cm sides was positioned between two aluminum plates. The top plate was fixed and contained a rectangular slot to hold an ultrasound transducer, while the bottom plate was oscillated by a linear motor. Sinusoidal compressions of the phantom were applied at frequencies from 0.5 to 3.5 Hz with a maximum strain of 5%. Loops of RF data were acquired using a GE Vingmed Vivid 7 system and a 2.5 MHz phased array transducer imaging at 43 fps. Acquisition frames were not synchronized to the compression. Displacement maps were generated using 2–D cross–correlation between the pre– and post–compressed RF frames; strain images were obtained from the derivative of the displacement maps. A finite element analysis model was also constructed to compare and quantify the displacement amplitude from the experimental RF data.

Results: Local displacements were estimated from the RF data frames acquired at the maximum frame rate of the ultrasound system, 43 fps. To evaluate the impact of lower frame rates on the resultant elastograms, the RF data frames were decimated by a factor of two, and local displacements computed, until the RF frames were too far apart to accurately estimate the sinusoidal compression frequency. Our results indicate that a frame rate of two times the sinusoidal compression frequency represents a minimum requirement for the estimation of the compression frequency from the displacement data. However, the displacement estimates obtained are more peaked when compared to the smooth sinusoidal variations in the displacement estimates obtained at higher frame rates. Frame rates on the order of ten times the sinusoidal compression frequency provide more consistent signal-to-noise ratio estimates as illustrated in Figure 1. Note that the signal–to–noise ratio is quite high even for frame–rates on the order of two times the compression frequency as shown in Figure 1. Results obtained using the finite element analysis model and the experimental results were consistent.

Figure 1:

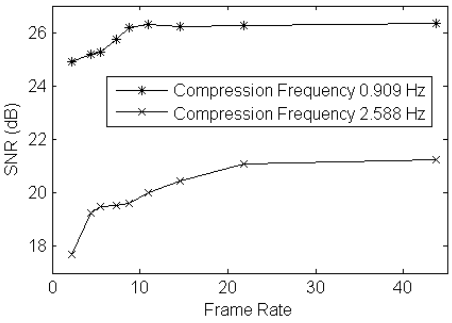

Conclusions: Accurate evaluation of cardiac tissue wall motion displacements and strain requires an ultrasound frame rates greater than two times the heart rate, although a frame rate of about two times the heart rate is sufficient to estimate the compression frequency.

References:

[1] Varghese T, Zagzebski JA, Rahko P, Breburda CS. Ultrasonic imaging of myocardial strain using cardiac elastography, Ultrason Imaging. 2003; 25(1):1–16.
[2] Konofagou EE, D'hooge J, Ophir J. Myocardial elastography– A feasibility study *in vivo*. Ultrasound Med Biol. 2002; 28(4):475–82.
[3] Chen, H., Shi H., Varghese T., Improvement of elastographic displacement estimation using a two–step cross-correlation method. Ultrasound Med Biol. 2006 (in press).

* *indicates Presenter*

125 **TRACKING OF APONEUROSIS MOTION DURING VOLUNTARY CONTRACTIONS OF THE TIBIALIS ANTERIOR MUSCLE.**

JW Farron[1], T Varghese[2,3], BC Heiderscheit[4], DG Thelen[1,3].*
[1]Mechanical Engineering, [2]Medical Physics, [3]Biomedical Engineering, [4]Orthopedics and Rehabilitation Departments, University of Wisconsin–Madison, Madison, WI, USA.

Background: Ultrasound is increasingly being used to measure *in–vivo* muscle and tendon motion. Prior studies have visually identified anatomical landmarks (e.g. the proximal and distal musculotendon junction) on successive images to estimate average fiber and tendon strain [1]. Recently, correlation-based analysis of B–mode images was introduced as a method to automatically track additional points on the musculotendon unit [2]. Further development of an elastographic approach to estimate spatial strain distribution is important for validating detailed biomechanical models of muscle [3].

Aims: The aim of this study was to compare correlation–based elastographic analyses of B–mode and radiofrequency (RF) images obtained during voluntary contractions of the tibialis anterior muscle.

Methods: The distal tibialis anterior muscle was imaged during voluntary isometric contraction-relaxation cycles up to 25% of maximum strength (Figure 1a). Radiofrequency (RF) data were acquired over a 30 mm deep by 40 mm wide (1036 x 360 pixel) viewing plane at 5 MHz center frequency using a Siemens Antares scanner equipped with a research interface, using a VFX 13–5 linear array transducer. A correlation–based tracking algorithm [4] was used to estimate the axial and lateral displacement of 10 kernels (1 mm x 1 mm) spaced equally along a 10 mm section of the distal aponeurosis (Figure 1b). This analysis was repeated with B–mode images (Figure 1c). The distance between the aponeurosis and kernels in the last frame was used as a measure of the tracking accuracy.

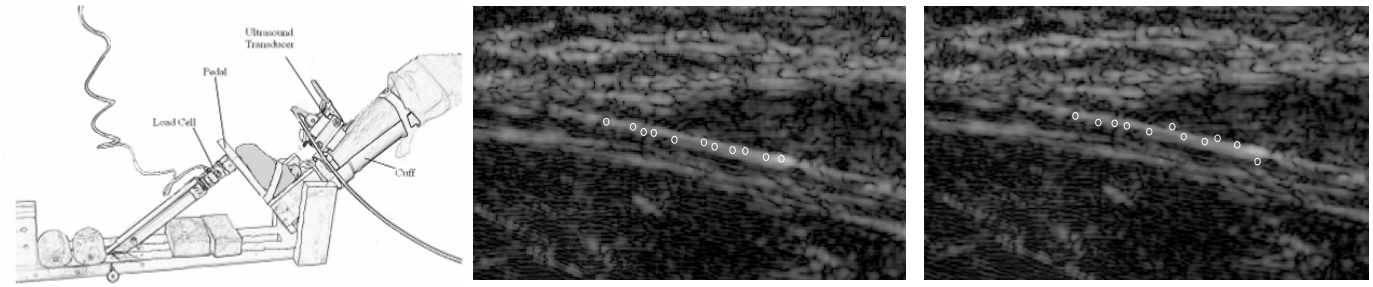

(a) (b) (c)

Figure 1: (a) Experimental setup; (b) Final locations of kernels after tracking RF data and (c) B–Mode images through a contraction–relaxation cycle.

Results: Tracking motion using RF data showed less deviation from the aponeurosis than using B–mode data. Over the contraction–relaxation cycle, individual kernels deviated an average of .02 mm from the best linear fit using the RF data, and 0.07 mm using the B–mode data. The final orientation of the linear fit lines was similar, with changes in angle of 0.5 and 0.4 degrees off the original aponeurosis orientation.

Conclusions: This study demonstrates the improved displacement resolution obtained using RF image data, compared to B–mode, to track aponeurosis motion during muscle contractions. The simultaneous tracking of proximal and distal aponeurosis motion facilitates a direct estimate of average muscle fiber strain and pennation [2]. Further refinement of this approach would provide a powerful tool for investigating the effects of injury, surgery and rehabilitation programs on *in–vivo* musculotendon mechanics.

Acknowledgements: Aircast Foundation, NFL Charities.

References:

[1] Fukunaga, T., et al., Muscle and tendon interaction during human movements. Exerc Sport Sci Rev, 2002. 30(3): p. 106-10.
[2] Loram, I.D., C.N. Maganaris, and M. Lakie, Use of ultrasound to make noninvasive *in vivo* measurement of continuous changes in human muscle contractile length. J Appl Physiol, 2006. 100(4): p. 1311–23.
[3] Blemker, S.S. and S.L. Delp, Three–dimensional representation of complex muscle architectures and geometries. Ann Biomed Eng, 2005. 33(5): p. 661–73.
[4] H. Shi and T. Varghese, Two–dimensional multi-level strain estimation for discontinuous tissue, Phys. Med. Biol. (in press), 2006.

098 **CLINICAL BREAST ELASTOGRAPHY: BLINDED READER PERFORMANCE AND STRATEGIES FOR IMPROVING READER PERFORMANCE.**

B. S. Garra[1], L. M. Mobbs[1], C. M. Chant[1], J. Ophir[2].*
[1]University of Vermont College of Medicine & Fletcher Allen Health Care, Burlington, VT, USA; [2]The University of Texas Health Science Center at Houston, Houston, TX, USA.

Background: Elastography is gradually finding increasing application in the characterization of breast masses since the ability of the technique to distinguish benign from malignant breast masses was demonstrated nearly ten years ago. Over the past several years, we have been conducting a clinical trial to determine the usefulness of elastography as an adjunct to mammography and sonography for the characterization of breast masses. As part of that study, a blinded reader evaluation of the performance of elastography alone for distinguishing benign from malignant breast lesions is being conducted. We now report the first results from that evaluation.

Aims: To demonstrate in a larger number of patients, the performance of elastography alone as a means of classifying breast lesions as benign or malignant. Also to present some characteristic features of various types of masses and to illustrate some strategies to improve the performance of breast elastography in a clinical environment.

Methods: 115 biopsy proven breast masses were studied using elastography and sonography. The elastograms were acquired using a Philips HDI 1000 scanner using a 7.5MHz linear array transducer. Up to 28 frames of RF data were acquired to generate each elastographic image. Both frame held and hand held elastograms were acquired. The elastograms were generated and then subjected to wavelet filtration to reduce noise and artifacts. The resulting elastograms were presented side by side with the corresponding grayscale sonogram for review by a single experienced reviewer who was blinded to the actual sonograms and biopsy results. A level of suspicion score (LOS) was assigned to each lesion using a 100 point scale based upon three features subjectively evaluated by the observer. The features were: lesion hardness relative to the surrounding tissue, lesion border characteristics and the difference in apparent size of the elastographic lesion relative to the sonographic lesion. Also, the transverse maximum diameters of the lesion on both the elastogram and sonogram were measured and compared. ROC analysis was used to evaluate the performance of the features.

Results: The area under the ROC curve using LOS for all lesions was 0.84 which indicates moderate performance. Using an LOS of 60, sensitivity was 70% and specificity was 89.4%. This performance seemed to be related to including cases in which the sonographic lesion was not identified on elastograms. Including such cases resulted in several missed cancers. Looking at 102 cases where a lesion could be seen on the elastograms, the Az improved to 0.90, a significant improvement. Using lesion hardness score alone resulted in an ROC area (Az) of 0.85 for lesions visible on elastography whereas using lesion size difference alone resulted in an ROC area of only 0.81.

Conclusions: Our results indicate that lesion hardness estimates, though subjective and difficult to make, may be more useful than lesion size difference estimates for distinguishing cancers from benign lesions. Combining both features together is the most effective strategy for correctly classifying lesions as definitely benign without missing any cancers. Our study also indicates that it is important NOT to classify lesions as benign if they are not visible on the elastogram. Avoiding classification of such cases only reduced the number of cases that could be classified by about 11%. Hopefully further improvements in elastographic image quality will further reduce this percentage.

Acknowledgements: This work was supported by NIH/NIBIB Program Project Grant #8 P01 EB0022105.

033 **ROC ANALYSIS OF BREAST ULTRASOUND ELASTICITY IMAGING.**

Elizabeth S. Burnside[1], Timothy .J Hall[1] Amy M. Sommer[1], Gale A. Sisney[1], Gina K. Hesley[2], Nicholas J. Hangiandreou[2], William E. Svensson[3].*

[1]Medical Physics Department, University of Wisconsin, 1530 MSC, 1300 University Avenue, Madison, WI 53706, USA; [2]Mayo Clinic, Rochester, MN, USA; [3]Charing Cross Hospital, London, England, UK.

Background: Garra, et al., published in 1997 [1] results of a study of breast elasticity imaging involving a small number of cases and a single observer. That study suggested that mechanical strain imaging could provide new information that might improve breast tumor diagnosis. That study also suggested improvement that should be made in the imaging system and in the study. Most notably, it was suggested that real–time elasticity imaging would significantly improve the ease of use, and more observers studying a larger pool of data would add to the significance of their findings.

Aims: To retrospectively determine the accuracy of the ultrasound (US) strain imaging to differentiate benign and malignant breast masses and thereby improve the decision to biopsy.

Methods: Approval for the study was obtained from the Institutional Review Board and informed consent obtained from patients who participated in image acquisition. Strain imaging was performed on 444 breast lesions in 406 patients. Lesions were imaged using free–hand compression and a real–time strain imaging algorithm. The highest–quality 50 malignant and 50 benign lesions were selected for a reader study. Three observers blinded to pathologic outcomes first interpreted B–mode images using BI-RADS descriptors and provided a probability of malignancy. Then the readers viewed the strain image appearance, made measurements and provided an updated probability of malignancy. ROC curves were constructed for each observer using probabilities assessed without and with strain. The areas under these curves (AUC), sensitivity and specificity were calculated and compared. Inter–observer variability was evaluated. We also analyzed whether the correlation between an automated and a subjective quality assessment predicted reader performance.

Results: Each reader's AUC improved when strain imaging was used to assess the probability of malignancy. The average AUC after strain imaging was significantly better than after B–mode (0.872 versus 0.902, $P = 0.012$). Using a threshold of 2% probability of malignancy, as a group, specificity with strain improved significantly over B–mode alone (0.140 versus 0.191, $P < 0.0001$) while achieving high sensitivity (0.986 versus 0.993, $P = 0.32$). Statistically significant inter–observer variability was observed ($p < 0.001$). In addition, the ability to accurately assess image quality appeared to correlate with observer performance.

Conclusions: US strain imaging has the potential to aid in the discrimination of benign and malignant breast masses. However, inter–observer variability and image quality affect performance.

Acknowledgements: This study was funded in part by a grant from the US Army (DAMD17–00–1–0596) and the NIH (R01CA100373). In addition, collaborators at Mayo and Charing Cross received support from Siemens Medical Solutions Ultrasound Group. We are also grateful to Siemens for the equipment loans that made this work possible.

Reference:

[1] Garra BS, Cespedes EI, Ophir J, et al. Elastography of breast lesions: initial clinical results. Radiology 1997; 202:79–86.

041 **CYST CHARACTERIZATION VIA DIFFERENTIAL CORRELATION COEFFICIENT VALUES FROM 2D AND 3D BREAST ELASTOGRAPHY.**

Rebecca C. Booi[1], Paul L. Carson[1], Matthew O'Donnell[1], Marilyn A. Roubidoux[1], Anne L. Hall[2], Jonathan M. Rubin[1].*

[1]University of Michigan, Ann Arbor, MI, USA; [2]General Electric Healthcare, Milwaukee, WI, USA.

Background: Ultrasound is often used as a supplement to mammography for distinguishing breast lesions, particularly between cysts and solid masses. However, approximately 2% of masses which could be mistaken for complex cysts are malignant [1]. The echoes in most complex cysts are caused by small particulate matter and imaging artifacts such as sidelobes from neighboring regions, reverberations and electronic noise [2]. Sidelobes and reverberations move at different rates as the tissue is compressed and electronic noise is uncorrelated. Therefore, speckle tracking algorithms should track these echoes poorly, and the resulting correlation coefficient in a cyst should be considerably lower than in surrounding tissue.

Aims: The goal of this study was to evaluate whether the differences in the correlation coefficient, (R), between breast tissue and cysts could easily identify cysts within tissue. This additional source of cyst characterization might reduce the number of biopsies of complex cysts. The fidelity of this technique would be increased if relative R values between hypoechoic cancers and tissue exhibited different trends than cysts and tissue.

Methods: Experiments were conducted with a GE Logiq 9 scanner using a 1D array operating at 7.5 MHz as part of a combined US/tomosynthesis system. Six human subjects (with 6 cysts, 3 cancers) were imaged. All US data were obtained through a TPX 2.5 mm paddle, and subject breasts were compressed similarly to mammography. For 2D data acquisition, 90 radiofrequency (RF) images were acquired by further compressing the breast up to 10% strain over 2 seconds. In 3D, 5 RF images were acquired over 5 elevational samples at 0.4 mm spacing for up to 3% strain over 7 sec. Images were correlated using 2D and 3D phase–sensitive speckle tracking algorithms and displacement estimates were accumulated. R values were measured in the lesion and the tissue.

Results: All R values in the cysts were lower than surrounding breast tissue, as expected. These poorer correlations were caused by random signal in the cysts which quickly changed between pre–compression and post–compression images, and thus could not be tracked. Additionally, poorer cyst correlation was observed using 3D elasticity versus 2D. With 2D elasticity, R values in the cysts were 7–29% lower than in the tissue. These differences increased with 3D elasticity by 4–7%. Additional decorrelation in cysts from 2D to 3D imaging was due to the increased kernel size and scanning time (which increased patient motion) inherent in 3D elasticity imaging, both of which increased the randomness of the cyst signal and resulted in poorer R values. Conversely, 2 of the 3 hypoechoic cancers imaged in 2D in this study had R values less than 10% lower than surrounding tissue, and 1 of the 3 cancers had a greater R than tissue.

Conclusions: This study suggests that cyst characterization in breast tissue might be improved by evaluating differential R values determined by elasticity imaging. The somewhat poorer correlation coefficients seen with 3D elastography might be further accentuated by increasing the number of elevational samples. Relative to surrounding tissue, correlation in cysts in this study was poorer than in hypoechoic cancers, improving the robustness of this technique. More human subjects will be evaluated in the future to verify these trends. Additional factors of cyst characterization, such as signal level and increased through–transmission, could be combined with differential correlation values for improved cyst identification.

Acknowledgements: Supported in part by NIH Grants R21–CA109440 and RO1–CA91713.

References:

[1] Louie L, Velez N, Earnest D, Staren ED. Management of nonpalpable ultrasound – indeterminate breast lesions. Surgery. 2003 Oct;134(4):667–73.

[2] Stavros, AT. Breast Ultrasound. Lippincott Williams & Wilkins; 2004.

** indicates Presenter*

042 **LIVER STIFFNESS MEASUREMENT IN MORBID AND MALIGNANT OBESITY BY TRANSIENT ELASTOGRAPHY.**

Véronique Miette[1], Céline Fournier[1], Laurent Sandrin[1].*
[1]Echosens, Research and Development Department, 153 avenue d'Italie, 75013 Paris, FRANCE.

Background: Fibroscan® (Echosens, Paris, France) [1] is based on transient elastography. This novel non-invasive and rapid device is used to assess liver fibrosis by measuring liver stiffness in adult patients. A limitation of Fibroscan®, like in other ultrasound techniques, is obesity. Soft tissue characteristics including absorption, aberration and reverberation determine the reliability of the elastographic results [2].

Aims: The purpose of this study was to improve and to evaluate the diagnosis accuracy on patients with morbid obesity defined as a body mass index (BMI) greater than or equal to 40 (BMI 40+) and malignant obesity (BMI 50+).

Methods: 27 patients (67% men, 33% women, median age 51.7 years (33 to 76 years), BMI 25 to 53 with chronic liver disease were prospectively included. Liver stiffness measurements were performed with a standard probe including a 3.5 MHz transducer and a dedicated probe with a 1.75 MHz transducer.

Measurements were obtained for each subject on the right lobe of the liver with both probes. The operator located a portion of the liver that was at least 4 cm thick and free of large vascular structures. The examiner took the measurements with the probe placed over the intercostal space and stopped the examination when 8 valid measurements or when 20 invalid measurements were obtained. Both entire examinations lasted approximately 15 minutes.

During a second step, the echo signals acquired were analyzed: cross–correlation data analysis and image processing were performed. Taking the abdominal wall thickness into account, the measurement depths were automatically adjusted between 20 and 120 mm.

Results: We noted that the new method improves the quality of the elastogram. A total of 718 measurements were performed. We note that the success rate (ratio of the number of valid measurements to the total number of measurements) was improved: 28% in the standard case and up to 41% with new algorithms and dedicated probe.

Conclusions: About 90% of morbidly obese patients show histological abnormalities of the liver and morbid obesity alone may lead to severe disease showing all the features of alcoholic hepatitis and may end in cirrhosis and liver failure. This study showed that obesity is no impediment to the FibroScan® examination, even with a BMI of up to 40.

Figure 1: Example of stiffness measured at a depth between 64 to 103 mm on patient with malignant obesity (BMI 53) and cirrhosis.

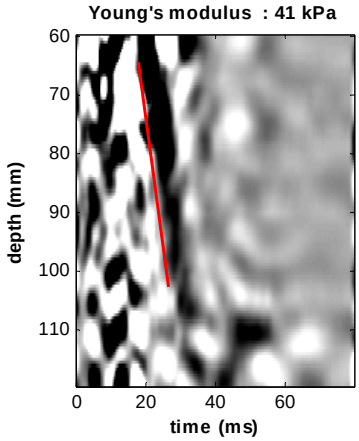

Acknowledgements: We thank Prof. Mathurin, Dr. Canva and Dr. Hollebecq, Service Hépathologie et Gastroenterologie, Hôpital Claude Huriez, CHRU de Lille, France.

References:

[1] Sandrin L et al, Transient elastography: a new non invasive method for assessment of hepatic fibrosis, Ultrasound in Medicine and Biology 2003;29(12):1705-1713.
[2] Hinkelman L et al, Measurements of ultrasonic pulse arrival time and energy level variations produced by propagation through abdominal wall, J. Acoust. Soc. Am. 95(1), January 1994 530:541.

100 **STRAIN CONTRAST FOR *IN VIVO* BREAST TISSUE.**

Amy M. Sommer[1], Timothy J. Hall[1], Elizabeth S. Burnside[1], Jingfeng Jiang[1].*
[1]University of Wisconsin–Madison, Madison, WI, USA.

Background and Aims: Our goal was to objectively study lesion contrast in elasticity images to aid in the diagnosis of a lesion as malignant or benign. Subjective analysis of a sequence of elasticity images of *in vivo* breast tissue suggests that many fibroadenomas (FA) lose contrast as deformation increases, although contrast for invasive ductal carcinomas (IDC) remains relatively constant.[1]

Methods: Radiofrequency (RF) echo data was acquired from a Siemens Elegra with real–time freehand elasticity imaging of *in vivo* breast tissue. An offline 2–D block matching algorithm was used to estimate tissue displacements and strain for a sequence of data. A reference frame in the sequence was chosen and the displacement field for each frame of RF data was used to warp that RF field back to the coordinate system of the reference frame. An area of fat within the reference frame was identified and manually traced by a radiologist. The lesion boundary was automatically segmented in the reference frame. Strain image contrast for the lesion was computed relative to the entire background and relative to fat for each frame in the sequence. Both elasticity contrasts were then plotted as a function of accumulated frame–average strain. This procedure has been performed so far for 13 FAs and 7 IDCs.

Results: The mean contrast relative to the entire background for FAs (0.67±0.12) is typically lower than for IDCs (0.72±0.07). The same is true for the mean contrast relative to fat for FAs (0.67±0.18) and IDCs (0.76±0.10). However, at the lowest deformation the FA contrast relative to the entire background (and relative to fat) is high and is comparable to that of IDCs. The FA contrast relative to the entire background (as well as relative to fat) often changes by 0.2 or more over approximately 10% accumulated frame–average strain, while the IDC contrast relative to the entire background (as well as relative to fat) remains reasonably constant over the same deformation range, with IDC contrast never changing by more than 0.18.

Conclusions: Calculating lesion contrast relative to the entire background leads to difficulties in comparing data sets, since the amount of glandular tissue and fat varies among patients. Initial studies show that calculating contrast relative to fat provides a slight advantage over calculating contrast compared to the entire background. Figures 1 and 2 show the advantage of calculating the contrast relative to the fat (dashed line) compared to calculating the contrast relative to the entire background (solid line) versus the accumulated strain for a FA and an IDC respectively. Strain image contrast for a single frame does not provide enough information to distinguish between benign and malignant lesions. Lesion contrast varies significantly with increasing deformation for *in vivo* FAs while staying relatively constant for *in vivo* IDCs. Elasticity contrast for a sequence of frames obtained over a range of deformations provides additional information for distinguishing between the most common solid benign and malignant lesions.

Acknowledgements: We are grateful for the support from the NIH (R01–CA100373), and to colleagues at the Mayo Clinic in Rochester, MN, USA, and the Charing Cross Hospital in London, UK for providing some of the data used in this study.

Reference:

[1] Hall, T.J., Zhu Y., Spalding C.S. *In vivo* real–time freehand palpation imaging. Ultrasound in Medicine & Biology 2003; 29(3): 427–35.

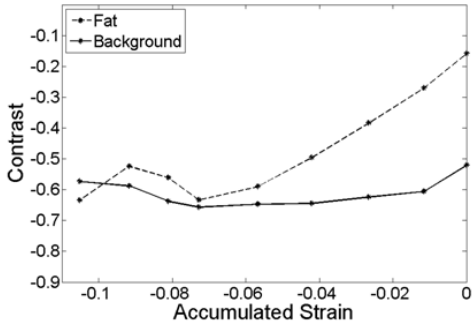

Figure 1: Fibroadenoma

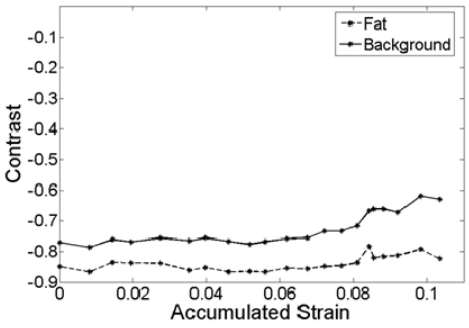

Figure 2: Invasive Ductal Carcinoma

* *indicates Presenter*

065 **HIGH RESOLUTION MAGNETIC RESONANCE ELASTOGRAPHY AT 7T: APPLICATION TO RHEOLOGY.**

B. Larrat[1], R. Sinkus[1], M. Tanter[1], M. Fink[1].*
[1]Laboratoire Ondes et Acoustique, ESPCI, 10 rue Vauquelin, 75005 Paris, FRANCE.

Background: The number of clinical applications for elastography as a new imaging modality is constantly growing [1]. The rheology of tissue is, however, far more complicated than a simple parallel arrangement of one spring with one dashpot [2]. In order to obtain maximum diagnostic gain from viscoelastic information, it is necessary to use the correct rheological model for the interpretation of the complex shear modulus G* in terms of solid and liquid component. This necessitates the measurement of G* within a reasonable bandwidth 1) for model identification and 2) for tissue characterization.

Aims: We propose to use a high-field MRI animal scanner for the assessment of the frequency–dependent behavior of G*. Experiment on living rats, *in–vitro* tissue specimens and various phantom materials were performed.

Methods: A 7 Tesla MRI-system (PharmaScan, Bruker, Ettlingen, Germany) with horizontal bore was utilized. A piezoelectric plate (PiezoSystems) with resonance frequency at 60Hz was used for mechanical excitation. The plate was mounted underneath the object of interrogation (Figure1a) leading to a compressional mode of excitation (up-down vibration). A modified spin–echo sequence with sinusoidal motion encoding gradients was used. The sequence was phase–locked to the mechanical excitation frequency. Given the small bore size, gradient strengths up to 300mT/m could be used. This allows visualization of wave–amplitudes as small as 100nm at in–plane resolutions of ~100µm. Experiments were performed between 100–800 Hz.

Results: Good wave penetration was observed in both *in–vitro* and *in–vivo* brain tissue (Figure 1b & c) at spatial resolutions down to 500µm in-plane (1mm through–plane). Figure 1d shows the reconstructed dynamic modulus (Gd) and loss modulus (Gl) of the complex shear modulus between 200Hz and 600Hz for *in–vitro* bovine liver tissue. We observe a power–law for the frequency behavior for Gd and Gl (i.e. $\sim\omega^{\alpha}$, $\alpha\sim0.9$) which is in agreement with the so–called spring–dashpot model. It is however noticeable, that the ratio of Gl/Gd does not follow the predictions of the spring–dashpot model. We find $Gl/Gl=\tan(0.5\pi*0.2)$ which is not equal to $\tan(0.5\pi\alpha)$ as expected from simple calculations [3]. These values are similar to what we measured in lamb brain tissue *in–vitro*.

Conclusions: The high resolution MRI system allows investigating the rheological properties of tissue over almost one order of magnitude in frequency (100–1000Hz). Thereby, the validity of various rheological models can be studied with absolute quantities in an unbiased manner (contrary to other techniques, like MTC [4]). Already at this level we observe deviations from theoretical predictions like the spring–dashpot model. This necessitates the development of new rheological models.

References:

[1] Huwart, L. *NMR Biomed.* 19(2), 173–179 (2006).
[2] Verdier, C. *Journal of Theoretical Medicine* 5(2), 67–91 (2003).
[3] Schiessel, H. et al. *J. Phys. A: Math. Gen.* (28), 6567–6584 (1995).
[4] Fabry, B. *Physical Review E.* (68), 041914 (2003).

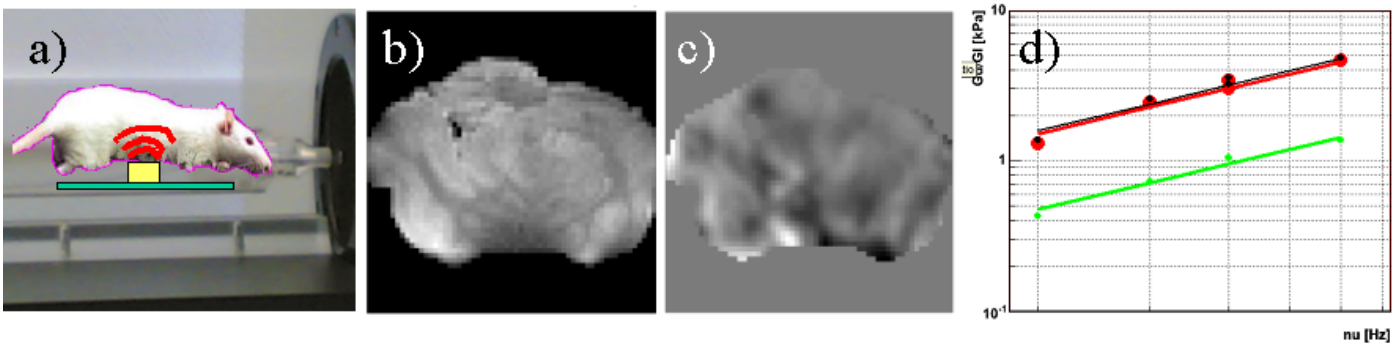

Figure 1: Experimental setup (a) for *in–vivo* and *in–vitro* experiments at the 7T horizontal MRI system. The object rests on the piezo-transducer, which vibrates in the up–down direction. *In–vitro* experiments with lamb brain [b): magnitude MR image, c): y-component of curl] showed very good wave penetration at 100Hz. d) Dynamic modulus (red) and loss modulus (green) as a function of frequency (200-600 Hz) for liver tissue *ex–vivo*. The absolute value of the complex shear modulus is shown in black.

* *indicates Presenter*

068 ***IN VIVO* 3D ELASTOGRAPHY OF INDUCED SKELETAL MUSCLE CONTRACTION.**

RGP Lopata[1], MM Nillesen[1], JP van Dijk[2], IH Gerrits[1], JM Thijssen[1], CL de Korte[1].*
[1]Clinical Physics Laboratory; [2]Department of Clinical Neurophysiology, Radboud University Nijmegen Medical Centre, Nijmegen, The NETHERLANDS.

Background: Cardiac strain imaging using real–time 3D ultrasound is a promising technique for early non–invasive diagnosis of congenital heart disease and/or heart failure. The 3D deformations and high heart rates can cause severe limitations to the accuracy of strain estimates. The contraction/relaxation cycle of the heart cannot be controlled. In neuro–physiological research, controlled contraction of skeletal muscle tissue is achieved using electrical stimulation. However, depending on the level of contraction, the imaging technique still requires a high frame rate. BiPlane imaging is a fast semi 3D imaging technique that enables strain estimation in 2 orthogonal planes.

Aims: In this study, 3D elastography of actively contracting skeletal muscle tissue is examined by determining strain in 3 orthogonal directions using BiPlane Imaging for normal and athletic volunteers.

Methods: Raw (rf) ultrasound data were acquired with a Philips SONOS 7500 live 3D ultrasound system, equipped with a X4 matrix array transducer and an RF–interface. An iterative 2D coarse–to–fine strain algorithm was implemented to estimate displacements in both orthogonal planes. Sub–sample and sub-line resolution was obtained by 2D parabolic interpolation of the data [1]. Elastograms were generated using a LSQ strain estimator. Triggered BiPlane imaging was performed during excitation of the left tibialis anterior (TA) muscle using a single pulse electrical stimulation of the peroneal nerve. The TA in the lower leg was chosen for its compact size and superficial position. Both isometric contraction (using a force transducer) and surface electromyography (EMG) were measured simultaneously and synchronized with the ultrasound data. Two normal volunteers and one endurance athlete were examined. After empirically finding the maximal stimulation level for each person (based on EMG), the level of stimulation was lowered stepwise until no or only little contraction was observed. The frame-to-frame deformation of the muscle during one contraction / relaxation cycle was measured twice for all subjects and compared with results of the force and EMG measurements.

Results: Using the iterative algorithm with 2D parabolic interpolation, axial and lateral displacements were estimated for a window of 0.60 mm (starting with a window of 2.40 mm and with an overlap of 50%). The axial and lateral elastograms were computed in both planes using the measured frame-to-frame displacements. Cumulative axial and lateral strain curves were obtained for manually segmented regions-of-interest (excluding bone and other tissue). The shape of the axial and lateral strain curves matched the measured force curve in both planes and corroborated isovolumetric contraction. Lateral expansion was observed in the cross–sectional plane, whereas contraction parallel to the muscle fibers was found. The endurance athlete revealed significantly higher maximum strain values (18% axial strain) than the untrained volunteers (6% axial strain). An excellent correlation between electrical stimulation and maximum strain in the muscle was found. For very low electrical stimulations, this correlation was weak; at lower excitation levels fewer motor units are stimulated and thus different parts of the muscle are excited.

Conclusions: Fast 3D Strain estimation using BiPlane imaging of actively contracting skeletal muscle tissue in a controlled environment is feasible.

Acknowledgements: The support of the Dutch Technology Foundation (STW) is acknowledged.

References:

[1] Lopata R.G.P. et al; *In Vivo* 3D Cardiac Elastography in an Animal Model and Human Heart, Proc. of The 5th Interl. Conf. On the Ultrasonic Measurement and Imaging of Tissue Elasticity. Snowbird, Utah, USA, p 75, Oct. 2006.
[2] Kallel, F. and Ophir, J.: A least squares estimator for elastography. Ultrasonic Imaging, Vol. 19 (3), pp. 195-208, 1997.

** indicates Presenter*

071 **THREE-DIMENSIONAL SONOELASTOGRAPHY FOR THERMAL LESION DETECTION IN AN *IN VIVO* SWINE MODEL.**

M Zhang[1], B Castañeda[1], J Christensen[1], W Saad[1], DJ Rubens[1], KJ Parker[1].*
[1]University of Rochester, Rochester, NY, USA.

Background: In the last two decades sonoelastography has been tested and verified in theoretical studies, acoustical phantoms, and thermal ablation studies in liver tissue *in vitro*. Radio frequency ablation (RFA), a minimally invasive thermal therapy, has been under investigation as an alternative to surgery for treating liver tumors. This study investigates the feasibility of detecting RFA lesions using *in vivo* 3D sonoelastography, which presents unique imaging challenges due to respiratory and cardiac motion. Furthermore, establishing efficacy in an *in vivo* animal model is an important step towards clinical implementation in humans.

Aims: To investigate the detectability of *in vivo* thermal lesions in porcine liver using real–time 2D and 3D sonoelastography.

Methods: The pig is anesthetized, and the abdomen is prepared and draped in the standard surgical manner. The liver is exposed through a midline incision. A RFA needle is then inserted into the porcine liver under ultrasound guidance. A lesion is created about 1 cm beneath the liver surface. Two mini–shakers (Bruel & Kjaer, Denmark) are applied on the liver surface. A sonoelastography volume is generated by acquiring a series of 2D images using a motorized tracking device (Velmex Inc., Bloomfield, NY). After *in vivo* imaging, the animal is sacrificed, and the liver is excised for *ex vivo* study. RFA lesions are harvested and measured with calipers and fluid displacement. The elastic contrast between the RFA lesion and untreated liver is obtained by viscoelastic testing.

Results: A total of twelve RFA lesions were created in three porcine livers, with volumes ranging from 0.2 cc to 3 cc. Preliminary results showed good correlation of lesion dimensions and volume between sonoelastography images and gross pathology for lesions of different sizes. For instance, the volume of a RFA lesion measured by fluid displacement was 3.0 cc while the sonoelastography volume of the same lesion was 2.94 cc. Figures 1 and 2 show the B–mode and sonoelastography image of a 1.5 cc lesion. Its major axes are 14.87 mm and 10.52 mm when measured in the sonoelastography image, while in gross pathology (Figure 3), they are 14.78 mm and 10.57 mm, respectively. An RFA lesion as small as 0.2 cc was also detected successfully *in vivo*.

Conclusions: Preliminary results show good correlation between 3D sonoelastography and gross pathology, supporting the feasibility of sonoelastography for lesion detection and volume estimation. *In vivo* 2D sonoelastography images of different-sized RFA lesions were acquired, showing the potential of sonoelastography as a real–time method to accurately monitor thermal therapy of tumors. More experiments are ongoing to advance our results.

Acknowledgements: This study was supported by Fischer Fund Grant 4-50275.

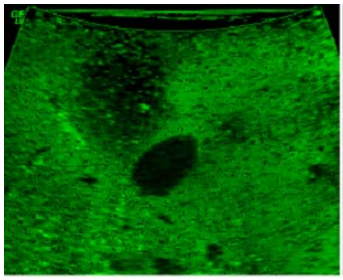

Figure 1: Sonoelastography image of an RFA lesion *in vivo*.

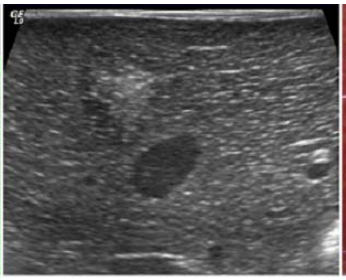

Figure 2: Corresponding B–mode image of the lesion.

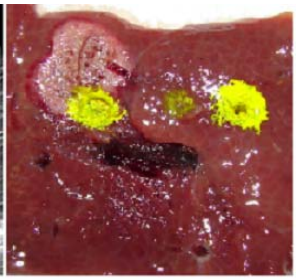

Figure 3: Gross pathology of the lesion.

004 **EFFICIENT ELIMINATION OF DROPOUTS IN DISPLACEMENT TRACKING.**

GM Treece[1], JE Lindop[1], AH Gee[1], RW Prager[1].*
[1]Department of Engineering, University of Cambridge, Cambridge, England, UK.

Background: Many ultrasound strain imaging techniques rely on estimating the relative displacement of pre– and post–deformation signals by maximizing a correlation–based measure. Exhaustive search is slow, particularly when using long windows to reduce noise. Reducing the search range by initializing with a previous displacement estimate speeds up computation, but can cause the search to converge one or more wavelengths of the probe center frequency from the correct location. Searching for the phase zero of the complex correlation [1] is very time–efficient, but implicitly limits the search range to one wavelength. Estimation errors lead to subsequent estimates tracking the phase zero at one or more wavelengths from the correct zero. Strain values derived from such estimates contain considerable noise, and, therefore, result in distinctive 'dropouts' in strain images based on the phase–zero method (Figure 1c).

Aims: To combine the efficiency of phase–zero tracking with the stability of an exhaustive search.

Methods: Rather than calculating displacement for each RF vector in turn, we calculated displacements row-wise for all RF vectors, gradually working down the ultrasound image (Figure 1a). At each stage, we stored the correlation (or SNR, or an estimate of SNR) at the eventual estimated location. We chose as our initial displacement estimate the displacement from a small range of vectors (typically ±2) in the previous row with the highest stored correlation. Very rarely, displacement estimates can be improved by repeating the process in the upward direction, at each point preserving displacements with the highest correlation from each pass.

Results: Figures 1 and 2 show typical *in vivo* and *in vitro* results using a 5–10MHz linear probe with a freehand protocol. Dropouts are eliminated from all of the 200 or so frames from each of these data sets. Only one phase–zero update is required per displacement estimate; by contrast the CA method [2] requires repeated phase–zero estimates at ½ wavelength spacing. The technique can also correct frames containing very little other than dropouts (Figure 2); this is not possible by the use of a median filter [3].

Conclusions: This method allows very fast phase–zero displacement tracking algorithms to be implemented, with very little additional overhead, whilst eliminating error propagation.

Acknowledgements: Graham Treece is supported by a Royal Academy of Engineering/EPSRC Research Fellowship.

References:

[1] JE Lindop, GM Treece, AH Gee and RW Prager, 3D Elastography Using Freehand Ultrasound, Ultrasound Med Biol 37 (4), 529–545 (2006).
[2] M Yamakawa and T Shiina, Strain Estimation Using the Extended Combined Autocorrelation Method, Jpn J Appl Phys 40, 3872–3876 (2001).
[3] Y Zhu and TJ Hall, A Modified Block Matching Method for Real–Time Freehand Strain Imaging, Ultrasonic Imaging 24, 161–176 (2002).

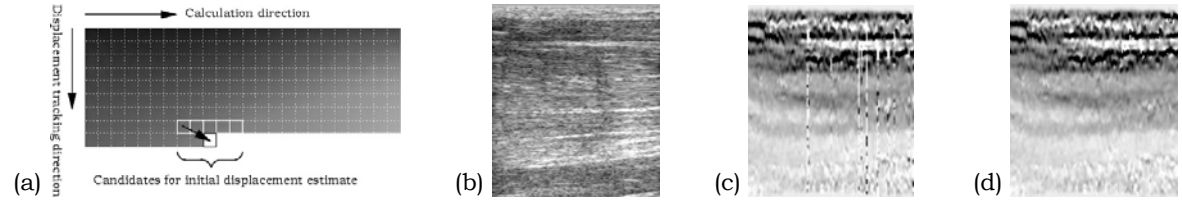

Figure 1: The ordering and initialization of displacement estimation (a), a B–scan of the upper arm (b), a corresponding strain image showing typical dropouts (c), and the dropouts are eliminated with negligible overhead (d).

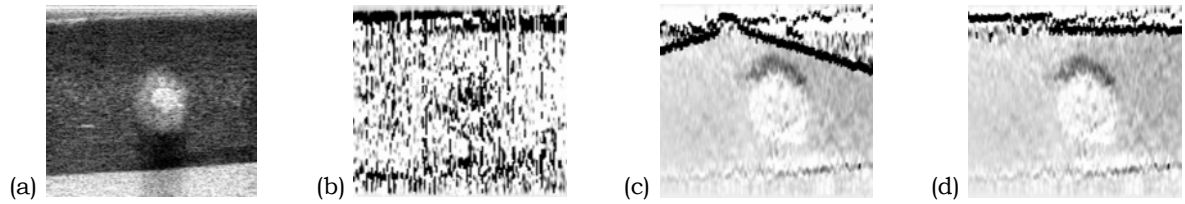

Figure 2: A B–scan of an olive embedded in jelly mixed with flour (a), the strain image completely obliterated by dropouts (b), the new algorithm revealing real strain data (c), a second upward pass eliminates dropouts entirely (d).

* *indicates Presenter*

088 **RESOLUTION OF AXIAL–SHEAR STRAIN ELASTOGRAPHY.**

A Thitai Kumar[1,2], R Righetti[1], J Ophir[1,2] and TA Krouskop[1,3].*
[1]The University of Texas Health Science Center Houston Medical School, Houston, TX, USA; [2]University of Houston, Houston, TX, USA; [3]Baylor College of Medicine, Houston, TX, USA.

Background: In conventional elastography, a quasi–static axial compression is applied to a tissue region, and the resulting local axial strain is estimated. The axial strain is estimated as the gradient in the axial direction of the axial displacements. If the gradient of the axial displacements is taken along the lateral direction, an estimate of the local axial–shear strain is obtained. This technique of mapping the local axial–shear strain due to quasi–static axial compression is defined as axial–shear strain elastography. The investigation of the spatial resolution of axial–shear elastography using a simulation study is presented here.

Methods: The resolution of axial–shear strain elastography was investigated using a single inclusion model, i.e., an elastically stiff lesion embedded in a homogeneously softer background. Resolution was defined as the smallest size of the inclusion for which the strain value at the inclusion/background interface was greater than a threshold, set as the average of the axial–shear strain value at the interface and the axial–shear strain inside the inclusion. The resolution was measured from the axial–shear strain profile oriented at 45º to the axis of beam propagation, due to the absence of axial–shear strain along the normal directions. The effects of the ultrasound (US) system parameters, such as bandwidth, beamwidth and pitch, along with signal processing parameters, such as correlation window length (W) and axial shift (ΔW) on the estimated resolution, were investigated.

Results: The results of this study showed that the resolution of axial–shear strain elastography (at 45º orientation) is determined by the bandwidth and the beamwidth. Interestingly, when the cross-correlation window length is scaled inversely to the bandwidth, the upper bound on the resolution is limited by the larger of the window length and the beamwidth (Figure 1). The results also showed a linear dependence of the resolution on the pitch (Figure 2). For a given US system, however, the resolution upper bound can be compromised by the choice of signal processing parameters.

Conclusions: We have shown that the resolution of axial–shear strain elastography in a direction oriented at 45º to the axis of the beam propagation is limited by the larger of the beamwidth and the window length. This was the case when the window lengths were scaled inversely to the bandwidth. We have also shown that for given values of beamwidth, pitch and bandwidth, the achievable resolution is limited by the window length used. The axial shift was found to have a weak influence on the results.

Acknowledgements: This work was supported in part by NIH program project grant P01–EB02105–13 awarded to the University of Texas Health Science Center Houston Medical School.

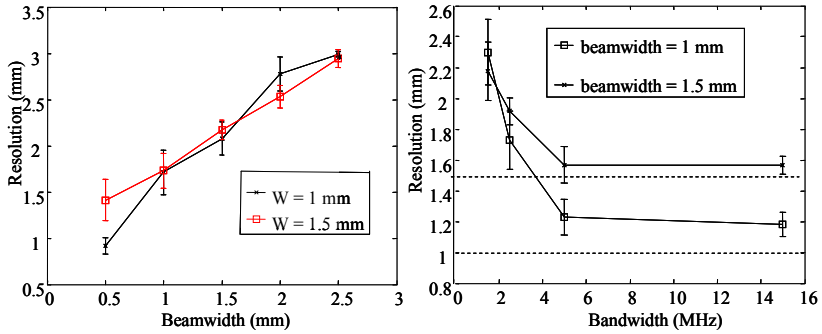

Figure 1: Estimated elastographic resolution (mm) as a function of beamwidth (a) and -3 dB bandwidth (MHz) (b). To obtain the plot in (a), the data were simulated for 5 MHz center frequency transducer, 50% fractional bandwidth and a 70% beam overlap. To obtain the plot in (b), the data were processed using a cross–correlation window length W=5λ while the beamwidth was maintained at 1 mm and ΔW= 0.2 W. The window length (in mm) corresponding to the bandwidth used are 2.5 mm, 1.5 mm, 0.75 mm and 0.25 mm.

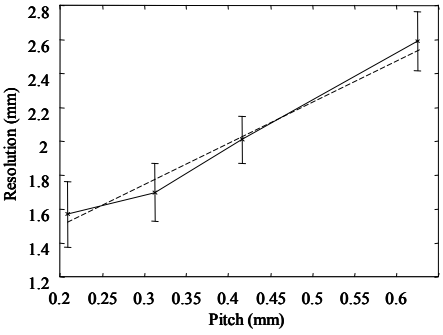

Figure 2: Estimated axial–shear strain elastographic resolution (mm) as a function of pitch (mm). The data were simulated for 5 MHz center frequency transducer and 50% fractional (-3 dB) bandwidth. The beamwidth was set at 1 mm. The data were processed with a window length W = 1 mm and window shift ΔW= 0.2 W.

001 **A NOVEL REAL–TIME SPECKLE TRACKING ALGORITHM USING DYNAMIC PROGRAMMING.**

J Jiang[1], TJ Hall[1].*
[1]Medical Physics Department, University of Wisconsin–Madison, Madison, WI, USA.

Background and Aims: Although tissue elasticity imaging appears to be quite promising clinically, the ability to accurately track *in vivo* tissue motion is still somewhat limited. This study is intended to develop a robust algorithm for real–time ultrasonic strain imaging using dynamic programming techniques.

Methods: From basic physics we know that tissue motion under external mechanical stimuli should be highly continuous. Therefore, the speckle tracking problem fits well within the general framework of the hidden Markov model and can be solved as an optimization problem. A dynamic programming technique [1] with a cost function combining correlation and motion continuity was used to regularize motion tracking. We have modified the classic 2–D block-matching algorithm to implement this idea. To achieve real–time performance, the dynamic programming regularization was only applied to a column of displacement data (the initial search) that is typically located at the center of the region of interest. Following the initial search, displacement estimation on either side of the initial column can be split into independent tasks for parallel processing under the guidance of its neighboring estimates.

Results: Radiofrequency (RF) echo data acquired from a Siemens Elegra with freehand scanning of *in vivo* breast tissue [2] and tissue mimicking phantoms were used to validate this algorithm. We found that the new algorithm provides more accurate displacement estimates than our previous algorithm for *in vivo* clinical data. In particular, the new algorithm is capable of tracking larger frame–average tissue deformation (~1-2%), thereby increasing strain image consistency in a sequence of images. The new algorithm can also tolerate larger local strain (~10%). Preliminary results also suggest that a significantly longer sequence of high contrast strain images (e.g. 45 vs. 15 in one cancer dataset) could be obtained with the new algorithm compared to the previous algorithm [3]. We also achieved more than 12 frames/second with a 3 cm x 3 cm region of interest, which is sufficient to provide real–time feedback during *in vivo* elasticity imaging.

Conclusions: A computationally efficient speckle tracking algorithm using dynamic programming is presented here, and our results are encouraging. We anticipate that this algorithm can significantly enhance the clinical utility of ultrasonic strain imaging system clinically by consistently providing high quality strain images.

Acknowledgements: This work is supported in part by grants from NIH–R01CA100373 and the University of Wisconsin–Madison.

References:

[1] A. J. Viterbi, “Error bounds for convolutional codes and asymptotically optimum decoding algorithm,” IEEE Transactions on Information Theory, vol. 13, pp. 260–269, 1967.
[2] T. J. Hall, Y. Zhu, and C. S. Spalding, "*In vivo* real–time freehand palpation imaging," *Ultrasound in Medicine & Biology*, vol. 29, pp. 427–35, 2003.
[3] Y. Zhu and T. J. Hall, "A modified block matching method for real–time freehand strain imaging," *Ultrasonic Imaging*, vol. 24, pp. 161–76, 2002.

* *indicates Presenter*

006 **RF SIGNAL PROCESSING USING FAST GAUSS–NEWTON OPTIMIZATION.**

J Fehrenbach[1], R Souchon[2].*
[1]Laboratoire MIP, Toulouse, FRANCE; [2]INSERM U556, Lyon, FRANCE.

Background: RF signal processing in elastography is usually performed using 1–dimensional cross-correlation algorithms between pre– and post–compression images. The displacement of each point of the tissue is estimated independently of its neighbors.

Aims: Our objective is to propose and evaluate an algorithm for displacement estimation that uses the 2-dimensional structure of the image. Because the displacement field in tissues is continuous, and most of the time smooth, we want to include this a–priori information in our algorithm.

Methods: The algorithm we propose is based on a Gauss–Newton least squares minimization, similar to the method described for a different purpose in [1]. Control points are placed in the domain, once their displacement is known we model the displacement of other points in the domain using bilinear interpolation. The displacement of the control points to be estimated is the displacement that minimizes a cost function. Our cost function is the squared difference between the post–compression signal and the pre–compression signal transported by the displacement field. A second term added to this cost function is a regularization term, and ensures that the displacement field will be smooth enough.

Results: When applied to synthetic data, our algorithm provides interesting results. Compared to a standard cross–correlation algorithm, for a suitable choice of parameters, both the elastographic signal-to–noise ratio (SNRe) and the spatial resolution are improved. For an application to real data, we present qualitative results that show that our method gives less noisy displacement estimates. Moreover, when only axial displacements are to be estimated, our algorithm has an efficient computation time (a few seconds for a non–optimized implementation).

Conclusions: We propose a 2–dimensional algorithm for displacement estimation. This algorithm seems to be promising, in the sense that it provides good spatial resolution and high SNRe as compared with standard cross–correlation algorithms. It should be evaluated on a wider set of real data; this evaluation should include quantitative comparison with traditional algorithms.

Acknowledgements: We thank Jean–Luc Gennisson (LOA, Paris, France) for providing us with the dynamic data. This work was supported in part by the National Cancer Institute (USA) Program Project Grant P01–CA64597 to the University of Texas Medical School at Houston; and by the ACINIM CNRS Project (France).

Reference:

[1] J Fehrenbach, M Masmoudi, R Souchon, P Trompette, Detection of Small Inclusions by Elastography, Inverse Problems 22 (2006), pp.1055–1069.

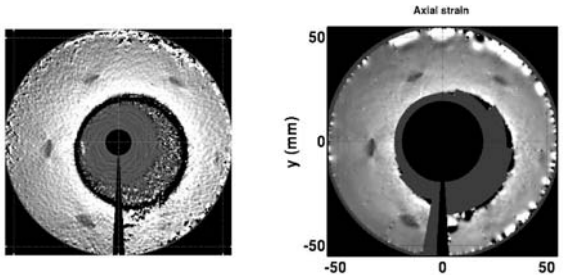

(a) (b)

Figure 1: Elastograms obtained by Radial Elastography
(a) cross–correlation method
(b) our method

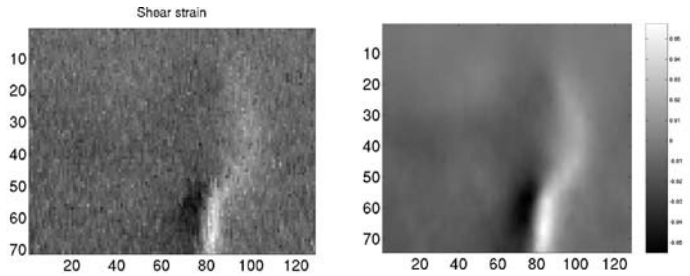

(a) (b)

Figure 2: Snapshots from a sequence of Dynamic Elastography
(a) cross–correlation method
(b) our method

054 **DISPLACEMENT ESTIMATORS IN ULTRASONIC ELASTOGRAPHY FOR FINITE DEFORMATIONS.**

Walaa Khaled[1], Stefan Reichling[2], Otto T. Bruhns[2], Helmut Ermert[1].*
[1]Institute of High Frequency Engineering; [2]Institute of Mechanics, Ruhr–University Bochum, Bochum, GERMANY.

Background: Mechanical properties of biological tissue represent important diagnostic information and are of histological and pathological relevance. In order to obtain the mechanical properties of tissue non-invasively, we developed a real–time strain imaging system for clinical applications. The output data of this system also allow an inverse elastography approach leading to the spatial distribution of the relative shear modulus of tissue. The elastography system calculates the displacements of an axially compressed medium by calculating delays from the ultrasonic echoes. The most commonly used techniques are based on cross–correlation methods (e.g. Phase Root Seeking (PRS) [1]). These were shown to be accurate but are heavily dependent on the compression magnitude and echo decorrelation.

Aims: In case of deformations larger than 1% cross–correlation methods based on radio–frequency (RF) data fail to estimate the correct displacement of the deformed tissue (Figure 1). A number of other techniques for the estimation of displacement based on Block Matching (e.g. Sum Absolute Differences (SAD)) have been explored [2]. As RF data is rarely available in conventional ultrasound machines, we propose in this work a strain imaging method using base–band envelope data. The envelope signals can be digitized at a lower sampling rate, and they require less storage and processing time. In this presentation the feasibility and accuracy of envelope data based strain imaging is extensively explored.

Methods: An inhomogeneous tissue phantom with a stiff cylindrical inclusion was used. The phantom was subjected to an initial deformation. A displacement of 20 mm (equivalent to 5% deformation) was applied in 20 steps. The elastograms were generated from RF data collected with a 9 MHz linear array transducer of the Siemens Sonoline machine with a conventional A/D board at a sampling frequency of 50 MHz and base–band data using PRS and SAD algorithms.

Results: The feasibility of these estimators was demonstrated using the measured real time ultrasound data of the tissue–mimicking phantom with a single and a double inclusion. The error calculated between simulated data and calculated results for the PRS was higher with increasing compression. However, using the SAD method combined with large deformations shows a very stable estimation of displacement. The feasibility of these methods was demonstrated using the measured real time ultrasound data of a tissue–mimicking phantom with a single and a double inclusion. The proposed methods appear promising for the qualitative differential diagnosis of lesions in the tissue.

Conclusions: The outcomes show that, especially in the case of compressions larger than 2%, block matching methods are more appropriate as a tissue displacement estimator.

Acknowledgements: This project is supported from the DFG (German Research Foundation; project ER 94/30–1)

References:

[1] Pesavento, A.; Perrey, C.; Kruger, M.; Ermert,.H.: A time–efficient and accurate strain estimation concept for ultrasonic elastography using iterative phase zero estimation. IEEE Trans. UFFC. Vol. 46 (1999), pp. 1057–1067.
[2] Lubinski, M.A.; Emilianov, S. Y.; O'Donnell, M.: Speckle tracking methods for ultrasonic elasticity imaging using short time correlation. IEEE Trans. UFFC. Vol.46 (1999) pp. 82–96.

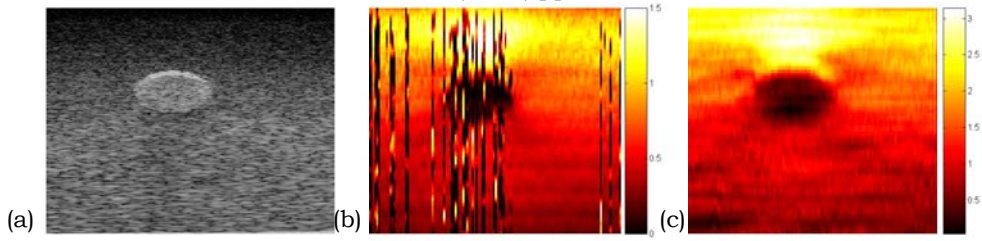

Figure 1: Tissue–mimicking phantom of PVA with a stiff cylindrical inclusion:
(a) B–mode image
(b) strain images calculated using the PRF algorithm at 1.5% deformation
(c) the 2D–SAD algorithm at 3% deformation

* *indicates Presenter*

057 **APPLICATION OF 2–D OPTIMIZED STRAIN ESTIMATION ALGORITHM TO DEFORMATION IMAGING OF BOVINE LIVERS *IN VITRO*.**

Elisabeth Brusseau[1], Jean–François Déprez[1], Olivier Basset[1].*
[1]CREATIS UMR CNRS 5515 INSERM U630, Lyon, FRANCE.

Background: In elastography, strain distribution needs to be estimated with high accuracy since clinician's interpretation and mechanical parameter reconstruction will be directly related to those estimations. Recently, we developed a 2–D strain estimation technique [1] that computes optimal deformation parameters through the constrained maximization of a similarity criterion. Encouraging initial data from simulations and phantom experiments were presented.

Aims: The objectives of this work are to assess the performance of the developed algorithm to image deformation of biological tissues and to correct the estimator accordingly if necessary.

Methods: The 2–D iterative and adaptive strain estimator described in [1] assumes that the physical compression of the medium results, within acquired RF images, in 2–D acoustical footprints that are axially time–delayed and scaled, as well as laterally shifted. Optimal parameters are estimated as the arguments that maximize the normalized correlation coefficient between the pre–compressed 2-D acoustical footprint and its deformed version compensated for the searched parameters. Strong constraints have been introduced to limit the occurrence of local maxima. This significantly increases the robustness of the estimation.

However, in biological application, we observed that stress induced signal variations may be of complex shape, and constrained optimization can sometimes remain insufficient to prevent the algorithm to converge towards a local solution. In these particular cases, finding the global maximum would require an initial configuration for the optimization, close to that of the solution. For those reasons, a correction procedure has been added, that uses the value of the normalized correlation coefficient (NCC) at the solution as an indicator of probable good or wrong (NCC<0.8) estimation. When a wrong estimation is suspected, parameters are recomputed, starting N=10 optimizations from N different initializations. The retained parameter values are those leading to the highest NCC.

Results: Tests were performed with several fresh cut specimens of bovine livers. Diseased areas were mimicked by generating harder small size lesions inside the tissues. Biological samples were deformed by lowering the probe, by small steps [0.2 mm – 0.4 mm] owing to the sample media thickness. RF data were acquired with a 7 MHz center frequency probe.

The resulting axial strain images demonstrate the ability of our technique to investigate biological media. Elastograms are smooth and exhibit the harder inclusions clearly. Axial displacements were also computed by integration of axial strains and their maximum values corroborate perfectly the experimental conditions of the load application. Finally, maps of the normalized correlation coefficients at the solutions were also investigated, appearing homogeneous with high mean values (reaching a peak of 0.97).

Conclusions: Results demonstrate that our technique, strengthened by the procedure that detects potential wrong estimates to then try to correct them, allows strain imaging of biological tissues. Future work will consist of continuing *in vitro* biological applications and beginning *in vivo* applications.

Acknowledgements: This work has been financially supported by the scientific committee of the INSA-Lyon, France.

Reference:

[1] E. Brusseau, J.F. Déprez, G. Said, O. Basset, 2D Strain estimation based on a Newton constrained minimization strategy. Application to Experimental Data, Proc. of The 4th International Conference on the Ultrasonic Measurement and Imaging of Tissue Elasticity, 2005, p 111. http://www.ece.rochester.edu/users/rcbu/conference/2005conf.htm

Figure 1: Result obtained with a sample of an *in vitro* bovine liver. The generated inclusion is clearly visible in the elastogram. In this case, the mean correlation coefficient has been estimated at 0.93.

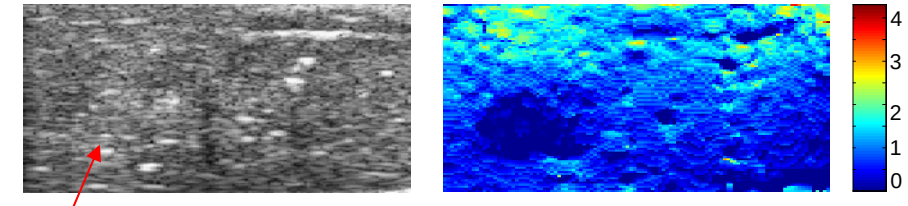

034 **IMAGING MYOCARDIAL HETEROGENEITY USING PROPAGATION OF PULSED VIBRATION FOR HEALTHY SUBJECTS AND PATIENTS WITH OLD MYOCARDIAL INFARCTION.**

Hiroshi Kanai[1], Sachiko Watanabe[2], Yoshifumi Saijo[1], Motonao Tanaka[1].*
[1]Tohoku University, Aramaki–aza–Aoba 6-6-05, Sendai 980–8579, Miyagi, JAPAN; [2]Miyagi Shakaihoken Hospital, Nakata–aza–Maeoki 143, Sendai 981–1103, Miyagi, JAPAN.

Background: It is well known that the diseased area due to old myocardial infarction (OMI) becomes fibrous.

Aims: This study shows that a novel method noninvasively visualizes myocardial heterogeneity for patients with OMI.

Methods: Using a sparse sector scan, the minute myocardial motions were measured simultaneously at about 1,000 points in the heart wall at a high frame rate (>400 Hz). We have found that a pulsed vibration is excited by aortic–valve closure [1]. The consecutive spatial distributions of the vibrations clearly reveal that the vibration propagates from the root of the aortic valve to the apex along the heart wall [2]. Since its propagation time along the heart wall and the duration period are only several milliseconds and its amplitude is about 100 micrometers, this phenomenon cannot be measured by conventional equipment. In this study, the method was applied to 7 healthy subjects and 5 patients with OMI. The spatial distribution of the propagation speed of the vibration is also visualized.

In Vivo Experiments: For all healthy subjects, the propagation of the pulsed vibration was clearly visible both in the longitudinal axis and apical views. Even for the healthy subjects, there is a spatial difference in the propagation speed; about 4 m/s for the strong echo area and about 3 m/s for the weak echo area, for 60 Hz component in the septum. For all patients with OMI, the vibration propagated in the normal region, but it did not propagate in the diseased area as shown in the consecutive panels of Figure 1 at 4 ms intervals.

Conclusions: These preliminary results indicate that the method has the potential for noninvasively revealing myocardial heterogeneity.

References:

[1] H. Kanai and Y. Koiwa: "Myocardial Rapid Velocity Distribution," *Ultrasound in Medicine and Biology*. Vol. 27, No. 4, pp. 481–498 (2001).
[2] H. Kanai: "Propagation of Spontaneously Actuated Pulsive Vibration in Human Heart Wall and *In Vivo* Viscoelasticity Estimation," *IEEE Transactions on Ultrasonics, Ferroelectrics, and Frequency Control*. Vol. 51, No. 11, pp. 1931–1942 (2005).
[3] H. Kanai, H. Hasegawa, N. Chubachi, Y. Koiwa, and M. Tanaka: "Noninvasive Evaluation of Local Myocardial Thickening and Its Color–Coded Imaging," *IEEE Transactions on Ultrasonics, Ferroelectrics, and Frequency Control*. Vol. 44, No. 4, pp. 752–768 (1997).

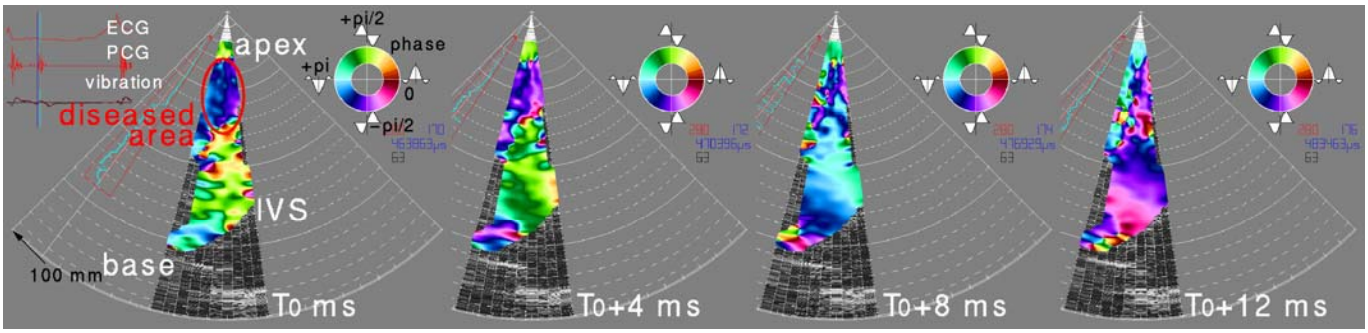

Figure 1: For a patient with old myocardial infarction, the developed method [2] was applied in the apical view. The vibration was measured at each point in the interventricular septum by the phased tracking method [3]. The phase of the 60 Hz component of each vibration signal was detected and its spatial distribution was shown at consecutive 4 ms intervals from the aortic valve closure time (T_0). As shown in these panels, the pulsed wave was spontaneously actuated by the closure of the aortic valve, and it propagated along the septum. However, it did not clearly propagate in the diseased region due to the myocardial infarction.

* *indicates Presenter*

067 ***IN VIVO* 3D CARDIAC ELASTOGRAPHY IN AN ANIMAL MODEL AND HUMAN HEART.**

RGP Lopata[1], MM Nillesen[1], FN van de Vosse[3], IH Gerrits[1], JM Thijssen[1], L Kapusta[2], CL de Korte[1].*
[1]Clinical Physics Laboratory, [2]Children's Heart Centre, Radboud University Nijmegen Medical Centre, Nijmegen, The Netherlands; [3]Department of BioMedical Engineering, Eindhoven University of Technology, Eindhoven, THE NETHERLANDS.

Background: Research in strain imaging can be extended towards a full 3D approach since the introduction of real–time 3D ultrasound imaging techniques. The complex and fast movements and deformations of the heart muscles require 3D+t data for accurate full 3D strain imaging. However, sub-optimal temporal resolution of 3D datasets is still a problem as well as the high computational load of 3D strain estimation. In this study, BiPlane imaging is used as a fast semi 3D imaging technique for measuring axial and lateral strain of the heart during the entire heart cycle.

Aims: In this study 3D strain imaging of actively contracting heart tissue is examined by determining strain in 3 orthogonal directions in the heart muscle using a fast 2D parabolic interpolation.

Methods: Raw (rf) ultrasound data were acquired with a Philips SONOS 7500 live 3D ultrasound system, equipped with an X4 matrix array transducer and an RF–interface. An iterative 2D coarse–to–fine strain algorithm (Method I) was implemented to estimate displacements. Sub–sample and sub–line resolution were obtained by 2D parabolic interpolation of the data for which a parabolic shape of the peak of the 2D cross–correlation was assumed. Hence, the displacements were easily found by solving a set of analytical expressions. In a previously developed algorithm (Method II [1]), the data were sub–sampled using spline interpolation (Method I) in both directions. To improve the signal correlation, the signal windows were re-aligned and locally stretched at each iteration using previously estimated displacement and strain values. The method was validated using simulated BiPlane data (Field II©, [2]) of a 3D Finite Element Model (FEM) simulated phantom containing a central cylindrical inclusion (four times higher Young's Modulus) and randomly distributed point scatterers. The FEM solutions were used to simulate images before and after compression. Elastograms were generated using the new and previous [2] methods, and a comparison was made using SNR_e and CNR_e values. Additionally, the method was evaluated using data obtained from beagles with an induced valvular aortic stenosis and from a trained athlete. BiPlane images were obtained during several heart cycles. A region in the lateral wall (parasternal view) was manually segmented in both planes and the frame–to–frame deformation of the muscle was measured. The cumulative axial and lateral strains were calculated after median 2D+t filtering of the displacements.

Results: Using the iterative algorithm with 2D parabolic interpolation, excellent correlation between simulated and measured axial strain was found for a window of only 0.60 mm and the elastographic signal to noise ratio (SNR_e) was 43dB, whereas the SNR_e of the previous method (Method II) was 39dB. In lateral and elevational direction, the SNR_e was considerably lower (12dB) but still exceeded the performance of the previous algorithm (SNR_e = 9dB). Furthermore, the computation time was decreased by a factor 200. The cumulative axial strain in the beagle with a valvar aortic stenosis revealed a maximum strain value of 50%. The lateral and elevational strain was considerably lower (approximately 20%). A drift in the strain values was removed by applying a linear trend correction algorithm. In the endurance athlete, the systolic phase revealed a rising slope (0.2s) to a maximum of 60% axial strain, whereas the diastolic decrease is much slower (0.6s). The lateral (-30%) and elevational strain (-20%) were considerably lower. Tracking the region of interest was necessary for generating valid cumulative strain curves. Besides region tracking, usage of the coarse–to–fine algorithm enabled cumulative displacement measurements up to 10.0 mm justifying the usage of the described interpolation method.

Conclusions: Fast 3D Strain estimation using bi–plane imaging of actively contracting heart tissue is feasible with promising outlook for extension to full 3D.

Acknowledgements: The support of the Dutch Technology Foundation (STW) is acknowledged.

References:

[1] Lopata R.G.P. et al; Comparison of three non–axial strain estimation techniques for 3D strain estimation in elastic materials and tissues, Proceedings of the 4th International Conf. on the Ultrasonic Measurement and Imaging of Tissue Elasticity. Austin, Texas, USA, p. 76, Oct., 2005.
[2] J.A. Jensen and N. B. Svendsen. Calculation of pressure fields from arbitrarily shaped, apodized and excited ultrasound transducers, IEEE Trans. Ultrason., Ferroelec., Freq. Contr., 39, pp. 262–267, 1992.

047 **TRANSIENT MR-ELASTOGRAPHY OF THE HEART.**

B Robert[1], R Sinkus[1], JL Gennisson[1], M Tanter[1], M Fink[1].*
[1]Laboratoire Ondes et Acoustique, ESPCI, Paris, FRANCE.

Aims: It is expected that the viscoelastic properties of the myocardium change locally depending on the degree of tissue damage, for instance, after an infarct. Thus, strain imaging like tagging [1] or DENSE [2] have been developed to provide information about regional abnormal mobility. Reduced strain response relative to known stress would thereby demonstrate increased stiffness. However, the stress is unknown for these kinds of measurements. Conversely, MR–Elastography (MRE) allows the assessment of inherent viscoelastic tissue parameters which are likely to characterize tissue damage in a more objective manner, and thus carry the potential to diagnose myocardial viability better. However, high resolution MRE necessitates the use of high frequency mechanical excitations (>200 Hz) in order to achieve a small wavelength (<1 cm) capable of resolving small regional defects within the myocardium. Because of the strong viscous properties of tissue at high frequencies, externally generated waves are damped in the overlying tissues and are unlikely to reach the heart with sufficient amplitude. To overcome this limitation, we propose using waves generated naturally during the heart cycle. Valve closure at the beginning and end of systole are believed to account for the 1st and 2nd heart sounds [3].

Methods: A retrospectively–gated ECG–triggered balanced gradient echo sequence was extended by a trapezoidal motion–encoding gradient (20 mT/m) ending just before the read–out gradient. Phase–locking the sequence to the 300 Hz component (wavelengths are sufficiently short within the 5 cm long septum) allows selecting TE=5 ms and TR=10 ms. Within a single breath hold of 20 s, 100 cardiac phases were acquired for a single slice with FOV=320 mm, slice thickness 8 mm, 128x128 resolution, α=50° and 72% phase sharing among neighboring cardiac phases. A 5–element cardiac coil was used in conjunction with SENSE (reduction factor 2) in order to get phase images.

Results: Figure1 shows the phase maps within the septum with and without Motion Encoding Gradient (MEG) in different directions (feet–head or through slice). The phase maps are acquired at the beginning and end of systole. Phase profiles are drawn along the dashed line for each image. A clear difference between with coding and without coding is visible for both heart sounds. Interestingly, strong wave–like modulations are visible for the M–direction during the 1st heart sound (1st heart sound: atrioventricular valve closure) but almost none are seen during the 2nd (2nd heart sound: semilunar valve closure). This observation is opposite for the S–direction: strong wave–like modulations are visible during the 2nd heart sound but almost none are seen during the 1st. The measured wavelengths in both cases are approximately 1cm.

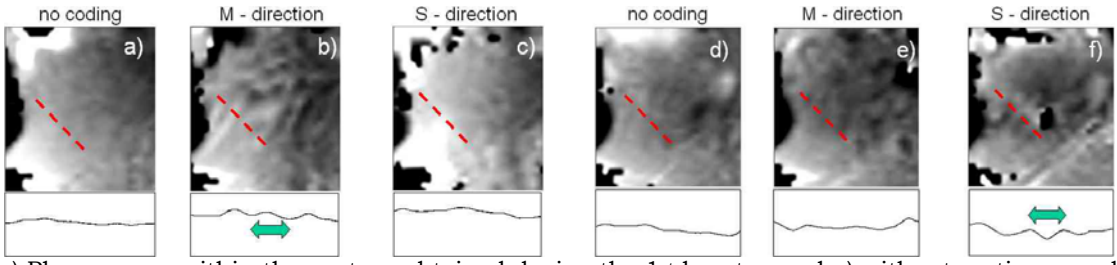

Figure1: a–c) Phase–maps within the septum obtained during the 1st heart sound a) without motion encoding, b) with coding in transverse (M) and c) in axial (S) direction. d–f) corresponding phase–maps obtained during 2nd heart sound. The profiles underneath each image show the phase values along the dashed line.

Conclusions: Heart elastography is a challenging new application. The classical motion encoding gradient in elastography, unfortunately, serves also as a velocity encoder. Thus, careful differentiation between bulk motion of the heart and true shear waves must be performed. Ultrasound has shown that 300 Hz shear waves travel at 3 m/s. Thus we cannot observe the wave propagation at a temporal resolution of 10 ms (100 heart phases); we observe the presence or absence of the waves. The different wave polarizations probably reflect the different sound origins. Further experiments are currently being conducted to explore the improvements achievable by stronger gradients (60 mT/m) and multi–slice experiments.

References:

[1] Wen et al, MRM 54:538–48,2005.
[2] Denny et al, MRM 49:743–54,2003.
[3] Kanai H, IEEE–UFFC 52(11):1–12, 2005.

* *indicates Presenter*

048 **NON–INVASIVE ELASTOGRAPHY OF CAROTID ARTERIES.**

Hermine Ribbers[1], Richard G.P. Lopata[1], Suzanne Holewijn[2], Gerard Pasterkamp[3], Jan D. Blankensteijn[2], Chris L. de Korte[1].*

[1]Clinical Physics Laboratory, [2]Department of Vascular Surgery, Radboud University Nijmegen Medical Center, Nijmegen, The NETHERLANDS; [3]Experimental Cardiology Laboratory, University Medical Center Utrecht, Utrecht, The NETHERLANDS.

Background: Cardiac disease and stroke are the major cause of death in the Western World. Atherosclerosis of the carotid artery is the most important predictor of stroke. Elastography is a technique used to assess the composition and vulnerability of an atherosclerotic plaque [1]. Contrary to intravascular applications, the ultrasound beam and radial strain are not aligned in non–invasive, transcutaneous acquisitions.

Aims: To determine two dimensional displacement and strain images of phantoms and carotid arteries *in vivo* and to reconstruct the radial and circumferential strain.

Methods: RF–data were acquired using a Philips SONOS 7500 live 3D ultrasound system, equipped with an L11 (3–11 MHz) linear array transducer and rf–interface. A homogeneous, hollow cylinder phantom (20% gelatin, 1% SiC scatterers (10 μm)) [4] was measured in a water tank at different intraluminal pressures [1]. In addition, measurements in patients (n=12) were made to evaluate the *in vivo* applicability of the technique. Longitudinal and cross–sectional recordings were made, both in phantoms and patients.

Strain along the ultrasound beam (axial strain) was determined using cross–correlation analysis for signal–windows from the pre– and post–compression data [2]. For lateral strain estimation, new ultrasound lines were interpolated between the acquired lines [2]. A cross–correlation based search algorithm was applied to determine lateral displacement and strain [3]. Radial and circumferential strain images were determined from the axial and lateral strain images using principal strain analysis or by using compounding of corrected axial strain images, acquired using different beam steering angles [4].

Results: Longitudinal, axial strain images showed a decreasing strain from the lumen–vessel wall interface to the outer region that can be described by a $1/r^2$ relationship [1]. The lateral strain images showed no strain in this direction indicating a plane strain situation. In the cross sectional view, compression of the material in regions at 12 and 6 o'clock was observed, whereas, expansion was observed in regions at 3 and 9 o'clock. This pattern is in accordance with theory but can only be partly corrected for; in the transition regions, zero axial strain was measured [5]. The lateral strain images showed a complimentary pattern. However, large artifacts were observed at the 5 and 7 o'clock positions. These artifacts are caused by the sharp angle the ultrasound beam makes with the interface at these crossings resulting in an alteration in the spatial distribution of ultrasound beams due to refraction [6]. Radial and circumferential strain images as reconstructed from the lateral and axial displacements were also influenced by the latter artifact. Using axial elastograms acquired at different beam steering angles, strain images without this artifact can be obtained by compounding.

In patients, low strain was observed in non–atherosclerotic artery walls. High and low strain regions were found in atherosclerotic plaques. High quality elastograms were generated both in longitudinal and cross-sectional views.

Conclusions: Two dimensional non–invasive elastography of atherosclerotic carotid arteries is feasible. Phantom studies revealed elastograms in accordance with theory. Additional *in vivo* validation is needed to assess the value of this technique for identifying plaque vulnerability and composition.

References:

1 de Korte CL, Céspedes EI, van der Steen AFW, Lancée CT. Intravascular elasticity imaging using ultrasound: feasibility studies in phantoms. *Ultras Med Biol* 1997;23(5):735–746.

2 Konofagou E, Ophir J. A new elastographic method for estimation and imaging of lateral displacements, lateral strains, corrected axial strains and Poisson's ratios in tissues. *Ultras Med Biol* 1998;24(8):1183–1199.

3 Lopata R, Nillesen M, Gerrits I, Thijssen J, Kapusta L, de Korte C. 3D Strain Estimation for Isotropic and Anisotropic Materials. *IEEE Ultrasonics Symposium Proceedings,* Rotterdam, The Netherlands 2005; 731–734.

4 Fung–Kee–Fung SD, Lee WN, Ingrassia CM, Costa KD, Konofagou EE. Angle–independent strain mapping in myocardial elastography. *IEEE Ultrasonics Symposium Proceedings*, Rotterdam, The Netherlands 2005; 516–519.

5 de Korte CL, Céspedes EI, van der Steen AFW. Influence of catheter position on Estimated Strain in Intravascular Elastography. *IEEE Trans UFFC* 1999; 46(3):616–625.

6 Thompson RS, Bambi G, Steel R, Tortoli P. Intraluminal ultrasound intensity distribution and backscattered Doppler power. UltrasMed Biol 2004; 30(11):1485–1494.

090 **MULTI–MODALTY IMAGING WITH ELASTICITY ASSESSMENT.**

Armen Sarvazyan[1].*
[1]Artann Laboratories, 1459 Lower Ferry Rd., Trenton, NJ 08618, USA.

Background: No single imaging technology is ideal for every disease. Because of the complementary nature of diagnostic information provided by different imaging modalities, fusion of data from different modalities is important for diagnosis and treatment monitoring. Since mechanical properties of tissues are shown to be highly sensitive to the conditions of tissue, the merging of elasticity data with diagnostic information from other sources appears to be an important aspect of the multi–modality imaging concept. One of the approaches to multi–modality imaging and the fusion of diagnostic information from diverse sources is model–based-imaging, that is, generating 2–D or 3–D images of an object integrating available information about that object in a simulated patient specific computer model [1].

Elasticity imaging is a modality which intrinsically is linked to other imaging modalities used for obtaining strain patterns in the tissue under different levels of loading. Detailed images necessary for the elasticity distribution assessment can be produced using a number of imaging modalities: MRI, ultrasound and X-ray. Fusion of mechanical information with other structural and functional tissue characteristics obtained by imaging modalities used for strain evaluation is an important aspect of elasticity imaging.

Aim: The objective of this presentation is to analyze the problem of merging diagnostic information obtained by different imaging modalities and, more specifically, to discuss numerous crossroads between tissue biomechanics and medical imaging in general.

Methods and Results: We analyzed in detail the problem of multi–modality imaging in regard to prostate and breast cancer diagnostics because the elasticity data were shown to be highly relevant for these particular applications. Various modalities, such as MRI, ultrasound, mammography and Mechanical Imaging based on measurements of stress patterns on the tissue surface and finding the solution to an inverse problem were considered. Numerous limitations on the applicability of the model–based multi-modality imaging concept were revealed. Composing a patient–specific 3–D model requires well defined and carefully validated algorithms for translating features of the object assessed by an imaging modality into the quantitative anatomical and histopathological parameters. Development of such algorithms cannot be accomplished without a comprehensive database relating measured variables with structural and other diagnostically relevant characteristics of the object.

Conclusions: Multi–modality imaging integrating structural, functional and biomechanical information has great potential for medical diagnostics and can be beneficial for treatment monitoring and as a tool for preoperative planning. However, numerous obstacles hinder the implementation and wide use of this concept.

Reference:

[1] AP Sarvazyan, LF Lizzi, and PNT Wells, "A new philosophy of medical imaging." Medical Hypotheses, 1991, vol. 36, pp. 327–335.

013 **INHOMOGENEITY OF THE TISSUE THERMAL PARAMETER OF EBBINI'S MODEL AND ITS DEPENDENCY ON TEMPERATURE.**

Chikayoshi Sumi[1], Hiroyuki Yanagimura[1], Tsuneaki Ooba[1] and Kyousuke Inoue[1].*
[1]Sophia University, 7-1, Kioicho, Chiyodaku, Tokyo, JAPAN.

Background: We have reported the methods for reconstructing the thermal properties [1,2] of living soft tissues such as conductivity, capacity and diffusivity for diagnosis and treatment (planning and controlling). Temperature distribution can be measured by ultrasonic imaging or MRI.

Aims: In this report, we focus on the application of the Ebbini's model for measuring temperature to the thermal property reconstructions. The method is proposed to measure temperature elevations for a short time generated by HIFU. We also used this method to measure the decrease of temperature during cooling down and temperature change for a long time due to thermal exposure. As the heat capacity of our target is large, the temperature change is slow (e.g., compared with a conductor). Here, for such cases, we report the accuracy of the temperature measurement. As the temperature change is expressed by the product of the thermal strain (i.e., elongation, shrinking and change of ultrasound speed) and tissue thermal parameter k described by the dependencies (coefficients) of the ultrasound speed and volume on temperature. The measurement accuracy is determined by the accuracies of the parameter k and strain measurement.

Methods: MCSPGM [3] enables accurate measurement of strain even using low SNR echo data. Then, using MCSPGM for a fresh calf liver, we measured the inhomogeneity of the thermal parameter k and the dependency on temperature. We changed the temperature of the target form 20 to 50ºC using hot water in a stepwise (total 15 steps, i.e., three repetitions of a set of increasing 0.2, 0.3, 0.4ºC, keeping the temperature for an hour, and increasing 9.1ºC) and measured the thermal strains generated during the respective temperature elevations in an ROI (27.0 mm x 22.8 mm) under a uniform temperature distribution (confirmed using five thermocouplers positioned every 5 mm in the depth).

Results: The B–mode image and measured strains are respectively shown in Figure 1a and 1b. The temperatures and the required times to increase the temperature are respectively described in the results. As the generated thermal strain became large at high temperatures, the dynamic ranges of the strain images were appropriately set. The means and standard deviations in the region A (ranging to the depth of 8.1 mm depicted in Figure 1a) vs. stages were evaluated. The region A had almost all parenchyma and no large blood vessels.

Due to heating, the tissues shrank. With increasing temperature, the absolute thermal parameter k became small (means of stages 6 to 8, i.e., 30.0 to 30.9ºC, -4.43×10^2 vs. 1 to 3, i.e., 20.0 to 20.9ºC, -6.13×10^2; means of 10, -6.16×10^2 vs. 5, -9.16×10^2). However, the results were also affected by the required time to increase the temperature (e.g., by 9.1ºC at 10, 5,905 vs. 5, 5,240 s). With increasing thermal exposure time, the parameter k becomes small. The dependency of the parameter k on the thermal exposure time can be clearly explained in the results of stages 4 and 9 (the tissues shrank during constant temperatures for one hour, i.e., -2.10×10^{-1} and -1.93×10^{-1}%). When the change of temperature was large and the temperatures were high, the standard deviation was also large. Moreover, a longer time was required to increase the temperature. However, although the magnitudes of strains changed, the similarity could be found in the strain images of the stages 1–15. Furthermore, the images have high correlations with the B–mode images. Thus, the imaging of the thermal strain and parameter k is useful for diagnosis.

For the stages of 40ºC, the shrinking was small in region A, due to the fact that the surrounding tissues of the large vessel (arrowed in Figure 1a) shrank largely and the specimen adhered at the US transducer. It was meaningful that we could measure the rapid shrinking (coagulation) of the surrounding tissues of the large vessel.

Conclusions: The thermal parameter k (i.e., temperature coefficient of US speed and volume) was inhomogeneous as well as dependent on temperature and thermal exposure time. MR measurement will also be reported.

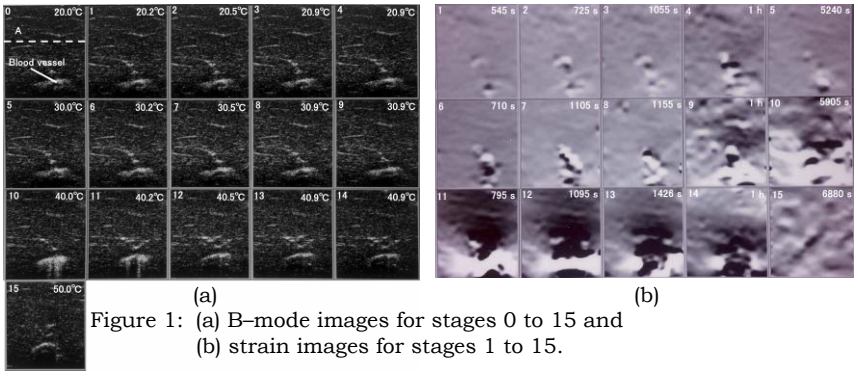

(a) (b)

Figure 1: (a) B–mode images for stages 0 to 15 and (b) strain images for stages 1 to 15.

References:
[1] C. Sumi, Proc. of IEEE Int. Ultrasonics Symp, pp. 21–25, 2005.
[2] C. Sumi, Proc. of the 3rd Int. Conf. on the Ultrason Meas & Imag of Tissue Elasticity, p73, 2004.
[3] C. Sumi, IEEE Trans. UFFC, vol. 46, pp. 158–166, 1999.

036 **ULTRASOUND INDUCED THERMAL STRAIN IMAGING (TSI) FOR ARTERIAL PLAQUE CHARACTERIZATION.**

K. Kim[1], S.–W. Huang[1], R.S. Witte[1], T. L. Hall[1], and M. O'Donnell[1].*
[1]Biomedical Engineering Department, University of Michigan, Ann Arbor, MI 48109, USA.

Background: Rupture–prone plaque consists of a large lipid–rich core and a thin fibrous cap. It is well known that lipids have a negative temperature dependence on the sound speed, whereas water–based tissues have positive temperature dependence [1]. The opposite sign in sound speed change with temperature rise of the two different tissue types creates the contrast required for resolving the fatty tissue from surrounding water–based tissue. Using a conventional ultrasound (US) scanner, the spatial distribution of temporal strain produced by changes in the sound speed with a controlled local temperature modulation can be imaged [2].

Aims: Using a 2–D phased array in combination with a conventional US scanner, the feasibility of ultrasound induced TSI for arterial vulnerable plaque characterization is demonstrated.

Methods: Among other heating sources, including microwave [3], ultrasound may be the best candidate for delivering energy locally and has simplicity of probe design for an existing conventional US scanner. Thermal lens effects and radiation force generated by the heating transducer, combined with motion artifacts, will be challenging issues to overcome for clinical applications. High resolution TSI using a conventional US scanner (iU22, Philips) was first applied to a uniform rubber phantom. 1 MHz 512 channel transducer array (Imasonic, Besançon, FRANCE) was used as a heating source. 2-D phase-sensitive, correlation–based speckle tracking was applied to map the spatial distribution of temporal strain across the sample. A rabbit kidney and a canine aorta with fat inside the lumen were prepared in a clear gel phantom. The fat was extracted from a chicken thigh. The heating beam was designed to cover 10 x 10 x 20 mm region. The heating of 800 ms was interleaved with the imaging of 200 ms. The thermal strain image of the kidney sample was compared with MRI fat quantification and histology.

Results: The temperature rise estimated by TSI in a rubber phantom was about 2ºC within 1 second using an average intensity of 100 W/cm^2. The thermal lens effect was also imaged by tracking the lateral displacement. To avoid artifacts due to radiation force, if any, the image frames before and after heating were averaged for about 150 ms after waiting about 20 ms when the heating beam was stopped. With the same intensity used above for 3 sec, the temperature inside kidney and canine aorta sample was increased by about 1°C. The fatty tissue surrounding the collecting system was clearly differentiated and 2–D TSI matches well with histology and MRI fat quantification. US induced TSI also clearly differentiate the fatty tissue inside of the lumen of the canine aorta.

Conclusions: These *in–vitro* preliminary results demonstrate the feasibility of noninvasive US induced TSI for arterial vulnerable plaque characterization using a commercial US scanner with a small temperature change over a relatively short period of time.

Acknowledgements: Work supported in part by NIH grants HL–47401 and HL–67647 and EB003451.

References:

[1] F. A. Duck, Physical Properties of Tissue. London: Academic, 1990.
[2] R. Seip, P. Van Baren, C. Simon, and E.S. Ebbinni "Non–invasive spatio–temporal temperature estimation using diagnostic ultrasound," IEEE Ultras Sympos Proc. 1613–1616, 1995.
[3] Y. Shi, R.S. Witte, and M. O'Donnell**,** Identification of Vulnerable Plaque Atherosclerotic Plaque Using an IVUS-Based Thermal Strain Imaging, IEEE Transactions on Ultrasonics, Ferroelectrics, and Frequency Control, Vol. 52, No. 5, (May 2005).

** indicates Presenter*

029 **ULTRASOUND BASED TEMPERATURE IMAGING FOR MONITORING RADIOFREQUENCY ABLATION.**

M Daniels[1], J Jiang[1], T Varghese[1], EL Madsen[1], JA Zagzebski[1].*
[1]University of Wisconsin–Madison, 1300 University Avenue, Rm. 1530, Madison, WI, USA.

Background: Radiofrequency (RF) ablation is the most common minimally invasive treatment in the United States for hepatocellular carcinoma and liver metastases. Clinicians have difficulty determining treated volumes after ablation, leading to tumor recurrence. Temperature imaging would allow clinicians to determine areas of the tumor that have reached high enough temperatures to cause cell death.

Aims: The purpose of this study was to determine the accuracy of temperature maps estimated from ultrasound signals. We present results of both finite element analysis (FEA) [1] and experiments using RF ablations of a tissue mimicking (TM) phantom.

Methods: FEA models were developed to determine the temperature distribution from an RF ablation electrode embedded in liver tissue. FEA analysis enabled creation of temperature and tissue expansion maps for a 12 minute ablation procedure. An initial frame of RF echo data was simulated assuming a spatially random distribution of scatterers. Then the thermal expansion maps were combined with speed of sound changes from the elevated temperatures, and these were used to create new sets of simulated ultrasound RF frames at specified intervals during the ablation procedure. Apparent tissue displacements were estimated and accumulated from consecutive simulated RF frames to generate temperature maps of the ablation. The temperature maps obtained from the accumulated displacements were compared to the original temperature maps created using the FEA analysis.

Experimentally, a RITA RF electrode was mounted in an apparatus containing pseudo–liquid tissue mimicking material with known thermal properties. Power was applied for approximately 12 minutes, heating the slurry. An Ultrasonix RP500 system was used for raw echo signal data acquisition during the TM phantom ablation procedure. The transducer was placed at a fixed position at the top of the TM material, with the RF ablation electrical grounding pad placed below the material. The temperature increase was monitored invasively using fiber optic temperature probes placed at specific locations in the phantom. The visibility of the tines of the electrode in the ultrasound image enabled a direct comparison of the temperature estimated from the ultrasound based displacement–gradient imaging to the fiber optic probe temperature on a very local basis.

Results: The temperature maps generated from the ultrasound echo signals exhibited a high level of correspondence with those created with FEA. In generating the temperature maps, both 1D and 2D cross–correlation (CC) methods were utilized. For a region of interest around a tine, the 2 DCC method underestimated the temperature around the tine by an average of 8%, while the 1D CC method overestimated the temperature around the tine by an average of 30% when compared to the actual FEA temperature [1]. The largest temperature gradient is exhibited at and around the tine, so this represents the worst case scenario. Even with this underestimation, the location of the RF ablation electrode tines can be easily visualized using the temperature maps, along with the zone of elevated temperatures due to the ablation. For the phantom ablation experiment, fiber optic probe measurements were compared to their corresponding values in the temperature map. The fiber optic probe temperature measurements correlated to within ±5ºC with those obtained using the noninvasive ultrasound–based temperature maps.

Conclusions: The temperature maps estimated using the ultrasound signals correlated well to the FEA generated temperature maps. A method of simulating the RF ablation procedure using FEA and creating temperature maps using ultrasound simulations is presented, along with experimental phantom results that demonstrate an accuracy of ±5ºC. Temperature mapping can therefore be used to visualize a zone of necrosis during an RF ablation procedure.

Reference:

[1] Daniels M, Varghese, T. Ultrasound Simulation of Real–Time Temperature Estimation during Radiofrequency Ablation using Finite Element Models. Ultrasound In Medicine & Biology (in press).

061 **TOWARD LIVER FIBROSIS STAGING WITH IMPULSIVE ACOUSTIC RADIATION FORCE.**

KR Nightingale[1], KD Frinkley[1], L Zhai[1], GE Trahey[1], ML Palmeri[1].*
[1]Duke University, Durham, NC, USA.

Background: Acoustic radiation force can be used to mechanically excite tissue in remote, focused locations, and the tissue response can be monitored using ultrasonic correlation based methods. The speed with which the resulting shear waves propagate away from the focal region can be estimated and used to quantify the material shear modulus, as was originally proposed by Sarvazyan et. al [1]. In practice, an algebraic inversion of the Helmholtz equation has been used to reconstruct shear wave speed, requiring extensive filtering and smoothing prior to 2nd order differentiation of displacement in both space and time, and excluding locations within the excitation region [2,3]. We have implemented a new approach that compares the temporal variations in displacement curves at multiple lateral and axial positions within and around the excitation region to estimate local shear wave speed without differentiation. In this work we compare the two methods on data from: 1) FEM simulations, 2) calibrated phantoms, and 3) *in vivo* human liver.

Aims: The overall purpose of this work is to determine a robust method for shear stiffness quantification for clinical application in staging liver fibrosis.

Methods: Three–dimensional Finite Element Method (FEM) models of the dynamic response of elastic media to impulsive acoustic radiation force excitations were used to study the accuracy of the proposed method in reconstructing stiffness of tissue ranging from 1 – 80 kPa [4]. Experiments were performed with a Siemens SONOLINE Antares™ Scanner with VF10–5 (5.7 MHz) and VF7–3 (4.2 MHz) linear arrays. Each interrogation had a reference tracking line and a high intensity pushing line, followed by a series of tracking A–lines. Multiple interrogations were performed, with the tracking lines and/or pushing lines sequentially interrogating different lateral locations. Displacements were determined via cross correlation using a three wavelength kernel with 99% overlap. For phantom studies, the reconstructed tissue stiffness estimates were compared with measurements using a mechanical indenter.

Results: The new reconstruction method generates consistent values with the algebraic inversion method, however the new method was found to be more robust in the presence of jitter and poor SNR. In the modeling studies, the shear moduli of elastic materials were able to be reconstructed within 10% of the actual moduli, with improving accuracy in stiffer media. In custom phantoms (gelatin bloom strengths: 100, 200 and 300), the Young's moduli (assuming a Poisson's ratio of 0.5) derived with the new method were: 5.8 (.3), 11.7 (.4), and 16.9 (1.2) kPa, respectively, comparing well with indenter measurements of 6.8 (.3), 12.2 (.1), and 16.6 (.1) kPa. *In vivo*, elastic moduli estimated with the new method were 7.8 (3.5), and 7.4 (1.3) kPa in two healthy volunteers, and the mean reconstructed moduli were within 1 kPa of each other on three different days.

Conclusions: The new method is applied both within and outside of the excitation region, and does not require 2nd order temporal and spatial differentiation of displacement data. The method is robust and generates consistent measurements over multiple acquisitions. Shear stiffness moduli are consistent with those reported in the literature for liver.

Acknowledgements: This work was supported by NIH grants R01 EB002132 and R01 CA114075. The authors would also like to thank Siemens Medical Solutions USA, Inc. Ultrasound Division for their technical assistance.

References:

[1] Sarvazyan A., Rudenko O., Swanson S., Fowlkes B., Emelianov S. "Shear wave elasticity imaging: A new ultrasonic technology of medical diagnostics", Ultrasound Med. Biol., 24(9):1419-1435, 1998.
[2] Nightingale KR, McAleavey SA, Trahey GE. "Shear wave generation using acoustic radiation force: *in vivo* and *ex vivo* results", Ultrasound Med. Biol., 29(2):1715:1723, 2003.
[3] Bercoff J., Tanter M., Fink M. "Supersonic shear imaging: a new technique for soft tissue elasticity mapping", IEEE UFFC, 51(4):396-409, 2004.
[4] Palmeri ML, Sharma AC, Bouchard RR, Nightingale RW, Nightingale KR. "A Finite-Element Method Model of Soft Tissue Response to Impulsive Acoustic Radiation Force," IEEE-UFFC, 52(10), 1699-1712, 2005.

* *indicates Presenter*

030 **REAL–TIME TISSUE COMPRESSION QUALITY FEEDBACK FOR OPTIMIZED FREEHAND ELASTICITY IMAGING.**

Emil G. Radulescu[1], Radu Alexandru[1], Regina Hooley[2], Liane E. Philpotts[2] and Heather Frimmer[2].*
[1]Aloka, US R&D, Wallingford, CT 06492, USA; [2]Department of Diagnostic Radiology, Yale University School of Medicine, New Haven, CT 06520, USA.

Background: As pathological conditions often produce changes in biological tissue stiffness, elasticity imaging provides valuable information, facilitating the detection and diagnosis process. Static elasticity imaging consists of applying a stress to the biological tissue and evaluating the response using conventional ultrasound and correlation methods. Real–time freehand elasticity imaging, as opposed to using motorized compression, makes the scanning process more controllable and allows for a larger variety of imaging locations. Its disadvantage, however, consists of exhaustive operator training, as obtaining superior quality strain images requires continuous adjustment of the compression technique. The sonographer needs to maintain a constant compression rate, exclusively on the axial direction of the imaging transducer, while avoiding lateral and out–of–plane tissue motions.

Aims: A compression analysis algorithm was designed to optimally estimate in real–time the strain image quality prior to actually computing the image by assessing the quantity and quality of tissue compression versus depth.

Methods: The algorithm employed a criterion for automatic selection of the most advantageous frame pairs (pre– and post–compression) producing elasticity images of optimal dynamic ranges (DRe) and signal-to-noise ratios (SNRe) while providing live graphical compression feedback to the operator. The algorithm was implemented on a modified commercial scanner (Aloka SSD5500) equipped with a newly developed static elasticity imaging module. The strain images were displayed in real–time using a graphic interface specially developed to include both the compression feedback and a combined B–Mode / strain display.

Results: Images of breast elasticity obtained at Yale New Haven Hospital, CT for various solid masses and cysts, including benign and malignant cases, validated the tissue compression quality feedback algorithm. Thirty, (30) breast masses were scanned during this initial phase. Elasticity image acquisition was facilitated by the graphical compression feedback, significantly reducing the learning period and improving the DRe and SNRe of the images. Figure 1 illustrates a case of biopsy proven infiltrating ductal carcinoma in a 49 year old patient. B–Mode image is shown on the left and the strain image is shown on the right, overlapped on the B–Mode image, as a transparent color map.

Conclusions: The frame pair selection criterion optimized the trade–off between the number of images obtained and their quality (DRe and SNRe) and reduced radically the amount of artifact in the images while lowering the computational burden. During the offline review process of the collected elasticity data, the information indicating the tissue compression quantity and quality was used to confirm the quality of raw data behind the elasticity images.

Acknowledgements: Ms. Rena Kathreptis and Mr. Lee Oppegaard of Aloka America are specially thanked for valuable advice and essential contribution to clinical evaluation.

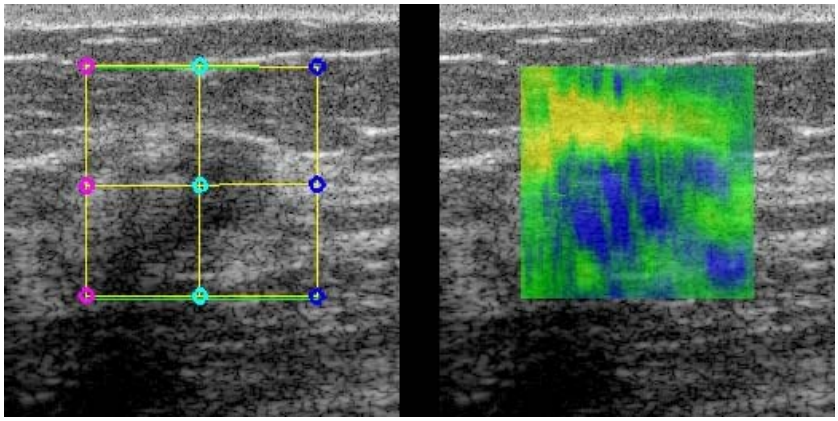

B–Mode image Strain image

Figure 1: Biopsy proven infiltrating ductal carcinoma.

031 **SONOELASTOGRAPHIC SHEAR VELOCITY IMAGING: AN APPLICATION OF CRAWLING WAVES.**

K Hoyt[1], KJ Parker[1], DJ Rubens[1].*
[1]University of Rochester, Rochester, NY, USA.

Aims: The objective of this study was to develop a novel sonoelastographic technique for estimating local shear velocities from propagating shear wave interference patterns termed crawling waves.

Background: It has been shown that interfering shear waves could produce slowly propagating interference patterns with an apparent velocity much less than the underlying true shear velocity. These crawling waves can be visualized in real–time using sonoelastography, which depicts the vibrational response of soft tissue owing to dynamic mechanical excitation. In general, crawling wave images describe shear wave propagation patterns and allow estimation of spatial elastic properties in tissue, namely, shear velocity distributions [1]. Since changes in tissue elasticity are indicative of an abnormal pathological process, imaging parameters such as shear velocity distributions may prove feasible for differentiating normal from abnormal tissues.

Methods: To evaluate our novel shear velocity estimation technique, a 1D sonoelastographic simulation program was developed. Simulation studies analyzed tradeoffs between various system level parameters and imaging conditions. A GE LOGIQ 9 scanner equipped for sonoelastography was used for experimental studies. Demodulated IQ colorflow data was transferred to an external computer for shear velocity image generation. In experiments, shear velocity images were generated using two homogeneous phantoms of different stiffness with true shear velocities obtained using time–of–flight measurements. Results from a heterogeneous phantom were compared to true shear velocities derived from mechanical measurements. Finally, shear velocity images were obtained from an *in vitro* prostate and compared to the final pathological diagnosis. For all experimental studies, crawling waves were induced using a pair of bending piezoelectric elements positioned on opposite sides of the phantoms or embedded tissue sample and vibrating at offset frequencies (e.g., 200 and 200.15 Hz) parallel to the US scan plane [1].

Results: Simulation results demonstrate that increasing kernel window size reduces shear velocity estimator noise, but compromises spatial resolution due to the moving window estimation approach. Increasing the source vibration frequency was shown to reduce estimator variance, but shear wave attenuation also increases at higher vibration frequencies owing to viscoelastic effects. Since attenuation effectively reduces the shear wave SNR (signal to noise ratio), this variable was assessed revealing that lower SNR levels produced substantial variability in shear velocity estimates. The effects of amplitude quantization were evaluated and results indicated that 4–bit display resolution produced more variability in the shear velocity estimates than that obtained using either 8–bit or 16–bit quantization (16–bit being the most accurate). Results from homogeneous phantoms demonstrated the ability of sonoelastographic shear velocity imaging to quantify the true underlying shear velocity distributions (less than 7% error) as verified using time–of–flight measurements. Furthermore, heterogeneous phantom results revealed the capacity for lesion detection (1 cm diameter inclusion) and shear velocity quantification as validated from mechanical measurements. Experimental results obtained from a prostate specimen depict two high-contrast regions of elevated shear velocity (Figure 1) that were confirmed as focal adenocarcinomas by pathology.

Conclusions: A novel sonoelastographic shear velocity imaging technique was developed and shown to produce results consistent with true shear velocities in simulation and phantom studies. High–contrast visualization of focal carcinomas was demonstrated, introducing the clinical potential.

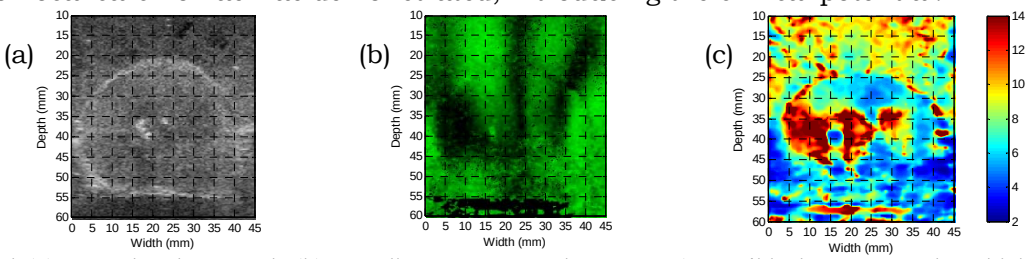

Figure 1: Matched (a) B–mode ultrasound, (b) Crawling wave sonoelastogram (green/black correspond to high/low vibrational amplitude, respectively) and (c) Shear velocity image in prostate. (See Proceedings on CD for color images.)

Acknowledgements: This work was supported in part by NIH 5 RO1 AG16317–03.

Reference:

[1] Wu Z, Hoyt K, Rubens, Parker KJ. Sonoelastographic imaging of interference patterns for estimation of shear velocity distributions in biomaterials. J Acoust Soc Am 2006; 120:1–11.

* *indicates Presenter*

040 **FEASIBILITY OF MUSCLE STRAIN IMAGING USING ULTRASOUND ELASTOGRAPHY DURING THERAPEUTIC BODY MOVEMENTS.**

John J. Triano[1], Helene M. Langevin[2], James R. Fox[3], Elisa E. Konofagou[4].*
[1]Canadian Memorial Chiropractic College, Research Department, Toronto, ON, CANADA; [2]Neurology and [3]Orthopedics Departments, University of Vermont, Burlington, VT, USA; [4]Department of Biomedical Engineering, Columbia University, New York, NY, USA.

Background: There is little information on the mechano–transduction of loads applied by manual treatments for LBP. Many tissues may be stimulated leading to biological responses [1,2]. It is critical to identify how loads distribute among the various layers. Information on load will advance the understanding by (1) informing on the mechanisms of action; (2) identifying the boundaries for safety; and (3) gaining insights on tissue biomarkers and how to improve clinical results (threshold, dosage and duration).

Aims: The feasibility of ultrasound elastography during continuous passive motion (CPM) for LBP to estimate tissue layer thicknesses and strains was studied.

Methods: Hand–held ultrasound B–scan and elastography were used during CPM (0.24 Hz, 15 degree lumbar excursion). A single volunteer was tested in prone and lateral bending CPM upright postural tasks (stand, bend, weight holding). The ultrasound transducer (Terason 2000, Teratech, Inc; 10 MHz, 24 frames/sec) was positioned 3 cm lateral to the midline at the L2/L3 interspace and stabilized manually. Cutaneous and subcutaneous thickness served to confirm negligible variation in manual compression. Tissue metrics were strata layer thicknesses and cumulative axial strains estimated using cross–correlation techniques [2].

Results: Ultrasound B–scan, cumulative strain over 5 seconds of flexion are shown (Figure 1). Percent change in thicknesses at motion extremes are in Table 1. It would be intuitive for both muscles (longissimus and multifidus) to deform similarly during passive motion. This was observed with erect active flexion and extension, but not with prone CPM. Apparent shearing action between muscle layers and non–uniformity of cumulative displacement and strain were observed. Strain images indicated axial compression and tension in the longissimus muscle during extension and flexion respectively, while the opposite was seen with the multifidus.

Layer	Left boundary	Right Boundary
Skin	0%	0%
Subcutaneous	2.24%	0%
Longissimus	4.5%	16.9%
Multifidus	-4.5%	-11.3%

Figure 1:

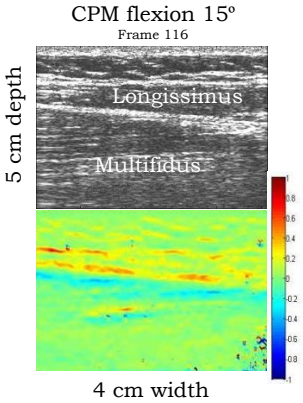

Conclusions: B–scan ultrasound during prone CPM demonstrated non–uniform and counter–intuitive directions of muscle motion, cumulative strain and changes in muscle thickness. Lateral bending and upright task behaviors were more in agreement with the intuitive expectations of uniform deformation across the two muscle layers. Standard assumptions regarding muscle loading in response to postural tasks may not apply to treatment conditions involving recumbence. Noninvasive elastography techniques appear adaptable to measure tissue strains of CPM clinical maneuvers. Future work will focus on stabilizing ultrasound transducer motion tracking, extending analyses to include lateral strain and tissue behaviors in healthy and unhealthy volunteers.

References:

[1] Herzog W. The mechanical, neuromuscular and physiologic effects produced by the spinal manipulation. In: Herzog W, editor. Clinical Biomechanics of Spinal Maniuplation. New York: Churchill Livingstone, 2000: 191–207.
[2] Ophir J, Cespedes I, Ponnekanti H, Yazdi Y, Li X. Elastography: a quantitative method for imaging the elasticity of biological tissues. Ultrason Imagning 1991; 13(2):111–134.

* *indicates Presenter*

022 **DYNAMIC MECHANICAL RESPONSE OF ELASTIC SPHERICAL INCLUSIONS TO ACOUSTIC RADIATION FORCE EXCITATION.**

ML Palmeri[1], SA McAleavey[2], KL Fong[1], GE Trahey[1], KR Nightingale[1].*
[1]Duke University, Durham, NC, USA; [2]University of Rochester, Rochester, NY, USA.

Background: Acoustic Radiation Force Impulse (ARFI) imaging has been used clinically to study the dynamic response of stiff inclusions relative to their background material to focused, impulsive acoustic radiation force excitations. Dynamic displacement data are typically displayed as a set of parametric images, including displacement immediately after excitation, maximum displacement, time to peak displacement, and recovery time from peak displacement. To date, however, no definitive trends have been established between these parametric images of spherical inclusions and the tissue's mechanical properties.

Aims: The purpose of this study is to correlate the dynamic behavior observed in these parametric images with the underlying elastic material properties of tissue.

Methods: Three–dimensional Finite Element Method (FEM) models of the dynamic response of elastic media to impulsive acoustic radiation force excitations are used to study the impact of spherical inclusions of varying size and stiffness on shear wave dynamics during ARFI imaging [1]. Field II, a linear acoustic field simulation package, is used to simulate the ultrasonic tracking of displaced acoustic scatterers in the modeled 3D volume of tissue [2,3]. The model results are compared with clinical and phantom data.

Results: Displacement magnitude, time to peak displacement, and recovery time are all inversely related to the Young's modulus of a homogeneous elastic media. Experimentally, pulse repetition frequency during displacement tracking can limit stiffness resolution using the time to peak displacement parameter. The excitation pulse duration also impacts the time to peak parameter, with longer pulses reducing the inertial effects present during impulsive excitations. Material density affects tissue dynamics, but is not expected to play a significant role in biological tissues. The presence of an elastic spherical inclusion in the imaged medium significantly alters the tissue dynamics in response to impulsive, focused acoustic radiation force excitations. Times to peak displacement for excitations within and outside an elastic inclusion are still indicative of local material stiffness; however, recovery times are altered due to the reflection and transmission of shear waves at the inclusion boundaries. These shear wave interactions cause stiffer inclusions to appear to be displaced longer than the more compliant background material. The magnitude of shear waves reflected at elastic lesion boundaries is dependent on the stiffness contrast between the inclusion and the background material, and the stiffness and size of the inclusion dictate when shear wave reflections within the lesion will interfere with one another. Jitter and bias associated with the ultrasonic displacement tracking also impact the estimation of a tissue's dynamic response to acoustic radiation force excitation.

Conclusions: Stiff inclusions appear to experience greater relative displacements than more compliant background material later in time after a radiation force excitation due to shear wave interference within the inclusion. Dynamic parameters (e.g., time to peak displacement) estimated in response to impulsive excitations are more readily correlated with quantifiable material properties than estimated displacement magnitudes.

Acknowledgements: This work was supported by NIH grants R01 EB002132, R01 CA114075, R01 CA114093 and the Coulter Foundation. The authors would also like to thank Siemens Medical Solutions USA, Inc. Ultrasound Division for their technical assistance.

References:

[1] Palmeri ML, Sharma AC, Bouchard RR, Nightingale RW, Nightingale KR. "A Finite–Element Method Model of Soft Tissue Response to Impulsive Acoustic Radiation Force," *IEEE-UFFC*, 52(10), 1699–1712, 2005.
[2] Jensen JA, Svendsen NB. "Calculation of Pressure Fields from Arbitrarily Shaped, Apodized, and Excited Ultrasound Transducers," *IEEE–UFFC*, 39(2), 262–267, 1992.
[3] Palmeri ML, McAleavey SA, Trahey GE, Nightingale KR. "Ultrasonic Tracking of Acoustic Radiation Force–Induced Displacements in Homogeneous Media," *IEEE–UFFC*, in press.

* *indicates Presenter*

077 **CONGRUENCE OF SONOELASTOGRAPHY CRAWLING WAVES AND MECHANICAL MEASUREMENTS FOR ESTIMATION OF VISCOELASTIC PROPERTIES OF SOFT TISSUES.**

Benjamin Castañeda[1], Man Zhang[1], Zhe C. Wu[1], Deborah J. Rubens[1], Kevin J. Parker[1].*
[1]University of Rochester, Rochester, New York, USA.

Background: The knowledge of mechanical properties of soft tissue is essential to optimize elasticity imaging modalities. Previously, we reported the agreement of two different methods for estimating the elastic moduli of soft tissues: Mechanical measurements (MM) fitted into a Kelvin–Voigt fractional derivative (KVFD) model and the Crawling Waves (CrW) method [1]. The estimation of the shear velocity of the CrW was done manually and therefore was prone to human error. We update this work by introducing a model–based semi–automatic algorithm to estimate shear wave velocity for the CrW method. We also present results for human prostate tissue, in addition to the elasticity modulus estimation for fresh and thermal–treated veal liver.

Aims: The first aim of the study is to measure reliably and accurately the viscoelastic properties of soft tissue. The second aim is to compare the results of two techniques: Sonoelastography Crawling Waves (CrW), and Mechanical Measurement (MM) results fitted into a Kelvin–Voigt fractional derivative (KVFD) model.

Methods: Fresh and thermal–treated veal liver tissue samples (~ 500cc volume) as well as excised prostate glands were directly placed in between a pair of shear wave sources. The wavelengths of shear wave interference patterns in sonoelastography images were measured ranging from 100 to 280Hz using a model–based algorithm. The algorithm pre–processed the image to increase the region of interest, which was then projected onto its horizontal axis. The projection was fitted to a cosine–squared model, which provides the estimation of the wavelength and therefore, the estimation of the shear wave velocity and the Young's modulus of the tissue.

For the MM, cylindrical cores (10 mm diameter, 8 mm length) were acquired from fresh/thermal–treated liver and prostate tissues. 5% compressive strain was applied over 1000 seconds. The stress–relaxation curve of each sample was fitted to a KVFD model. Finally, the complex elastic modulus at any frequency was obtained by the Fourier transform of the time domain response.

Results: Table 1 shows the estimated Young's Modulus for raw liver, thermal–treated liver and human prostate using CrW and MM. Figure 1 shows the comparison of CrW and MM for a prostate gland where particular care was taken to extract cores from the region where CrW were measured. Both methods provide similar results.

Conclusions: The CrW method provides estimations of the Young's moduli of the fresh veal liver, thermal–treated liver and human prostate, which are congruent with the MM results. The new model-based image–processing algorithm improves the measurements obtained from CrW. These results suggest that CrW can be adapted for *in vivo* use to measure tissue properties. The stress–relaxation test produces repeatable results, which fit well to the KVFD model. The methodology used in this study can be applied to other soft tissues.

Acknowledgements: This study was partly supported by NIH grant 5 RO1 AG016317–05.

Reference:

[1] M. Zhang, Z.C. Wu, D.J. Rubens, K.J. Parker, "Mechanical measurement of elastic properties of bovine liver and human prostate under compression", Proc. of The 4th. Int. Conf. Ultrason. Meas. Imag. Tissue Elasticity, pp. 130, 2005.

Raw Veal Liver					
Frequency (Hz)	100	120	150	180	
E CrW (kPa)	5.5	8.2	10.7	11.1	
E MM (kPa)	11.2	11.5	11.8	12.0	
Thermal Ablated Veal Liver					
Frequency (Hz)	150	180	200	220	240
E CrW (kPa)	247	405	365	360	476
E MM (kPa)	351	363	370	376	382
Human Prostate					
Frequency (Hz)	100	120	140	160	180
E CrW (kPa)	20.8	24.0	24.9	25.4	26.3
E MM (kPa)	20.7	21.7	22.6	23.5	24.2

Table 1: Young's moduli estimation using CrW and MM

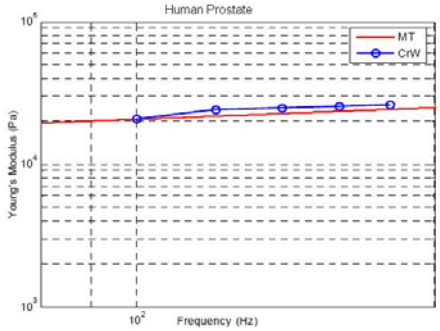

Figure 1: Frequency dependent elastic moduli of human prostate

115 **STIFFNESS RECONSTRUCTION OF HUMAN MUSCLE TISSUE.**

Jeong–Rock Yoon[1], Joyce R. McLaughlin[2], Stephen F. Levinson[3].*
[1]Clemson University, O–225 Martin Hall, Box 340975, Clemson, SC, 29634–0975, USA; [2]Rensselaer Polytechnic Institute, 110 8th street, Troy, NY, 12180–3590, USA; [3]Wayne State University, 261 Mack Boulevard, Detroit, MI, 48201, USA.

Background: Some human tissues are anisotropic, and a typical example is muscle tissue. In [1] Levinson has presented early results for quadriceps muscle that show a linear relation between Young's modulus and applied load during static contractions in muscle, as well as some viscoelastic implications from a multi frequency experiment. Doppler imaging was used in [1] with a relatively slow frame rate. New data using Fink's supersonic transient elastography technique in human biceps muscle and magnetic resonance elastography (MRE) data from human calf muscle from the Mayo clinic provides an opportunity for a better viscoelastic reconstruction. A comparison of both methods is also feasible.

Aims: We target: (1) elastic and viscoelastic changes related to the orientation of muscle fibers, imaging of longitudinal and transverse shear moduli, and wave spreading due to viscoelasticity; and (2) verification of a linear relationship between muscle stiffening and applied load which induces muscle contraction. MRE data is also compared to ultrasound data.

Methods: The arrival time algorithm [2] is a successful algorithm to reconstruct the shear wave speed in transient experiments, effectively utilizing propagating wave fronts. A modified arrival time algorithm [3] including the viscoelastic spreading effect, can provide the reconstruction of some viscoelastic properties as well as shear wave speed. On the other hand, variance controlled harmonic reconstruction in [4], incorporating local SNR information, provided shear stiffness as well as viscoelastic information in MRE. We used three reconstruction methods to evaluate supersonic imaging data in human biceps muscle and MRE data in human calf muscle. Many different experimental variables (different loads, different imaging angle between the imaging plane and muscle fiber) were considered.

Results: From supersonic transient elastography data (biceps muscle), we produced reconstruction images of the shear wave speed and some viscoelastic properties depending on the muscle fiber orientation. We also observed changes in elastic properties depending on the applied load. Reconstructions for MRE data (calf muscle) were also compared to the supersonic imaging results.

Conclusions: The elastic properties (shear wave speed, viscoelasticity) changes in human muscle tissue depending on the fiber orientation, and applied force can be imaged with some muscle differentiation seen in the images.

Acknowledgements: The supersonic ultrasound data were obtained from the laboratory of M Fink at Laboratoire Ondes et Acoustique, ESPCI, Paris, France, and the magnetic resonance elastography data was provided by R Ehman at Mayo Clinic, Rochester, MN, USA.

References:

[1] S Levinson, M Shinagawa, T Sato, Sonoelastic determination of human skeletal muscle elasticity, J. Biomechanics, vol 28, no 10, 1145–1154, 1995.
[2] L Ji, J McLaughlin, D Renzi, JR Yoon, Interior elastodynamics inverse problems: shear wave speed reconstruction in transient elastography, Inverse Problems, vol 19, S1–S29, 2003.
[3] J Klein, J McLaughlin, Effects of viscoelasticity in shear wave speed reconstruction, Proc. of The 4th International Conference on the Ultrasonic Measurement and Imaging of Tissue Elasticity, 53, 2005.
[4] J McLaughlin, D Renzi, JR Yoon, R Ehman, A Manduca, Variation controlled shear stiffness images for MRE data, 3rd IEEE International Symposium on Biomedical Imaging: Macro to Nano, 960–963, 2006.

* *indicates Presenter*

117 **BIOLOGICAL IMPLICATIONS OF MUSCLE ELASTICITY AND VISCOSITY.**

Stephen F. Levinson[1], Armen Sarvazyan[2], Jeong–Rock Yoon[3], Joyce R. McLaughlin[4], Oleg Rudenko[5].*
[1]Wayne State University, 261 Mack Boulevard, Detroit, MI, 48201, USA; [2]Artann Laboratories, Inc., 1457 Lower Ferry Road, West Trenton, NJ, 08618–1414, USA; [3]Clemson University, O–225 Martin Hall, Box 340975, Clemson, SC, 29634-0975, USA; [4]Rensselaer Polytechnic Institute, 110 8th street, Troy, NY, 12180–3590, USA; [5]M.V. Lomonosov Moscow State University, Vorob'evy gory, 119992, Moscow, RUSSIAN FEDERATION.

Background: Skeletal muscle represents one of the most mechanically complex of biological tissues. It is dynamic, elastic, highly viscous and anisotropic. We have previously reported on data obtained using supersonic shear wave imaging (SSI) and magnetic resonance elastography (MRE). Based on these data, we have determined that both elasticity and viscosity are highly anisotropic and that, rather than being a passive parameter, viscosity changes dramatically with contraction. With the application of new inversion algorithms, we now have the opportunity to quantify these properties and draw inferences based on classical mechanics and biologic function. Our work has spawned interest in developing new mathematical models derived from the molecular basis of muscle contraction.

Aims: Elastography makes it feasible to measure both shear muscle elasticity and viscosity as a function of fiber orientation and the contractile state. We seek to better understand the relationship between the anisotropic viscoelastic properties of skeletal muscle and muscle function. Further, we intend to examine and challenge the adequacy of existing biomechanical models of muscle and to develop new models as appropriate.

Methods: Data previously obtained from the human biceps brachialis muscle as a function of applied load using SSI [1] and from the gastrocnemius–soleus muscle group using MRE [2] were used in this study. Our approaches to inversion of these data are being presented separately. The data were assessed in terms of their potential physiologic bases and relationships to known and theoretical aspects molecular biology. The potential implications in terms of the biomechanical aspects of muscle function were also explored.

Results: A representative time–lapse SSI image is shown in Figure 1. Elasticity and viscosity were derived from this and similar images, and from MRE data. Both properties were found to be strongly affected by muscle fiber orientation and the contractile state. None of the existing models of muscle contraction and muscle biomechanics that we have studied can adequately explain the phenomena observed. The data are consistent, however, with aspects of muscle physiology and function. A new model that is based on the molecular biology of crossbridge activity shows significant promise in light of the data presented [3].

Conclusions: The viscoelastic properties of skeletal muscle can be reconstructed from SSI and MRE data as a function of fiber orientation and contractile state. Although correlations with function and physiology can be drawn, new biomechanical models may be required to adequately represent the results obtained.

Acknowledgements: The supersonic ultrasound data was obtained from the laboratory of M Fink at Laboratoire Ondes et Acoustique, ESPCI, Paris, France, and the magnetic resonance elastography data was provided by R Ehman at Mayo Clinic, Rochester, MN, USA.

References:

[1] J Bercoff, M Tanter, M Fink. Supersonic shear imaging: a new technique for soft tissue elasticity mapping. IEEE Trans Ultrason Ferroelect Freq Control, vol 51, 396–409, 2004.
[2] J Basford, T Jenkyn, K An, R Ehman, G Heers, K Kaufman. Evaluation of healthy and diseased muscle with magnetic resonance elastography. Arch Phys Med Rehabil, vol 83, 1530–6, 2002.
[3] O Rudenko, A Sarvazyan. Wave Biomechanics of Skeletal Muscle. Acoustical Physics No. 6, in press, 2006.

Figure 1: Composite image showing a 3 frame sequence of displacement data. Frame 1 is shown in red, Frame 2 in green and Frame 3 in blue.

025 **TWO–DIMENSIONAL MULTI–LEVEL STRAIN ESTIMATION FOR DISCONTINUOUS TISSUE.**

H.Shi[1], T Varghese[1].*
[1]University of Wisconsin–Madison, 1530 MSC, 1300 University Avenue, Madison, WI, USA.

Background: A large number of strain estimation methods presented in the literature are based on an assumption of tissue continuity that establishes a continuous displacement field. However, in certain locations in the body such as in the arteries *in–vivo* scanning may produce displacement fields that are discontinuous between the two walls of the artery. Many of the displacement or strain estimators fail when the displacement fields are discontinuous.

Aims: In this work, we present a new 2D multi–level motion or displacement tracking method using 2D cross–correlation for accurate estimation of the strain for discontinuous tissue.

Methods: A 2D multi–level cross–correlation method to compute local displacement fields and strains in discontinuous media was used. Coarse displacement estimates are initially obtained using sub-sampled B-mode data using a multi–level pyramid algorithm. The coarse displacement estimates are then utilized to guide the high resolution estimation on the lowest level of the pyramid containing the RF echo signal data. This method combines the advantages provided by the robustness of B–mode envelope tracking and the precision obtained using RF motion tracking to obtain high resolution displacement and strain estimates. After motion or displacement tracking at each level of the pyramid, we utilize the normalized cross-correlation coefficient as a confidence measure corresponding to the reliability of the displacement estimate. Displacement estimates with a low normalized cross–correlation coefficient are replaced or interpolated from surrounding displacement estimates that possess a higher normalized cross–correlation value.

Results: The 2D multi–level method is evaluated using both finite element analysis (FEA) based ultrasound simulations and experimental data acquired on the carotid artery. Results obtained from the FEA based simulations demonstrate the effectiveness of the 2D multi–level method for strain estimation in discontinuous media. We compare the strain estimation performance of 1D cross–correlation and 2D cross-correlation based on the displacement continuity assumption to the 2D multi–level method. Our results illustrate that all of the methods based on the displacement continuity assumption fail to estimate strains on the distal boundary of the vessel wall, where only the 2D multi–level method provides consistent results.

The effectiveness of this method is also demonstrated on *in–vivo* data obtained on the carotid artery, where the two walls of the artery are separated by blood leading to discontinuous media. *In–vivo* scanning of the carotid plaque is performed using a Siemens Antares ultrasound system with an ultrasound research interface.

Conclusions: We demonstrate the feasibility of utilizing a 2D multi–level cross–correlation based method to compute local displacements and strain for discontinuous tissue. The FEA simulations and *in–vivo* experimental data demonstrate the improvement in the strain estimation performance over algorithms based on the tissue continuity assumption.

* *indicates Presenter*

079 **A METHOD FOR IMAGING THE TIME–DEPENDENT MECHANICAL BEHAVIOR OF POROELASTIC MATERIALS USING AXIAL STRAIN ELASTOGRAPHY.**

Raffaella Righetti[1], Mariapaola Righetti[2], Jonathan Ophir[1], Thomas A. Krouskop[3].*
[1]The University of Texas Health Science Center Houston Medical School, 6431 Fannin St., Houston, TX, 77030, USA; [2]University of Florence, Via S. Marta 3, Florence, 50139, ITALY; [3]Baylor College of Medicine, One Baylor Plaza, Houston, TX, 77030, USA.

Background: The time–dependent mechanical behavior of poroelastic materials can be tested using a number of compression methods. In the field of elastography, poroelastograms are usually generated as ratios between lateral and axial strain elastograms acquired from a poroelastic material undergoing stress relaxation [1]. In a homogeneously poroelastic cylindrical sample under stress relaxation, the axial strain distribution does not change significantly with time, while the lateral strain distribution decays in an exponential manner, which depends on the geometry, and the elastic and permeability properties of the sample. If the poroelastic sample is subjected to a creep experiment, instead, temporal changes occur both in the axial strain and the lateral strain distributions [2].

Aims: In this paper, we investigate the feasibility of imaging the behavior of poroelastic materials using axial strain elastograms obtained from porous samples in a creep test.

Methods: Axial strain, lateral strain and effective Poisson's ratio elastograms and poroelastograms were generated from cylindrical tofu phantoms subjected to an unconfined sustained constant load. The constant load compression was applied using a mechanical device built in our laboratory that allows the application of a wide range of axial forces. For comparison, gelatin phantoms of similar geometry were also tested. Simulations were performed to corroborate the experimental findings.

Results: The results of our study demonstrate that in creep experiments, both axial strain elastograms and lateral strain elastograms exhibit a time–dependent behavior that depends on the geometry and the elastic and permeability properties of the material. Samples with different poroelastic properties were found to be characterized by significantly different axial strain time constants as well as lateral strain time constants. The effective Poisson's ratio elastogram time constants were found not to be statistically significantly different from those obtained from the same materials under stress relaxation. Axial strain and lateral strain elastograms obtained from gelatin phantoms showed no significant changes with time.

Conclusions: Creep experiments can be used to generate time–dependent changes in the axial strain elastograms of poroelastic materials. These time–dependent changes can be exploited to distinguish between homogeneous materials having different poroelastic properties. The use of axial strain elastograms for imaging the time–dependent mechanical behavior of poroelastic materials would be of great advantage to overcome image quality limitations typical of lateral strain elastograms. This cannot be accomplished using stress relaxation experiments, since during stress relaxation, the axial strain distribution is expected not to change appreciably with time. In creep experiments, lateral strain elastograms may still be required for the estimation of the time–dependent mechanical behavior of the effective Poisson's ratio of the material, particularly in the case of non–homogeneous poroelastic samples.

Acknowledgements: This work was partially supported by NCI Program Project PO1–CA64597–12 and by funding from John S. Dunn foundation to The University of Texas Health Science Center Houston Medical School.

References:

[1] Righetti R, Ophir J, Srinivasan S, Krouskop TA. The feasibility of using elastography for imaging the Poisson's ratio in porous media. Ultras. Med. Biol., vol. 30(2): 215–228, 2004.
[2] Armstrong CG, Lai WM, Mow VC. An analysis of the unconfined compression of articular cartilage. J. Biomech. Eng., vol. 106: 165–173, 1984.

064 **THE SPATIO–TEMPORAL BEHAVIOUR OF THE STRAIN FIELD IN LAYERED POROELASTIC MEDIA.**

Gearóid P. Berry[1], Nigel L. Bush[1], Jeffrey C. Bamber[1].*
[1]Institute of Cancer Research, 15 Cotswold Road, Sutton, Surrey, England, UK.

Background: Soft tissues contain mobile fluid which can be displaced by compressing the tissue. In an attempt to model the influence of this compression–induced fluid flow on tissue mechanical behaviour, soft tissue has previously been treated as a poroelastic material [1]. Furthermore, elastographic techniques have previously been used to image the time-evolution of the compression–induced strain field in homogeneous cylindrical poroelastic phantoms and time–dependent spatially–varying behaviour consistent with the predictions of poroelastic theory has been observed [2,3]. However, before investigating the clinical applicability of poroelastic strain imaging techniques *in vivo*, it would first be desirable to investigate their performance in more complex phantom materials that more closely resemble the anatomical structure of soft biological tissue.

Aims: The aim of this current study was to generalise previous work by determining if elastographic techniques could be used to image and interpret the time–evolution of the strain in heterogeneous layered poroelastic samples.

Methods: Using finite element simulation, the governing equations of poroelasticity [4] were solved to predict the behaviour of the strain field in layered poroelastic models. Pseudo–static elastographic techniques were also applied to image the time–evolution of the strain field in layered poroelastic phantoms where the poroelastic properties were varied between the different layers.

Results: The imaged compression–induced strain field exhibited time–dependent spatially–varying behaviour consistent with the predictions of the finite element simulation.

Conclusions: This study has determined that elastographic techniques may be used to image and interpret the behaviour of the strain field inside layered poroelastic phantoms. The nature of the observed strain behaviour revealed both the location of the mobile fluid and the flow path taken by the fluid as it was expressed from the phantom. Such information might be of clinical value in the assessment and diagnosis of lymphoedema as well as in the differential diagnosis of tumour tissue.

Acknowledgements: This work was supported by grants from the Institute of Cancer Research and the Engineering and Physical Sciences Research Council, UK.

References:

[1] Berry GP, Bamber JC, Armstrong CG, Miller NR, Barbone PE. Towards an acoustic model–based poroelastic imaging method: I. Theoretical foundation. Ultrasound Med Biol 2006;32(4):547–567.
[2] Berry GP, Bamber JC, Armstrong C, Miller NR. Towards a model–based poroelastic imaging method. Proceedings of the Third International Conference on the Ultrasonic Measurement and Imaging of Tissue Elasticity. October 17–20, Cumbria, UK: 2004b: p96 (abstract).
[3] Berry GP, Bamber JC, Bush NL, Miller NR. The spatio–temporal variation of the strain field inside compressed poroelastic materials. Proceedings of the Fourth International Conference on the Ultrasonic Measurement and Imaging of Tissue Elasticity. October 16–19, Austin, TX, USA: 2005a: p97 (abstract).
[4] Biot MA. General Theory of Three-Dimensional Consolidation. J Applied Physics 1941;12:155–164.

* *indicates Presenter*

104 **CALIBRATION CURVES FOR NONLINEAR QUANTIFICATION OF TISSUE ELASTICITY WITH SCANNING ACOUSTIC MICROSCOPY.**

J. L. Katz[1,2], O. Marangos[1], Y. Wang[2], P. Spencer[2], A. Misra[1].*
[1]School of Computing and Engineering; [2]School of Dentistry, University of Missouri–Kansas City, Kansas City, MO 64110, USA.

Background: Scanning acoustic microscopy (SAM) is one of the few nondestructive techniques that provide very high resolution micromechanical properties of samples from low reflectance biological tissues to quite high reflectance metals and ceramics [1]. What is obtained on a SAM image is a mapping of the reflection coefficient, $r = (Z_2-Z_1)/(Z_2+Z_1)$, where Z_2 and Z_1 are the acoustic impedances ($Z = \rho c$) of the material being studied and the acoustic coupling fluid respectively [2,3].

Aims: To quantify the micromechanical properties of materials by measurement of the reflection coefficient requires calibration of the received signal amplitude as related to the reflection coefficients of known materials. This is based on the common assumption that the received signal amplitude is proportional to the reflection coefficient. There are several cases in which simple linear fits could result in erroneous results: (1) clearly when the linear fit does not agree with the theoretical relationship; (2) if the reflectance of the target material lies below the lowest or above the highest of the calibration materials; and (3) the target material has continuous reflectances over a wide range. Also of concern is that materials with very low r values ($r \sim <0.2$) may not provide a strong signal so that system amplification settings have to be used in order to obtain a measurable signal.

Methods: Therefore, for any quantification purposes, the calibration has to be performed for the specific material as well as for the specific acoustic imaging system. In this continuing study, we analyze the signals from SAM in frequency and time domains to obtain gain functions for various system amplification settings. The gain functions are found to significantly depend upon both the material reflectance as well as the frequency at high amplification settings. These gain functions are then used to predict the relationships between reflection coefficients and Fourier amplitude or average power. These analyses were applied to develop calibration curves for the WINSAM 100 SAM system (Kramer Scientific Instruments GmbH, Herborn, Germany) using a 30 MHz central frequency transducer (KSI PT30–002).

Results: Nine reference materials with acoustic impedance ranging from 2.3 MRayl to 99.58 MRayl were used; these are shown in the following table. Using such analyses makes it now possible to separate materials' effects from system electronic effects, resulting in better estimates of errors in the material properties being measured. From the frequency domain calculation it is clear, that at a given gain setting, the gain function has an inverse relationship with reflectance. Thus the gain function serves to saturate the signal for high reflectance materials. As in the case of the frequency domain calculation, excellent agreement is obtained in the time domain calculation for gain settings of –10 and 0 dB. However, at 8 dB gain setting the predicted values deviate for high reflectance material. This deviation is a result of nonlinear behavior of the gain function at such high gain settings. Also, the predicted results using the time domain fits are very close to those obtained for the 3 dB bandwidth frequencies.

Material		ρ (g/cm³)	c (m/s)	Z = ρc (MRayl)	R_{th}
Calibration Materials	Tungsten (W)	19.07	5222	99.58	0.97
	Copper (Cu)	8.72	4662	40.7	0.93
	Brass	8.37	4195	35.1	0.92
	Aluminum (Al)	2.76	6268	17.3	0.84
	PVC	1.41	2366	3.3	0.38
	PETG	1.27	2325	2.9	0.33
	Polycarbonate	1.19	2270	2.7	0.29
	Polypropylene	0.90	2640	2.4	0.23
	HDPE	0.95	2439	2.3	0.21
Validation Materials	LDPE	0.91	2071	1.9	0.12
	TPX®	0.82	2180	1.7	0.09
Couplant	Water (24°C)	1.00	1495	1.5	-

Conclusions: To assess the applicability of the above calculations, the developed calibration curves were validated by comparison with independently measured reflection coefficients for the two lowest impedance materials, LDPE and TPX®. The comparisons show that the predicted reflection coefficients are within 10% of the theoretical values.

Acknowledgements: This research supported in part by: USPHS Research Grants DE14392, National Institute of Dental and Craniofacial Research (PS); USPHS Major Instrumentation Grant RR16710 (PS); DE 15281 (YW); National Institutes of Health, Heart, Lung, Blood Institute, NIH R01 HL69064–01–05 (JLK); FDA Project KG001436 (JLK); UMKC Chancellor's Interdisciplinary Ph.D. Fellowship (OM). Research performed in UMKC Center for Research on Interfacial Structure and Properties (UMKC–CRISP).

References:

[1] Briggs G. A. Acoustic Microscopy. Oxford, UK: Clarendon; 1992.
[2] Raum K., Jenderka K. V., Klemenz A., Brandt J. Multilayer Analysis: Quantitative Scanning Acoustic Microscopy for Tissue Characterization at a Microscopic Scale. IEEE Transactions on Ultrasonics, Ferroelectrics, and Frequency Control 50(5): 507–516, 2003.
[3] Hirsekorn S., Pangraz S., Weides G., Arnold W. Measurement of Elastic Impedance With High Spatial Resolution Using Acoustic Microscopy. Applied Physics Letters 67(6): 745–747, 1995.

021 **CONTRAST–TRANSFER EFFICIENCY FOR ELECTRODE DISPLACEMENT ELASTOGRAPHY.**

Shyam Bharat[1], Tomy Varghese[1].*
[1]University of Wisconsin–Madison, 1530 MSC, 1300 University Avenue, Madison, WI, USA.

Background: Electrode displacement elastography is a strain imaging method that can be used for *in vivo* imaging of radiofrequency (RF) ablation–induced lesions in abdominal organs such as the liver and kidney [1]. In this technique, tissue motion or deformation is introduced by displacing the same electrode used to create the lesion, and strain images are generated from ultrasound echo signals acquired before and after the electrode–induced displacements.

Aims: The local strains imaged depend on the modulus distribution of the tissue region being scanned. Therefore, a quantitative evaluation of the contrast transfer efficiency from modulus contrast to strain contrast in electrode–displacement elastograms is warranted. The contrast–transfer efficiency (CTE) has been utilized earlier for external compression elastography [2,3]. In this study, we present a CTE formalism for electrode displacement elastography.

Methods: The CTE is defined as the ratio (in dB) of the observed elastographic strain contrast and the underlying true modulus contrast. The variations of the CTE parameter as a function of the underlying true modulus contrast, applied displacements and distance of the inclusion from the surface of the ultrasound transducer were investigated using finite element analysis. The results of these finite element simulations were incorporated into a frequency–domain ultrasound simulation program, to study the impact of the ultrasound–based strain estimation noise artifacts on the CTE. Validation of the finite element simulation results was also achieved by imaging a custom-made tissue–mimicking (TM) phantom containing a single spherical inclusion with a mock RF electrode embedded in it.

Results: The CTE was compared for both electrode displacement and external compression elastography. The trend in the CTE was similar for both methods, in that stiffer inclusions in a softer background exhibited higher CTE values than softer inclusions in a stiffer background. Also, both methods show the highest CTE when the inclusion had the same underlying elastic modulus as the background. However, while this maximum CTE value was 0dB for external compression elastography, it was greater than 10dB for electrode displacement elastography. For all cases of stiffer inclusions in a softer background, the electrode displacement method exhibited CTE values approximately 10dB above that seen in the external compression method. The CTE was fairly independent of the applied incremental displacements (in the range of displacements studied), while it decreased marginally with the distance of the inclusion from the surface of the transducer. Results from the ultrasound simulation program and the TM phantom were in excellent agreement with the finite element simulations.

Conclusions: CTE values in excess of 0dB are indicative of the fact that, in electrode displacement elastography, the observed strain contrast is higher than the underlying modulus contrast, for stiffer inclusions in a softer background. This property of electrode displacement elastography could be useful for clearly delineating the boundaries of lesions or tumors that are marginally stiffer than surrounding normal tissue, since the corresponding strain contrast on electrode displacement elastograms is expected to be higher than the underlying modulus contrast, based on the results of this study.

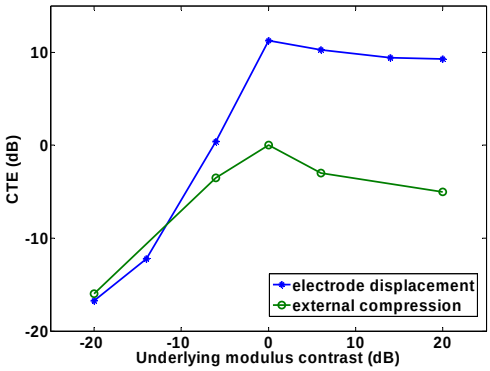

References:

[1] Varghese T, Zagzebski JA and Lee FT, Jr. 2002. Elastographic Imaging of Thermal Lesions in the Liver *in vivo* following Radiofrequency Ablation: Preliminary results, *Ultrasound Med Biol*, 28, 1467–73.
[2] Ponnekanti H, Ophir J, Yijun H and Cespedes I 1995. Fundamental Mechanical Limitations on the Visualization of Elasticity Contrast in Elastography, *Ultrasound Med Biol*, 21, 533-43.
[3] Kallel F, Bertrand M and Ophir J 1996. Fundamental Limitations on the Contrast–Transfer Efficiency in Elastography: An Analytic Study, *Ultrasound Med Biol*, 22, 463-70.

* *indicates Presenter*

087 **FORWARD SIMULATIONS FOR DETERMINING THE DETECTABILITY OF SMALL INCLUSIONS WITH DYNAMIC ELASTOGRAPHY.**

Jeremy McNamara[1], Larisa Goldmints[1], Antoinette M. Maniatty[1].*
[1]Rensselaer Polytechnic Institute, Jonsson Engineering Center 2049, 110 8th Street, Troy, NY, USA.

Aims: The goal of this work is to determine the sensitivity of the observed changes in tissue dynamic motion to the size and stiffness of an inclusion as well as the frequency of the propagating shear wave and background stiffness. The purpose of this study is to provide an indication of the detectability of the inclusion. If the perturbation of the tissue displacement due to the inclusion is less than the error from modeling or measurement, then it becomes difficult to detect the inclusion. The directional dependence of the wave speed for a regular array of rod–shaped inclusions is also studied for different frequencies.

Background: Currently, many researchers are developing methods to reconstruct tissue elastic properties from elastographic measurements for diagnostic use in the medical field [1,2]. A natural question that arises is: What is the minimum size or stiffness contrast of a tumor that can be detected using this method. Studies have been performed in 2–D at a single frequency, and it was found that the perturbation in the displacement field due to a stiff inclusion is proportional to the area of the inclusion and slightly less than proportional to the contrast ratio between the inclusion and surrounding tissue. Evidence of this relationship in 2–D motivates further studies that can establish a similar relationship in 3–D and at different frequencies. Separately, studies have been performed on quasi–composite samples consisting of a background matrix and stiffer included parallel rods, to simulate an anisotropic inclusion, for example, due to blood vessels running along the same direction. An orientation–dependent relationship has been identified between the shear wave wavelength and relative shear wave speeds in the rods and background matrix. At larger wavelengths, the shear wave sees the inclusion as a homogeneous, composite material, but at shorter wavelengths, a differentiation in speeds along different directions that is not predicted for a homogenized composite, suggests that the wave sees the rods and matrix separately.

Methods: A forward simulation is performed using a finite element method in space and finite difference method in time. The finite element code uses general 3–D equations of elasto–dynamics for the solution. A special finite element formulation, with piece–wise tri–linear interpolation of the displacement field and piece–wise constant interpolation of the pressure field is used in order to handle the nearly incompressible behavior of tissue. The finite element parallel code is written in C. PETSc functions are used to simplify partitioning and parallelization of the algorithm. Contrast ratio and size of inclusion will be varied, and simulations will be performed at various frequencies.

Results: Standard deviations in the displacement field from that without an inclusion are calculated for each of the simulations over spatial and temporal domains with varying contrast ratio and inclusion size. From these, a relationship is determined for the detectability of the inclusion with respect to the contrast ratio and size. In addition, the effect of frequency and the background stiffness, which together control the wavelength, on detectability will be noted.

Conclusions: This study should provide greater insight into shear wave imaging techniques and give a better understanding of the limits of detection. In addition, the frequency dependence of detection should allow researchers to optimize their studies to maximize detectability of inclusions.

Acknowledgements: This work has been supported by the National Science Foundation through grant DMS-0101458 and by the National Institutes of Health through grant 5 R21 EB003000–02. The authors thank J. McLaughlin, E. Park, and D. Renzi at Rensselaer for many valuable discussions.

References:

[1] J. McLaughlin and D. Renzi, "Shear Wave Speed Recovery in Transient Elastography and Supersonic Imaging Using Propagating Fronts", Inverse Problems, Vol. 22, April 2006, pp. 681–706.
[2] E. Park and A.M. Maniatty, "Shear Modulus Reconstruction in Dynamic Elastography: Time Harmonic Case", accepted, Physics in Medicine and Biology, 51:15 August, 2006, pp. 3697–3721.

038 **SOME RESULTS ON THE CONDITIONING OF THE INVERSE PROBLEM OF IMAGING IN MAGNETIC RESONANCE ELASTOGRAPHY.**

David J.N. Wall[1], Peter Olsson[2], Elijah E.W. Van Houten[3].*

[1]Centre for Bioengineering, Department of Mathematics & Statistics, University of Canterbury PB4800 Christchurch, NEW ZEALAND; [2]Department of Applied Mechanics, Chalmers University of Technology, SE-412 96 Gothenburg, SWEDEN; [3]Department of Mechanical Engineering, University of Canterbury, PB4800 Christchurch, NEW ZEALAND.

Background: The imaging problem of elastography is an inverse problem. The nature of an inverse problem is that it is ill–conditioned. We consider properties of the mathematical map which describes how the elastic properties of the tissue being reconstructed vary with the field measured by Magnetic Resonance Imaging. This map is a nonlinear mapping and our interest is in proving certain conditioning and regularity results for this operator which occurs naturally in this problem of imaging in elastography. In this treatment, we consider the tissue to be linearly elastic, isotropic and spatially heterogeneous. We determine the conditioning of this problem of function reconstruction, in particular for the density and stiffness functions.

Aims: We examine the Fréchet derivative of the nonlinear mapping, which enables us to describe the properties of how the field affects the individual maps to the density and stiffness functions. This paper illustrates how use of the implicit function theorem and the techniques developed in [1] can considerably simplify the analysis of Fréchet differentiability and regularity properties of this underlying operator.

Results: We present new results which show that the stiffness map is relatively well conditioned, whereas the density map suffers from medium ill–conditioning. Computational work has been done previously to study the sensitivity of these maps [2], but our work here is analytical.

The validity of the Newton–Kantorovich methods for the computational solution of this inverse problem is directly linked to the Fréchet differentiability of the appropriate nonlinear operator, which we justify.

Conclusions: The choice of elastic properties for imaging in elastography research remains an open question at this point; the use of the analytical methods described here will help to predict and understand the value and reliability of different parameterizations of elasticity imaging. Furthermore, results indicate significant work needs to be done to achieve effective multi–parameter reconstructive imaging.

Acknowledgements: This work was initiated while one of the authors (DJNW) was visiting the Chalmers University of Technology, and he thanks the University for possibility of the visit and the hospitality received.

References:

[1] T. J. Connolly and D. J. N. Wall. On Fréchet differentiability of some non–linear operators occurring in inverse problems; an implicit function theorem approach. *Inverse Problems*, 6:949–966, 1990.

[2] Elijah E. W. Van Houten, Marvin M. Doyley, Francis E. Kennedy, Keith D. Paulsen, and John B. Weaver. A three-parameter mechanical property reconstruction method for MR–based elastic property imaging. *IEEE Transactions on Medical Imaging*, 24(3):311–324, March 2005.

* *indicates Presenter*

116 **VARIANCE CONTROLLED SHEAR STIFFNESS IMAGING IN MAGNETIC RESONANCE ELASTOGRAPHY.**

JR McLaughlin[1], D Renzi[1], J R Yoon[2].*
[1]Rensselaer Polytechnic Institute, Troy, NY, USA; [2]Clemson University, Clemson, SC, USA.

Background: Magnetic Resonance Elastography is a new imaging technique to measure the stiffness of tissue. In this experiment, a single frequency mechanical excitation is applied to the surface of an object and the interior displacement, U, of the resulting time harmonic wave is measured with MR. Under some assumptions, the displacement satisfies the Helmholtz equation, $\omega^2 U = \mu \Delta U$, and the shear modulus, μ, can be found simply by calculating $\mu = -\omega^2 U / \Delta U$. Typically the displacements are first filtered, then $\mu = -\omega^2 U / \Delta U$ is numerically calculated, and because small quantities in the denominator can lead to outliers, a median filter is applied to the shear modulus.

Aims: We apply MRE to a phantom experiment performed at the Mayo Clinic by Richard Ehman. The phantom contains a large 1.7 cm inclusion and a second very small 3 mm inclusion. The amplitude behind the large inclusion is very small, so the SNR varies substantially across the medium. There is a tradeoff between creating a good image of the small inclusion and generating artifacts in the low SNR regions. The aim of this work is to generate high quality images that both recover the small inclusion and do not have artifacts in the low SNR regions by equalizing the variance of the reconstructed shear modulus across the medium.

Methods: We first decompose the displacement into phase and amplitude. This is required because the most important term in shear modulus recovery is a first derivative phase term, and calculating the second derivatives in the Laplacian over smooth the information rich first derivative phase term. We used a statistically based averaging scheme to calculate all derivatives, and choose the parameters such that the first and second derivative terms have the same variance. Then we apply a median filter to the shear modulus, where the support of the median filter is adjusted according to the SNR to equalize the variance of the recovered modulus across the medium.

Results: We apply this method to a phantom experiment containing a small 3 mm inclusion with a stiffness contrast of about 6. We are able to recover the full contrast of the small inclusion without creating artifacts in the low SNR regions.

Conclusions: In MRE, the SNR can vary significantly across the medium, which creates a tradeoff between resolution in high SNR regions and artifacts in low SNR regions. Furthermore, the information rich first derivative phase terms can be over smoothed when calculating the Laplacian, causing a loss of resolution. When these issues are taken into account by equalizing the variance across the image, we can generate an improved reconstruction that has better resolution in high SNR regions without creating artifacts in low SNR regions.

113 **NONLINEAR ELASTICITY IMAGING: RECOVERING NONLINEAR ELASTIC PARAMETERS USING HIGHER ORDER FINITE ELEMENTS.**

NH Gokhale[1], MS Richards[1], CE Rivas[1], R Leiderman[1], PE Barbone[1] and AA Oberai[1,2].*
[1]Boston University, Boston, MA, USA; [2]Rensselaer Polytechnics Institute, Troy, NY, USA.

Background: It is well known that the mechanical properties of soft tissue can change with tissue pathology. For example, it is observed that the elastic (shear) modulus of malignant breast masses is typically an order of magnitude higher than the background of normal soft tissue. In addition, it is known that with increasing applied strain the stiffness of cancerous soft tissues increases more rapidly than the background of non-malignant soft tissues [1,2]. While many attempts have been made to image and map the linear elastic properties of soft tissue [3–6], relatively few attempts have been made to account for both large deformation and material non–linearity in reconstructing the elastic properties of soft tissue. One notable exception is the work of Skovoroda [7], which accounts for large deformations but uses a linear constitutive model.

Aims: The objective of our present work is to develop, implement and test algorithms to reconstruct the material parameters in non–linear, large deformation hyperelastic tissue models, given "measured" displacement fields.

Methods: The overall problem was formulated as a constrained minimization problem. The constraint took the form of a finite element (FEM) model for the hyperelastic tissue response. In the forward FEM model, due consideration was given to issues of mesh locking which were avoided by the use of higher order finite elements. The optimization problem was solved efficiently using a quasi–Newton method and the adjoint method. A novel initialization technique was used to further accelerate the inverse problem solution. By using a very good guess of the displacement field (corresponding to the previous material property update), we avoided solving a complete non–linear problem at every inversion iteration.

Results: We present numerical examples highlighting the roles, respectively, of geometric nonlinearity, material nonlinearity and combined geometric and material nonlinearities. Where appropriate, comparisons to linear elastic reconstructions are given. The acceleration technique described above speeds the solution of the inverse problem by about a factor of 20.

Conclusions: An efficient method for reconstructing material property maps in hyperelastic constitutive relations in the limit of incompressibility is presented. Numerical examples are presented to show the efficiency of this approach. Future applications include mapping the non–linear material parameters in soft tissue for medical diagnosis (biomechanical imaging) and computer assisted surgery.

Acknowledgements: This work was supported by the DOD Breast Cancer Research Program (Award No. W81XWh-04–1–0763) and NSF.

References:

[1] Kroukop TA, Wheeler TM, Kallel F, Garra BS and Hall T. Elastic moduli of breast and prostate tissues under compression. Ultrasonic Imaging 20:260–274, 1998.
[2] Wellman P, Howe RH, Dalton E and Kern KA. Breast tissue stiffness in compression is correlated to histological diagnosis. Technical Report, Harvard Biorobotics Laboratory, 1999.
[3] Oberai AA, Gokhale NH, Feijoo GR. Solution of inverse problems in elasticity imaging using the adjoint method. Inverse Problems 19:297–313 2003.
[4] Oberai AA, Gokhale NH, Doyley MM, Bamber JC. Evaluation of the adjoint equation based algorithm in elasticity imaging. Physics in Medicine and Biology 49:2955–2974, 2004.
[5] Doyley MM, Meaney PM, Bamber JC. Evaluation of an iterative method for quantitative elastography. Physics in Medicine and Biology 45:1521, 2000.
[6] Miga MI. A new approach to elastography using mutual information and finite elements. Physics in Medicine and Biology 48(6):467–480, 2003.
[7] Skovoroda AR, Lubinski MA, Emelianov SY and O'Donnell M. Reconstructive elasticity imaging for large deformations. IEEE Transactions of Ultrasonics, Ferroelectrics and Frequency Control, 46:523, 1999.

** indicates Presenter*

111 **ESTIMATION OF TISSUE ELASTICITY PARAMETERS USING A SIMILARITY BASED APPROACH.**

Junbo Li[1], Yaoyao Cui[1], Michael Kadour[1], Alison Noble[1].*
[1]Wolfson Medical Vision Lab, Department of Engineering Science, University of Oxford, Parks Road, Oxford, OX1 3PJ, England, UK.

Background: The *in vivo* estimation of tissue elasticity parameters is important for realistic tissue deformation modeling and diagnostic tasks such as cancer detection. So far the commonly used approach involves solving the so–called inverse elasticity problem of recovering elastic parameters from displacement measurements. A limiting factor in this solution is the accuracy of displacement estimation. Recently, a general approach to elasticity imaging was introduced by Miga [1] that attempts to relate the inverse reconstruction problem to the problem of non–rigid image registration. Our presentation, which reports on a continuation of our previous work in ultrasound elasticity imaging [2], follows this similarity based approach and explores its potential benefits for ultrasound elasticity imaging of the breast.

Methods: We consider the inverse elasticity problem as a global optimal problem based on the similarity measures of the observed and the model–deformed ultrasound images and build the inverse problem within the framework of non–rigid image registration. Different similarity metrics for ultrasound images have been employed. An obvious advantage of the proposed method was that no explicit displacement estimation step was needed. The displacement calculation was actually embedded in the optimization process. The main error sources related to the validity of the deformation model and the signal–to–noise ratio of the recorded images. A split–and–merge approach was used based on the local mismatch of the model–deformed and the observed image and the inverse problem was solved iteratively.

Results: We evaluate the performance of the similarity–based inverse elasticity imaging method through a series of experiments with synthetic images, phantom data for which the "ground–truth" was known and *in vivo* breast ultrasound data. Some preliminary results illustrate the effectiveness of the method (Figure 1).

References:

[1] Washington, C.W., Miga, M.I.: Modality Independent Elastography (MIE): A New Approach to Elasticity Imaging. IEEE Trans. on Medical Imaging 23 9 (2004) 1117–1128.
[2] Li, J., Cui, Y., Noble, J.A.: Inverse elasticity reconstruction based on an image–similarity measure approach, Proc. of the Third International Conference on the Ultrasonic Measurement and Imaging of Tissue Elasticity, Windermere, Cumbria, UK (2004).

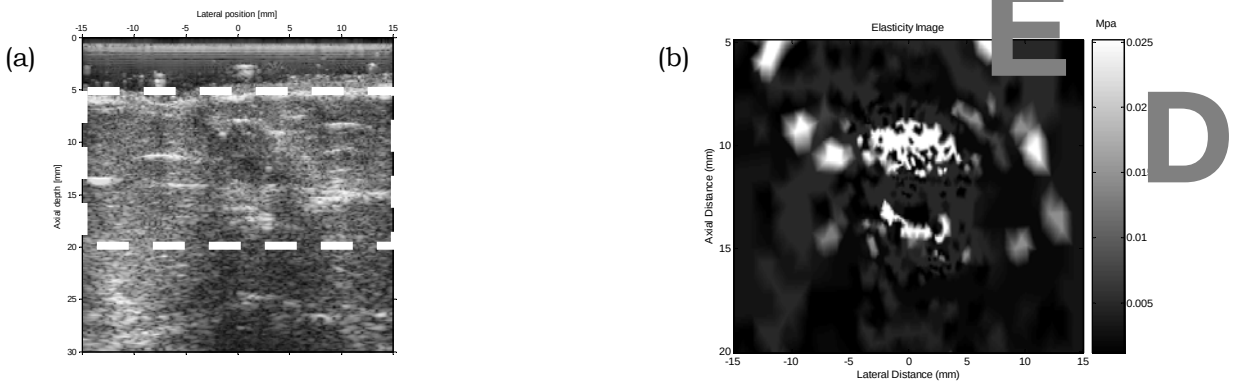

Figure 1: *In vivo* elasticity imaging of the breast tissue with a scar. (a) illustrates the B–mode image and (b) shows the elasticity image.

082 **VISCOELASTIC TISSUE PROPERTY MEASUREMENT USING HIGH FREQUENCY ULTRASOUND.**

D. Liu[1], E. S. Ebbini[2].*
[1,2]University of Minnesota, Minneapolis, MN, USA.

Background: The advantages of high frequency ultrasound system (HFUS) in dermatology and ophthalmology have been proven, but results on quantitative imaging with HFUS are mixed at best [1]. With the current 20–40 MHz imaging system, it is difficult to distinguish between hypoechoic structures such as tumors, nevi, sebaceous glands and hair follicles [1]. One solution is to use even higher frequencies (40-60 MHz) as nicely illustrated in [2], but this still will not address the quantitative imaging limitations. A controlled application of acoustic radiation force (ARF) with appropriate modeling to allow for localized tissue property measurement may provide an important tool towards mitigating this impediment.

Aims: Our aim is to develop a high frequency ultrasound system for quantitative imaging of viscoelastic properties of thin tissue samples (e.g. skin and subcutaneous tissue).

Methods: The core component was a dual–element concave transducer with a highly focused PZT–4 transducer (5 MHz, 20 mm diameter, $f_{\#}$ = 0.625) for localized application of ARF and an inner PVDF imaging transducer (25 MHz, 100% BW, 6 mm diameter, $f_{\#}$ = 2) for monitoring of the induced shift. The application of ARF pulses and M–mode imaging were synchronized so that the entire dynamics of the tissue deformation can be captured at PRF values up to 10 kHz without interference from ARF pulses. In addition, coded excitation technique was utilized to improve SNR as well as suppress the strong interference imposed by the highly concave structure of PZT–4 transducer in imaging and motion tracking. Captured RF data was first evaluated using a correlation based shift estimation algorithm to produce spatio–temporal displacement maps along the axial direction. These displacement maps were used as input to an extended Kalman filter (EKF) for on–line tracking of the shear modulus and shear viscosity. The EKF simultaneously estimated the state and parameter values utilizing a second order constitutive model of viscoelastic response with unknown parameters. It also allowed for incorporation of both input and measurement noise models. The former was significant since local variations in absorption and/or ARF beam distortions are inevitable in practice and cannot be predicted precisely *in situ*. The system was tested using tissue mimicking phantoms described by Nightingale *et al* [3]. The shear modulus values estimated were consistent with the published values for the phantom used (we have tested phantoms with 0.1, 0.5, and 1.6 kPa). Shear viscosity was also estimated with consistent results from sample to sample (we still do not have an independent measurement for this parameter). A composite phantom (a stiff sample covered with a thin soft layer) and a phantom with an inclusion were tested as well.

Results: All results obtained indicated that the highly focused ARF transducer design was suitable for localized generation of viscoelastic response in thin tissue sample (<1 mm thick) in water with the response almost independent of boundary effects. The results also demonstrated that maximum displacement may not be a robust indicator of stiffness for thin tissue samples when boundary effects are significant.

Conclusions: The use of highly localized ARF beam and the EKF utilization of the full transients of the tissue displacements are necessary for quantitative viscoelastic tissue property measurement near boundaries.

References:

[1] Diane M. Thiboutot, "Dermatological applications of high–frequency ultrasound," in Proc. SPIE, Medical Imaging, 1999.
[2] F.S. Foster, C.J. Pavlin, K.A. Harasiewicz, D.A. Christopher, and D.H. Turnbull, "Advances in ultrasound biomicroscopy," Ultrasound in Medicine & Biology, vol. 26, pp. 1–27, 2000.
[3] K.R. Nightingale, M.L. Palmeri, R.W. Nightingale, and G.E. Trahey, "On the feasibility of remote palpation using acoustic radiation force," J. Acoust. Soc. Am., vol. 110, pp.625–634, July 2001.

* *indicates Presenter*

108 **ESTIMATION OF POISSON'S RATIO BY USING FORCE AND DEFORMATION INFORMATION FROM SINGLE INDENTATION.**

Yongping Zheng[1], Alex P.C. Choi[1], Carrie H. Y. Ling[1].*
[1]The Hong Kong Polytechnic University, Hong Kong, CHINA.

Background: Indentation is an *in–vivo* measurement for determining mechanical properties of biological tissue such as articular cartilage (AC). Hayes *et al.* developed a solution for indentation of the AC by using a flat–ended cylindrical rigid indentor [1]. From the force–deformation data obtained from an indentation test, the Young's modulus of the tissue can be calculated based on a known Poisson's ratio. However, the estimation error of Young's modulus E may be greatly increased due to the uncertainty of the Poisson's ratio. Recently, methods have been proposed to use two indentation tests conducted with two different sized indentors to extract the Young's modulus and Poisson's ratio simultaneously [2,3].

Aims: In this study, a novel method is proposed to extract the Young's modulus together with Poisson's ratio of the tissue simultaneously from the force–deformation data obtained from a single indentation.

Methods: In an indentation experiment, the Young's modulus E can be determined by the following equation [1]:

$$E = \frac{(1-\nu^2)}{2a\kappa(\nu, a/h)} \cdot \frac{P}{w} \qquad \text{Equation 1}$$

where E is Young's modulus, P is the indentation force, υ is the Poisson's ratio, w is the indentation depth, a is the radius of the indentor, h is the original thickness of the tissue, k is a scaling factor which depends on the aspect ratio a/h and Poisson's ratios υ. According to the results of Zhang *et al* [4]:

$$E = \frac{(1-\nu^2)}{2a\kappa_n(\nu, a/h, w/h)} \cdot \frac{P}{w} \qquad \text{Equation 2}$$

It is obvious that the scaling factor κ_n in Equation 2 includes the effects of deformation w/h. Moreover, it was revealed that κ_n almost linearly depends on the deformation w. Therefore, κ_n can be written as:

$$\kappa_n(a/h, \nu, w/h) = \kappa(a/h, \nu) \cdot (1 + \beta\, w/h) \qquad \text{Equation 3}$$

where β is a factor that depends on the aspect ratio and Poisson's ratio, therefore, $\beta=\beta(\upsilon,a/h)$ and we calculated β for various aspect ratio a/h (0.2 – 2.0) and Poisson's ratio υ (0.1 – 0.5) according to the table of $\kappa(\upsilon,a/h,w/h)$ [4]. By substituting Equation 3 into Equation 2, then Equation 2 becomes $P/w=c+c\beta\cdot w/h$, where $c = (2\cdot a\cdot E)\cdot\kappa(a/h,\upsilon)/(1-\upsilon^2)$, is the y–intercept of the linear relationship between P/w and w/h. The slope of this linear relationship is $c\beta$. The Poisson's ratio can be determined by using the β table together with the force–deformation data. Then, the Young's modulus can be further estimated using Equation 2.

Using finite element simulation software, ABAQUS, the axisymmetric indentations with assigned Young's modulus and Poisson's ratio (60 kPa and 0.45, respectively) for aspect ratios equal to 1.0 was established. The radius of the indentor was set to 4.5 mm. The calculated Poisson's ratio and Young's modulus were obtained when the deformation ratio w/h was equal to 0.01, 0.025. 0.05 and 0.1. Finally, the effect of the incorrect assumption of the Poisson's ratio was studied by fixing the Poisson's ratio (0.3 ~ 0.5) in the calculation of the Young's modulus.

Results: By using our proposed method, the estimation errors of Poisson's ratio and Young's modulus ranged from -1.7% to -2.6% and 3.0% to 4.3%, respectively. In comparison with the estimation error of Young's modulus with fixed Poisson's ratio (0.3 ~ 0.5) which ranged from -19.1% to 42.8%, it was found that our method can not only greatly improve the estimation error of Young's modulus, but also perform simultaneous calculation of Poisson's ratio and Young's modulus.

Conclusions: This study demonstrated the feasibility of the proposed method for simultaneous calculation of Poisson's ratio and Young's modulus using a single indentation with high accuracy. Further studies are required to verify the results obtained by the proposed method using experimental tests on phantoms with different material properties.

Acknowledgements: This work is supported by the Research Grants Council of Hong Kong (PolyU 5245/03E) and The Hong Kong Polytechnic University.

References:

[1] Hayes WC, et al., Biomech 5: 541–551 (1972).
[2] Jin H and Lewis JL, J Biomech Eng 126: 138–145 (2004).
[3] Choi APC and Zheng YP, Med Biol Eng Comp 43: 258–264 (2005).
[4] Zhang M, et al., Med Eng Phys 19: 512–517 (1997).

070 **APPLICATION OF A 2D ELASTOGRAPHIC TECHNIQUE FOR EARLY DETECTION OF PRESSURE ULCERS: PRELIMINARY RESULTS.**

JF Déprez[1], E Brusseau[1], O Basset.*
[1]Creatis, Lyon, FRANCE.

Background: A pressure ulcer is a damaged tissue area induced by an unrelieved pressure compressing the tissue during a prolonged period of immobility. This pathology concerns subjects with either limited mobility or impaired sensitivity. The level of pressure required to produce an ulcer varies significantly from one person to another. Moreover, the lack of information and studies on the development of this pathology makes its prevention and early detection difficult.

However, it is known that muscles are more vulnerable to mechanical loading than skin since muscle may be in contact with bony protuberance [1]. Thus lesions originate in the deep muscle tissues before developing on the surface. Moreover, using an animal model, Gefen et al. [2] demonstrated significant stiffening (1.8–fold to 3.3–fold) of damaged areas. This makes elastography a promising tool for understanding pressure ulcer formation.

Aims: In this work, we investigated the possibility of detecting pressure ulcers at an early stage, using a 2D strain estimation technique.

Methods: To mimic an ulcer at an early stage, a numerical phantom was designed, composed of 3 distinct regions, a bony protuberance (Young's Modulus = 10 GPa), the healthy tissue area (50 kPa) and the lesion itself (100 kPa), located near the bone. An axial compression of 3% was applied on the top surface while the bone remained fixed, and medium deformation was calculated with a finite element modeling. The corresponding pre– and post–compression radiofrequency (RF) ultrasound images were generated with the Field II software.

Due to the configuration of the tissues, the phantom experienced large lateral displacements during the load. This induced major changes in the acoustical footprints, and decorrelation between pre– and post-compression signals. The 2D strain estimator recently developed by our group was therefore used to process data [3]. This model was based on a constrained optimization strategy and computes the axial strain while considering lateral motion, which improves robustness with regard to decorrelation.

Results: While the ulcer cannot be detected on an echogram (Figure 2), computed strain maps (Figure 3) were of great help for distinction between the lesion, the healthy tissues and the bone; the deformation of the bone was almost zero, and the mean axial strain of the ulcer was half that of surrounding tissues (2.5% vs. 5%). Moreover, the boundary between the healthy region and the pathological area was very sharp, which again emphasized the lesion. Finally, the absolute maximum lateral displacement reached 0.41 mm. This represented 70% of the axial maximum displacement (0.58 mm) and justified the need for using a 2D approach.

Conclusions: First, this study demonstrated that the detection of a pressure ulcer at an early stage was feasible using simulated data. The potential of our 2D elastographic method was also shown in a situation with large lateral displacements. Additional studies are now planed on *in vitro* and *in vivo* data.

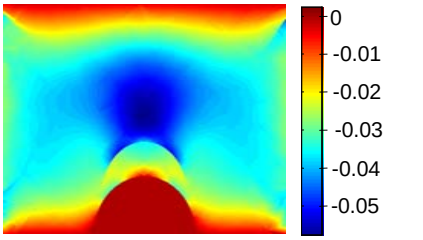

Figure 1: Theoretical axial strain (%)

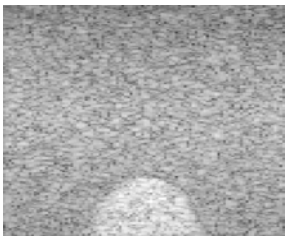
Figure 2: Echogram

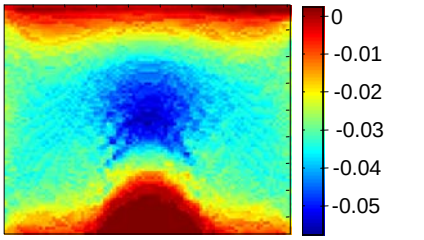

Figure 3: Computed axial strain (%)

References:

[1] G.T. Nola, L.M. Vistnes, Differential response of skin and muscle in the experimental production of pressure sores. Plast. Reconstr. Surg. 66:728–733.

[2] A. Gefen, N. Gefen, E. Linder–Ganz, S.S. Margulies, *In vivo* muscle stiffening under bone compression promotes deep pressure sores, Trans. of the ASME 127: 512–524.

[3] E. Brusseau, J.F. Déprez, G. Said, O. Basset, 2D Strain estimation based on a Newton constrained minimization strategy: Application to Experimental Data, Proc. of The 4th International Conference on the Ultrasonic Measurement and Imaging of Tissue Elasticity, 2005, p 111. http://www.ece.rochester.edu/users/rcbu/conference/2005conf.htm.

* *indicates Presenter*

052 **ULTRAFAST ULTRASONIC IMAGING APPLIED TO MEASUREMENTS OF *IN VIVO* MUSCLE CONTRACTION FEATURES.**

Thomas Deffieux[1], Jean–Luc Gennisson[1], Mickaël Tanter[1] and Mathias Fink[1].*
[1]Laboratoire Ondes et Acoustique, UMR 7587, ESPCI, 10 rue Vauquelin 75005 Paris, FRANCE.

Background: Numerous monitoring techniques are commonly used to study muscular or neuromuscular diseases. Among them, Electromyography (EMG), Mechanomyography and Acceleromyography offer time accurate measurements but poor spatial resolution. Conversely, Cine Phase Contrast Magnetic Resonance Imaging or Doppler Tissue Imaging offers good spatial resolution but low sampling rate.

Aims: The goal of this study is to propose a new tool to image the contraction of a muscle *in vivo*. This imaging device retains very good spatial resolution as well as a very high frame rate to extract significant parameters such as contraction and relaxation time, velocity or contracting fiber bundle position.

Methods: The method uses an ultrafast ultrasound imaging device to follow the displacements of the muscle tissue during a contraction. The ultrafast scanner drives an 8 MHz 128 element ultrasonic probe and can take up to 5000 frames per second with sub–millimeter resolution [1]. Displacements as low as one micron are computed from the one dimensional axial cross–correlation of two successive images [2]. The ultrafast scanner is set up to trigger an electro-stimulation device connected to a pair of electrodes placed on the biceps brachii motor point or its associated nerve. The ultrasound array is either placed parallel or perpendicular to the muscle fibers.

Results and Conclusion: Experiments show that it is possible to localize the contracting fiber bundles as well as to extract the main temporal features of the contraction in real time during one single transient excitation. Such features are the contraction time, the relaxation time and the velocity distribution.

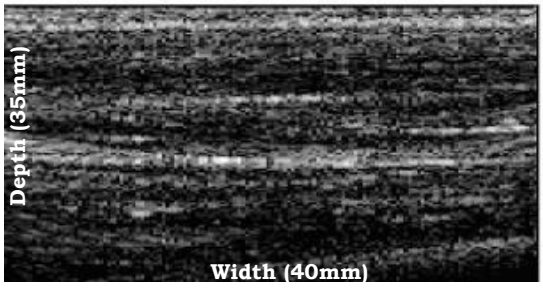

Figure 1: B–Mode image of the biceps brachii (35 x 40 mm^2).

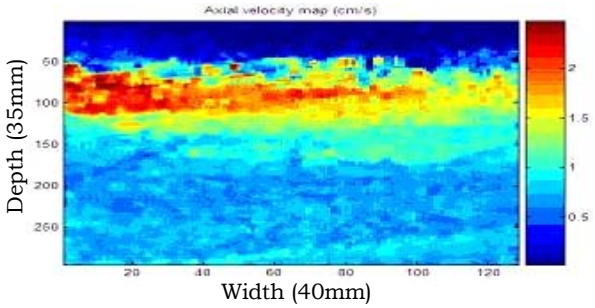

Figure 2: Axial velocity map (35 x 40 mm^2) computed from relative axial displacements between successive images.

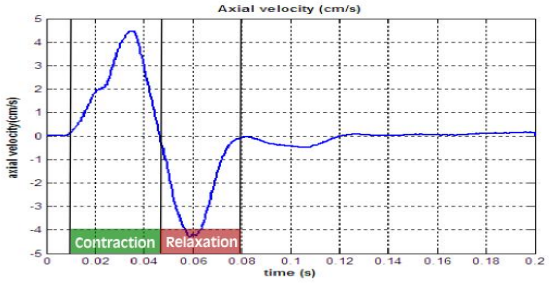

Figure 3: Axial velocity as a function of time, corresponding to a small region of fibers after excitation.

The ultrafast ultrasound modality device, coupled with an EMG device, will provide an optimal tool to understand the link between electrical and mechanical activities of the muscle and its possible associated disorders.

References:

[1] L. Sandrin, M. Tanter, S. Catheline, and M. Fink, "Shear modulus imaging using 2D transient elastography", IEEE Trans. Ultrason., Ferroelec., Freq. Contr. 49, 426–435 (2002).
[2] J. Ophir, I. Céspedes, H. Ponnekanti, Y. Yasdi, and X. Li, "Elastography: a quantitative method for imaging the elasticity of biological soft tissues", Ultrason. Imaging 13, 111–134 (1991).

* *indicates Presenter*

005 **LOCATION ESTIMATION INCREASES THE ACCURACY OF ULTRASONIC STRAIN ESTIMATES.**

JE Lindop[1], GM Treece[1], AH Gee[1], RW Prager[1].*
[1]University of Cambridge, Cambridge, England, UK.

Background: Strain estimation is fundamental to elasticity imaging in general. It usually begins with displacement estimation by comparing finite length windows of RF ultrasound signals recorded before and after tissue deformation. Strain is estimated by taking the gradient, commonly assuming that each displacement applies at the window centre. However, amplitude variation perturbs the location at which the displacement estimate is valid [1]. This is a significant source of strain estimation noise, which we refer to as amplitude modulation (AM). It can be reduced by amplitude compression [2] or adaptive stretching [3].

Aims: To develop a technique for estimating the location at which each displacement estimate is valid. To evaluate this technique in the context of strain estimation and compare with existing approaches. We have called our algorithm "Amplitude Modulation Correction" (AMC).

Methods: RF data from homogeneous scattering fields at compressive strains in the range 0.01%–4.0% were simulated using Field II [4] with an SNR of 20 dB. This provided the basis for recording estimation performance (SNR_e). A correlation coefficient maximizer (CCM) and efficient correlation phase zero search (EPZS) were compared with and without enhancement by amplitude compression and AMC. Adaptive strain estimation (ASE) using Sum of Absolute Differences served as a benchmark. A range of window lengths (2.8–27.1λ) were employed, λ being the wavelength at the probe centre frequency, while window spacing and least squares gradient estimation length were held constant. Performance was averaged over multiple datasets to ensure the production of reliable results, which were verified by qualitative assessment of *in vitro* and *in vivo* strain images.

Results: AMC improved the performance of both CCM and EPZS for short windows, though the improvement was greatest for EPZS with longer windows, in which case it usually outperforms ASE. Figure 1 shows selected quantitative results. The occurrence of artifacts correlated with features in the B-scans was also reduced. An example is shown in Figure 2.

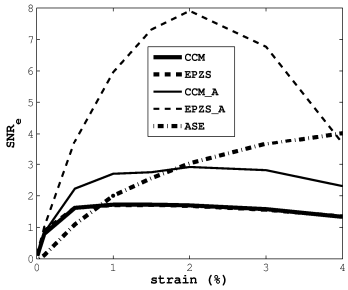

Figure 1: SNR_e against strain for various algorithms using 13.5λ windows. The curves for CCM and EPZS overlap. CCM_A and EPZS_A are enhanced by AMC.

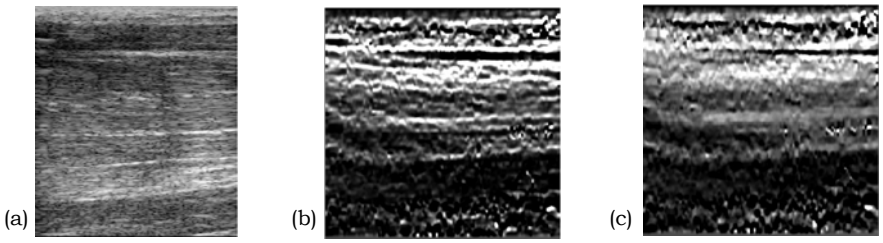

Figure 2: Scan of bicep.
(a) B–mode image displays amplitude variation.
(b) Strain image from EPZS with 13.5λ windows and 1 mm least squares gradient estimation. White represents 1.5% extension and black represents zero strain. The SNR_e is moderate and many AM artifacts are present.
(c) Strain image from EPZS_A shows that AMC improves the SNR and removes most of the artifacts that correlate with amplitude variation.

Conclusions: AMC substantially reduces the level of noise in strain estimates from window displacements, and performs better than amplitude compression. It yields competitive performance for phase–based algorithms even compared to adaptive methods. The computational cost of location estimation is negligible, so AMC could be applied in systems that require real time processing.

References:

[1] I Céspedes and J Ophir. Reduction of image noise in elastography. Ultrason. Imag., 15:89–102, 1993.
[2] JE Lindop, GM Treece, AH Gee and RW Prager, 3D elastography using freehand ultrasound, Ultrasound Med. Biol., 37 (4):529–545, 2006.
[3] SK Alam, J Ophir, and EE Konofagou. An adaptive strain estimator for elastography. IEEE T. Ultrason. Ferr., 45(2):461–472, 1998.
[4] JA Jensen. Field: a program for simulating ultrasound systems. In Proceedings of the 10th Nordic–Baltic Conference on Biomedical Imaging, 4:351–353, 1996.

* *indicates Presenter*

060 **THE K–SIGMA FILTER: A NEW CORRELATION–BASED FILTER FOR STRAIN IMAGING.**

Rémi Souchon[1], Jean–Yves Chapelon[1].*
INSERM UMR 556, 151 crs Albert Thomas, 69424 Lyon cedex 03, FRANCE.

Background: In ultrasonic elastography, strain is typically estimated from the gradient of time delay estimates (TDEs), the latter being obtained using a cross–correlation method (Ophir et al. 1991). Filtering of the TDEs is usually necessary because the gradient operator amplifies noise [2,3].

Aims: Design a TDE filter that uses additional information – namely the cross–correlation coefficient (ρ) associated with each individual window – to achieve high elastographic signal–to–noise ratio (*SNRe*), while preserving sharp spatial resolution.

Methods: The standard deviation (σ) associated with each individual TDE can be interpreted as a confidence interval: assuming the TDEs are normally distributed, there is a 68% chance that the true TD is within the range $\Delta t \pm \sigma$ (Δt is the TDE obtained from cross–correlation). In practice, the interval σ is unknown, but it can be estimated from the cross–correlation coefficient ρ, which is readily available, based on equations derived from [4]. For each TDE, the filter processes as such:

1. Estimate σ from ρ
2. Calculate the intermediate value $\tau = (\Delta t_{i+1}+\Delta t_{i-1})/2$
3. Replace Δt_i by $\Delta t_i^f = \begin{cases} \Delta t_i - K\sigma & \text{if} \quad \tau \le \Delta t_i - K\sigma \\ \tau & \text{if} \quad \Delta t_i - K\sigma \le \tau \le \Delta t_i + K\sigma \\ \Delta t_i + K\sigma & \text{if} \quad \Delta t_i + K\sigma \le \tau \end{cases}$

Δt_i denotes the current TDE, Δt_{i-1} and Δt_{i+1} denote its two neighbors, and K is a weighting parameter. In the second step, the intermediate value τ is the TDE that achieves the highest *SNRe* locally (because Δt_{i-1}, τ, and Δt_{i+1} are exactly aligned). The third step forces the filtered value Δt_i^f to remain within the confidence interval $\Delta t_i \pm K\sigma$. It allows the filter to make large variations for low–correlation estimates (associated with large σ), and only small corrections around high–correlation estimates, considered more reliable, (associated with small σ). Note that K=1 corresponds to forcing all filtered values to remain within the 68% confidence interval, K=2 to remain within the 95% confidence interval. Once all TDE along a line have been processed, Steps 2 and 3 can be repeated to further improve *SNRe*. The new filter was tested by measuring *SNRe* and resolution in simulations and in experimental data. Two commonly used filters (moving average and 2D median) were used as gold standard for comparison.

Results: Figure 1 shows *SNRe* vs. nb of iterations in simulated RF data. Figure 2 shows *SNRe* vs. axial resolution: the 3σ filter was able to improve *SNRe* by a factor of 22 while increasing resolution from 1.2 to 2 mm only. Figure 3 shows an elastogram in a resolution phantom (a) without and (b) with the 3σ filter.

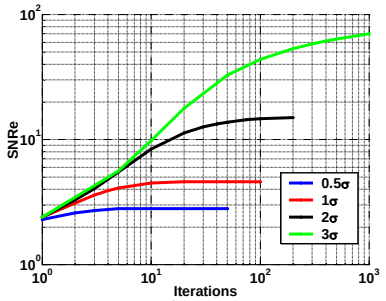

Figure 1

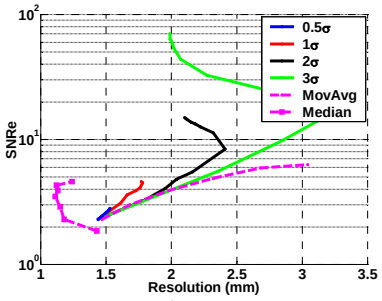

Figure 2

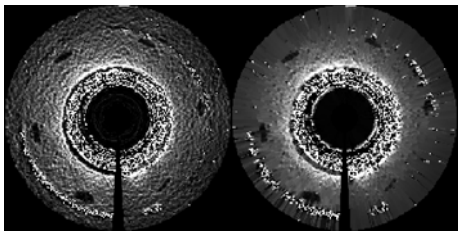
Figure 3

Conclusions: The proposed filter uses additional information (cross–correlation coefficients) to provide low–noise, high–resolution elastograms. It can be combined with any gradient operator (LSQ, staggering, optimal DD, etc.). It is fast and can be implemented in real–time even for a large number of iterations.

Acknowledgements: This work was funded by NIH Program Project Grant P01–CA64597 (later reassigned to P01-EB) to the University of Texas in Houston.

References:

[1] Ophir et al: Elastography: a method for imaging the elasticity of biological tissues. Ultrasonic Imaging 13, 111-134, 1991.
[2] Kallel et al: A least squares estimator for elastography. Ultrasonic Imaging 19, 195-208, 1997.
[3] Luo J et al., Axial strain calculation using a low-pass digital differentiator in ultrasound elastography. IEEE Trans Ultrason Ferroelectr Freq Control 51(9), 1119-1127, 2004.
[4] Varghese and Ophir: A theoretical framework for performance characterization of elastography: The Strain Filter. IEEE Trans Ultrason Ferroel Freq Cont 44(1), 164-172, 1997.

* *indicates Presenter*

009 **COMPARISON OF MULTIDIMENSIONAL DISPLACEMENT VECTOR AND STRAIN TENSOR MEASUREMENT METHODS THROUGH SIMULATIONS AND PHANTOM EXPERIMENTS.**

Chikayoshi Sumi[1] and Tomonori Ebisawa[1].*
[1]Sophia University, 7-1, Kioicho, Chiyodaku, Tokyo, JAPAN.

Background: We have reported three methods of measuring a multidimensional displacement vector, i.e., the multidimensional autocorrelation method (MAM) and multidimensional Doppler method (MDM) using an instantaneous ultrasound signal phase [1]; multidimensional cross–spectrum phase gradient method (MCSPGM) using a local phase characteristics [2]. High measurement accuracy is achieved by combining one of the methods with the lateral Gaussian envelope cosine modulation method (LGECMM) [1] or multidirectional synthetic aperture method (MDSAM) [3]. MAM and MDM require less computational time and provide real–time measurements. Furthermore, we also reported a direct strain measurement method based on the autocorrelation method [4].

Aims: The measurement accuracies of the methods are specifically investigated using simulated noisy echo data and experimental phantom data.

Methods: (1) *Simulations:* 2D displacement vector measurements (0.01 mm, 0.01 mm) are simulated, assuming that LGECMM is used. The 2D echo data obtained before and after a single pulse repetition interval are simulated by convolving 2D Gaussian–envelope PSF ($\sigma_x = \sigma_y = 0.4$ mm) with white noise. The measurement accuracy is evaluated using SNR by changing lateral modulation frequency at an ultrasound frequency of 3.5 MHz (a typical lower ultrasound frequency that we use). White noise is added to the simulated echo data.
(2) *Phantom experiments:* Compression was mechanically applied to an agar phantom in the axial direction using the transducer. The phantom (height, 60.0 mm) had a cylindrical stiff inclusion (dia. = 15.0 mm) at a depth of 15.0 mm. 7.5 MHz ultrasound frequency was used. Here, the lateral modulation was not performed. The result of 1D AM is also shown.

Results: (1) *Simulations:* Table I summarizes the accuracies of the methods (a: MAM; d: MDM; c: MCSPGM) for echo data SNR (∞, 20 and 0.7 dB), lateral modulation frequency (higher and lower than 2.0 mm^{-1}), and moving–average width and local region size. From this table, we can conclude that at low lateral modulation frequencies, the order of accuracies (both axial and lateral displacements) is MAM, MCSPGM and MDM when the local echo data SNR is high, whereas the order is inverted when the local echo data SNR is low (i.e., MDM, MCSPGM and MAM). Moreover, MDM is robust for the use of a small moving–average width compared with MAM. That is, MAM is weak for a local low–echo–data SNR case, whereas MDM is robust for such a case. However, at high lateral modulation frequencies with noise, the measurement accuracies of MAM, MDM and MCSPGM are comparable, although when using high SNR echo data, MAM is the most accurate of all the methods.
(2) *Phantom experiments:* Axial strain images obtained by the above methods are shown in Figure 1a–1e when sufficiently large strains were generated (i.e., approximately 2.0%). The detectability of the images obtained by MCSPGM, MAM, MDM and 1D AM [i.e., Figure 1a–1d] are respectively superior to those of the infinitesimally compressed case, e.g., 0.067% (not shown). However, for the direct strain measurement method (Figure 1e), the detectability was not improved. This is because, although the contrast in strains was enhanced, the decorrelation noise caused by the lateral displacement was also enhanced by the large compression, i.e., the generated noise was amplified twice by the differentiation.

Table I: Order of accuracies of axial and lateral displacements for echo data SNRs of ∞, 20 and 0.7 dB at high lateral modulation frequencies, i.e., > 2.0 mm^{-1}. The order described in parentheses is for low lateral modulation frequencies, i.e., < 2.0 mm^{-1} when the order is different from that for the high lateral modulation frequencies.

Width (size)	Axial (∞ dB)	Lateral (∞ dB)	Axial (20 dB)	Lateral (20 dB)	Axial (0.7 dB)	Lateral (0.7 dB)
64×64	a,c,d	a,c,d	a,d,c	a,c,d	d,c,a	d,c,a
32×32	a,c,d	a,d,c (a,c,d)	a,d,c	a,d,c (d,c,a)	-	-
16×16	a,d,c	a,d,c	a,d,c (d,c,a)	a,d,c (d,c,a)	-	-
8×8	a,d,c (d,c,a)	a,d,c (d,c,a)	d,a,c (d,c,a)	d,a,c (d,c,a)	-	-

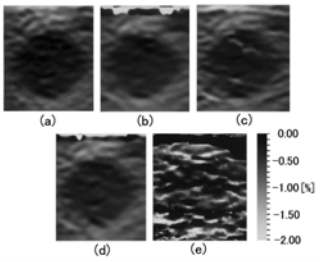

Figure 1: Phantom experiments.

Conclusions: The measurement accuracies were compared.

References:
[1] C. Sumi, Proc. of IEEE International Ultrasonics Symposium (CD-ROM), pp. 1771–1776, September 2005.
[2] C. Sumi, IEEE Trans. on UFFC, vol. 46, no. 1, pp. 158–166, January 1999.
[3] C. Sumi, IEEE Trans. on UFFC, vol. 52, no. 10, pp. 1670–1689, 2005.
[4] C. Sumi, "Direct strain measurement method based on autocorrelation method," Proc. of the Third International Conference on the Ultrasonic Measurement and Imaging of Tissue Elasticity, p. 64, Cumbria, October 2004. http://www.ece.rochester.edu/users/rcbu/conference/2004conf.htm

* *indicates Presenter*

003 **A NOVEL LATERAL MOTION TRACKING ALGORITHM AND ITS APPLICATIONS IN SHEAR STRAIN IMAGING: A FEASBILITY STUDY.**

J Jiang[1], TJ Hall[1].*
[1]Medical Physics Department, University of Wisconsin–Madison, Madison, WI, USA.

Background and Aims: Ultrasonic strain imaging systems provide useful information in breast tumor characterization [1,2]. In this technique, tissue displacements along the insonification direction (i.e., axial direction) are often measured to assess "relative stiffness", while the displacements perpendicular to the beam (i.e. lateral displacements), necessary for accurate motion tracking, are typically discarded in image formation due to their poor accuracy. However, for some applications such as Young's modulus reconstruction and estimating local shear strains, both components of the 2D displacement vector are essential. In this study, we aim to improve the quality of lateral displacements, by taking advantage of the superior quality in the axial displacements in a two step process.

Methods: First, a modified 2D block–matching algorithm (BMA) [3] is used to obtain axial and lateral displacements. Then, an optical flow–based algorithm is used iteratively to further enhance the accuracy of lateral displacements. We assume that the local tissue motion in a small region (e.g. 1 mm square) follows a 2D affine model containing six parameters (axial and lateral translations, axial and lateral stretches, and axial and lateral shearing). There are two significant differences compared to the Lagrangian speckle model [4]. The first significant modification is parameter reduction. Since we have great confidence in the estimated axial displacements and strains, we treat the axial stretch and translation as known parameters. The lateral stretch can also be treated as a known parameter if the tissue incompressibility is enforced. Therefore, only three parameters (one lateral translation and two shearing) need to be solved iteratively using the classic optical flow technique [5]. The second modification is that the optical flow is used to estimate sub–pixel lateral displacements using the coarse tissue motion measured by the robust BMA. Therefore, it is unlikely that the algorithm converges to wrong local minima.

The improved lateral displacements along with the estimated axial displacements can be used to form local shear images to assess local tissue mobility. Generally, lateral tissue motion may result in echo signal decorrelation, severely corrupting the axial displacement estimates. Therefore, the improved lateral displacements may also be applied to enhance the quality of axial displacement.

Results: Through computer simulations, our results suggested the proposed method can significantly reduce the lateral displacement estimate error variances compared to the block–matching algorithm. Radiofrequency (RF) echo data acquired from a Siemems Elegra with freehand scanning of *in vivo* breast tissue [2] were also used to validate this method. Through processing of *in vivo* breast tissue data (4 data sets with two fibroadenomas and two malignant tumors (one invasive ductal carcinoma and one invasive apocrine carcinoma), we found that the presence of large local shear strains around the two benign breast lesions (i.e. halo shaped rings) are easily observed but cannot be seen in two malignant cases. Since low mobility is related to invasive breast lesions, our preliminary findings suggests that studying tissue mobility of *in vivo* breast lesions may actually offer valuable information in lesion characterization.

Conclusions: In this study, a new lateral displacement algorithm is presented, and our results show that it is possible to measure lateral displacements with reasonably good precision. With this improvement, local shear strains can be estimated, thereby providing additional information for breast tumor differentiation.

Acknowledgements: This work is supported in part by grants from NIH–R01CA100373 and the University of Wisconsin–Madison.

References:

[1] B. S. Garra, et al., "Elastography of breast lesions: initial clinical results," *Radiology*, vol. 202, 1997.
[2] T. J. Hall, Y. Zhu, and C. S. Spalding, "*In vivo* real–time freehand palpation imaging," *UMB*, vol. 29, 2003.
[3] J. Jiang and T. J. Hall, "A novel real–time speckle tracking algorithms and its applications in strain imaging," AIUM Annual Conference, Washington DC, 2006.
[4] R. Maurice and M. Bertrand, "Lagrangian speckle model and tissue–motion estimation: Theory," IEEE Trans. Med. Imaging, vol. 18, 1999.
[5] J. L. Barron, et al., "Performance of Optical Flow Techniques," *Int J Comp Vis*, vol. 12, 1994.

089 **SNR, CNR AND THEIR TRADE–OFF WITH RESOLUTION IN AXIAL-SHEAR STRAIN ELASTOGRAPHY.**

A Thitai Kumar[1,2], J Ophir[1,2] and TA Krouskop[1,3].*
[1]The University of Texas Health Science Center Houston Medical School, Houston, TX, USA; [2]University of Houston, Houston, TX, USA; [3]Baylor College of Medicine, Houston, TX, USA.

Background: In axial–shear strain elastography, the local axial–shear strain created in an inhomogeneous material, due to application of quasi–static axial compression, is imaged. It is known that the shear strains generated near the interface between the different materials in an inhomogeneous material are dependent upon the bonding at the interface, orientation of interface with respect to direction of normal compression and Young's modulus contrast between the two materials among others [1]. Therefore, estimating the shear strains may provide information on the bonding at the internal interfaces. Further, shear strains are by definition sum of two components, the axial–shear strain and lateral–shear strain [1]. In this paper, we study the signal–to–noise ratio (SNR), contrast–to–noise ratio (CNR) and their trade–offs with resolution of the axial–shear strain elastography through simulations and experiments.

Methods: The SNR and CNR of axial–shear strain elastography were both investigated using a single inclusion model, i.e., an elastically stiff lesion embedded in a homogeneously softer background. SNR was computed as the mean–to–standard deviation of the axial–shear strain estimates in the target while CNR was computed as the difference between axial–shear strain estimates from the target and the background scaled to the average noise. Here, the target was defined as the peak in the axial–shear strain profile taken along a 45º orientation with respect to axis of compression. Since the axial–shear strain value changed spatially, the mean and standard deviation of the estimates needed to compute SNR and CNR were obtained from the same location but over a number of independent realizations. The behavior of resolution (obtained from Reference [2]) for various system and signal processing parameters was compared with behavior of the CNR and SNR to understand the trade–off between them.

Results: The results of the study showed that CNR and SNR of axial–shear strain elastography have a band–pass like filter in the strain domain that is similar to that of axial strain elastography (Figure 1). As the beamwidth increased, the noise and the peak axial–shear strain value both decreased. Thus, the CNR/SNR remain almost constant (Figure 2). However, as the pitch increased, only the noise decreased leading to an increase in CNR/SNR (Figure 3). As expected, the CNR/SNR did not show any trend with correlation window length and axial shift. The results showed that unlike axial strain elastography, a trade–off between CNR/SNR and resolution exists only with the pitch and not with signal processing parameters in axial–shear strain elastography.

Conclusions: We have shown that there exists a range of applied axial strain that favors higher CNR values than others. CNR/SNR does not show a trend with correlation window length and therefore, one can choose window length to obtain better resolution. However, unlike axial elastography, the CNR/SNR cannot be improved with signal processing parameters alone.

Acknowledgements: This work was supported in part by NIH program project grant P01–EB02105–12 awarded to The University of Texas Health Science Center Houston Medical School.

References:

[1] Timoshenko SP and Goodier JN. *Theory of Elasticity* (McGraw-Hill, New York, pp 8–11, 1970).
[2] Thitai Kumar A, Righetti R, Ophir J and Krouskop TA. Resolution of axial–shear strain elastography, Proc. of The 5th International Conference on Ultrasonic Measurement and Imaging of Tissue Elasticity, p 69, 2006.

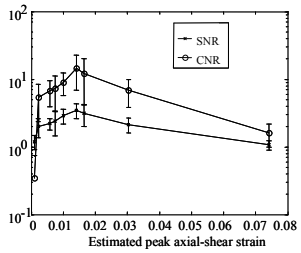

Figure 1: Plot of the SNR and CNR as a function of estimated peak axial-shear strain.

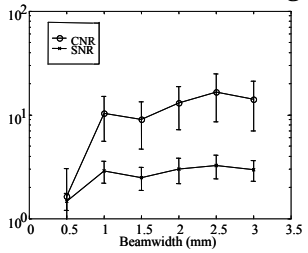

Figure 2: Plot of the SNR and CNR as a function of beam width.

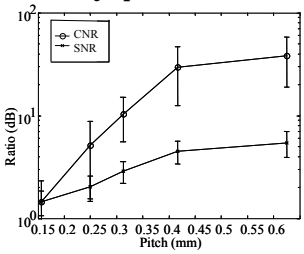

Figure 3: Plot of the SNR and CNR as a function of pitch.

* *indicates Presenter*

105 **REAL–TIME LEAST–SQUARES STRAIN ESTIMATOR FOR ELASTOGRAPHY.**

R Zahiri–Azar[1], SE Salcudean[1].*
[1]University of British Columbia, Vancouver, BC, CANADA.

Background: Elastography as an imaging technique has been well established in the literature [1] and has been shown to be useful in different clinical applications. Typically in elastography, strain is estimated by applying a gradient operator on the previously obtained time–delays. To reduce the noise amplification due to the gradient operation and improve the elastographic signal–to–noise ratio (SNRe), the Least Squares strain Estimator (LSE) was introduced [2]. LSE fits a line to a vector or "kernel" of displacement estimates. The slope of this line provides an estimate of the local strain that averages out noise at the expense of resolution. The larger the kernel, the better the SNRe [3].

Aims and Methods: We present a real-time implementation of the LSE strain estimation method and an associated user interface that allows exploration of the tradeoff between axial resolution Ra and SNRe. Since only the slopes of the piecewise fitted lines contain the information, a 1D displacement vector d with m points around a given kernel of n point can be modeled by $d(i+j)=a(i)j+b(i)$ where i is the kernel counter (i.e. $i0[0\ldots m-n]$) and j is the kernel index (i.e.$j0[0\ldots n-1]$), and $a(i)$ and $b(i)$ are constant. This way the closed form least squares estimation of $a(i)$ for each kernel, which is an estimate of the strain at the middle of the i^{th} kernel, can be formulated as:

$$\hat{a}(i) = \frac{n\sum_{j=0}^{n-1} jd(i+j) - \sum_{j=0}^{n-1} j\sum_{j=0}^{n-1} d(i+j)}{n\sum_{j=0}^{n-1} j^2 - (\sum_{j=0}^{n-1} j)^2}, \quad i = 0\ldots m-n.$$

$\sum_{j=0}^{n-1} j = n(n-1)/2$, $\sum_{j=0}^{n-1} j^2 = n(n-1)(2n-1)/6$ can be calculated up front for all kernels. $\sum_{j=0}^{n-1} d(i+j)$, $\sum_{j=0}^{n-1} jd(i+j)$ can be computed with a *for loop* up to the size of the kernel compared to [2] that requires six sum of products calculations, matrix inversion plus extra overhead to put the data in matrix form. For odd kernel sizes by indexing from –n/2 to n/2 the closed form can be further simplified to $\hat{a}(i) = \sum_{j=-n/2}^{n/2} jd(i+j) / \sum_{j=-n/2}^{n/2} j^2$.

Results and Conclusions: The trade–offs between the axial resolution Ra and SNRe have been determined from 1D simulation of RF data and are shown in Figure 1 below. As suggested in [3], Ra decreases linearly with kernel size while SNRe increases super linearly. This allows the generation of smooth images with large kernels to easily recognize features at larger scale while details can be examined with a small kernel that preserves resolution. An interface was implemented on an Ultrasonix 500RP machine to allow the user to adjust the image in real time.

References:

[1] J. Ophir et al, "Elastography, a quantitative method for imaging the elasticity of biological tissue", Ultrasonic Imaging Vol. 13, pp. 111–34, 1991.
[2] F. Kallel, and J. Ophir, "A least–squares strain estimator for elastography", Ultrasonic Imaging 19, pp. 195–208, 1997.
[3] S. Srinivasan, R. Righetti, and J. Ophir, "Tradeoffs between the axial resolution and the signal–to–noise ratio in elastography." Ultrasound in Medicine and Biology, Vol. 29, No. 6, pp. 847–866, 2003.
[4] R. Zahiri–Azar, SE Salcudean, "Motion Estimation in Ultrasound Images using Time Domain Cross Correlation with Prior Estimates", IEEE Transaction on Biomedical Imaging, in press.

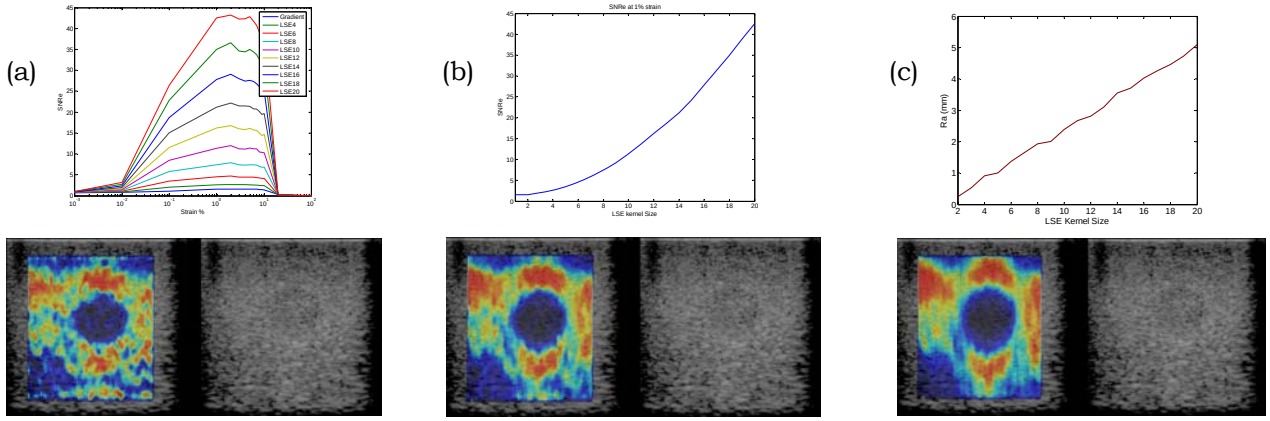

Figure 1: Improvement in the strain filter of the TDPE algorithm (a), SNRe at 1% strain (b), and elastograms (bottom) and degradation in the axial resolution (c) as the kernel size of LSE increases (fs=40 MHz, fo=5MHz, W=1mm, 50% overlap).

085 **ELASTICITY IMAGING IN THE TREATMENT OF LOBULAR BREAST CARCINOMA: A CASE STUDY.**

J R Resnick[1], S Good[1], D Paul[1], L Fan[1], S Barnes[1], J Hanson[2].*
[1]Siemens Medical Solutions USA, Inc., Ultrasound Division, 1230 Shorebird Way, Mountain View, CA, 94043, USA; [2]Swedish Medical Center, 1221 Madison Suite 400, Seattle, WA, 98104, USA.

Background: Medical ultrasonic imaging has traditionally been used as a diagnostic tool. Increasingly, however, ultrasonic imaging is finding a role in treatment and therapy. In this case study, we illustrate how B–mode imaging and ultrasonic elasticity imaging together may be of use in planning breast surgery.

Aims: To illustrate in a case study how elasticity imaging might effectively complement other imaging modalities in planning for treatment of lobular breast carcinoma.

Methods: The patient in this study is a 55 year old female. In March, 2006, the patient's mammogram showed architectural distortion in the central and outer portions of the right breast. This was deemed suspicious, and led to an ultrasound exam five days later. B–mode imaging revealed a number of ill-defined hypoechoic solid masses in the breast, with extensive shadowing. The shadowing prevented clear visualization of tissue beneath the hypoechoic areas, and made it impossible to determine whether there was penetration of the masses to the chest wall. Breast biopsy confirmed lobular breast carcinoma. Subsequently, to better characterize the size and extent of the masses, the patient was imaged with magnetic resonance imaging (MRI). Five days later, the patient was scanned using an ACUSON Antares™ ultrasound system equipped with prototype real time simultaneous B–mode and elasticity imaging capability.

Results: *Ultrasound:* The ill–defined hypoechoic regions seen in the initial B–mode imaging were much better defined as regions of elevated relative stiffness on the elasticity image. The areas of elevated stiffness did not appear to penetrate to the chest wall.

MRI: The MRI images showed the outer and middle third of the breast to include a series of irregular masses, and confirmed that the masses did not extend into the chest wall.

Surgery: Indications that the carcinoma did not extend to the chest wall led to greater confidence in the surgical planning. Mastectomy was performed to remove the right breast, while the muscle layer beneath the breast was left intact.

Other comments: The period from the initial B–mode imaging to the final MRI report was a time of stress and uncertainty for the patient and her family. Reducing uncertainty as early as possible after initial diagnosis reduces patient stress. If elasticity imaging had been performed and had reported results at the same time as the initial B–mode exam, the patient's stress and anxiety in waiting for the final MRI report might have been reduced.

Conclusions: This is but a single case history, and more cases would be required to draw general conclusions. (We hope this report may result in opportunities to study additional cases.) Nonetheless, these results suggest that by helping to delineate the size and extent of lobular breast carcinoma, ultrasonic elasticity imaging could play a valuable role in treatment planning and patient care.

Acknowledgements: We are grateful to the patient in this study, for providing us access to her medical and imaging records, and for her grace, courage, and determination, which continue to inspire us.

(a) B–mode image 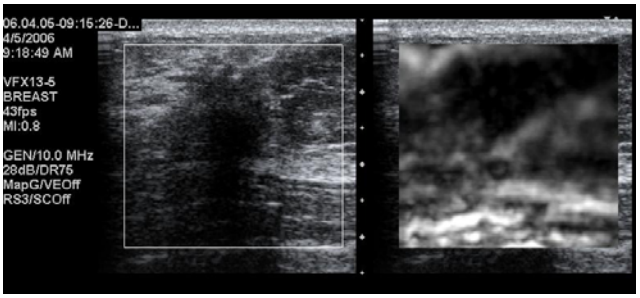

(b) Elasticity image

Figure 1: Lower boundary of hypoechoic solid mass in the B-mode image (a) is ill-defined. In the elasticity image (b), the lower boundary of the stiffer mass (large dark region) shows as bounded below by softer tissue (grey) and the layered muscle and fascial areas (bright bands.) (Elasticity Image Scale: black = most stiff, white = least stiff)

050 **MR–ELASTOGRAPHY IS CAPABLE OF INCREASING THE SPECIFICITY OF MR-MAMMOGRAPHY – INFLUENCE OF RHEOLOGY ON THE DIAGNOSTIC GAIN.**

R. Sinkus[1], K. Siegmann[2], M. Tanter[1], T. Xydeas[2], Mathias Fink[1].*
[1]Laboratoire Ondes et Acoustique, ESPCI, 10 rue Vauquelin, 75005 Paris, FRANCE; [2]Radiology Department, University Tübingen, Tübingen, GERMANY.

Background: MR–Mammography using contrast agents is a technique with a sensitivity close to 100%. It lacks, however, specificity which limits its potential application for breast cancer screening [1]. In order to prevent an unacceptable amount of false–positive cases, and even worse, false–negative cases, additional techniques such as breast ultrasound and X–ray mammography are used routinely. The importance of palpation in the process of breast cancer diagnosis is undisputed. However, this method lacks precision and objectivity because it relies on individual perception and skill. Moreover, sensitivity is low especially in case of small tumors [2].

Aims: We investigated 68 patients (38 malignant and 30 benign) to see whether MR-elastography as an adjunct to MR–mammography is capable of increasing the specificity.

Methods: MR–mammography (MRM) and MR–elastography (MRE) were performed within the same session without re–positioning the patient (Figure 1a). Maximum signal enhancement due to bolus application (gadopentetate dimeglumine) overlaid in color on T1–weighted images showed the location of the suspicious lesion very well (Figure 1b). The time course of signal change was evaluated within a region–of–interest (ROI) over ~8minutes post bolus injection. Its temporal shape together with structural information about the shape of the lesion was condensed into the BIRADS classification [3], which represents the currently accepted system for diagnosis of MRM in order to differentiate between benign and malignant lesions. Afterwards, 3D-MRE was performed as a targeted measurement [4]. MRE provided the complex shear modulus G*. Since tissue resembles a complex rheological structure [5], we investigated the performance of three rheological models: the Voigt model, the Maxwell model and the springpot model [6].

Results: Malignant tumors were typically well visualized on the elasticity maps reconstructed with the Maxwell model (Figure 1c), on the viscosity maps reconstructed with the Voigt model (Figure 1d) and the exponent α of the springpot model. The other viscoelastic parameters demonstrated very poor lesion visibility. The BIRADS classification yielded an area of Az=0.86±0.04 under the ROC–curve. When linearly combining BIRADS with the viscoelastic parameters (equal weight and prior to addition individually renormalized to the interval [0–1]) we obtained Az=0.92±0.03 for BIRADS+ηVoigt (p=0.057), Az=0.93±0.03 for BIRADS+μMaxwell (p=0.064) and Az=0.95±0.02 for BIRADS+α (p=0.024). The combination with α demonstrated the lowest value for the significance level.

Conclusions: MRE is capable of improving the specificity of MRM. At a sensitivity of ~95%, the specificity is improved by ~23% when compared to the performance of BIRADS alone. The improvement depends on the rheological model chosen to interpret the complex shear modulus G* in terms of solid and liquid component.

References:

[1] Kuhl, C.K. & Schild,H.H. *JMRI.* 12, 965-974 (2000).
[2] Bancej, C. et al. *J. Med. Screen.* 10(1), 16-21 (2003).
[3] American College of Radiology (ACR). Breast Imaging Reporting and Data System® (BI-RADS®) Atlas. 3rd ed. Reston (VA), American College of Radiology (2003).
[4] Sinkus, R. *Magn Reson Imaging* 23(2), 159-165 (2005).
[5] Verdier, C. *Journal of Theoretical Medicine* 5(2), 67-91 (2003).
[6] Schiessel, H. et al. *J. Phys. A: Math. Gen.* (28), 6567-6584 (1995).

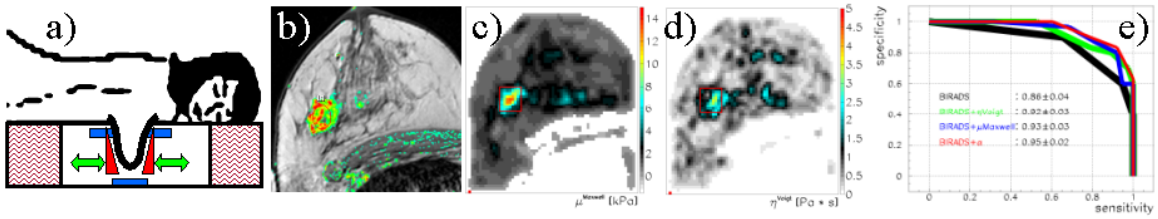

Figure 1: a) Experimental setup with the patient in prone position. MR–receiver coils (blue) and mechanical transducers (red) allow to perform MRM and MRE within the same session. b) T1-weighted axial image with maximum signal change overlaid in color. c) Reconstructed map of Maxwell elasticity and d) Voigt viscosity. e) ROC curves for BIRADS (black), BIRADS+ηVoigt (green), BIRADS+μMaxwell (blue) and BIRADS+α (red).

* *indicates Presenter*

093 **CLINICAL APPLICATIONS OF A REAL TIME ELASTOGRAPHY TECHNIQUE IN BREAST IMAGING.**

RG Barr[1,2].*

[1]Radiology Consultants, Youngstown, Ohio, USA; [2]Northeastern Ohio University College of Medicine, Rootstown, Ohio, USA.

Background: Elastography can provide diagnostic information of breast masses which is otherwise not available in routine clinical practice. This information can improve both the sensitivity and specificity in ultrasound breast cancer detection.

Aims: To demonstrate the clinical utility of a real–time robust elastographic technique in detection and characterization of breast masses, and to present initial results of a pilot study.

Methods: 100 breast lesions were evaluated with a real–time free hand elastography technique which displays both the B–mode image and its corresponding elastogram. Images were obtained on either an Elegra or Antares Ultrasound System (Siemens Ultrasound) modified with elastography software utilizing the 13 MHz linear probe. The lesions were pathologically proven by FNA, biopsy or clinical course (hematoma). The lesions included both benign (cysts, complex cysts, fibroadenomas, lipoma, epidermoid cyst, hematoma) and malignant lesions. The largest dimension of a lesion obtained on an image pair (B-mode image and its corresponding elastogram) was used to characterize the lesion as benign or malignant. In the image pair, if the largest dimension of the lesion in the elastogram was equal to or larger than the corresponding dimension in the B–mode image, the lesion was characterized as malignant. If the largest dimension of the lesion in the B–mode image was larger than the corresponding dimension in the elastogram, the lesion was characterized as benign.

Results: 77 benign and 23 malignant lesions were evaluated. Of the 77 benign lesions, all demonstrated an elastographic image that was smaller in the dimensional length than the B–mode image. Of the 23 malignant lesions, all demonstrated an elastogram image larger in the dimensional length than the B-mode image. (Sensitivity 100%, specificity 100%). Characteristic elasticity patterns for specific pathology were identified. See Figures below for typical image pairs. Figure 1 is a benign lesion, fibroadenoma, and Figure 2 is a malignant lesion, invasive ductal carcinoma.

Conclusions: Initial results of adding real–time breast elastography in the characterization of breast lesions demonstrate the elastographic patterns can be used to characterize lesions as benign or malignant with a >95% accuracy. In our initial evaluation of adding real–time elastography to the clinical evaluation of breast abnormalities, the elastogram added additional clinically useful information in a large portion of cases. Larger multi–center trials are needed to confirm our initial findings and determine the sensitivity and specificity of this technique.

Acknowledgements: This work was supported in part by a grant from Siemens Ultrasound.

References:

[1] Ophir, J., Céspedes, I., Maklad, N. F., and Ponnekanti, H.: "Elastography: A Method for Imaging the Elastic Properties of Tissue *In-Vivo*". Chapter 7 In Ultrasonic Tissue Characterization, M. Tanaka et al., eds., Springer Verlag, Publ., Tokyo, pp 95-123, 1996.

[2] Garra, B.S., Céspedes, I., Ophir, J., Spratt, S., Zuurbier, R. A., Magnant, C. M. and Pennanen, M. F.: Elastography of Breast lesions: initial clinical results. Radiology, Vol. 202, pp. 79-86, 1997.

[3] Svensson WE et al. Elasticity Imaging of 67 Cancers and 167 Benign Breast Lesions Shows That It Could Halve Biopsy Rates of Benign Lesions. Proceedings of the 4th Int'l Conference on the Measurement and Imaging of Tissue Elasticity 2005, p. 87.

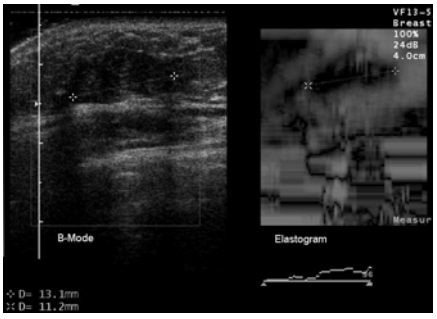

Figure 1: Benign Lesion, Fibroadenoma

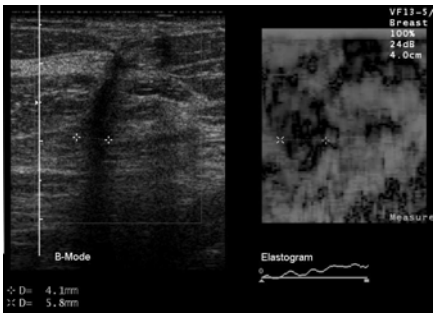

Figure 2: Malignant Lesion, Invasive Ductal Carcinoma

* *indicates Presenter*

099 **BREAST LESION SIZE IN ELASTICITY IMAGING.**

Amy M. Sommer[1], Elizabeth S. Burnside[1], Gale A. Sisney[1], Gina K. Hesley[2], Timothy J. Hall[1].*
[1]University of Wisconsin–Madison, Madison, WI, USA; [2]Mayo Clinic, Rochester, MN, USA.

Background and Aims: Our goal was to compare the lesion size in B–mode with that in elasticity images as a potential aide in the diagnosis of breast lesions. Elasticity images of *in vivo* breast tissue demonstrate that malignant lesions typically appear larger in elasticity images than in B–mode images, while benign lesions typically do not [1–3]. Automated and manual boundary segmentation in the elasticity image was compared to manually drawn boundaries in B–mode.

Methods: Radiofrequency (RF) echo data was acquired from a Siemens Elegra with real–time freehand elasticity imaging of *in vivo* breast tissue. A 2–D block matching algorithm was used offline to estimate tissue displacements for a sequence of data from which elasticity images were formed [4,5]. Fifty (50) benign and fifty (50) malignant lesions were chosen from 444 lesions to represent the total data set. The highest quality frames [6] were selected from each data set, and three radiologists independently viewed the B–mode sequences, chose a representative frame and drew the lesion boundary. The radiologists then viewed the corresponding edited B–mode and elasticity images, chose a representative frame and drew the lesion boundary in the elasticity image. The ratio of the lesion area in the elasticity image to that in the B-mode image was found. An automated segmentation algorithm was used to obtain a lesion boundary in the highest quality elasticity image in each sequence. The lesion size ratios from manual segmentation were then compared to those from the automated segmentation.

Results: A threshold for the lesion size ratio above which all malignant tumors fall had few benign lesions below it for manual segmentation by three radiologists (A – 3, B – 5, C – 1), but that number increased with the use of an automated boundary in the elasticity image and the radiologist drawn B–mode boundary (A – 13, B – 12, C – 10).

Conclusions: Lesion size in elasticity images compared to that in B–mode images is a predictive measure of malignancy. However, large variability exists among the three radiologists' manually drawn lesion boundaries and the automated boundaries in some elasticity images, suggesting that the radiologists were biased towards tracing in strain images what was seen in the B–mode as opposed to confidently interpreting the elasticity image. Figure 1a shows the B–mode image of a lesion that likely influenced the manually drawn boundary (dashed line) in the elasticity image (b) compared to the automated boundary (solid line).

Acknowledgements: We are grateful for the support from the NIH (R01–CA100373), and to colleagues at the Mayo Clinic in Rochester, MN, USA, and the Charing Cross Hospital in London, England, UK, for providing some of the data used in this study.

References:

[1] Garra, BS, et al. Elastography of breast lesions: initial clinical results. Radiology 1997; 202(1):79–86.
[2] Hall, TJ, Zhu Y, Spalding CS *In vivo* real–time freehand palpation imaging. Ultrasound Med Biol 29: 427–35, 2003
[3] Regner, D.M., et al. Breast lesions: evaluation with US strain imaging – clinical experience of multiple observers. Radiology 2006; 238(2):425–37.
[4] Zhu, Y. and T.J. Hall. A modified block matching method for real–time freehand strain imaging. Ultrasonic Imaging 2002; 34(3):161–76.
[5] Jiang J, Hall T.J., Sommer A.M. Simultaneous performance assessment and image formation: A novel method for performance validation of ultrasonic strain imaging. Submitted for publication in IEEE TMI, 2006.
[6] Jiang J, Hall T.J., Sommer A.M. A novel performance descriptor for ultrasonic strain imaging: A preliminary study. In press IEEE UFFC 2006.

Figure 1: (a): B–Mode Image (b): Elasticity Image

049 **VASCULAR ACOUSTIC RADIATION FORCE IMPULSE IMAGING (ARFI) IMAGING OF POPLITEAL AND CAROTID ARTERIES: *IN VIVO* RESULTS.**

Douglas Dumont[1], Jeremy Dahl[1], Elizabeth Miller[1], Jason Allen[1], Gregg Trahey[1].*
[1]Duke University, Durham, NC, 27708, USA.

Aims: To describe results from a pilot study involving twenty–nine patients with diagnosed vascular disease and thirty–two subjects with no prior history of vascular disease.

Background: Peripheral arterial disease of the lower extremities affects approximately one-third of Americans over 55, with ten percent of cases requiring surgical intervention. Despite its clinical prevalence, the disease is often under–diagnosed, with some studies suggesting that 68% of cases are asymptomatic [1]. Of similar concern is the rupture of vulnerable carotid plaques, leading to potentially fatal thrombi. Imaging techniques that can reliably characterize and identify both peripheral arterial disease and atherosclerotic plaque can be beneficial for improving patient outcome. One method that shows promise for vascular imaging is Acoustic Radiation Force Impulse Imaging (ARFI) [2], an imaging technique that uses radiation force to displace tissue.

Methods: ARFI imaging data were acquired from both popliteal arteries of twenty–eight healthy subjects and twenty–four patients with diagnosed peripheral arterial disease. ARFI imaging data were also obtained from the common and internal carotid arteries of four healthy subjects and five patients with diagnosed cardiovascular disease. Custom ECG–gated sequences were used to acquire data during vessel diastole and vessel systole. ARFI displacement images were then computed from the longitudinal segments of the vessels.

Results: Of the 104 datasets (n=52 subjects) acquired from the popliteal artery, 57 provided viable ARFI results, showing well defined vascular walls and plaque and excellent spatial registration between conventional B–mode images and ARFI displacement images. It was generally noted that the majority of the non–viable datasets were either from a) relatively deep popliteal arteries in which the popliteal distal wall was deeper than 37mm or b) popliteal arteries in which the lumen and vascular walls were poorly defined by conventional ultrasound. Improvements in ARFI imaging at depth have increased the yield of viable datasets from 44% to 65% over the course of the popliteal study. Percent–yield of viable images was not a factor for the carotid study. For viable ARFI images, we observe that vascular walls displace less than surrounding tissue, suggesting that it is stiffer. For viable ARFI images, we observe that plaques visible in B–mode are well characterized in corresponding ARFI images.

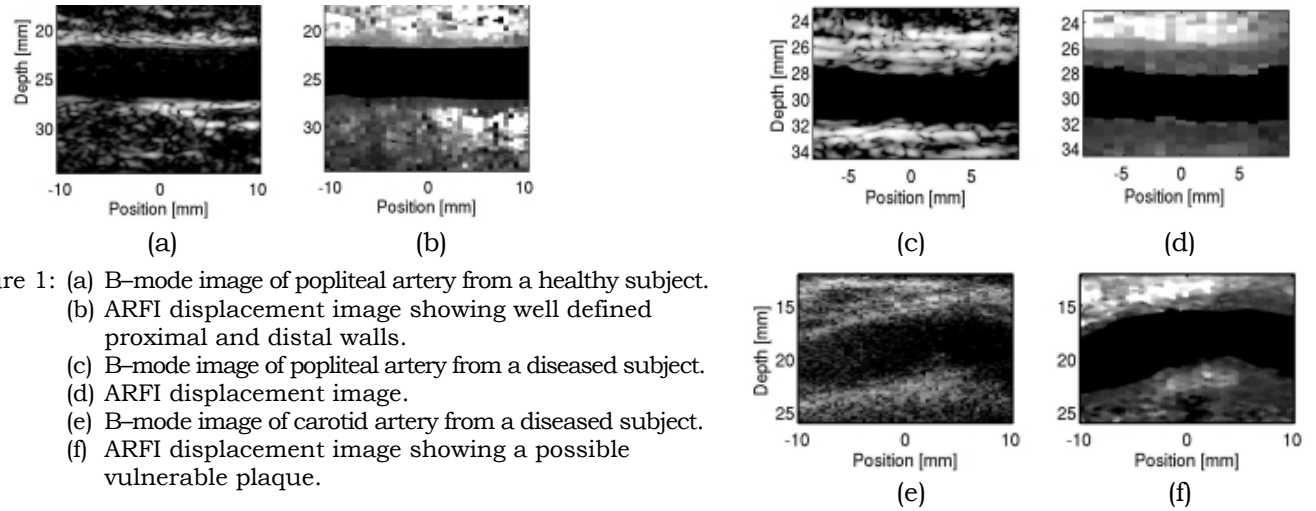

Figure 1: (a) B–mode image of popliteal artery from a healthy subject.
(b) ARFI displacement image showing well defined proximal and distal walls.
(c) B–mode image of popliteal artery from a diseased subject.
(d) ARFI displacement image.
(e) B–mode image of carotid artery from a diseased subject.
(f) ARFI displacement image showing a possible vulnerable plaque.

Conclusions: ARFI imaging shows promise in vascular imaging applications, especially in superficial peripheral arteries such as the carotid artery in which energy loss due to attenuation is reduced.

Acknowledgements: This work is supported by NIH Grants HL075485 and 5T32EB001040.

References:

[1] R. Dieter, W. Chu, J. Pacamowski, P. McBride, and T. Tanke. The significance of lower extremity peripheral arterial disease. Clin. Cardiology. 25:3-10,2002.
[2] G. Trahey, M. Palmeri, R. Bentley, and K. Nightingale. Acoustic Radiation Force Impulse Imaging of the mechanical properties of arteries: *in vivo* and *ex vivo* results. Ultrasound Med. Biol. 30:1163:1171, 2004.

* *indicates Presenter*

094 **PRELIMINARY POROELASTOGRAPHY RESULTS ON LYMPHEDEMATOUS TISSUES *IN VIVO*.**

Raffaella Righetti[1], Brian S. Garra[2], Louise M. Mobbs[2], Christina M. Chant[2], Jonathan Ophir[1].*
[1]The University of Texas Health Science Center Houston Medical School, 6431 Fannin St., Houston, TX, 77030, USA; [2]The University of Vermont College of Medicine, 111 Colchester Av., Burlington, VT, 05401, USA.

Background: We have recently reported the results of an *in vivo* poroelastographic experiment on a subject having chronic lymphedema in the right upper arm, a condition that is characterized by a significant amount of free fluid [1]. The experiment was performed by using a novel compression/acquisition methodology, which allowed maintaining high correlation values during the entire acquisition interval. In this paper, we report on additional recent results from two other patients.

Methods: Two experiments were performed *in vivo*. The first experiment consisted of acquiring poroelastographic data from the forearm subcutis of a female subject (age 65) having chronic lymphedema (advanced stage 2 lymphedema, per the criteria of International Staging of Lymphedema). The second experiment consisted of acquiring poroelastographic data from the legs of a female subject (age 46) having advanced stage 1 lymphedema in the right upper leg and a regular stage 1 lymphedema in the left upper leg (per the criteria of International Staging of Lymphedema). Data were acquired at the University of Vermont using the Philips HDI–1000 system with a 7.5 MHz linear array transducer, 50% bandwidth, 1 mm beamwidth and a 20 MHz sampling frequency. The RF data were then sent to The University of Texas, where they were used to generate poroelastograms [1] and to analyze the effects of the physiological factors on the attainable image quality of the poroelastograms [2].

Results: The results on the lymphedema arm suggest a spatially non–homogeneous effective Poisson's ratio distribution, which decreases in time in local regions of the abnormal tissue. Unlike the poroelastogram obtained from the arm, the poroelastograms from the legs show a temporal monotonic decrease of the effective Poisson's ratio values in all image regions. For the purpose of illustration, a sonogram and corresponding poroelastogram obtained from matching subcutis areas in an edematous leg are shown in Figure 1. This 38 mm x 20 mm area is indicated by the box on the sonogram. The decorrelation analysis study showed an exponential decay of the mean cross–correlation coefficient values with time, with time constants in general exceeding 1s. These decorrelation results are in general agreement with the results in the livers and thyroids reported in [2], although they indicate order–of–magnitude greater time constants (i.e., slower decay) than those found in the livers and thyroids.

Conclusions: These preliminary results confirm our earlier observation that poroelastic effects that include spatial segmentation effects of the effective Poisson's ratio as well as temporal stress relaxation effects exist in lymphedema, and that it may be technically feasible to generate poroelastograms from lymphedematous tissues *in vivo*. They also suggest that subcutis tissues may be significantly less sensitive to physiological decorrelation noise than liver and thyroid, probably due to their extremity position, a favorable condition for generating poroelastograms *in vivo*.

Acknowledgements: This work was supported by NCI Program Project PO1-CA64597-12 and by funding from John S. Dunn foundation to The University of Texas Health Science at Houston.

References:

[1] Righetti R, Ophir J, Garra BS, Chandrasekhar RM, Krouskop TA. A new method for generating poroelastograms in noisy environments. Ultrasonic Imaging, vol. 27: 201-211, 2005.
[2] Chandrasekhar RM, Ophir J, Krouskop TA, Ophir K. Effects of physiological tissue motion on predicted elastographic image quality *in vivo*. Ultras. Med. Biol., 2006 (in press).

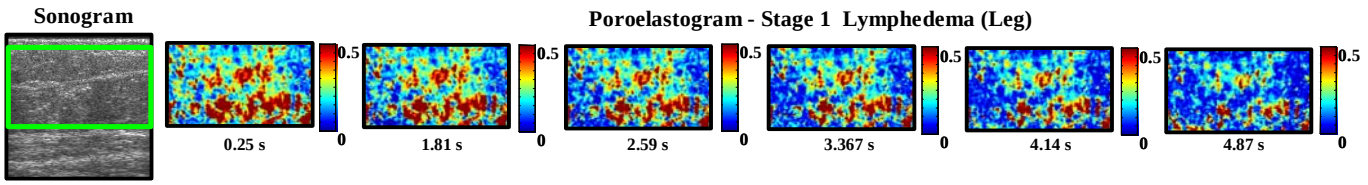

Figure 1

086 **THYROID STIFFNESS INDEX FROM THYROID ELASTOGRAPHY USING CAROTID ARTERY PULSATION: CORRELATION WITH FINE NEEDLE ASPIRATION BIOPSY.**

Unmin Bae[1], Manjiri Dighe[1], Vijay Shamdasani[1] and Yongmin Kim[1].*
[1]University of Washington, Seattle, WA, USA.

Background: Thyroid elastography has shown the potential for non–invasive differential diagnosis of thyroid nodules. With the conventional approach, freehand compression is applied on the neck area, and the resulting strain is estimated from ultrasound signals. However, the quality of strain images and the resulting diagnostic performance have been reported to be greatly affected by decorrelation noise that is mainly caused by undesirable motion of the carotid artery during external freehand compression and pulsation. We have studied the feasibility of thyroid elastography using pulsation of carotid artery as the compression source and found that carotid artery pulsation can serve as a repeatable and operator-independent compression source for thyroid elastography.

Aim: For a differential diagnosis of thyroid nodules, we aim to develop a measure of thyroid tissue stiffness using the pulsation–based thyroid elastography and correlate it with the diagnosis from the fine needle aspiration (FNA) biopsy.

Method: A pilot study is being conducted at the University of Washington. An Institutional Review Board approval was obtained from the Human Subjects Division. Ultrasound examinations were performed for the study prior to the FNA. Baseband ultrasound data of thyroid nodules were acquired using an Hitachi EUB–5500 ultrasound machine. Strain was estimated off–line using the angular strain method [2]. Since carotid artery pulsation was used as the compression source, the strain near the carotid artery can indicate the amount of compression applied by carotid artery pulsation. Thyroid stiffness index (TSI) was computed as the ratio of strain near the carotid artery (high–strain region) to that of a stiff area (low-strain region) inside a thyroid nodule. Higher TSI means smaller strain for a given amount of compression, indicating stiffer thyroid tissue.

Results: TSI for a case of papillary carcinoma was 44.7 whereas that for a case of follicular neoplasm was 12.4. TSI for benign nodular goiter with and without interstitial fibrosis was 24.4 and 16.3, respectively, indicating the fibrosis contributes to increasing tissue stiffness. For a nodule that appears to be solid in B–mode but was ruled out as being cystic from the FNA, TSI was 7.3. For 17 thyroid nodules (from 15 patients) with a definite FNA diagnosis, TSI for papillary carcinoma was higher than other lesions, such as follicular neoplasm and nodular goiter, indicating that papillary carcinoma is stiffer than other lesions (p=0.01). This finding is consistent with the *in vitro* stiffness measurements of thyroid lesions [1] and indicates that TSI may be useful in differentiating the papillary carcinoma, the majority (~80%) of thyroid cancer, from other lesions.

Conclusion: TSI from thyroid elastography using carotid artery pulsation shows a good correlation with pathological findings from the fine needle aspiration biopsy. TSI needs to be further evaluated with post-surgical histology in the future. TSI may provide a quantitative measure of thyroid stiffness for non-invasive differential diagnosis of thyroid nodules.

References:

[1] A. Lyshchik, T. Higashi, R. Asato, et al., "Elastic moduli of thyroid tissues under compression," Ultrasonic Imaging, vol. 27, pp. 101-110, 2005.
[2] U. Bae and Y. Kim, "Angular strain method for strain estimation in ultrasound elasticity imaging," Proc. of The 4th International Conference on the Ultrasonic Measurement and Imaging of Tissue Elasticity, Austin, Texas, USA, 2005.

* *indicates Presenter*

102 **EXPERIMENTAL VALIDATION OF TISSUE MOTION TRACKING RESOLUTION LIMITS FOR THE DIGITAL PULSED PHASE LOCKED LOOP.**

Ted Lynch[1], Samuel Guy[1], Randi Saunders[1].*
[1]Luna Innovations Incorporated, Hampton, VA 23666, USA.

Background: Previous theoretical analysis has indicated that a digital implementation of the pulsed phased locked loop (PPLL) could track tissue motion on the order of 8 nanometers when the signal to noise ratio was 50 dB [1]. The digital PPLL has since been reduced to practice, and here we compare experimental results with our previous theoretical analysis.

Aims: The aim of this work is to establish the performance limits of the digital PPLL as a method for measuring tissue motion.

Methods: Corbin Sim–TestTM Ballistic Test Media [2], a tissue mimicking material, was placed on a metal plate. The material is made from animal protein and has a density and elasticity that closely match that of live animal muscle tissue. Small amplitude vibrations in the metal plate were created using a standard stereo speaker driven with a function generator. The motion of the metal plate was measured through the tissue mimicking material using the digital PPLL. The digital PPLL data were validated using a non–contact displacement transducer with nanometer resolution (Micro-Epsilon, Inc.: Raleigh, NC). To determine the resolution limits of the digital PPLL, the amplitude of vibration in the plate was decreased by lowering the drive voltage on the function generator until the limit of PPLL detection was reached. The process was repeated over a range of vibration frequencies from 1-1000 Hz.

Results: Preliminary results indicate that at a vibration frequency of 1000 Hz, the digital PPLL can track displacement amplitudes down to 30 nm. Animal model and clinical test data obtained while testing one potential application of the technology-the noninvasive estimation of internal pressures–will also be discussed in relation to these results.

Conclusions: High–resolution measurement of tissue motion has numerous potential applications, including the noninvasive measurement of intracranial pressure and intramuscular pressure, both of which have been tested clinically at the University of California, San Diego [3,4].

Acknowledgements: Funding provided by the U.S. Army Research Office under SBIR contract DAAD19-03-C-01391. The content does not reflect the position or policy of the U.S. Government, and no official endorsement should be inferred.

References:

[1] T Lynch, et al. "High Resolution Time of Flight Measurements with the Pulsed Phase Locked Loop." Proc. of The 4th International Conference on the Ultrasonic Measurement and Imaging of Tissue Elasticity, p 80, 2005. http://www.ece.rochester.edu/users/rcbu/conference/2005conf.htm.
[2] Corbin Manufacturing & Supply, Inc. PO Box 2659 White City, OR 97503 USA. http://www.bulletswage.com/sim-test.htm.
[3] JM Wiemann, et al. "Noninvasive Measurement of Intramuscular Pressure in a Model Compartment Syndrome." J Orthop Trauma (in review) 2006.
[4] Ueno T, Macias BR, Yost WT, Hargens AR. "Noninvasive assessment of intracranial pressure waveforms by using pulsed phase lock loop technology." J Neurosurg. 2005 Aug;103(2):361–7.

032 **ANTHROPOMORPHIC UTERINE PHANTOMS FOR TESTING ELASTOGRAPHY SYSTEMS.**

Maritza A. Hobson[1], Gary R. Frank[1], Tomy Varghese[1], Ernest L. Madsen[1].*
[1]Medical Physics Department, University of Wisconsin–Madison, 1300 University Avenue, 1530 MSC, Madison, WI 53706, USA.

Aims: To develop and test anthropomorphic uterine phantoms for mimicking *in vivo* ultrasound (US) strain imaging using saline infused sonohysterography (SIS) to provide the needed compressions. Such an anthropomorphic uterine phantom may aid in the development of software for uterine strain imaging.

Background: Uterine strain imaging has been successful in differentiating between endometrial polyps and leiomyomas in excised uteri [1]. An anthropomorphic uterine phantom that mimics the SIS method could help determine whether or not the current strain imaging methods would be successful *in vivo*. Kiss *et al* [2] determined the average Young's moduli values for excised normal uterine and cervical tissue, and the appropriate safflower oil–in–gelatin dispersion materials can be chosen to mimic the uterine, cervical and fibroid tissue using these values.

Methods: The dimensions and shapes of the components of the uterus phantom are modeled after the typical uterus of a pre–menopausal woman with no children. An anterior/posterior view of the phantom design is shown in Figure 1. A 10% safflower–oil–in–gelatin dispersion material was used in 3 mm diameter spheres that represent fibroids randomly distributed in the myometrium and cervix; 80% oil represents fat; and 50% oil represents the myometrium and cervical tissues. US test cylinders and samples for dynamic testing of each component were made at the time of phantom production. Methods for determining the US speed of sound, attenuation and Young's modulus have been described previously [3]. A Siemens Antares with VFX 13–5 and 9–4 transducers were used to obtain radiofrequency (RF) data during a 9% volume expansion of the endometrial cavity. RF data was post–processed using a 2–D block matching algorithm to generate strain images [4]. RF data will also be acquired using the Aloka.

Results: The 10%, 50%, and 80% oil–in–gelatin materials had Young's moduli of 82.4, 30.0, and 8.66 kPa, respectively; speeds of sound were 1581, 1520, and 1486 m/s; and attenuation coefficients/frequency at 7 MHz of 0.34, 0.41, and 0.61 dB/cm/MHz. Figure 2 shows a strain image (bottom) obtained on a Siemens Antares showing a stiffer 3 mm inclusion in the surrounding myometrium. The strain image was obtained after up–sampling in the axial direction six times, which could limit the feasibility of real–time imaging using SIS for compression.

Conclusions: The first uterine phantom performed very well and was shown to be durable and give reproducible results. Phantoms with more complex geometries will be constructed and will include other oil concentrations for endometrial polyps, adenomyosis and other uterine conditions once *in vitro* mechanical properties have been determined. It is anticipated that insight into the feasibility of SIS strain imaging will be enhanced via availability of these phantoms.

References:

[1] Hobson, M.A. *et al.* Elastographic Imaging of Uterine Tissue. Proc. of The 4th Int. Conf. on Ultrasonic Measurement and Imaging of Tissue Elasticity. Lake Travis, TX, USA, p.104, 2005.
[2] Kiss, M.Z. *et al.* Frequency–dependent Complex Mod. Of the Uterus: Preliminary Results. *Physics in Medicine and Biology*, 2006. In press.
[3] Madsen, E.L. *et al.* Stability of Heterogeneous Elastography Phantoms made from Oil Dispersions in Aqueous Gels. *Ultrasound in Med. & Biol.* 32.3: 261–270, 2006.
[4] Zhu, Y. and T.J. Hall. A mod. block matching method for real–time freehand strain im. *Ultra. Im.* 24: 161–176, 2002.

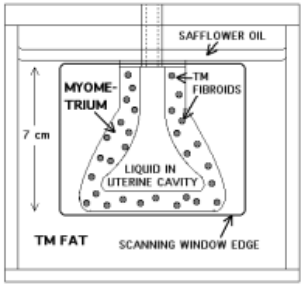

Figure 1: Uterine Phantom Anterior/Posterior View

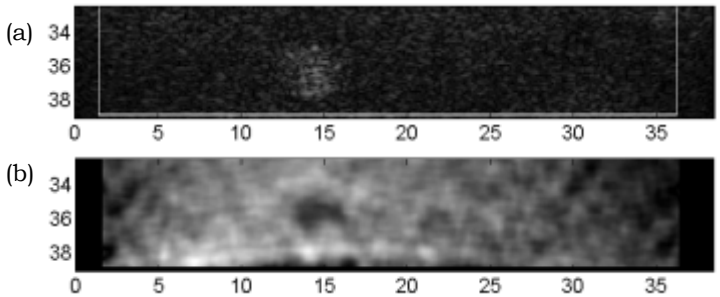

Figure 2: B–mode Image (a) and Strain Image (b) of 3 mm fibroid. Scales are in mm.

* *indicates Presenter*

059 **ULTRASOUND ELASTOGRAPHY AND BACKSCATTER ATTENUATION TOMOGRAPHY AS METHODS FOR IONIZING RADIATION DOSIMETRY: A FEASIBILITY STUDY.**

Jeffrey C. Bamber[1], Nigel L. Bush[1], Jamie Trap[1], Mike Partridge[1].*
[1]Joint Department of Physics, Institute of Cancer Research and Royal Marsden NHS Trust, Downs Road, Sutton, Surrey, SM2 5PT, England, UK.

Background: In recent years there has been interest in the use of polymer gels for ionizing radiation dosimetry [1]. Gel dosimetry is based on the principle that radiation–induced polymerization results in a change in a calibrated physical property of the gel that can be measured non–invasively and interpreted as an accurate and repeatable measure of dose. Various gels have been developed for this purpose and a variety of physical properties have been explored for use as the readout variable, including optical absorption, magnetic resonance relaxation, ultrasonic speed and ultrasonic absorption. All of these physical variables may be imaged and hence provide the possibility for measuring absorbed radiation dose distributions in three dimensions, which would permit verification of complex radiotherapy treatments. Magnetic resonance imaging represents a costly and inconvenient approach to the problem, which is one reason why optical and ultrasound imaging methods have been investigated. To date, neither has provided the combined levels desired for convenience of use, spatial resolution, accuracy and precision of dose estimation. For ultrasound [2], it would appear that part of this problem has arisen from the use of methods that reconstruct images of sound speed or attenuation coefficient from transmission projections of time–of–flight or signal–loss, using relatively unfocused sound beams. This has limited the spatial resolution and resulted in image artefacts.

Aims: To evaluate the feasibility and potential for two new methods of imaging the three–dimensional ionizing radiation dose distribution in radiation sensitive gels; viz. elastography and backscatter attenuation tomography.

Methods: For the first time, MAGIC (Methacrylic and Ascorbic acid in Gelatine initiated by Copper) gels were manufactured containing ultrasound scatterers, taking care to avoid oxygen contamination that would otherwise act as an undesired source of gel polymerization. Gels were irradiated in the sealed moulds in which they were created, to produce approximately square or cylindrical regions of gel exposed to a given dose in a background of unexposed gel. After allowing time for the resulting polymerization to stabilize, the gels were removed from the moulds for imaging, using either (1) a well–established freehand elastography method that involves a hand–induced motion of the transducer to apply compressive force to the gel, followed by a 2–D RF echo cross–correlation estimation of the resulting displacement distribution, and a linear least squares axial strain estimation, or (2) a backscatter attenuation estimator that worked by applying the same linear least squares gradient estimator used in elastography to the log backscatter magnitude versus depth. The backscatter attenuation images were then improved by an angular compounding, i.e. averaging the attenuation estimates obtained from multiple viewing angles.

Results: Both methods clearly visualized the presence of large (4cm) very high dose (40–100 Gy) regions in the gels. The attenuation method, unsurprisingly, required a high degree of spatial homogeneity in the local number density of scatterers, which was not achieved for all the gels manufactured. Freehand elastography was better in this respect, and a relatively small (~7.5mm radius) cylindrical region exposed to a 40 Gy dose was clearly depicted.

Conclusions: It is relatively easy to load MAGIC gels with ultrasound scatterers without introducing oxygen contamination, and it is possible, in elastographic and backscatter attenuation images, to visually detect regions in such gels that have been exposed to ionizing radiation. The results indicate that it would be worthwhile developing improved backscatter gel manufacturing and imaging methods for carrying out detailed studies of the accuracy, precision and spatial resolution of dose measurement, and for comparison with existing gel dosimetry readout techniques. It may also be worth considered radiation sensitive gels as a basis for constructing elastographic phantoms with controlled stiffness distributions.

Acknowledgements: This work was supported by funding from the EPSRC.

References:

[1] Trapp J, Partridge M, Hansen V, Childs P, Bedford J, Warrington J, Leach MO, Webb S (2004). The use of gel dosimetry for verification of electron and photon treatment plans in carcinoma of the scalp. Phys Med Biol; 49:1625–1635.
[2] Mather M L, Baldock C (2003) Ultrasound tomography imaging of radiation dose distributions in polymer gel dosimeters: Preliminary study. Med Phys; 30:2140–2148.

026 **NON–CONTACT FOCUSED ACOUSTIC RADIATION FORCE TECHNIQUE FOR THE BIOMECHANICAL CHARACTERISATION OF AN AMPUTEE'S RESIDUAL LIMB.**

Helen Mulvana[1], Sandy Cochran[2], Bill Spence[1], Stephan Solomonidis[1].*
[1]University of Strathclyde, Glasgow, Scotland, UK; [2]University of Paisley, Paisley, Scotland, UK.

Background: Qualitative assessment via palpation is the dominant technique used by prosthetists to assess the elastic properties of the lower–limb amputee's residual limb tissue. The efficacy of this method is subject to the skill of the prosthetist, prone to error and cannot be automated. Attempts to quantify tissue elasticity have been made for other applications such as the detection of cancerous tumours. The result is elastography imaging, where ultrasound is used to recover qualitative strain data displayed in grey scale. The development of an equivalent technique for quantitative tissue evaluation would assist the prosthetist in finding areas most suited to load bearing and requiring pressure relief.

Aims: This study aims to develop a technique for ultrasonic stimulation of tissue to enable biomechanical assessment of an amputee's residual limb prior to prosthesis fitting.

Methods: Experiments based on previously published work [1], were conducted to establish the use of a two–element piezoceramic confocal array transducer as a device for non–contact, low frequency tissue excitation. The two elements were driven at high frequencies, F_n and $F_n + \delta f$, and the nonlinear nature of the propagation medium was used to create sum ($2F_n$) and difference (δf) frequencies at the focal point. Since high frequencies are strongly attenuated, the low frequency of interest remains.

Results: In the present study, a PZ27 focusing bowl (Ferroperm A/S, Kvistgaard, Denmark) was used with an outer diameter of 44.45 mm, focal length of 63.5 mm and centre frequency $F_n \approx 1.7$ MHz to excite tissue mimicking material. As a comparison, a flat, circular PZ27 element was also studied, with an RX771 lens (Robnor Resins Ltd., Swindon, UK) bonded to it. Each element of the arrays was driven using a separate 33220A signal generator (Agilent, South Queensferry, UK), and power amplification was used to reduce the propagation distance required to create the parametric array and to create a low frequency acoustic radiation force of magnitude appropriate for soft tissue displacement to be measured using an 8103 hydrophone (Bruel and Kjaer, Naerum, Denmark).

Conclusions: The results provide indications of the feasibility of focused, low–frequency acoustic interrogation of tissue as a tool in the quantitative assessment of the amputee's residual limb as an aid during prosthesis fitting. Further investigation towards practical application is suggested.

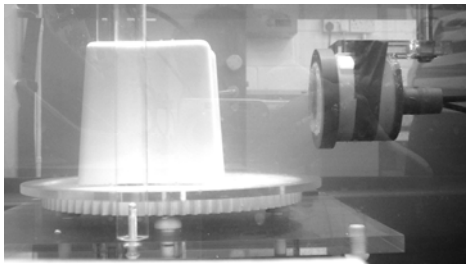

Figure 1

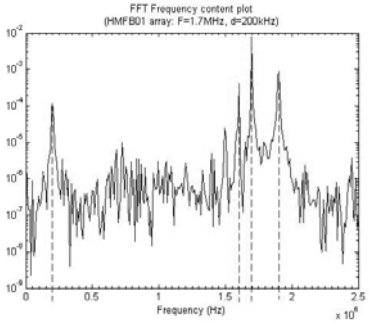

Figure 2

Acknowledgements: H. Mulvana is supported by the UK EPSRC Doctoral Training Centre in Medical Devices. The authors also acknowledge the support of P. Connolly and C. Kapatos.

Reference:

[1] M. Fatemi & J. F. Greenleaf, "Vibro–acoustography: An imaging modality based on ultrasound–stimulated acoustic emission," Proc. Nat. Acad. Sci. USA, vol. 96, pp. 6603–6608, June 1999.

* *indicates Presenter*

069 **QUANTIZATION OF TISSUE VISCO–ELASTICITY FROM MEASURED DISPERSION OF SHEAR WAVE SPEED: A PRACTICAL STUDY.**

Shigao Chen[1], Randall Kinnick[1], James F. Greenleaf[1].*
[1]Mayo Clinic College of Medicine, 200 First Street SW, Rochester, MN, 55905, USA.

Background: Tissue elasticity imaging with ultrasound provides valuable information about tissue wellness in an inexpensive way thus has great clinical potential. Currently most methods only provide a relative mapping of tissue elasticity. While they are useful in detecting abnormal lesions, other clinical applications may require *quantitative* measurement (i.e., in Pascal scale) of tissue elasticity. In addition, tissue *viscosity*, another important index of the tissue state, is usually neglected, often causing significant bias to elasticity estimation.

Aims: Our goal is to produce an apparatus for noninvasive, biopsy–like quantification of tissue elasticity and viscosity with high accuracy.

Methods: Radiation force from an amplitude modulated ultrasound beam is used to generate monochromatic shear waves of various frequencies (one frequency at a time) within the studied tissue. The propagation speed of each shear wave is estimated by tracking its phase shift over a known propagation distance, using a special ultrasound detection method developed by us. The challenge is that vibrations due to ultrasound radiation force are very small (down to 10^{-7}m) and are difficult to measure with traditional pulse echo ultrasound methods. Using *a priori* knowledge of the vibration frequency, we are able to apply Kalman filtering to the detected signal and reliably extract the phase of the small vibrations. The shear wave propagation speeds thus measured at multiple frequencies are then fit with a theoretical dispersion formula to estimate tissue elasticity and viscosity. A special ultrasound pulse sequence has been developed to allow vibration generation and detection with a single array transducer, which simplifies the measurement setup and makes this method compatible with commercial ultrasound scanners.

Results: In one experiment, shear waves were induced by mechanically vibrating a glass tube glued to a through–hole cut within a striated muscle of beef. The dispersions along and across the muscle fibers measured by our ultrasound motion detection method are shown in Figure 1. The estimated elasticity and viscosity match literature results (μ_1~49 kPa, μ_2~15 Pa·s along the fibers and μ_1~25 kPa, μ_2~3.3 Pa·s across the fibers) [1]. In another experiment, two transducers driven by the special ultrasound pulse sequence were used to simulate the performance of this method with a single array transducer. Results along fibers of another beef muscle sample shown in Figure 2 are close to those in Figure 1. Figure 2 also presents the results obtained in a rabbit liver sample.

Conclusions: Tissue elasticity and viscosity can be accurately quantified from the dispersion of shear wave propagation speed. This method can be implemented with a single array transducer of a commercial ultrasound scanner. Measurement results are independent of the beam shape and intensity of the vibration-generating ultrasound.

Reference:

[1] Catheline S et al., Measuring of viscoelastic properties of homogeneous soft solid using transient elastography: an inverse problem approach. J Acoust Soc Am 2004; 116(6):3734–3741.

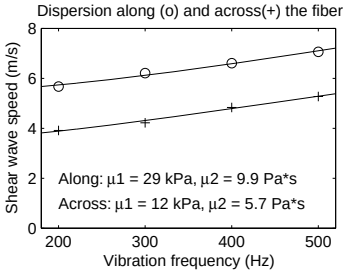

Figure 1: Dispersion of shear wave speed along and across beef muscle fibers. Shear waves were induced by mechanical vibration. Moduli were estimated from fit to Voigt model.

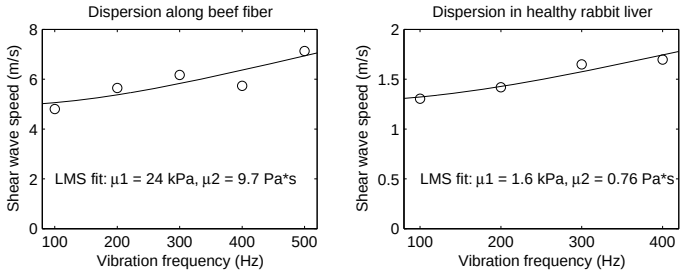

Figure 2: Shear wave speed dispersion measured along the beef muscle and a liver sample. Two transducers were used to simulate the performance of a single array transducer driven by a special pulse sequence allowing simultaneous vibration generation and detection. Voigt model was fit to data to estimate moduli.

076 **BREAST MECHANICAL IMAGER – AN ELASTICITY IMAGING DEVICE BASED ON DYNAMIC MEASUREMENT OF SURFACE STRESS PATTERNS.**

Vladimir Egorov[1], Jae Son[2], Suren Airapetian[1] and Armen Sarvazyan[1].*
[1]Artann Laboratories, 1459 Lower Ferry Rd., Trenton, NJ 08618, USA; [2]Medical Tactile, Inc., 5757 Century Blvd., Ste. 600, Los Angeles, CA 90045, USA.

Background: Mechanical Imaging (MI), which is being developed at Artann Laboratories during last 10 years [1], yields a 3–D map of tissue elasticity. MI closely mimics manual palpation since the MI probe with a pressure sensor array mounted on the probe acts similarly to a human hand during Clinical Breast Examination (CBE). In essence, MI "captures the sense of touch" and stores it permanently in digital format for analysis and comparison. Laboratory studies on tissue phantoms have shown that the MI is more sensitive than manual palpation [2].

Aim: The objective of this study is the development and validation of the Breast Mechanical Imager (BMI), an elasticity imaging device based on measurement of the stress pattern on the surface of the breast. BMI provides real time detection and imaging of breast tissue abnormalities and assessment of breast nodule features such as size, shape, consistency/hardness and mobility.

Methods: Figure 1 shows the BMI including a probe, (A), with a pressure sensor array, an electronic unit, (B), and a touch-screen laptop computer. The pressure sensor array is installed on the probe head surface and contacting the breast skin through a disposable elastic protective cover during the examination procedure. The probe head measures 50 mm x 40 mm having a radius of curvature of 38 mm. The pressure sensor array comprises 192 (16 x 12) pressure sensors covering 40 mm x 30 mm. Each pressure sensor has rectangular pressure sensing area of 2.5 mm x 2.5 mm (Medical Tactile, Inc., CA) and has sensitivity of about 0.05 kPa and hysteresis of 2–3% of the operational range. The breast examination procedure includes two modes: total breast examination (Mode 1) to detect suspicious sites and detailed local scan (Mode 2) to characterize in detail the initial findings. The breast examination in Mode 1 takes 30–40 seconds; a single local scan in Mode 2 takes 20–30 seconds. The laptop has touch screen capability and wireless connection with a printer to spool the automatically–generated examination report after the examination is completed.

Results: Laboratory testing on breast phantoms and an on–going clinical study demonstrated that current data acquisition rate 20 frames per second provide reliable 3–D images of underlying breast tissue structures with increased hardness and calculated values of lesion sizes, shape characterization, lesion mobility and Young's modulus evaluation. Figure 2 represents an example of visualized invasive ductal carcinoma, confirmed by biopsy pathology report.

Conclusions: BMI has potential to become a diagnostic and cancer screening tool that could enhance CBE through its higher sensitivity, quantitative record storage, ease–of–use, portability, minimal training required and inherent low cost.

Acknowledgements: This work is supported by NIH grant 5 R44 CA091392. The authors would like to thank Thomas J. Kearney, M.D., of the Cancer Institute of New Jersey, for the assistance in clinical study.

References:

[1] A. Sarvazyan, "Mechanical Imaging: A new technology for medical diagnostics." Int. J. Med. Inf., 1998, vol. 49, pp. 195–216.
[2] A. Sarvazyan, "Computerized palpation is more sensitive than human finger," Proc. 12th Int. Symposium on Biomedical Measurements and Instrumentation, Dubrovnik–Croatia, 1998, pp. 523–524.

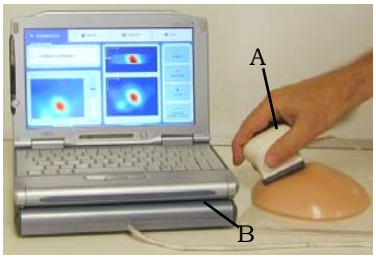

Figure 1: General view of BMI (see text)

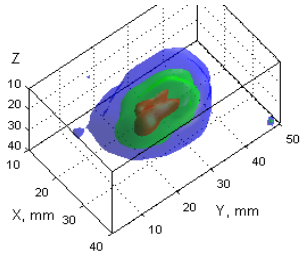

Figure 2: Recorded image of a lesion, histologically confirmed invasive ductal carcinoma.

* *indicates Presenter*

028 **MULTI–LAYERED PLAQUE VASCULAR PHANTOMS FOR ACOUSTIC RADIATION FORCE IMPULSE IMAGING.**

Douglas Dumont[1], Mike Mathis[1], Liang Zhai[1], Brian Fahey[1], Gregg E. Trahey[1].*
[1]Duke University, Department of Biomedical Engineering, Durham, NC, 27708, USA.

Aims: To construct and quantify multilayer composite vascular phantoms for Acoustic Radiation Force Impulse (ARFI) Imaging.

Background: Changes in vascular stiffness are often associated with corresponding changes in pathology. For example, it is generally accepted that atherosclerosis leads to a stiffening of the vascular wall and that thin fibrous–cap plaques may have increased risk of rupture, leading to acute cardiac events [1]. Thus, early detection and classification of vascular disease is important for guiding therapy. One method that shows promise for vascular imaging is Acoustic Radiation Force Impulse Imaging (ARFI) [2].

Previous work has demonstrated that Polyvinyl Alcohol (PVA) Cryogels are a suitable phantom material for vascular elasticity imaging [3,4]. This paper will describe new Cryogel phantoms for ARFI imaging that model soft and calcified plaques for various occlusion sizes. ARFI imaging results are also described for homogeneous and multilayer cryogel phantoms of varying stiffness.

Methods: Vascular phantoms were constructed by dissolving PVA particles into water at 94°C. Graphite particles were added to function as ultrasound scatterers. The resulting solution was cooled to room temperature before being cast into custom–made vessel molds. PVA stiffness was controlled by using freeze–thaw cycles to crosslink the solution. Each cycle consisted of freezing the PVA solution to -6°C for twelve hours and thawing to room temperature for twelve hours. Bi–layer phantom molds were constructed to model the vascular adventitia and intima–media. Calcified and soft plaque phantoms were constructed with 16%, 44% and 76% stenosis. Plaque stiffness was controlled by varying the number of freeze–thaw cycles for the occlusions. Phantoms were pressurized from 0kPa to 18kPa and imaged in cross–section and longitudinal planes using previously described ARFI techniques [2]. Plaque and wall sections were segmented from ARFI displacement data and volume rendered to produce three-dimensional visualizations of phantom structures.

Results: Preliminary ARFI results show high contrast between phantom layers and plaque occlusions that are not readily apparent with conventional ultrasound. Both occlusion types and sizes were visualized in the corresponding displacement images, with more compliant occlusions exhibiting higher contrast than stiffer occlusions of similar size.

Figure 1:
a) Conventional B–mode image of a compliant plaque phantom with a 44% stenosis.
b) Resulting ARFI displacement image with plaque visualized.
c) Conventional B–mode image of a stiff plaque phantom with bi–layer vascular wall.
d) Resulting ARFI displacement image showing definition of the more compliant outer layer.

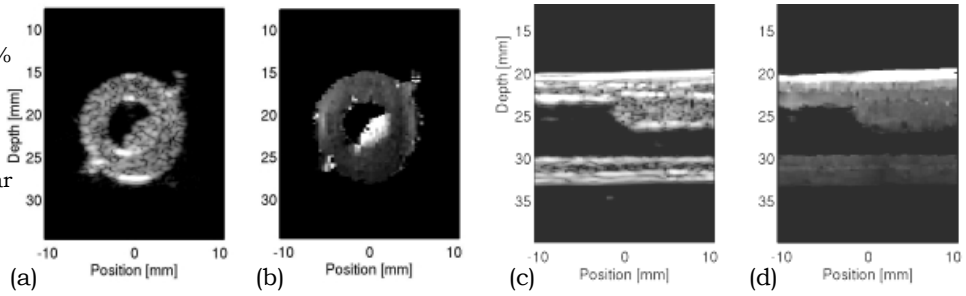

Conclusions: PVA cryogel is a suitable material for constructing multi–layer vascular phantoms with both hard and soft occlusions of various sizes. Further research will include modeling of more heterogeneous plaque structures, including thin–cap plaques.

Acknowledgements: We would like to thank Siemens for in–kind support and NIH Grants HL075485 and 5T32EB001040.

References:

[1] L. Troplseki, D. Salunke, and J. Humphries. On the mechanical behavior of athesclerotic plaque. Trans. 20th Ann Meet Soc Biomat, 18, 1994.
[2] G. Trahey, M. Palmeri, R. Bentley, and K. Nightingale. Acoustic Radiation Force Impulse Imaging of the mechanical properties of arteries: *in vivo* and *ex vivo* results. Ultrasound Med. Biol. 30:1163:1171, 2004.
[3] K. Chu and B. Rutt. Polyvinyl alchohol cryogel: An ideal phantom material for MR studies of arterial flow and elasticity. Magnetic Resonance in Medicine, 37:314–319, 1997.
[4] S. Nadkarni, H. Austin, G. Mills, D. Boughner, and A. Fenster. A pulsating coronary vessel phantom for two– and three–dimensional intravascular ultrasound studies. Ultrasound Med. Biol., 29(4):621–628, 2003.

106 **DEVELOPMENT OF A THREE–DIMENSIONAL TISSUE ELASTICITY MICROSCOPE.**

Tsuyoshi Shiina[1], Masashi Yoshida[1], Makoto Yamakawa[1], Naotaka Nitta[2], Tsuyoshi Mitake[3].*
[1]Graduate School of Systems and Information Engineering, University of Tsukuba, Tsukuba, JAPAN; [2]National Institute of Advanced Industrial Science and Technology, Tsukuba, JAPAN; [3]Research and Development Center, Hitachi Medical Corporation, Kashiwa, JAPAN.

Background: Some approaches for microscopic measurement of tissue elasticity have been proposed. These approaches emphasize high spatial resolution with high frequency ultrasound, so thin slices of tissue must be used. However, such thin slices are two–dimensional distributions, and real mechanical properties of tissue are apt to change when tissues are sliced thinly since the tissue microstructure is destroyed. To evaluate the mechanical properties of tissues under clinical conditions, it is important to measure the three–dimensional distribution of mechanical properties for relatively thick samples that preserve the microstructure of tissues. In addition, viscosity is another important parameter for tissue characterization, although most methods have so far have only tried to measure elasticity. For the purpose of improving precision of diagnosis based on tissue characterization, imaging of mechanical properties of tissue such as elasticity has been investigated. Recently, practical equipment for assessing tissue elasticity as strain images has been developed and used for diagnosing diseases such as breast cancers. To evaluate the stages of a progressive disease and to discriminate benign from malignant tumors, it is important to clarify the relationship between of the elasticity of tissues and their pathological conditions. There are some pioneering reports (1) on measurement of elastic modulus of tissues such as extracted breast. However, in order to examine the pathological correlations of the tissue elasticity, we need to compare the elasticity of each tissue element with the corresponding histological data.

Aims: From this viewpoint, we are developing a three–dimensional elasticity microscope for accumulating quantitative data on the mechanical properties of tissues.

Methods: First, in order to validate the feasibility of our approaches, we constructed a measurement system using relatively low frequency, 5 MHz. Many sets of volumetric data of echo signals from sample were captured with cyclic compression and relaxation. During the process of compression (relaxation), the pressure level was also recorded. Many sets of three–dimensional distributions of axial strain and elastic modulus data were calculated. At the same time, we also tried to compose three–dimensional images of hysteresis parameters which characterize the local viscoelasticity.

Results: Results of experiments using phantoms showed that three–dimensional distributions of elastic moduli were obtained with reasonable resolution and precision by our basic system (Figure 1). Next, considering the appropriate penetration depth and spatial resolution, the center frequency was set to 20-30MHz and the sample thickness was about 5 mm. The precision of the method was evaluated by comparing results by finite–element simulation and measurements of phantom inclusion with a cross-sectional diameter of different sizes. The spatial resolution is estimated to about 0.2 mm for elastic modulus.

Figure 1:

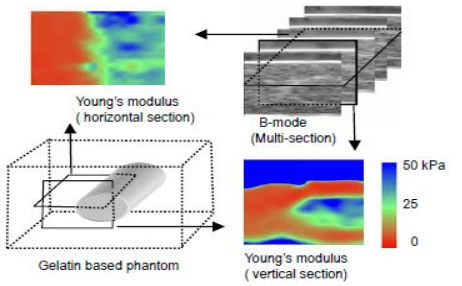

An example of 3-D elastic modulus measurement

Conclusions: Finally, we will show results of an experiment on extracted tissues to demonstrate the potential of the three-dimensional elasticity microscope.

References:

[1] T.A.Krouskop, T.M. Wheeler, F. Kallel, B.S. Garra, T.J. Hall, "Elastic Moduli of Breast and Prostate Tissue Under Compression," *Ultrason. Imaging*, vol.20, pp.260–274, 1998.
[2] N.A. Cohn, S.Y. Emelianov, M.A. Lubinski, M. O'Donnell, "An elasticity microscope. Part I: Methods," *IEEE Trans. Ultrason., Ferroelect., Freq. Contr.*, Vol. 44, No. 6, pp. 1304–1319, 1997.
[3] N. Nitta, T. Shiina and E. Ueno, "Hysteresis Parameter Imaging of Soft Tissue under Quasi–Static Deformation", *2003 IEEE International Ultrasonics Symposium Proceedings,* pp.1606–1609, 2003.

* *indicates Presenter*

121 **VOLUME ELASTICITY IMAGING WITH A 2–D CAPACITIVE MICRO–MACHINED ULTRASOUND TRANSDUCER (CMUT) ARRAY.**

Ted G. Fisher[1], Timothy J. Hall[1], Satchi Panda[2], Jingfeng Jiang[1], Jeff Resnick[2], Steve Barnes[2], Ernest L. Madsen[1].*

[1]Medical Physics Department, University of Wisconsin–Madison, 1530 MSC, 1300 University Avenue, Madison, WI 53706, USA; [2]Siemens Medical Solutions USA, Inc., Ultrasound Division, 1230 Shorebird Way, Mountain View, CA 94043, USA.

Background: A significant issue in clinical ultrasound imaging with typical 1–D array transducers is the inability to observe an abnormality in perpendicular image planes to rule out pseudo–lesions. The difficulty of this task is increased with elasticity imaging where some lesions are difficult to image in perpendicular planes. Further, because of the underlying mechanics of the elasticity imaging data acquisition problem, it is often difficult to obtain strain images of an *in vivo* lesion in multiple parallel planes. Volume ultrasound data acquisition simultaneously addresses both of these problems. However, until recently, the only ultrasound systems designed for volume data acquisition were either designed for cardiac or obstetrics applications and were not suitable for our applications in breast imaging. The advent of capacitive micro–machined ultrasound transducers (CMUTs) has created an opportunity to manufacture reliable, relatively low cost 2–D array systems with impressive performance. This paper presents the results of elasticity imaging with 3–D volume data acquired using a 2–D CMUT.

Aims: Assess the performance of various motion tracking strategies applied to a 3–D RF echo data set from an oil–in–gelatin phantom [1] with spherical targets for a multi–step deformation totaling about 15% axial strain.

Methods: A prototype 9 MHz 2–D CMUT array [2] connected to a Siemens SONOLINE Antares was used to acquire RF echo data from a 100 mm x 100 mm x 70 mm oil–in–gelatin phantom containing two 10 mm diameter spherical inclusions that have a 5:1 elastic contrast with the background. The transducer was mounted in a fixture that was used to apply a series of controlled compressions of 1.5-2% axial strain up to a total of about 15% strain. Elevation motion of the sphere was larger than the acoustic beam width so as to require 3–D tracking. This CMUT array images like a 1–D linear array in generating a 2–D image in the azimuthal plane, and it acquires a 3–D volume by electronically stepping the 2–D imaging plane in the elevational direction. Each volume acquisition acquired 312 A–lines in each image plane and 140 image planes in a 40 mm (axial) x 37 mm (lateral) x 29 mm (elevational) volume. Motion in the phantom was tracked with off–line data processing using three approaches: (1) 2–D block matching in single planes (pairing the same pre– and post–deformation planes), (2) 3–D tracking in the 'best' plane (select pairing of pre– and post–deformation planes), and (3) 3–D tracking combining block matching results from multiple planes. The contrast to noise ratios (CNRs) for the three motion tracking approaches were compared as a metric of performance. The volume strain image data were automatically segmented with a level sets algorithm and morphological operations to obtain surface rendered movies of the sphere through the 15% deformation. The volume of the rendered target was compared to the known sphere volume as another metric of strain image performance.

Results: The CNR increased with increasingly sophisticated motion tracking (2.33 ± 0.80, 3.78 ± 0.70, 4.22 ± 0.40 for the 2–D, 3–D 'best' plane and 3–D multi–plane tracking, respectively). The volume of the segmented target was estimated to be 0.44 ± 0.01 mm^3 compared to the known 0.52 mm^3 sphere volume. The accuracy of this estimate can easily be improved with segmentation algorithm optimization.

Conclusions: These results demonstrate the improvement in motion tracking available through 3–D tracking. This work also demonstrates that volume data acquisition allows accurate motion tracking and axial strain image formation for an entire target (within the field of view). Volume data acquisition with 2-D arrays will provide a major advancement in the capabilities of elasticity imaging systems.

Acknowledgements: This study was funded in part by a grant from the NIH (R01CA100373). We are also grateful to Siemens for the equipment loan that made this work possible.

References:

[1] Madsen EL, Hobson MA, Shi H, Varghese T, Frank GR. Stability of heterogeneous elastography phantoms made from oil dispersions in aqueous gels. Ultrasound Med Biol 2006;32:261–270.

[2] Daft C, Wagner P, Panda S, Ladabaum I. Elevation beam profile control with bias polarity patterns applied to microfabricated ultrasound transducers. 2003 IEEE Ultrasonics Symposium Proceedings (2):1578–1581, 2003.

118 **ANALYZING THE EFFECT OF VISCOELASTICY IN SHEAR WAVE SPEED IMAGES WITH SUPERSONIC IMAGING DATA.**

J. R. McLaughlin[1], D. Renzi[1], J. Klein[1], J–R. Yoon[2].*
[1]Rensselaer Polytechnic Institute, Troy, NY, USA; [2]Clemson University, Clemson, SC, USA.

Background: In supersonic imaging [1], a sequence of interior radiation force pulses is made along a line at a speed faster than the tissue shear wave speed. A wave propagates away from this line source. Time traces of displacement are created at each point in an image plane with the ultrafast imaging system developed in the laboratory of Mathias Fink. The time traces in measured data exhibit the effects of viscoelasticity showing wave spreading and amplitude decay [2]. Furthermore, the time traces are used to determine the arrival time at each point in the image plane of the wave front produced by the experiment.

Aims: The aim of this work is to analyze viscoelastic models, to show how these models yield wave spreading and amplitude decay and to accurately determine the arrival time. An additional goal is to exhibit the positive impact this improved arrival time has on shear wave speed(s) recovery and images of viscoelastic parameters.

Methods: We develop a parameterized model for wave spreading (and amplitude decay) which is derived from our viscoelastic model. Fast optimization procedures are employed to identify arrival times. The level curve method for the Arrival Time algorithm is used for shear wave speed, or multiple speeds and viscoelastic parameters, recovery.

Results: Shear wave speed(s) recovery with this improved arrival time identification procedure significantly improves shear wave speed(s) recovery in supersonic imaging. Viscoelastic parameters are also estimated.

Conclusions: Viscoelastic models, and in particular the wave spreading and amplitude decay implied by those models, provides improved inverse algorithms, for improved shear wave speed(s), and viscoelastic, imaging with supersonic imaging data.

Acknowledgements: This work is partially supported by NIH and ONR.

References:

[1] Joyce R. McLaughlin and Daniel Renzi, "Shear Wave Speed Recovery In Transient Elastography And Supersonic Imaging Using Propagating Fronts", Inverse Problem Vol.22, April 2006, pp.681–706.
[2] Joyce R. McLaughlin and Daniel Renzi, "Using Level Set Based Inversion of Arrival Times To Recover Shear Wavespeed In Transient Elastography And Supersonic Imaging", Inverse Problems, Vol.22, April 2006, pp.707–725.
[3] Bercoff J., Tanter M. and Fink M. 2004, "Supersonic shear imaging: a new technique for soft tissue elasticity mapping", IEEE Transactions on Ultrasonics, Ferroelectrics and Frequency control, 19 396–409.

* *indicates Presenter*

015 **SHEAR STRAIN ELASTOGRAMS INDUCED BY SHEAR DEFORMATION.**

Min Rao[1], E.L. Madsen[1], Tomy Varghese[1].*
[1]University of Wisconsin–Madison, 1530 Medical Science Center, 1300 University Ave., Madison, WI, USA.

Background: Elastography has been shown to be capable of tumor detection in the breast and prostate. However, some benign lesions, such as fibroadenomas in the breast, may have similar modulus values to infiltrating ductal carcinomas. Hence, to assess the malignancy of a detected lesion, axial strain imaging alone may not be sufficient. Garra et al [1] have shown that discrepancies between the size of lesions on sonograms and strain images may be a promising way to distinguish benign from malignant lesions. Konofagou et al [2] have shown that the shear strain estimates may provide supplementary information on the bonding between the tumor and the surrounding tissue. This property can characterize different tissue elements based on their mobility. However, the amount of shear strains obtained under an axial compression is usually small and hard to control. In addition, the shear strains of bound and unbound inclusions exhibit similar patterns due to the axial compression applied, as shown in Figure 1.

Aims: We illustrate using Finite–element analysis that significant differences can be observed in the shear strains induced by a lateral shear deformation for bound and unbound inclusions, as shown in Figure 2. In this study, ultrasound (US) simulation and phantom experiments were performed to demonstrate the feasibility and advantage of using shear strain images induced by a lateral shear deformation to distinguish benign from malignant tumors.

Methods: Shear strain elastograms (SSEs) induced by shear deformation were obtained on two inclusion phantoms. Both ultrasound simulation and tissue–mimicking phantom experiments were performed. The first phantom simulated the case of a malignant tumor, with the inclusion fully bounded to the surrounding medium. The second phantom simulated the case of a benign tumor, with the inclusion loosely bounded to the background. To induce a lateral shear deformation experimentally, the phantom was placed on a plate, attached to a stepper motor that introduces a lateral translation, while keeping the top surface of the phantom fixed. To fix the top surface, a compression plate with a rectangular slot for the transducer face was mounted on a linear stage driven by a second stepper motor in the axial direction. The surface of the plates was made coarse to prevent slipping between the plate and the phantom. After the RF data was acquired, a 2–D block matching algorithm was used to track the axial and lateral displacement. Components of the shear strain tensor, including the axial shear and lateral shear strains, were obtained from the displacement vectors using a least squares strain estimator.

Results: Simulation and experimental results show that increased shear strains are generated at the boundary between the inclusion and background for the unbounded case, which is not observed for the bounded inclusion. This difference in the shear strain patterns between bound and unbounded cases is significant compared to the shear strain patterns observed in shear strain images with only an axial compression.

Conclusions: SSEs obtained under a shear deformation may be helpful for differentiating benign and malignant tumors. Future work will deal with *in vitro* experiments on tissue samples and *in vivo* experiments.

Acknowledgements: This work is supported by Komen grant BCTR0601153.

References:

[1] Garra, B.S., Cespedes, E.I., Ophir, J., Spratt, S.R., Zuurbier, R.A., Magnant, C.M., and Pennanen, M. F., Elastography of breast lesions: Initial clinical results, Radiology, vol. 202, pp. 79–86, 1997.
[2] Konofagou, E.E., Harrigan, T., and Ophir, J., Shear strain estimation and lesion mobility assessment in elastography, Ultrasonics, vol. 38, pp. 400–404, 2000.

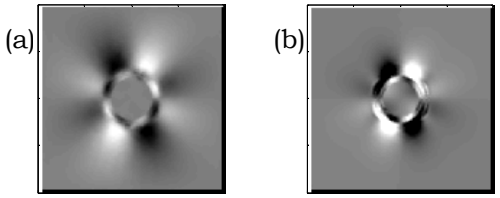

Figure 1: Finite–element calculated shear strains induced by an axial compression for a bounded (a) and an unbounded inclusion (b).

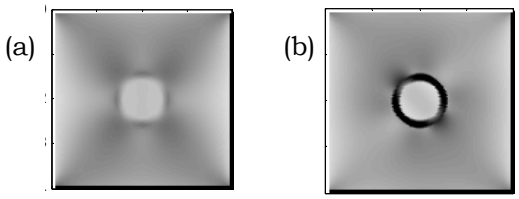

Figure 2: Finite–element calculated shear strains induced by a lateral shear deformation for a bounded (a) and an unbounded inclusion (b).

053 **ELASTIC IMAGING AT FINITE DEFORMATIONS.**

Stefan Reichling[1], Walaa Khaled[2], Otto T. Bruhns[1], Helmut Ermert[2].*
[1]Institute of Mechanics, [2]Institute of High Frequency Engineering, Ruhr–University Bochum, Bochum, GERMANY.

Background: Since material properties of soft tissue cannot be estimated directly *in vivo*, many numerical approaches for indirectly determining the material behavior have been developed [1–4]. Commonly, they are referred to as elasticity imaging. Using those methods, the displacement in the compression direction of the inhomogeneous tissue–like body under consideration is first measured by applying a quasi–static load. Subsequently, this displacement field is used as input for computing the distribution of material properties inside the sample. Although soft tissue is generally anisotropic, (quasi) incompressible and viscoelastic, the classical linearized, isotropic elasticity theory is usually adopted. In so doing, the distribution of the shear modulus μ can be estimated. However, if the deformation in the elastic body becomes too large, the assumptions implied by the linearized elasticity theory are not fulfilled any more. Consequently, Skovoroda et al. [2] proposed to use a geometrically exact description of the deformation. Since a linear elastic material model was adopted in [2], the range of application of the advocated method was nevertheless restricted. More precisely, all approaches which can be found in the literature are generally limited to measuring systems characterized by small (or moderate) deformations.

Aims: In this paper, an iterative approach is presented to estimate the shear modulus distribution of an incompressible, elastic body. The presented method is capable of taking into account large elastic deformations.

Methods: An iterative approach was developed. Using the presented algorithm, the distance between the measured displacement field, u^m, and a determined displacement field, u, is minimized with respect to the shear modulus, μ, using an appropriate norm, cf. [3,4]. Therefore, the estimation of the displacement, u, is required in every iteration step. For that purpose, an isotropic and hyperelastic material model is adopted. The incompressibility condition within the non–linear finite element computation is approximated by using a three–field variational principle depending on the displacement, u, the pressure, p, and the dilatation θ, cf. [5].

Results and Conclusions: The applicability as well as the performance of the approach is demonstrated by some 2D numerical examples and ultrasound measurements with PVA phantoms.

Acknowledgements: For the financial support within the project BR 580/32–1 the DFG (German Research Foundation) is gratefully acknowledged.

References:

[1] Sumi C, Suzuki A and Nakayama K. Estimation of Shear Modulus Distribution in Soft Tissue from Strain Distribution. IEEE Transactions on Biomedical Engineering, 42, pages 193–202, 1995.
[2] Skovoroda AR, Lubinski MA, Emelianov SY and O'Donnell M. Reconstructive Elasticity Imaging for Large Deformations. IEEE Transactions on Ultrasonics, Ferroelectrics, and Frequency Control, 46, pages 523–535, 1999.
[3] Kallel F and Bertrand M. Tissue Elasticity Reconstruction Using Linear Perturbation Method. IEEE Transactions on Medical Imaging, 15, pages 299–313, 1996.
[4] Oberai AA, Gokhale NH and Feijóo GR. Solution of inverse problems in elasticity imaging using the adjoint method. Inverse Problems, 19, pages 297–313, 2003.
[5] Simo J and Taylor R. Quasi–incompressible finite elasticity in principal stretches. Continuum basis and numerical algorithms. Computer Methods in Applied Mechanics and Engineering, 85, pages 273–310, 1991.

* *indicates Presenter*

058 **SIMULATIONS OF MOTION DETECTION USING A COMBINED ARRAY FOR LOCALIZED HARMONIC MOTION IMAGING.**

Janne Heikkilä[1], Kullervo Hynynen[2].*
[1]University of Kuopio, Department of Physics, Savilahdentie 9, Kuopio, 70211, FINLAND; [2]Sunnybrook Health Sciences Centre, 2075 Bayview Avenue, Toronto, ON, M4N 3M5, CANADA.

Background: Development of new noninvasive ultrasound radiation force techniques to explore mechanical properties of soft tissues has been in a focus of intensive research during the past few years. There are many applications in which these techniques have been used, e.g. ultrasound surgery monitoring [1], mammography [2], detecting calcifications in arteries [3] and measurement of arterial wall elasticity [4]. Some of these techniques are based on measurement of sound emission caused by dynamic radiation force stimulation [5] and others are based on measurement of actual tissue motion produced by the stimulation force.

Aims: In Localized Harmonic Motion Imaging (LHMI) [6], dynamic radiation force stimulation is used to induce harmonic displacements in a target, which are pulse–echo imaged and used in the estimation of elastic properties of the target. The aim of this study was to simulate feasibility of different pulse–echo fields to detect displacements in soft tissue, and the efficiency of the method to detect the vibration distribution and amplitude has been investigated.

Methods: We used simulated vibration distribution caused by an amplitude modulated radiation force field in a homogeneous 8x8x8 cm^3 soft tissue domain. The focal point of the stimulation was the center point of the soft tissue domain. We used a linear phased array that consisted of 128 geometrically focused elements. The height of the transducer was 28 mm and the length was 92 mm. The fixed focal depth of the elements was 40 mm. The vibration distribution was pulse–echo imaged using focused tracking beams produced by 2-32 electronically focused transducer elements. The location of the tracking elements in the transducer was moved across the center axis of the transducer. The focal depth of the tracking beam was the same as the stimulation depth, but, in the lateral direction, the focus was in the middle of the tracking beams. The frequency of the tracking fields was 5.5 MHz. The rf echoes of pulse–echo imaging were simulated using FIELD II. The cross–correlation of the rf signals was used in the displacement analysis.

Results: The results indicated that the displacement amplitude and distribution can be detected using pulse–echo imaging. The maximum displacement at the stimulation point was 4.3 μm, and the maximum displacements measured using different numbers of tracking elements (2, 4, 8, 16, and 32) were: 2.2 μm, 2.6 μm, 3.1 μm, 3.6 μm and 3.5 μm. The differences between the full–width half–maximums (FWHM) of the measured and real distributions in the direction perpendicular to the center axis of the transducer were similarly: 91%, 63%, 34%, 17% and 23%. The results showed that in this case 16 tracking elements were needed to achieve the realistic vibration amplitude and distribution.

Conclusions: In conclusion, we found that a small number of elements of a phased array can be used to detect the displacement distribution and maximum vibration amplitudes while other elements can be used to stimulate the target. In addition, as it can be seen from the results, the better the tracking beam is focused, the better the displacements can be tracked. This means that there are many parameters that effect the efficiency of the tracking beams (e.g. frequency, location of the tracking elements, etc.), and these effects need to be investigated in the future.

Acknowledgements: This study has been supported by The Academy of Finland (13614).

References:

[1] Konofagou E, Thierman J, Hynynen K. A focused ultrasound method for synchronous diagnostic and therapeutic applications - a simulation study, *Physics Med Biol* 46, 2967–2984 (2001).
[2] Nightingale KR, Nightingale RW, Palmeri ML, Trahey GT. A finite element model of remote palpation of breast lesions using radiation force: Factors affecting tissue displacement, *Ultrason Imaging* 22, 35–54 (2000).
[3] Trahey GE, Palmeri ML, Bentley RC, Nightingale KR. Acoustic radiation force impulse imaging of the mechanical properties of arteries: *In vivo* and *ex vivo* results, *Ultrasound Med Biol* 30, 1163–1171 (2004).
[4] Karjalainen T, Hynynen K. Ultrasound stimulated acoustic emission in the measurement of elasticity of arterial wall, *Proc IEEE Ultrasonics Symp*, 1929–1932 (2002).
[5] Fatemi M, Greenleaf JF. Ultrasound–stimulated vibro–acoustic spectrography, *Science* 280, 82–85 (1998).
[6] Konofagou E, Hynynen K. Localized harmonic motion imaging: theory, simulations and experiments. *Ultrasound Med Biol* 29, 1405–1413 (2003).

027 **PRINCIPAL COMPONENT ANALYSIS: SHEAR STRAIN EFFECTS.**

Hao Chen[1], Tomy Varghese[1].*
[1]University of Wisconsin–Madison, 1530 MSC, 1300 University Avenue, Madison, WI, USA.

Background: Elastography or elasticity imaging techniques that image the local stiffness properties of tissue are relatively new technique for non–invasive investigation of tissue mechanical properties. In elastographic imaging, tissue is deformed using a quasi–static deformation, with pre– and post-compression radiofrequency (rf) data frames acquired. Local strains are computed from the gradient of the displacement field along the axial direction between the pre– and post–compression echo signal frames.

Aims: The components of stress normal to the beam direction in the ultrasound image plane are shear stresses which exist in tissue during the quasi–static deformation. These shear stresses are usually caused by lateral or elevational motion during deformation. The shear stress may introduce relative shifts in the tissues without a change in the volume, leading to the gradient of the relative shift being equal to zero theoretically due to the minimal or zero volume change. However, strain noise artifacts are still introduced into the strain image with these relative shifts. In this work, we evaluated the impact of shear stresses using principal component analysis (PCA) and compared these results to the commonly estimated axial and lateral strain estimates. The shear strains are quantified using the shear angle while applying the deformation.

Methods: We demonstrated the impact of shear strain effects on strain tensor images (axial and lateral) utilizing both simulation and experimental data obtained using tissue–mimicking (TM) phantoms. For small axial deformations, shear strains can significantly reduce strain image quality quantified using the elastographic signal–to–noise (SNR_e) and contrast–to–noise (CNR_e) ratios. Shear strain effects also increase the noise level of strain tensor images even for larger axial deformations. On the other hand, PCA can be used to project the strain tensor images into the first and second principal component images that provide significantly better and reproducible strain images.

Experimental data were acquired using a real–time clinical Siemens Antares® Ultrasound Scanner with an ultrasound research interface using a VFX–13–5 linear array transducer. To induce a lateral shear deformation experimentally, the TM phantom was placed on a plate, attached to a stepper motor that introduces a lateral translation, while keeping the top surface of the phantom fixed. The top surface of the phantom was fixed using a compression plate with a rectangular slot for the transducer and mounted to a linear stage driven by a second stepper motor in the axial direction. The surface of the top and bottom plates was coarse to prevent slippage between the plate and the phantom. Axial compression of 0%, 1% and 2% were applied to the phantom over lateral shear angle deformation ranging from 0° to 9.5°.

Results: The SNR_e and CNR_e values obtained were over 10 dB better for the first and second PCA components over the entire range of shear deformations when compared to the axial and lateral strain tensors for the 0% axial deformation. The SNR_e and CNR_e values, however, showed a decreasing trend for the larger shear angles with axial compression of 1% and 2% and the error bars between the PCA and strain tensor components did not overlap. Significant improvements in the SNR_e and CNR_e values were still observed with both the applied axial compression and shear deformations.

Conclusions: In this work, we demonstrated the improvement obtained using the first and second PCA strain images in terms of the SNR_e and CNR_e over conventional strain tensor estimation. Both simulation and experimental data using TM phantoms demonstrated this improvement. Principal component strain images can provide good quality strain images even in the presence of large lateral shear effects.

Reference:

[1] Varghese T, Ophir J, Konofagou E, Kallel F, Righetti R. Tradeoffs in elastographic imaging. *Ultrason Imaging* 2001; 23: 216–248.

051 **A 3D TRANSIENT ELASTOGRAPHY SYSTEM DESIGNED FOR *IN VIVO* BREAST EXAMINATION.**

Jean–Luc Gennisson[1], Thomas Deffieux[1], Ralph Sinkus[1], Mathieu Pernot[1], Mickaël Tanter[1], Mathias Fink[1].*
[1]Laboratoire Ondes et Acoustique, UMR 7587, ESPCI, 10 rue Vauquelin 75005 Paris, FRANCE.

Background: Most ultrasound based elastography systems only estimate one or two dimensional (2D) displacements within a plane. Therefore, as at least one displacement component is missing, the three dimensional (3D) wave equation cannot be fully solved, and the shear modulus estimation is biased. Moreover, the lack of the third displacement component does not allow the use of the curl operator to remove longitudinal waves.

Aims: The goal of the proposed system is to provide an automated tool to scan the three dimensional displacement field within a volume. The three dimensional wave equation is then solved to estimate the shear modulus. The device is designed to easily allow further *in vivo* breast examinations.

Methods: We developed an ultrasound based elastography system for data acquisition in combination with 2D vector displacement estimation within the plane of the ultrasound beam. The vector displacement estimation is achieved using the concept of adaptive sub-apertures during the receive beam forming process [1]. The object of interest is scanned using a standard ultrasonic probe (4.5 MHz, 128 elements) from different directions on a circular orbit (Figure 1). The transducer is translated perpendicular to the orbit (~10 times) for each angle which leads to several block datasets (~30 blocks) each containing 2D displacement information. Thereby, the displacement of each voxel within the object is measured several times from different directions. This provides a high resolution volumetric 3D displacement field after transforming each dataset from polar to Cartesian coordinates. The data acquisition system is contained within a water tank underneath a standard breast biopsy table. This enables *in vivo* measurements with the patient in the prone position.

Results and Conclusions: Initial phantom experiments were conducted with steady state mechanical excitation at 80 Hz. Inclusions were clearly visible in the complex shear modulus map as reconstructed from the inversion of the full 3D wave equation. Taking benefit of the ultrafast acquisition speed of our ultrasound system, the proposed method allows measuring volumetric datasets at several mechanical excitation frequencies within a clinically acceptable time. The method provides, for each voxel, the relationship between frequency and complex shear modulus which in turn is linked to the underlying rheology of the material. This represents the proof of concept for a spectroscopic approach of elastography suitable for clinical application. Initial results were obtained from phantoms and excised specimens. Results showed the expected variation of G_d and G_l as a function of frequency. The system enables the study of rheological properties of tumors which should further extend the diagnostic capability of elastography.

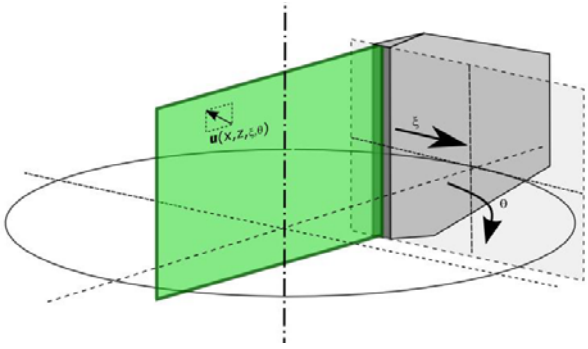

Figure 1: Ultrasound transducer array motion sequence. The transducer is rotated to an angle θ and translated along the ξ axis. For each position (θ,ξ) of the array, the 2D displacement field u(x,z) in the associated image plane is acquired.

Reference:

[1] J. Bercoff, M. Tanter, L. Sandrin, M. Fink, "Ultrafast compound imaging for 2D motion vector estimation: Application to transient elastography", IEEE Trans. Ultraso., Ferroelc, Freq. Contr. 49 (10), pp. 1363–1374, 2002.

066 **NON–INVASIVE VASCULAR ULTRASOUND ELASTOGRAPHY OF CAROTID ARTERIES: AN UPDATE ON A PHASE 1 CLINICAL STUDY.**

G Cloutier[1], RL Maurice[1], C Schmitt[1], MF Giroux[2], G Soulez[2].*
[1]Laboratory of Biorheology and Medical Ultrasonics, University of Montréal Hospital Research Center, Montréal, Quebec, CANADA; [2]Radiology Department, University of Montréal Hospital, Montréal, Quebec, CANADA.

Background: Only a minority of patients with carotid artery diseases will experience warning symptoms since the majority of strokes are caused by previously asymptomatic lesions. Since morbidity and mortality after acute strokes are unacceptably high, patients should be diagnosed and treated before they develop any symptoms.

Methods: Recently, a new method was developed to non–invasively assess vascular elasticity maps (NIVE, Non–Invasive Vascular Elastography) [1]. The method relies on the Lagrangian Speckle Model Estimator (LSME), which is a 2D algorithm providing all components of the deformation matrix. Radio-frequency (RF) ultrasound signals (Sonix RP, Ultrasonix, Vancouver, Canada) were recorded with a linear array transducer (L14-5/38) at a frame rate of 19 images/s in age–matched normal subjects and patients with severe carotid artery diseases (phase 1 clinical study). Cross–sectional and longitudinal images of carotids were acquired. Each image was divided into overlapping small windows and the LSME was applied to each window to obtain elastograms of the axial strain and axial shear strain.

Results: Reproducible elastograms were obtained as a function of time within a cardiac cycle and between cycles. Stress–strain modulus 2D distributions were computed for the group of normal subjects. Segmentation of plaque regions with different mechanical properties was possible. Elasticity distributions of healthy carotid walls were in agreement with the literature (cumulative strains below 5%). For patients with heterogeneous plaques, the axial strains were variable and shear values as high as 25% were detected at the interfaces of hard plaques and more compliant vascular tissues. Figure 1 shows typical axial strain and axial shear elastograms of a patient with a calcified plaque (Figure reproduced from [2]).

Conclusion: The feasibility of this new ultrasound imaging method is currently under evaluation. The Lagrangian speckle model algorithm, which provides axial and lateral strains, and axial and lateral shear estimations, may prove to be a unique approach for stroke prevention.

Acknowledgements: This work was supported by a VRQ–Univalor research grant and by a grant of the Canadian Institutes of Health Research (#PPP–78763). Dr Cloutier is recipient of a National Scientist award, Dr. Maurice of a Research Scholarship award, and Dr. Soulez of a Clinical Scholarship award of the Fonds de la Recherche en Santé du Québec.

References:

[1] Maurice R.L., Ohayon J., Frétigny Y., Bertrand M., Soulez G., Cloutier G., Non–invasive vascular elastography: Theoretical framework, *IEEE Trans. Med. Imag.*, 23 (2): 164–180, 2004.
[2] Schmitt C., Soulez G., Maurice R.L., Giroux M.F., Cloutier G., Non–invasive vascular elastography (NIVE): Toward a complementary characterization tool of atherosclerosis in carotid arteries, *Ultrasound Med. Biol.*, submitted, 2006.

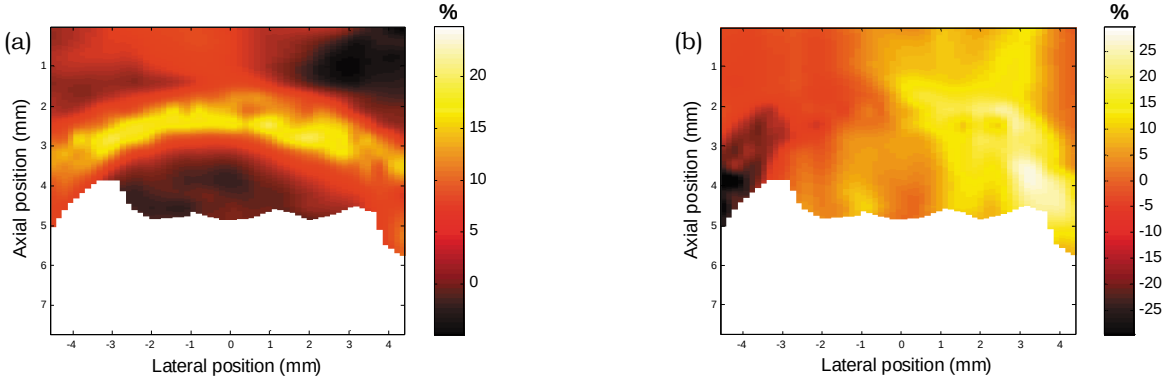

Figure 1: Cumulated axial strain (a) and axial shear (b) averaged on 7 consecutive cardiac cycles and estimated from RF sequences acquired from the proximal left internal carotid at the maximal stenosis position. The color scale gives the strain and shear in percent. The lumen is segmented in white.

* *indicates Presenter*

037 **STRAIN ESTIMATION OF ARTERIAL WALL WITH GLOBAL MOTION TRACKING: A PHANTOM STUDY.**

Hideyuki Hasegawa[1] and Hiroshi Kanai[1].*
[1]Graduate School of Engineering, Tohoku University, Aramaki–aza–Aoba 6–6–05, Sendai 980-8579, Miyagi, JAPAN.

Background: Pathological change of the arterial wall leads to significant change in elasticity [1]. We have been studying the measurement of elasticity of the arterial wall with ultrasound. The *phase tracking method* [2], previously developed by our group, estimates the displacement distribution of the arterial wall using the phase shift of echoes to obtain strain and elasticity. In this method, a high frame rate (200-300 Hz) is used to prevent aliasing. However, aliasing is mainly caused by large global motion of the arterial wall and, thus, the phase shift due to strain between successive frames becomes minute. Echoes from the arterial wall are composed of echoes from the lumen/intima and media/adventitia interfaces and from scatterers inside the wall. Although the phase shift between successive frames is minute, the *phase tracking method* accurately estimates the difference between the displacements of these interfaces (strain of the entire wall) because the echoes from these interfaces are stable against the pulsitility of the heartbeat. However, it is difficult to accurately estimate the strain inside the wall because echoes from scatterers are less stable in comparison with those from interfaces.

Aims: The phase shift of echoes between successive frames caused by strain is small, and the echoes from scatterers inside the wall fluctuate more easily by the pulsitility of the heartbeat. Therefore, to increase the phase shift of echoes due to strain, the phase shift of echoes is estimated by correlating the frame at the R–wave of electrocardiogram (before deformation) with that at the maximum strain. The time when the strain becomes the maximum is determined by the displacement waveform of the lumen/intima interface which is estimated by the *phase tracking method* based on the stable echo from the lumen/intima interface. Furthermore, before correlating the frames at the R–wave and at the maximum strain, the global translational motion is compensated using the displacement of the lumen/intima interface obtained by the *phase tracking method*.

Methods: A homogeneous cylindrical phantom (external and internal diameters: 8 and 10 mm) containing 5% carbon powder was measured with 10 MHz linear ultrasound probe. The scan plane was parallel to the axis of the phantom, and the directions of all ultrasonic beams coincided with the radial direction of the phantom. The change in internal pressure, which was applied using a flow pump, was measured by a pressure sensor.

Results: Figure 1(a) shows the strain distribution along the radial direction of the phantom obtained by the *phase tracking method*. To obtain the maximum strain by this method, the phase shift of each succeeding two frames was accumulated. Plots and vertical bars show means and the standard deviations for 46 ultrasonic beams. In Figure 1(a), mean values tended to follow the theoretical value, however, large variances were found. Figure 1(b) shows the strain distribution obtained by the proposed method. Variances in the estimated strain distributions were greatly reduced, and mean values were in good agreement with the theoretical values.

Conclusions: Strain estimates were greatly improved by correlating the frame before deformation with that at the maximum deformation with global translational motion compensation. The proposed method was considered to be more suitable for estimating the small strain of the arterial wall in comparison with the method in which the minute phase shift between successive frames is used for the strain estimation.

References:

[1] R. T. Lee, A. J. Grodzinsky, E. H. Frank, *et al.*, *Circulation*, 83, 1764-1770, 1991.
[2] H. Kanai, M. Sato, N. Chubachi, *et al.*, *IEEE Trans. Ultrason. Ferroelect. Freq. Contr.*, 43, 791-810, 1996.

Figure 1:
Radial Strain distributions of the cylindrical phantom obtained by
(a) the *phase tracking method* and
(b) the proposed method.

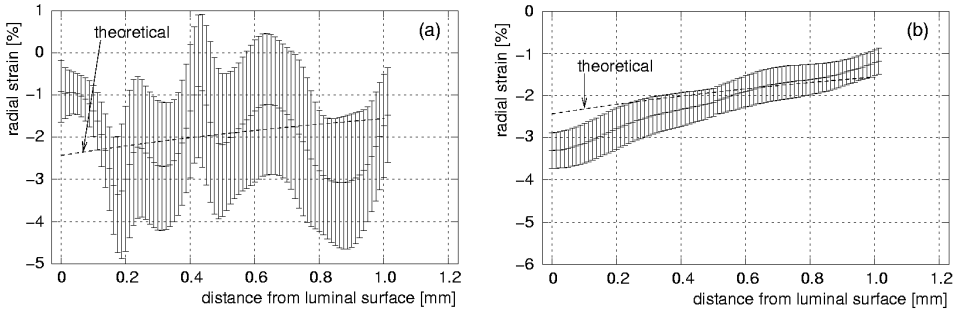

(a) The *Phase Tracking Method* (b) The Proposed Method

110 **GAINING NEW INSIGHTS ON THE RELATIONSHIP BETWEEN STRUCTURE, PROPERTY AND FUNCTION IN THE DIABETIC HEART USING ELASTOGRAPHY IMAGING.**

M Bilgen[1,2], J Gauch[3], R Loganathan[4], T Alrefae[5], E Popel[3], MD Alenezy[5], I V Smirnova[4].*
[1]Hoglund Brain Imaging Center, [2]Molecular and Integrative Physiology, [4]Physical Therapy & Rehabilitation Science, The University of Kansas Medical Center, Kansas City, KS, USA; [3]Electrical Engineering and Computer Science and [5]Physics Departments, Kansas University, Lawrence, KS, USA.

Background: The diabetic heart is targeted by both coronary and non–coronary pathology that eventually result in cardiac failure [1]. The failure to maintain tissue glucose homeostasis compromises cardiac structure and function in humans and experimental animal models of diabetes mellitus. The myocardial damage due to chronic hyperglycemia is a key property of the diabetic cardiomyopathy (DCM) and occurs as a result of abnormal metabolic and cell signaling pathways. In addition to myocardial damage, DCM is manifested by deposition of interstitial collagen in the myocardial tissue. These pathological features compromise the normal contractility and compliance of the diabetic myocardial tissue [2,3]. Elastography imaging offers new opportunities to gain new insights on the relationship between structure, property and function of diabetic heart.

Aims: This presentation aims to demonstrate the utility of elastography imaging to assess the impaired relaxation and contraction and wall motion abnormalities in the heart of an experimental diabetic rat model.

Methods: All procedures on animals were approved by the University of Kansas Medical Center Institutional Animal Care and Use Committee. Male Sprague–Dawley rats, aged 2 months, with an initial mean body mass of 250 g were made diabetic using a single intraperitoneal injection of streptozotocin. Diabetes was confirmed by measuring the non–fasting plasma glucose level ($\geq$ 300 mg/dl) two days following the injection.

At the end of 9 weeks of diabetes, the rats were anesthetized using 1.5% isofluorane in a mixture of air and oxygen (60% and 40% respectively). Cardiac magnetic resonance imaging (MRI) was performed using a 9.4 T horizontal bore scanner (Varian Inc., Palo Alto, CA, USA) and 60 mm radio frequency volume coil. EKG gated gradient echo based tagged–cine images were captured from short and long axis views of the heart. The cardiac cycle was temporally resolved into 10 equally incremented phases. The following settings were used for image acquisition: TR/TE = 25/2.44 ms, number of averages = 1, field of view = 60 x 60 mm, image matrix = 256 x 256, slice thickness = 2.0 mm, and width=0.3 mm and separation = 0.8 mm for the square grid tag lines.

Results: Figure 1 shows tagged images acquired during systolic phase of the cardiac cycle from a rat heart in short and long axis views. Using such images, the cardiac output can be quantified from the spatial motion occurring in the left ventricular wall and the degree of myocardial deformation can be computed in each square grid placed in the wall. Our current efforts are focused on developing computational algorithms based on optical flow, harmonic phase and watershed approaches to accurately quantify the motion and map the deformation profile as an indicator of local tissue stiffness.

Conclusions: Altered tissue structure from abnormal accumulation of interstitial collagen in diabetes leads to changes in the biomechanical properties of the myocardium, which ultimately results in compromised function. Quantitative measurements on the myocardial deformation may serve as an important bio–imaging marker reflecting the state of the cardiac tissue and a viable indicator for inspecting the condition of the diabetic heart.

References:
[1] Fisher M. *Heart* 90:336–340, 2004.
[2] Loganathan R et al. Int. J. of Cardiovascular Imaging. Int. Journal of Cardiovascular Imaging. 22:81–90, 2006.
[3] Loganathan R et al. Cardiovasc Diabetol. Online. 5:7, 2006.

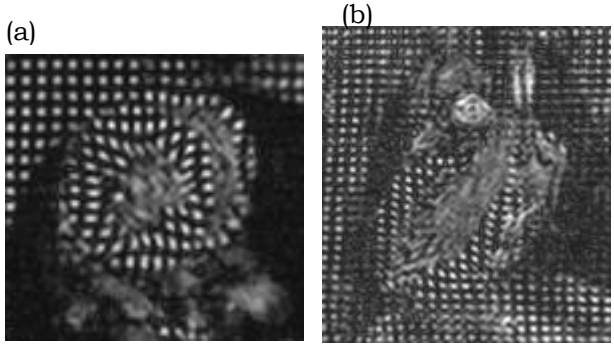

Figure 1: Tagged cine images showing the snapshot of rat heart in short (a) and long (b) axis views.

* *indicates Presenter*

046 **MECHANICAL VISCOELASTIC VARIATIONS OF *IN VIVO* CAROTID ATHEROMAS USING EXTERNAL ULTRASOUND.**

M McCormick[1], H Shi[1], C Mitchell[1], MA Kliewer[1], R. Dempsey[1], T Varghese[1].*
[1]University of Wisconsin–Madison, 1530 MSC, 1300 University Avenue, Madison, WI, USA.

Background: The majority of strokes are believed to be caused by the rupture of atherosclerotic plaques in the carotid arteries [1], thereby introducing emboli that occlude vessels in the brain. Methods to assess the vulnerability of carotid plaques to rupture are desirable for determining patient stroke risk and to decide on appropriate treatment options. Radial displacements and strains in the arterial wall have been utilized to measure vessel wall characteristics using measurements of pulse wave velocity [2] and diameter changes of the vessel wall [3]. However, the lateral displacements and shear strains in the vessel wall have not been carefully studied [4].

Aims: Tissue deformation in the vessel and plaque occurs due to the variations in blood pressure during the cardiac cycle. These deformations are visualized using diagnostic ultrasound. Our aim is to quantify radial strains in plaques and shear strains using external diagnostic ultrasound imaging techniques.

Methods: *In vivo* radiofrequency (RF) ultrasound data were collected from 12 subjects with atherosclerotic plaques using a commercial Siemens Antares clinical ultrasound scanner with an ultrasound research interface. RF data in a 3.8 cm x 3 cm region was acquired using a VFX 13–5 linear array transducer with a transmit waveform centered at 11 MHz at a frame rate of 30 frames/sec. Two measurements were evaluated. In the first case, two plaque regions of interest, (ROI) 0.4 mm x 1.5 mm, adjacent in the radial direction, and neighboring the lumen were selected. The inter–frame radial displacement of these regions was tracked with 2D cross correlation methods. Radial strain and plaque shear deformation was defined similar to that discussed in references [4, 5].

Results: Radial plaque strain was found to vary greatly across subjects and at different locations along the plaque. Generally, plaque that experienced large strains corresponded to a B–mode presentation consistent with soft plaques. However, low strain was observed with calcified plaques and soft plaques closer to the vessel wall. Shear strains were successfully quantified and large values of shear were observed.

Conclusions: Radial strains in plaque may be not only a function of plaque modulus, but also of plaque morphology, pressure waveform, and modulus properties of the surrounding tissues. Plaque shear occurs during the cardiac cycle and can be quantified. The amount of shear likely depends on the plaque modulus, the degree of protrusion into the lumen, and the pressure waveform.

References:

[1] Landwehr P, Schulte O, Voshage G. Ultrasound examination of carotid and vertebral arteries. *European Radiology.* 2001;11:1521–1534.
[2] Nagai Y, Fleg JL, et al., Carotid arterial stiffness as a surrogate for aortic stiffness: relationship between carotid artery pressure–strain elastic modulus and aortic pulse wave velocity, Ultrasound Med Biol. 1999, 25(2):181–188.
[3] Meinders JM, Hoeks AP, Simultaneous assessment of diameter and pressure waveforms in the carotid artery, Ultrasound Med Biol. 2004, 30(2):147–154.
[4] Cinthio M, Ahlgren AR, Bergkvist J, Jansson T, Persson HW, Lindstrom K. Longitudinal movements and resulting shear strain of the arterial wall. *American Journal of Physiology–Heart and Circulatory Physiology*. 2006;291:H394–H402.
[5] Holzapfel GA, Sommer G, Gasser CT, Regitnig P. Determination of layer–specific mechanical properties of human coronary arteries with nonatherosclerotic intimal thickening and related constitutive modeling. *American Journal of Physiology-Heart and Circulatory Physiology*. 2005;289:H2048–H2058.

035 **LOCAL UNDISTENDED ARTERIAL ELASTIC MODULUS RECONSTRUCTION USING *IN VIVO* STRAIN IMAGING AND PULSE WAVE VELOCITY.**

K. Kim[1], W.F. Weitzel[2], C. Jia[1], J.M. Rubin[3], T.J. Kolias[2] and M. O'Donnell[1].*
[1]Biomedical Engineering, [2]Internal Medicine and [3]Radiology Departments, University of Michigan, Ann Arbor, MI 48109, USA.

Background: Arterial compliance has been shown to be a strong indicator of vascular disease, cardiovascular disease and peripheral vascular occlusive disease [1]. Stiffening of the arterial wall results in lowering strain and increasing Pulse Wave Velocity (PWV) [2].

Aims: To fully characterize arterial elasticity over a large dynamic range, we applied a pressure equalization technique to compensate for the mean arterial pressure and enable reconstruction of the un-distended arterial elastic modulus reconstruction *in vivo*. Local un–distended arterial elastic modulus reconstruction can identify subtle arterial elasticity change.

Methods: Local PWV was taken using the same commercial ultrasound probe used for the strain measurement but at very high frame rates (up to 500 fps). For both strain and PWV measurements, an ultrasound correlation–based, phase–sensitive, speckle–tracking algorithm was employed. A simple model, assuming negligible effects by surrounding tissue, relates elastic modulus, E, of the artery wall to pulse pressure (Δp) and inter–cardiac strain ($\Delta\varepsilon$) by $E=[\Delta p/\Delta\varepsilon]$ where K contains geometric factors [3]. The Moens–Kotewerg equation for a tethered elastic tube was used for PWV. In both cases, artery geometrical factors, including inner and outer radius, need to be determined. Arterial inner radius can be measured from B–scan and correlation maps at relatively high accuracy. Combining these two equations leads to a single equation for the ratio of outer to inner radii (b/a):

$$(\frac{\Delta p}{\Delta \varepsilon})\frac{(\frac{b}{a})^2}{[(\frac{b}{a})+1]^3}=(\frac{\rho}{4})PWV^2$$

assuming incompressibility. Only one positive and real solution greater than unity is taken. To validate the technique using a commercial ultrasound probe, longitudinal and transverse scans were performed on an artery phantom connected to a pulsatile pump. To assess clinical feasibility, an *in vivo* free–hand ultrasound scanning procedure was performed, with IRB approval, on a recruited subject with an artery-vein bypass at the anastomosis of the local vein graft. Transverse and longitudinal scanning was performed on the vein side of the anastomosis while compressing to a pressure equaling diastolic pressure.

Results: The internal pulse pressure was measured at 138 mmHg. The intramural strain was 19%, and PWV was estimated to be 8.3 m/s. The inner radius of the phantom was 4.62 mm, and the density was 861 Kg/m^3. Using the equation above, the outer radius was determined to be 7.95 mm with 2% error. The reconstructed elastic modulus from these two independent measurements was 120 kPa compared to the direct mechanical measurement of 139 kPa. The reconstruction technique was validated within 15% error. For the human subject, the pulse pressure (120/76 mmHg) induced intramural strain was 15%, and PWV was 4.3 m/s under physiologic pressure and after pressure equalization the strain increased to 65% and PWV decreased to 1.7 m/s. Elastic moduli with and without compression were fit to a pure exponential function describing the nonlinear elasticity of the arterial wall. The exponent (slope of log-liner fit) was 3.1 and the un–distended vein elastic modulus was estimated to be 7.2 kPa.

Conclusions: With only two measurement points at different intraluminal pressures (i.e., strain preloads), the elastic property of the blood vessel was fully characterized demonstrating the feasibility of determining the un–distended elastic modulus *in vivo*.

Acknowledgements: Work supported in part by NIH grants HL-67647, HL-68658 and a grant from the Renal Research Institute.

References:

[1] Blacher J, Pannier B, Guerin A *et al.* Carotidarterial stiffness as a predictor of cardiovascular and all–cause mortality in end–stage renal disease. Hypertension 1998;32:570–574.
[2] Eriksson A, Greiff E, Loupas T, Persson M, Pesque P. Arterial pulse wave velocity with tissue Doppler imaging. Ultrasound in Med. & Biol. 2002; vol.28: No.5 :571–580.
[3] Kang Kim, W.F. Weitzel, J.M. Rubin, Hua Xie, Xunchang Chen, M. O'Donnell, Vascular Intramural Strain Imaging Using Arterial Pressure Equalization, Ultrasound in Med. & Biol. 30(6):761–771, 2004.

* *indicates Presenter*

114 **INVESTIGATION OF LOCALLY CONSTANT ASSUMPTION FOR INVERSE PROBLEM IN ELASTOGRAPHY.**

Kui Lin[1], Joyce R. McLaughlin[1].*
[1]Rensselaer Polytechnic Institute, Troy, NY, USA.

Background: In current elasticity studies, it is common to start from the general elastic equation in isotropic, homogeneous media. Full three–dimensional displacement measurements are needed to recover shear modulus from the general equation. By assuming incompressibility of the tissue or phantom and neglecting pressure, an acoustic wave equation can be derived for the forward problem model which effectively decouples the three components of displacement. When using this mathematical model for the inverse problem to recover shear modulus, the locally constant assumption is widely accepted; this assumption eliminates the terms containing the first derivatives of the shear modulus. The inverse problem method associated with this assumption is called the direct inversion. Alternatively, the first derivative terms of shear modulus which are contained in the original mathematical model, can be included when solving the inverse problem. In this case, the inverse problem method involves the solution of a first order partial differential equation, which we will call the full inversion method.

Aims: Our target is to investigate the relative difference of shear modulus recoveries from the direct inversion and the full inversion methods. We aim to establish an upper bound for the relative difference and to demonstrate when the full inversion method can provide more accurate reconstructions.

Methods: We used analytical methods to establish the bound and finite difference based numerical methods for both the direct and full inversion algorithms. We used variance controlled methods to differentiate the data in both algorithms and first order p.d.e. numerical schemes to reconstruct the elastic modulus for the full inversion method.

Results: We derived an error bound for the relative difference between the shear modulus reconstruction from the full and direct inversion methods, and showed examples exhibiting the differences between the recoveries from the full and direct inversion methods.

Conclusions: With good quality data, the full inversion method can provide more accurate solutions to the inverse problem particularly in the regions surrounding inclusions.

Acknowledgements: We acknowledge NIH and NSF for partial support of this work. This work was performed at IPRPI, the Inverse Problem Center at Rensselaer Polytechnic Institute.

References:

[1] David Gilbarg and Neil S. Trudinger. “Elliptic Partial Differential Equations of Second Order”. Springer, 3rd edition, 1997.
[2] Robert S. Anderssen and Markus Hegland. “For Numerical Differentiation, Dimensionality can be a blessing”. Mathematics of Computation, Volume 68, Number 227, Pages 1121–1141, 1999.
[3] Joyce R. McLaughlin, Daniel Renzi, Jeong–Rock Yoon, R. L. Ehman and A. Manducca, "Variance Controlled Shear Stiffness Images for MRE Data", IEEE International Symposium on Biomedical Imaging: Macro to Nano, 2006, pp. 960–963.

119 **MODEL–BASED VISCOELASTIC TISSUE CHARACTERIZATION FROM HIGH FREQUENCY ULTRASOUND MEASUREMENTS.**

B.B. Guzina[1], E. Ebbini[2], K. Tuleubekov[1], D. Liu[2].*

[1]Civil Engineering, University of Minnesota, 500 Pillsbury Dr SE, Minneapolis, MN 55455, USA; [2]Electrical & Computer Engineering, University of Minnesota, 200 Union St SE, Minneapolis, MN 55455, USA.

Background: One of the key prerequisites in quantitative ultrasound (US) imaging of cancerous lesions is a proper account for the mechanical properties of healthy (i.e. background) tissue [1]. Despite the highly complex nature of the underlying cellular structure, there is mounting evidence [2,3] that the transient tissue response to e.g. US excitation can be reasonably approximated using theory of viscoelasticity. Notwithstanding the significant advances made to date [e.g. 4–7], a reliable estimation of the viscoelastic tissue properties from (either *in–vitro* or *in–vivo*) US and other modalities remains an open research question.

Aims: Focused primarily on skin imaging applications, this study aims to develop a rigorous inverse solution for the viscoelastic characterization of subcutaneous tissues from high-frequency US measurements. With the use of a suitable visco–elastodynamic model that effectively (1) simulates the acoustic radiation force (ARF) and (2) accounts for the presence of proximate material interfaces (e.g. the skin surface or an underlying bone), the proposed methodology has potential applications to both laboratory (*in–vitro*) and *in–vivo* applications. Performance of the model is examined using HFUS experiments on tissue–mimicking (4 and 11mm thick) phantom specimens.

Methods: By means of an exact 3D wave propagation model [8] for a layered viscoelastic solid (Figure 1b), a rational analytical and computational framework is developed for the US characterization of lossy tissues. For generality the solution is established in terms of the fractional Zener model [9], a causal generalization of the standard linear solid (Figure 1a). To cater for realistic applications, the problem is formulated in a Bayesian setting for the US testing configurations involving a highly-focused radiation force and tissue motion estimates collected along the A–line that is coaxial with transducer axis (Figure 1c). For a rigorous treatment of the gradient search technique employed by the inverse solution, necessary sensitivities of the predictive model (with respect to viscoelastic tissue parameters) are evaluated analytically.

Results: Through numerical simulations, it was shown that a proper account for proximate material interfaces, e.g. skin surface (in terms of the layered model) was essential for the success of the inverse solution. Validity of the layered viscoelastic model and tissue characterization methodology was examined by comparison with HFUS measurements (Figure1c) performed on 4mm thick phantom samples (Figure 1d).

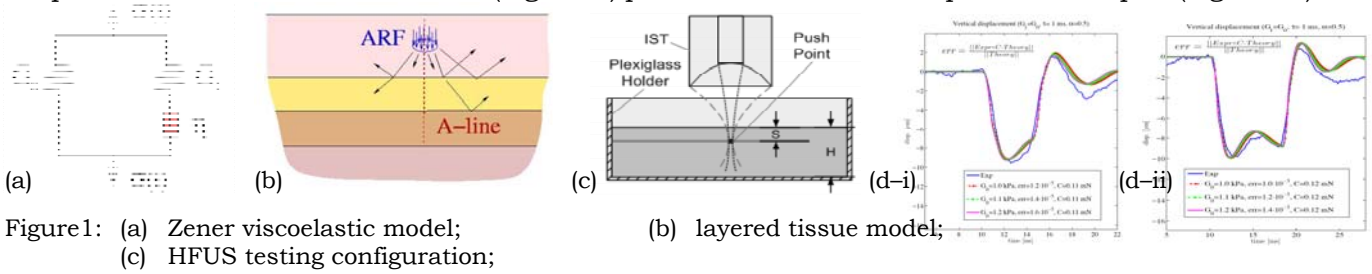

(a) (b) (c) (d–i) (d–ii)

Figure1: (a) Zener viscoelastic model; (b) layered tissue model;
(c) HFUS testing configuration;
(d) experiment versus layered viscoelastic theory – transient particle motion @ 1.1mm depth in the H=4 mm phantom: 4 ms (d–i) and 8 ms (d–ii) square ARF pulse.

Conclusions: Through a systematic computational and experimental study, it is shown (1) that a layered viscoelastic model provides an effective tool for simulating the transient response of subcutaneous tissues to HFUS excitation, and (2) that an "on–line" characterization of tissue viscoelasticity may be possible in the context of HFUS testing configurations such as those illustrated in Figure 1c.

References:

[1] MS Richards, AJ Moskowitz, AL Lerner, DJ Rubens, KJ Parker (2002) *Proc. IEEE Ultrasonic Symp.,* 2, 1639–42.
[2] AV Kobelev RM Kobeleva, YL Protstenko, V Berman, OA Kobelev (2005), *Proc. Mater. Res. Soc. Symp.,* 874, 9–14.
[3] A Oza, R Vanderby Jr, RS Lakes (2006) *Int. J. Mech. Sci.*, 48, 662–73.
[4] LS Taylor, AL Lerner, DJ Rubens, KJ Parker (2002) *ASME BED Publication,* 54, *Advances in Bioenginering*, 447–8.
[5] N Nitta, T Shiina, E Ueno (2002) *Proc IEEE Ultrasonic Symp.*, 2, 1885–89.
[6] MZ Kiss, T Varghese, TJ Hall (2004) *Phys. Med. Biol.*, 49, 4207–18.
[7] D Valtorta, E. Mazza (2005), *Medical Image Analysis*, 9, 481–90.
[8] BB Guzina and RYS Pak (2001) *Quart. J. Mech. Appl. Math.*, 54, 13–37.
[9] T Pritz (1999) *J. Sound Vibration*, 228, 1145–1165.

* *indicates Presenter*

012 **COMPARISON OF MULTIDIMENSIONAL SHEAR MODULUS RECONSTRUCTION METHODS THROUGH SIMULATIONS AND PHANTOM EXPERIMENTS.**

Chikayoshi Sumi[1], Daisuke Kikuchi[1], Yuuichi Shimada[1] and Shouta Nojiri[1].*
[1]Sophia University, 7-1, Kioicho, Chiyodaku, Tokyo, JAPAN.

Background: As a differential diagnosis technique for living soft tissues, we are developing ultrasonic-strain–measurement–based shear modulus reconstruction methods. Previously, we reported three–dimensional (3D) and 2D reconstruction methods utilizing a typical Poisson's ratio very close to 0.5 (nearly incompressible) [1,2]. However, because a decrease in the accuracy of reconstructed value was confirmed to be due to the difference between the original value and the set value, we proposed 3D and 2D methods of reconstructing Poisson's ratio as well. Furthermore, we proposed methods of reconstructing density and dealing with dynamic deformation. However, due to tissue incompressibility, the reconstructions of shear modulus, Poisson's ratio, and density became unstable. Last year [3], to obtain stable, unique reconstructions, we reported a new reconstruction method using mean normal stress approximated by the product of one of Lame's constants λ and volume strain as an unknown [4]. This method also enables stable, unique reconstructions of shear modulus and density under the condition that the mean normal stress remains unknown. A 2D phantom experimental result obtained by the new method was already presented [3].

Aims: In this report, the reconstruction accuracies (reconstruction values and spatial resolutions) and computation times of the methods are compared through simulations and phantom experiments.

Methods: To improve reconstruction speed (i.e., convergence speed of the conjugate gradient method), when the orders of the magnitudes of the coefficients multiplied by shear modulus, density and Poisson's ratio markedly differ from each other, a constant is multiplied by the respective coefficients such that the orders become the same (i.e., eigenvalues of matrix are regulated). (1) *Simulations:* The phantom includes a spherical inclusion having a different shear modulus and Poisson's ratio form those of the surrounding region. (2) *Phantom Experiments:* An agar phantom having an inclusion of a different shear modulus was used. 2D reconstructions were performed using the new method and previous method. The 2D strain tensor is obtained by differentiating the 2D displacement vector data measured using our developed multidimensional autocorrelation method (MAM). Specifically, here lateral modulation is not performed. Instead, the regularization is only implemented on the lateral displacement to stably obtain the data. The 3D reconstruction was also performed.

Results: Compared with the previously developed reconstruction method of shear modulus utilizing a typical Poisson's ratio [1,2], the new method realizes real–time reconstructions of the shear modulus together with the Poisson's ratio and density, although the new method requires a slightly more time to complete the reconstructions. (1) *Simulations:* We showed artifacts of the new method due to the low dimensionality (i.e., 2D) of the reconstructions [3], whereas those of the previous methods due to inhomogeneity of Poisson's ratio (Inclusions having higher or lower shear moduli and respectively higher and lower Poisson's ratios than the surrounding regions, the high shear moduli were estimated to be lower and higher than the original values and vice versa). Occasionally, the shear elasticity is reversely estimated (high or low). (2) *Phantom Experiments:* Figure 1 shows the reconstructions obtained using (a) the new method (remaining mean normal stress as a unknown) and the previous method using (b) a 2D stress condition and (c) 2D strain condition. For 2D reconstruction when the Poisson's ratio is homogeneous, as shown in the simulations, the previous method using a 2D stress condition yielded more accurate reconstruction than the new method. Primary 3D reconstructions were also obtained.

Conclusions: The new method allows for dealing with arbitrary soft tissues (i.e., incompressible or compressible tissues, inhomogeneous Poisson's ratio). This new reconstruction method is considered to be particularly suitable to 3D reconstruction. However, as the most soft tissues are considered to be incompressible (i.e., an almost constant Poisson's ratio), the suitability of the new and previously developed methods must also be experimentally compared using living soft tissues. If the target tissue is homogeneously incompressible, the previous method using a 2D stress condition is also useful.

References:

[1] C. Sumi etal, IEEE Trans. on BME, vol. 42, no. 2, pp. 193–202, 1995.
[2] C. Sumi, IEEE Trans. on UFFC, vol. 52, no. 10, pp. 1670–1689, 2005.
[3] C. Sumi, Proc of IEEE International Ultrasonics Symposium (CD–ROM), pp. 1771–1776, September, 2005.
[4] C. Sumi, "Reconstructions of shear modulus, Poisson's ratio and density using approximate mean normal stress as unknown", IEEE Trans. on UFFC (in press).

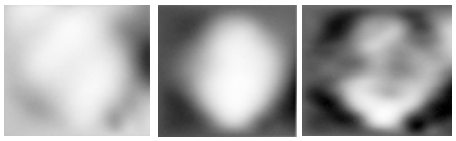

(a) (b) (c)
Figure 1: Agar phantom experiments.

097 **DOMAIN DECOMPOSITION OF THE ELASTICITY IMAGING PROBLEM: EXPERIENCE WITH A SUBZONE BASED MAGNETIC RESONANCE ELASTOGRAPHY APPROACH.**

EEW Van Houten[1], HU Berger[1], MD McGarry[1], MM Doyley[2], JB Weaver[3] and KD Paulsen[2].*
[1]University of Canterbury, Christchurch, NEW ZEALAND; [2]Thayer School of Engineering, Dartmouth College, Hanover, NH, USA; [3]Dartmouth–Hitchcock Medical Center, Lebanon, NH, USA.

Background: In general, the elasticity imaging problem is an ill–posed inverse problem whose quality of solution depends on factors such as the condition of the forward and inverse operator, the size of the parameter set being imaged and the regularity of the data within the imaging domain. Some of these factors are related to the fundamental nature of the model underpinning the inversion process while others are more dependent on aspects of the data itself (e.g. is motion quasi–static or harmonic, is the imaging region constrained or generally unconstrained, etc.). Many of these data specific aspects of the elasticity imaging problem can be controlled by modifying the local scope of the imaging domain. This is easily achieved in MR Elastography, where measured motion data is available throughout the imaging region. Here, we take advantage of this domain flexibility to examine reconstruction behavior across a variety of imaging factors.

Aims: We investigate the behavior of the elasticity imaging problem using a subzone based MR Elastography method [1]. This method decomposes the global imaging domain into "subzones" of variable size and proceeds with reconstruction at the local level. This allows the study of variation in the reconstruction process with respect to parameter size, relative wavelength, etc., without loss of parameter or motion resolution.

Methods: To explore the effects of these various reconstruction factors we made use of both simulated and measured data. Simulated data provided precise control over the imaging problem, while measured data ensured relevance to actual imaging conditions. Solutions were investigated for a variety of property contrasts, relative motion wavelengths, sizes of the parameter set, boundary conditions and proximities to resonant frequencies.

Results: We present new results showing that the stability of the reconstruction process is greatly affected by the effective constraint of the boundary conditions used, especially within the proximity to resonant frequencies. Additionally, the size of the parameter set for the resulting image has a strong effect on both solution time and accuracy. As the relative wavelength within the imaging domain decreases, the number of resonance points and local minima increase, making reconstruction particularly difficult in these conditions.

Conclusions: Just what the ideal data set to facilitate elasticity imaging would look like is an open question. The study presented here aims to help clarify some of the relationships between the data, the underlying property description and the elastic property reconstruction process that drive these problems. Control of the imaging domain allows further control of the factors which can work for or against a quality image. There are limits to what domain control alone can achieve, however, and further developments in the forward models and inverse methods may provide even better elasticity imaging results.

Reference:

[1] E.E.W. Van Houten, K.D. Paulsen, M.I. Miga, F.E. Kennedy and J.B. Weaver, "*An overlapping subzone technique for MR based elastic property reconstruction*", Magnetic Resonance in Medicine, 1999, 42(4), pp 779–786.

* *indicates Presenter*

045 **MEASUREMENTS OF ATTENUATION IN COPOLYMER–IN–OIL PHANTOMS USING TRANSIENT ELASTOGRAPHY.**

Cécile Bastard[1], Véronique Miette[1], Laurent Sandrin[1].*
[1]Echosens, Research and Development Department, 153 avenue d'Italie, 75013 Paris, FRANCE.

Background: The Fibroscan (Echosens, Paris, France) is a transient elastography based device used to quantify liver fibrosis by following the propagation of a low frequency shear wave. In its present state, the device only permits the measurement of the shear wave velocity. It would be interesting to adapt the existing device to enable the measurement of the shear wave attenuation since this would lead to an estimate of viscosity which may be a clinically relevant parameter for the assessment of fatty tissue in liver [1].

Aims: In the first stage, the aim was to develop a method to measure shear wave attenuation in new copolymer–in–oil phantoms using transient elastography in transmit mode [2].

Methods: The experimental setup is composed of a piston and an ultrasonic transducer placed on both sides of the phantom. The piston is used to generate a 50 Hz shear wave. The experiments were performed on three phantoms made with SEBS (Styrene–Ethylene/Butylene–Styrene) copolymer (4 %), silica (1% for acoustical scattering) and mineral oil of three different cinematic viscosities (35 mm^2/s, 87 mm^2/s and 220 mm^2/s at 20°C).

The first step of the developed method consists of experimentally measuring the strain rate induced in phantoms by a low–frequency shear wave, which allows the computation of the variation of the shear wave amplitude as a function of depth which includes both attenuation due to viscosity and geometrical attenuation due to diffraction effects.

In the second step, we simulate the strain rate by computing the theoretical response from a piston, using a non viscous model [3] and the experimentally measured shear wave velocity. The amplitude variation obtained in this second step is purely related to diffraction and can be used to compensate for the geometrical attenuation in the experimental data. It is therefore possible to measure the attenuation coefficient due to viscosity. Attenuation measurements were repeated 10 times in each of the three phantoms.

Results: Attenuation coefficients (standard deviation) were respectively 55.1 (0.5) Np/m, 60.9 (0.4) Np/m and 78.3 (3.1) Np/m in phantoms with low, medium and high viscosity.

Conclusions: Attenuation measurements are feasible with transient elastography in transmit mode. The method developed may be adapted to reflection mode in order to be used clinically.

References:

[1] EM. Brunt, Nonalcoholic steatohepatitis: pathologic features and differential diagnosis, Semin Diagn Pathol, Vol. 22, No.4, November 2005.
[2] L. Sandrin, M. Tanter, J. L. Gennisson, S. Catheline and M. Fink, Shear elasticity probe for soft tissues with 1–D transient elastography, IEEE Trans. on ultrasonics, ferroelectrics, and frequency control, Vol. 49, No.4, April 2002.
[3] L. Sandrin, D. Cassereau, M. Fink, The role of the coupling term in transient elastography, Journal of the Acoustical Society of America, Vol. 115, No. 1, January 2004.

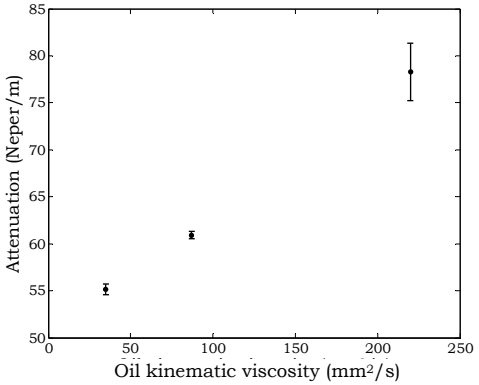

Figure 1: Attenuation measured in the three tested phantoms.

056 **SKIN ELASTOGRAPHY IN BREAST CANCER RELATED LYMPHOEDEMA PATIENTS UNDER SURFACE TENSILE LOADING.**

L. V. Coutts[1], J. C. Bamber[1], N. R. Miller[1], P Mortimer[1].*
[1]Institute of Cancer Research and Royal Marsden NHS Trust, Sutton, Surrey, England, UK.

Aims: Our aim was to evaluate the ability to use elastography to investigate the effects of surface tensile loading, of varying direction, on the normal and shear strain generated within skin and the underlying tissue layers in both the contralateral and ipsilateral arms of lymphoedema patients (n = 7) and in healthy volunteers (n = 5).

Background: The measurement of skin elasticity has the potential to play an important role in the clinical assessment of a range of skin conditions, including skin cancer, radiation fibrosis and lymphoedema, but many of these applications require highly local values of elastic properties to be measured. Existing methods, such as measuring strain while applying suction, torsion or a uniaxial load, provide only an overall value of skin stiffness on a scale no smaller than centimetres. Furthermore, these methods do not provide information about how the strain propagates to underlying tissue layers.

Methods: Elastograms were produced using two different imaging modalities, ultrasound and optical imaging. In both cases, an Extensometer (Cardiff Biometrics, UK) was used to apply a pseudo–static linear tensile strain to the surface of the forearm. This device also measured the load and the surface strain. For the ultrasound study, a sequence of RF images was acquired using a Zonare Ultrasound Scanner at 8.5 MHz while applying a 20% strain. Incremental tracking was used to form lateral displacement images and least squares strain estimation produced normal and shear strain images. The optical method used an approach known as photometric stereo (University of West of England) to obtain images of the skin surface topography before and after the application of a 1.25% strain. The optical elastograms were formed as previously described [1]. For both imaging modalities, data were acquired in two different loading directions, along and across the arm, to investigate anisotropy.

Results: The Extensometer results showed that the pronounced anisotropy observed in healthy volunteers disappears in lymphoedema patients. In both healthy volunteers and the unaffected (contralateral) arm of lymphoedema patients, the relative stiffness (measured as the ratio of load to surface strain) was approximately twice as large along the arm as across the arm. However, in the affected (ipsilateral) arm of lymphoedema patients, this ratio was 0.90 +/-0.27 (1 SD).

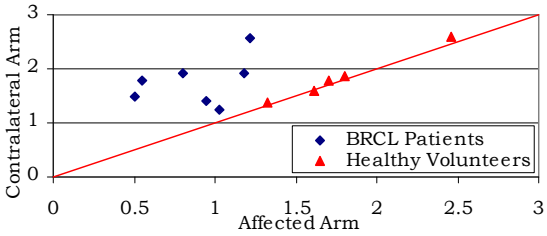

Figure 1: Skin stiffness anisotropy, defined as the ratio of stiffness in the stiffest direction to that in the softest direction, in contralateral and ipsilateral arms of breast cancer related lymphedema (BCRL) patients and healthy volunteers.

Ultrasound elastography showed that, in all subjects, despite the use of surface tensile loads, the strain propagated down into the subcutis. Furthermore, lymphoedema was found to increase the amount of strain propagated into the muscle layer. The ratio of the strain in the muscle to the strain in the subcutis was twice as large for the ipsilateral arm of lymphoedema patients as for both the patients' contralateral arms and for the healthy volunteers. Optical elastograms of the skin surface showed that the standard deviation on the mean surface strain was three times larger for the contralateral arm than for the ipsilateral arm.

Conclusions: These preliminary results show that lymphoedema affects the mechanical properties of skin and the underlying tissue layers in ways that can be measured using all three techniques (Extensometer, ultrasound elastography and optical elastography). Further work is required to determine the precise role and value of each technique in diagnosing and assessing lymphoedema.

Acknowledgements: This work is supported by funding from the EPSRC.

Reference:

[1] Coutts, L.V., Bamber, J.C., Miller, N.R., Feasibility of Skin Surface Elastography by Tracking Surface Topography, Proc. of The Third International Conference on the Ultrasonic Measurement and Imaging of Tissue Elasticity, Lake Windermere, UK, p 112, 17–20 October 2004.

* *indicates Presenter*

073 **ASSESSMENT OF MECHANICAL PROPERTIES AND GEOMETRICAL FEATURES OF THE PROSTATE BY A MECHANICAL IMAGING DEVICE.**

Vladimir Egorov[1], Suren Airapetian[1] and Armen Sarvazyan[1].*
[1]Artann Laboratories, 1459 Lower Ferry Rd., Trenton, NJ 08618, USA.

Background: Mechanical Imaging (MI), which has been in development at Artann Laboratories for the last 10 years [1], has yielded a 3–D map of tissue elasticity. At the same time, MI closely mimics manual palpation since the MI transrectal probe with a pressure sensor array mounted on its tip acts in a manner similar to a human finger during prostate palpation, slightly compressing the prostate with the probe.

Aims: The objective of this study is the development and validation of the Prostate Mechanical Imager (PMI), a device for real time imaging of the prostate and assessment of prostate features such as size, shape, consistency/hardness, and nodularity.

Methods: The transrectal probe (1) is comprised of two separate pressure sensor arrays and orientation sensors as shown in Figure 1. The first pressure sensor array, with 128 sensors (Pressure Profile Systems, CA), is installed on the probe scanning surface (2) to make contact with the prostate through the rectal wall during the examination procedure. The second pressure sensor array is installed on the surface of the probe shaft (3) for assessment of the pressure pattern in the sphincter area. The probe's 3–D orientation system (4) is comprised of three–axis magnetic sensor and two-axis acceleration sensor. In real–time, the examiner sees two orthogonal prostate cross–sections (Figure 2A) showing the relative location of the probe's pressure sensitive area in both projections. The total prostate scan takes 40–60 seconds to create and the collected data are instantly saved in digital format along with the integrated 3–D prostate image (Figure 2B).

Results: Laboratory testing on prostate phantoms demonstrated that 5 successive compressions of the probe against the phantom are sufficient to provide a clear 3–D integrated image. Multiple (10–15) compressions provide size evaluation reproducibility within 6%, nodule size assessment had STD of about 8% and the integral prostate phantom hardness evaluation of less than 15%. An on–going clinical study revealed that in 83.9% of the cases, 141 of 168 patients, the PMI yielded sufficient data for quantitative assessment of the gland parameters. PMI produced nodule detection sensitivity of 79%, specificity of 62%, and positive predictive value of 33%. The area under the Receiver Operating Characteristic (ROC) curve for nodule detection was 81%.

Conclusions: PMI provides documented 3–D mechanical prostate images with quantitative evaluation of prostate features such as size, shape, hardness and nodularity. The results obtained on model systems and in an on–going clinical study have proven that PMI has potential to become a diagnostic tool that could largely supplant DRE through its higher sensitivity, quantitative record storage, ease–of–use and inherent low cost.

Acknowledgements: This work is supported by NIH grant 5 R44 CA082620. The authors would like to thank Robert E Weiss of the Urology Division, Robert Wood Johnson Medical School, NJ, USA, for the assistance in the clinical study.

Reference:

[1] A. Sarvazyan, "Mechanical Imaging: A new technology for medical diagnostics." Int. J. Med. Inf., 1998, vol. 49, pp. 195–216.

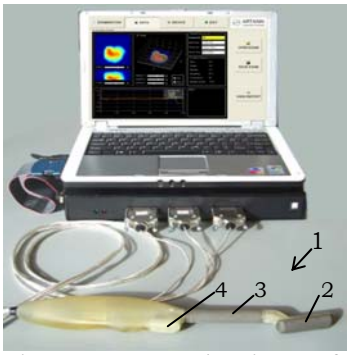

Figure 1: General view of PMI (see text)

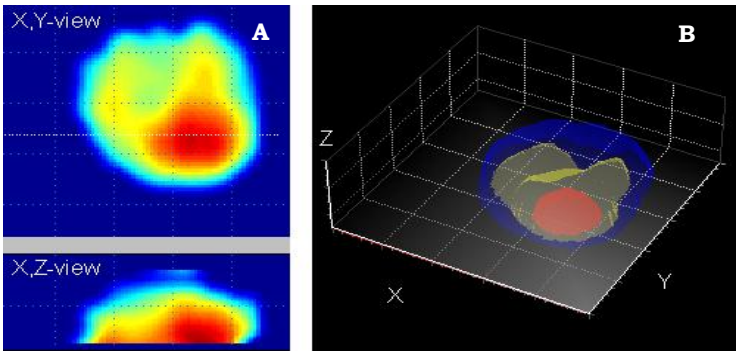

Figure 2: Prostate frontal and transversal cross–sections (A); 3–D integrated prostate image (B).

* *indicates Presenter*

080 **WAVE ATTENUATION AND POISSON'S RATIO IN DEFORMED MOUSE MAMMARY TUMOR.**

Hirohito Kobayashi[1]*, *Ray Vanderby*[1].
[1]Orthopedics & Rehabilitation Department, University of Wisconsin–Madison, Madison, WI, USA.

Aims: To evaluate the wave attenuation coefficient and Poisson's ratio in a compressed mammary tumor based on acousto–elasticity.

Background: Because wave attenuation is widely believed to be tissue specific [1,2], a significant number of ultrasound studies have been conducted on different tissues in their normal, non–deformed state. Elastography is a new ultrasound–based technique to evaluate tissue elasticity that has been developed over the past decade and a half which is gaining popularity as a modality for medical imaging. We proposed a similar technique based on the rigorous mathematical theory termed acousto–elasticity. Both techniques require echo measurements from a deformed state for elastic properties, but, to our knowledge, neither technique has previously evaluated wave attenuation properties in deformed tissues. In this study, we use acousto–elastic theory to evaluate the strain dependent tissue stiffness in compressed mouse mammary tumors. We then evaluated the wave attenuation properties of these tumors with the same measured wave echo data and with the assistance of the strain dependent stiffness (from our acousto–elastic technique). Finally, we evaluate Poisson's ratio $\nu(E)$ as a function of Green strain E in the deformed tumors by assuming the tissue tangential modulus $Ey(E)$ and tissue stiffness $C_{11}(E)$ are related by the following equation.

$$C_{11}(E) = \frac{1-\nu(E)}{(1-2\nu(E))(1+\nu(E))} Ey(E) \qquad \text{Equation 1}$$

Methods: Mammary tumor from a mouse was sandwiched between 4% agar slabs and mounted on a testing machine. The tumor was compressed from 0–20% of its original thickness in 2% increments. At each compression step, the applied force and ultrasound reflection echo were measured. First, the strain dependent stiffness was evaluated from the echo from the front interface based on acousto–elasticity. Using evaluated stiffness, the wave attenuation coefficient was evaluated with the echo from the back interface. Finally, the Poisson's ratio was evaluated as the ratio of stiffness and tangential modulus.

Results: For the mouse mammary tumor, both the wave attenuation coefficient and Poisson's ratio were found to be strain dependent and can be expressed by the following functions:

Wave attenuation coefficient: $a = 0.89(1.52E + 100.1E^2 - 283E^3)$ (Np/cm) Equation 2

Poisson's ratio: $\nu = \frac{1}{2} - \frac{672 + 17488E - 389904E^2 + 238216E^3}{12000022 - 5.819328E^6 - 11991256E^2 + 17987032E^3 + 59554E^4}$ Equation 3

Conclusions: The wave attenuation coefficient and Poisson's ratio were found to be strain dependent.

Acknowledgements: This work was supported by Wallace H. Coulter Foundation Translational Research Partnership Award.

Figure1: Test setup

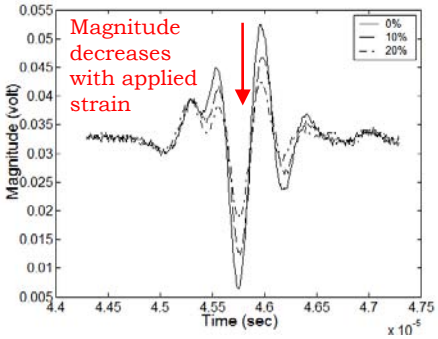

Figure 2: Echoes from the front interface
Echoes at 0%, 10% and 20% strain

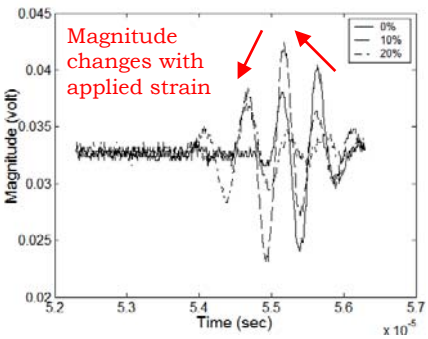

Figure 3: Echoes from back interface
0 – >10%: Echo Increased
10 – >20%: Echo Decreased

References:
[1] F. Dunn et al.,1969, "Biomedical Engineering", p. 303 McGraw–Hill.
[2] N. Akashi et al., 1995, J. Acoust.Soc. Am., Vol. 98, p. 3035–3039.

* *indicates Presenter*

109 **MEASUREMENT OF STIFFNESS OF ARTICULAR CARTILAGE BEFORE AND AFTER DEGENERATION USING WATER JET ULTRASOUND INDENTATION.**

M.H. Lu[1], Y.P. Zheng[1], C.H.Y. Ling[1].*
[1]The Hong Kong Polytechnic University, Hong Kong, CHINA.

Background: Articular cartilage is a biological weight–bearing tissue covering the bony ends of articulating joints. Subtle changes in structure or amount of its proteoglycans and collagen fibers can lead to the degeneration of cartilage and ultimately to loss of function. Osteoarthritis is one of the most frequent causes of physical disability among adults. However, it is still difficult to detect the early signs of osteoarthritis by existing X–ray, magnetic resonance imaging (MRI) and arthroscopy and assess the outcomes of various treatments. High frequency ultrasound has recently been demonstrated to be very suitable for the assessment of articular cartilage. Results have also shown that the combination of ultrasound parameters and elasticity can provide more comprehensive assessment for various cartilage defects. Earlier, we have developed a water jet ultrasound indentation technique [1], which has the potential to provide the simultaneous measurement of these parameters. It uses a water jet to deform the tissue and to provide a passage for focused high frequency ultrasound to reach the tissue to detect its thickness and deformation.

Aims: The aim of this study was to use water jet ultrasound indentation to measure the stiffness and ultrasound reflection ratio of articular cartilage specimens before and after the simulated degeneration caused by digestion by enzymes.

Methods: The ultrasound water indentation system was comprised of a focused high–frequency ultrasound transducer, a water beam ejector and a pressure sensor [1]. The water beam at a diameter of 1.9 mm served as a compressor as well as a medium for ultrasound propagation. The tissue deformation was estimated from the ultrasound echoes reflected from the tissue. Eight fresh mature bovine patellae without obvious lesions were obtained from the local slaughterhouse. They were first tested at 3 selected sites using the water jet indentation and conventional mechanical indentation. After that, simulated degeneration of articular cartilage was achieved by a trypsin digestion (0.25% trypsin solution, 4 hours, 37ºC) to remove the proteoglycan [2]. The degenerated articular cartilage specimens were then tested again using the water jet indentation and conventional mechanical indentation. The cartilage was first preloaded with a water pressure of 20 kPa for 3 seconds, and then it was indented with the pressure increasing to approximately 180 kPa within 1 second. The loading and unloading process repeated for 3 cycles at each measurement site. The ultrasound signals were continuously recorded during the whole process and used for off–line analysis to extract the stiffness and the ultrasound reflection ratio.

Results: Using the ultrasound water jet indentation system, a cartilage stiffness ratio of 433.0 ± 150.0 kPa was found for the intact samples and a stiffness ratio of 97.4 ± 29.3 kPa for the degenerated samples. Using the mechanical indentation system, a Young's modulus of 848.0 ± 277.0 kPa was obtained for the native cartilage samples and a Young's modulus of 205.6 ± 124.9 kPa for the degenerated samples. The elastic modulus was significantly reduced after treatment with trypsin, independent of the measurement method used. The stiffness ratio was reduced by 79% ($p < 0.001$, Paired T–test, SPSS) measured with the ultrasound water jet indentation system and by 76% ($p < 0.001$) using the mechanical indentation system. The stiffness ratio obtained using the ultrasound water jet indentation system was found to be very well correlated with the Young's modulus measured by the mechanical indentation with a correlation ratio of $r = 0.94$. For the ultrasound reflection measurements, a decrease of 35.64% ± 19.51% of the peak–to–peak amplitude at the interface of water/cartilage surface ($p < 0.001$, $n = 24$) was found after the cartilage sample was treated by the trypsin, and a decrease of 9.24% ± 8.17% was found at the interface of cartilage/subcondral bone.

Conclusions: We successfully demonstrated that the water jet ultrasound indentation could be used to simultaneously measure the mechanical and acoustic properties of articular cartilage. The measured parameters could differentiate the intact and degenerated articular cartilage.

Acknowledgements: This project was supported by the The Hong Kong Research Grant Council (B–Q754).

References:

[1] Lu MH, et al. Development of a water jet ultrasound indentation system. Ultrasound Med Biol 31: 817–26, 2005.
[2] Zheng YP, et al. Biomechanical assessment of digested cartilage using ultrasound. Med Biol Eng Comp 39: 534-541, 2001.

Snowbird Village Map

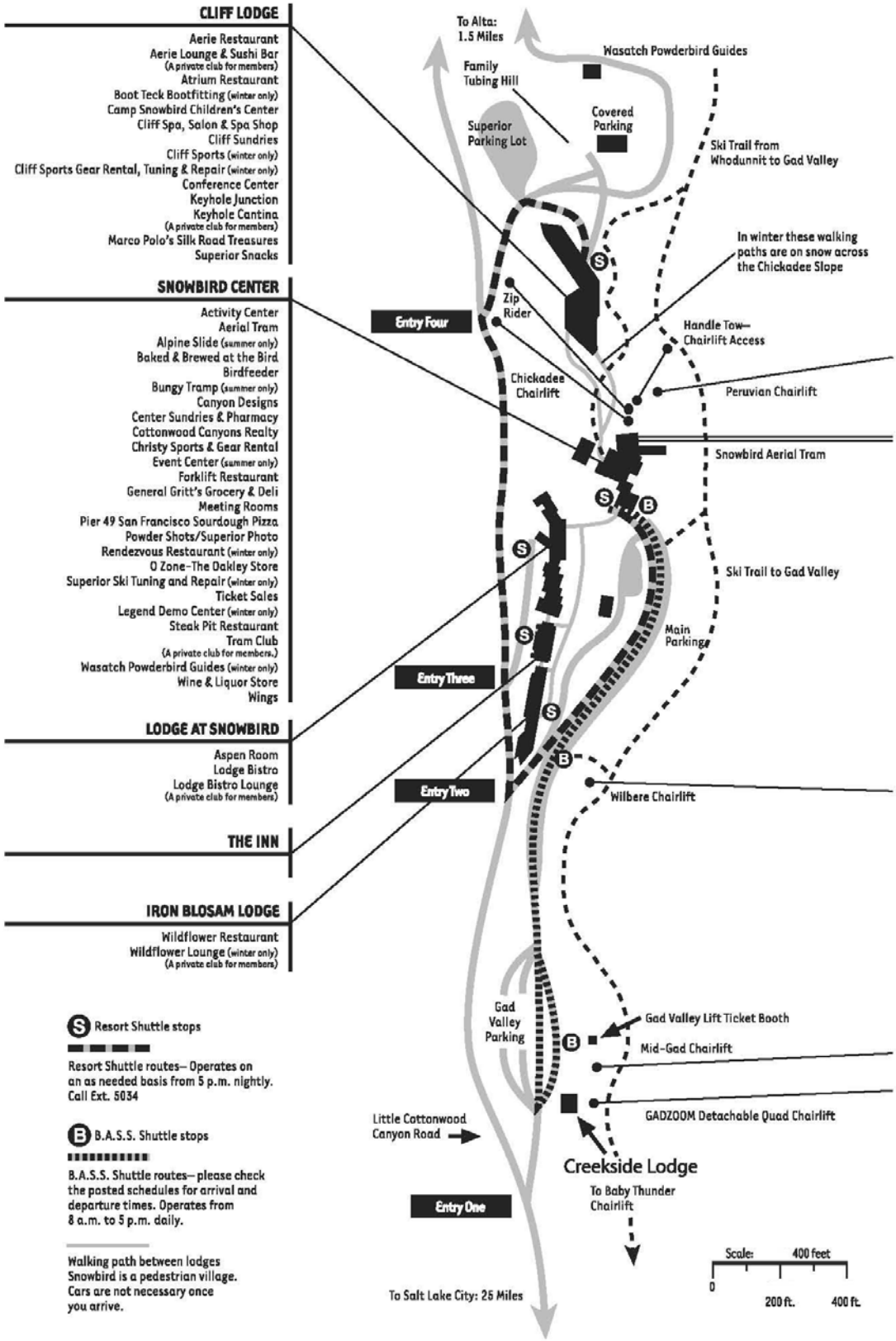

Cliff Lodge Conference Center

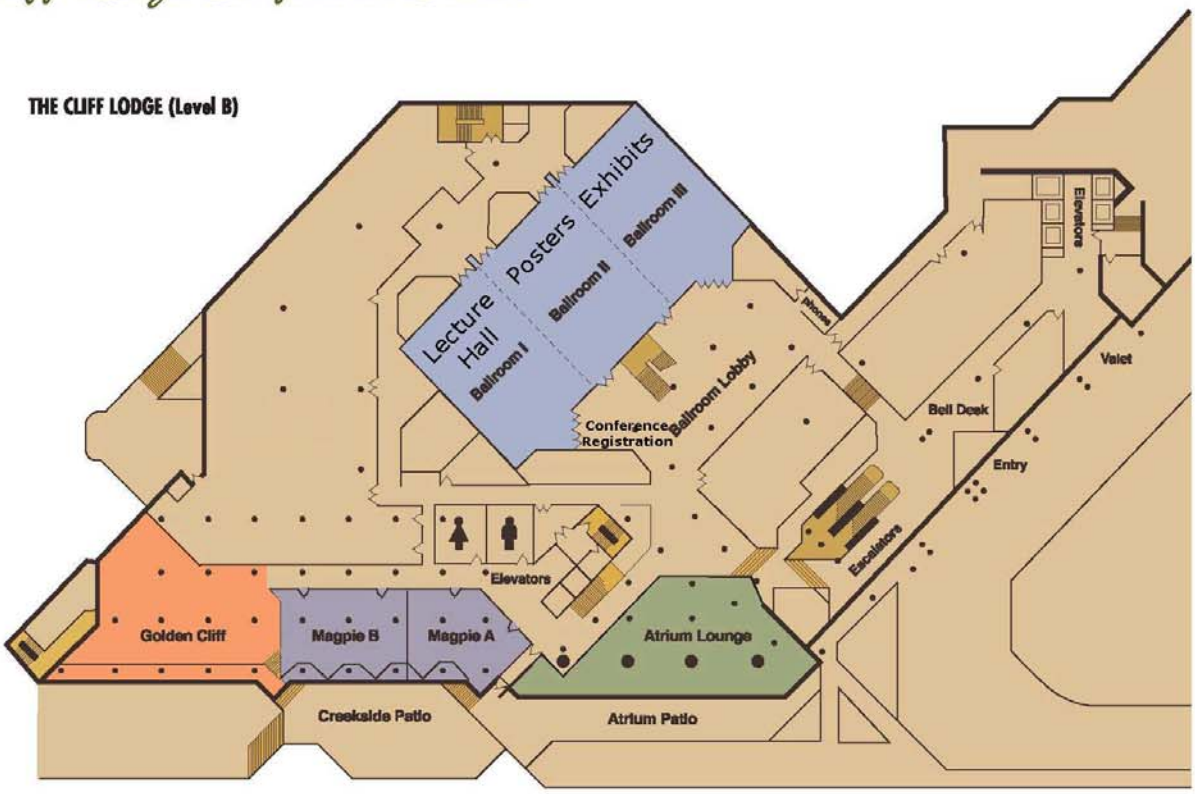

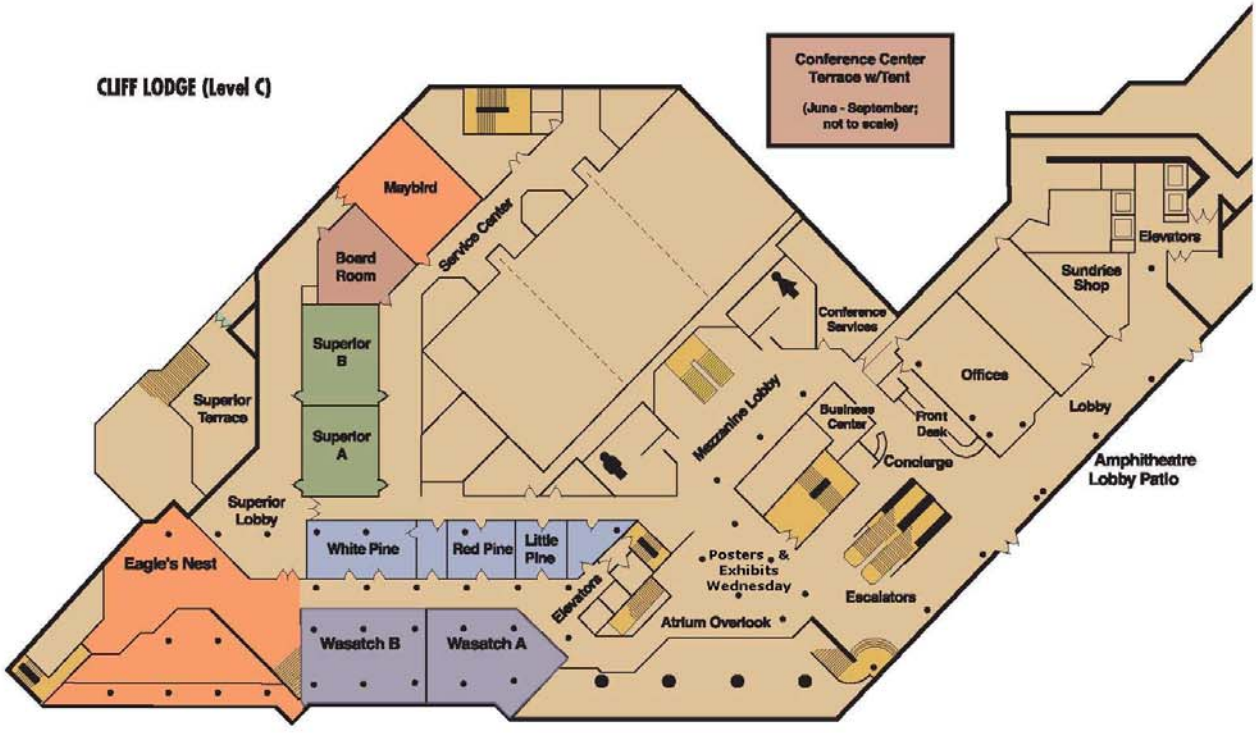

Please Fill Out Both Sides

Conference Evaluation and Questionnaire

OVERALL CONFERENCE:

	Poor		Mid		Excellent
Overall Conference Evaluation	1	2	3	4	5
General comments:					

SCIENTIFIC PROGRAM

	Poor		Mid		Excellent
Quality of the Presentations	1	2	3	4	5
Relevance of Presentations to the Conference's Theme	1	2	3	4	5
Time Allotted for Presentations too much time = 5/ just right = 3/too little time = 1	1		3		5
Time Allotted for Discussion too much time = 5/ just right = 3/too little time = 1	1		3		5
Poster Session	1	2	3	4	5
Tutorials	1	2	3	4	5
Equipment Exhibit	1	2	3	4	5
Student Participation	1	2	3	4	5
Additional comments:					

CONFERENCE MATERIALS:

	Poor		Mid		Excellent
Printed Proceedings Book	1	2	3	4	5
CD Proceedings	1	2	3	4	5
Other Registration Materials	1	2	3	4	5
I would like future abstracts to be expanded up to 2 pages each				Yes	No
I would like to submit my full PPT presentation to appear on the Conference website				Yes	No
Additional comments:					

CONFERENCE FACILITIES & SOCIAL PROGRAM

	Poor		Mid		Excellent
Lecture Hall	1	2	3	4	5
Registration Desk	1	2	3	4	5
Meals: Dining facilities	1	2	3	4	5
Conference Breakfasts and Lunches	1	2	3	4	5
Conference Dinner and Concert	1	2	3	4	5
Coffee Breaks	1	2	3	4	5
Opening Oktoberfest Reception	1	2	3	4	5
Closing Pizza Party					
Audio–Visual	1	2	3	4	5
Additional comments:					

Please Fill Out Both Sides

Conference Evaluation and Questionnaire

VENUE AND HOTEL

SCORING:	Very Poor		Mid		Excellent
Venue – Snowbird, Utah and Environs	1	2	3	4	5
Would you return to this city?	Yes		Perhaps		No
Area Attractions	1	2	3	4	5
Hotel: Overall	1	2	3	4	5
Reservations	1	2	3	4	5
Transportation and Accessibility	1	2	3	4	5
Reception and Check – In	1	2	3	4	5
Accommodations	1	2	3	4	5
Facilities	1	2	3	4	5
Parking	1	2	3	4	5
Would you return to this hotel?	Yes		Perhaps		No
Additional comments:					

CONFERENCE ADMINISTRATION

SCORING:	Very Poor		Mid		Excellent
Website	1	2	3	4	5
Registration off–site	1	2	3	4	5
Registration on–site	1	2	3	4	5
Administrative staff	1	2	3	4	5
Correspondence	1	2	3	4	5
Additional comments:					

GENERAL INFORMATION

I am a Returning Delegate	Yes		No
I plan to attend the next conference	Yes	Perhaps	No
and present a paper(s) / poster(s)	Yes	Perhaps	No
Other(s) from my lab would attend the next conference	Yes	Perhaps	No
and he/she / they would present a paper(s) / poster(s)	Yes	Perhaps	No
How did you learn of this conference? (Check all that apply)	☐ Email Announcement		
☐ Internet	☐ Website		
☐ Other	☐ Colleague		
Tutorial Topic Suggestions for next year:			
Additional Comments, Improvements or Suggestions:			

If you would be willing to host the Conference in your city, please give your name to the Conference Staff.
Questions or comments are welcome at any time at <elasticity.conference@uth.tmc.edu>